Integration of electric vehicles into microgrids and distribution grid

Department of Electrical and Information Engineering
Industry 4.0
Ph.D. Program
SSD: ING-IND/33– ELECTRICAL POWER SYSTEMS

Final Dissertation

Integration of electric vehicles into microgrids and distribution grid

---

by
Marasciuolo Francesca

Supervisor:

Prof. Maria Dicorato

Coordinator of Ph.D. Program:
Prof. Caterina Ciminelli

Course n°36, 01/11/2020-31/01/2024

Politecnico di Bari

LIBERATORIA PER L'ARCHIVIAZIONE DELLA TESI DI DOTTORATO

Al Magnifico Rettore
del Politecnico di Bari

Il/la sottoscritto/a Marasciuolo Francesca nato/a a Trani (BT) il 16/05/1995

residente a Trani (BT) in via Benedetto Croce, 6 e-mail francesca.marasciuolo@poliba.it

iscritto al 3° anno di Corso di Dottorato di Ricerca in Industria 4.0 ciclo 36

ed essendo stato ammesso a sostenere l'esame finale con la prevista discussione della tesi dal titolo:

"Integration of electric vehicles into microgrids and distribution grid"

DICHIARA

1) di essere consapevole che, ai sensi del D.P.R. n. 445 del 28.12.2000, le dichiarazioni mendaci, la falsità negli atti e l'uso di atti falsi sono puniti ai sensi del codice penale e delle Leggi speciali in materia, e che nel caso ricorressero dette ipotesi, decade fin dall'inizio e senza necessità di nessuna formalità dai benefici conseguenti al provvedimento emanato sulla base di tali dichiarazioni;
2) di essere iscritto al Corso di Dottorato di ricerca Industria 4.0 ciclo 36, corso attivato ai sensi del "*Regolamento dei Corsi di Dottorato di ricerca del Politecnico di Bari*", emanato con D.R. n.286 del 01.07.2013;
3) di essere pienamente a conoscenza delle disposizioni contenute nel predetto Regolamento in merito alla procedura di deposito, pubblicazione e autoarchiviazione della tesi di dottorato nell'Archivio Istituzionale ad accesso aperto alla letteratura scientifica;
4) di essere consapevole che attraverso l'autoarchiviazione delle tesi nell'Archivio Istituzionale ad accesso aperto alla letteratura scientifica del Politecnico di Bari (IRIS-POLIBA), l'Ateneo archivierà e renderà consultabile in rete (nel rispetto della Policy di Ateneo di cui al D.R. 642 del 13.11.2015) il testo completo della tesi di dottorato, fatta salva la possibilità di sottoscrizione di apposite licenze per le relative condizioni di utilizzo (di cui al sito http://www.creativecommons.it/Licenze), e fatte salve, altresì, le eventuali esigenze di "embargo", legate a strette considerazioni sulla tutelabilità e sfruttamento industriale/commerciale dei contenuti della tesi, da rappresentarsi mediante compilazione e sottoscrizione del modulo in calce (Richiesta di embargo);
5) che la tesi da depositare in IRIS-POLIBA, in formato digitale (PDF/A) sarà del tutto identica a quelle **consegnate**/inviate/da inviarsi ai componenti della commissione per l'esame finale e a qualsiasi altra copia depositata presso gli Uffici del Politecnico di Bari in forma cartacea o digitale, ovvero a quella da discutere in sede di esame finale, a quella da depositare, a cura dell'Ateneo, presso le Biblioteche Nazionali Centrali di Roma e Firenze e presso tutti gli Uffici competenti per legge al momento del deposito stesso, e che di conseguenza va esclusa qualsiasi responsabilità del Politecnico di Bari per quanto riguarda eventuali errori, imprecisioni o omissioni nei contenuti della tesi;
6) che il contenuto e l'organizzazione della tesi è opera originale realizzata dal sottoscritto e non compromette in alcun modo i diritti di terzi, ivi compresi quelli relativi alla sicurezza dei dati personali; che pertanto il Politecnico di Bari ed i suoi funzionari sono in ogni caso esenti da responsabilità di qualsivoglia natura: civile, amministrativa e penale e saranno dal sottoscritto tenuti indenni da qualsiasi richiesta o rivendicazione da parte di terzi;
7) che il contenuto della tesi non infrange in alcun modo il diritto d'Autore né gli obblighi connessi alla salvaguardia di diritti morali od economici di altri autori o di altri aventi diritto, sia per testi, immagini, foto, tabelle, o altre parti di cui la tesi è composta.

Luogo e data Bari, 02/04/2024 Firma 

Il/La sottoscritto, con l'autoarchiviazione della propria tesi di dottorato nell'Archivio Istituzionale ad accesso aperto del Politecnico di Bari (POLIBA-IRIS), pur mantenendo su di essa tutti i diritti d'autore, morali ed economici, ai sensi della normativa vigente (Legge 633/1941 e ss.mm.ii.),

CONCEDE

- al Politecnico di Bari il permesso di trasferire l'opera su qualsiasi supporto e di convertirla in qualsiasi formato al fine di una corretta conservazione nel tempo. Il Politecnico di Bari garantisce che non verrà effettuata alcuna modifica al contenuto e alla struttura dell'opera.
- al Politecnico di Bari la possibilità di riprodurre l'opera in più di una copia per fini di sicurezza, back-up e conservazione.

Luogo e data Bari, 02/04/2024 Firma 

Politecnico di Bari

Department of Electrical and Information Engineering
Industry 4.0
Ph.D. Program
SSD: ING-IND/33–ELECTRICAL POWER SYSTEMS

Final Dissertation

Integration of electric vehicles into microgrids and distribution grid

by
Marasciuolo Francesca:

Referees:
Prof. Luigi Martirano
Prof. Andrea Bonfiglio

Supervisors:
Prof. Maria Dicorato

Coordinator of Ph.D Program:
Prof. Caterina Ciminelli

Course n°36, 01/11/2020-31/01/2024

Abstract

This thesis reports the results of the three-years activities carried out during the XXXVI cycle of the Ph.D. course in Industry 4.0 of Politecnico di Bari.

The main goal of this work regards the integration of electric vehicles into microgrids and distribution networks by means of technological solutions and operation programming methodologies covering different approaches of the involved actors. Charging infrastructures in DC microgrid architectures that involve renewable energy resources, electrochemical storage systems are considered promising for numerous fields of implementation. In addition, vehicle-to-grid technology allows electric vehicles to be exploited as additional storage systems further to smart charge regulation. The potential of these systems lies in the possibility of coordinating all resources by means of optimization algorithms for operation planning, in order to achieve economic and technical objectives, and to enable the microgrid to perform various functions by means of its resources including electric vehicles, such as reserve provision, supporting active power for electricity grids, controlling peak shaving and load shifting, and regulating voltage and frequency.

The control of the microgrid is entrusted to the energy management system, which is able to set the optimal level of power exchange between components, depending on certain objectives by means of manifold procedures accounting for specific issues related to electric vehicles and relevant charging stations, energy storage and renewable sources. Analogously, the integration of electric vehicles in wider frameworks such as energy communities and distribution networks requires

proper energy management functions dealing with technical and economic challenges while interacting with microgrid-level energy management system or smart charging stations. In particular, a first analysis deals with day-ahead planning procedure for microgrids supplying electric vehicles, based on assumptions and forecasts, with a focus on the possibility of internal reserve provision and the integration of fast-charge stations. Monitoring and measurement systems play a central role in a microgrid, as they provide data from the field to the management system. Within this framework, another research topic focuses on the analysis of a monitoring architecture for data acquisition and control command communication between the energy management system and field devices. Furthermore, the possibility of aggregating microgrids into energy communities is addressed through a day-ahead scheduling strategy for managing the resources of DC microgrids within community with the aim of respecting the power exchange in a first level procedure, while ensuring internal reserve levels to cope with forecast errors in photovoltaic generation as well. In addition, the effects of integrating electric vehicles on distribution networks is assessed by defining methodologies and simulation tools for managing vehicle charging. In particular, the economic and environmental impact of operating electric vehicles in parking lots, and the role of integrated stationary storage systems in achieving economic and environmental benefits is evaluated through optimization strategies with technical and economic objectives. Finally, the development of multi-objective strategies, based on microgrid and distribution network planning methodologies, allows to assess the effects of these systems on distribution network operation, laying the basis for studying the role of energy communities integrated into distribution networks.

The thesis work is framed in the activities developed by power system group at Politecnico di Bari within EU H2020 projects (CONNECT and PROGRESSUS) culminated with the realization of a DC microgrid for supplying electric vehicles as project use case.

Sommario

Questo lavoro di tesi riporta i risultati di tre anni di attività svolte durante il XXXVI ciclo del corso di dottorato in Industria 4.0 del Politecnico di Bari.

L'obiettivo principale del lavoro è incentrato sull'integrazione dei veicoli elettrici nelle microreti e nelle reti di distribuzione mediante soluzioni tecnologiche e metodologie di programmazione con diversi approcci dei soggetti coinvolti nella loro gestione. Le infrastrutture di ricarica in architetture di microreti in corrente continua che coinvolgono anche risorse energetiche rinnovabili, e sistemi di accumulo elettrochimico sono tra le più promettenti per i numerosi campi di implementazione. Inoltre, la tecnologia vehicle-to-grid permette di utilizzare i veicoli elettrici come sistemi di accumulo aggiuntivi oltre a controllare i processi di carica. Il potenziale di questi sistemi risiede nella possibilità di coordinare tutte le risorse mediante algoritmi di ottimizzazione, al fine di raggiungere obiettivi economici e tecnici, e di abilitare la microrete a diverse funzioni, come la fornitura di riserve, il supporto di potenza attiva per le reti elettriche, il controllo dei picchi di carico, la regolazione della tensione e della frequenza.

Il controllo della microrete è affidato al sistema di gestione dell'energia, in grado di impostare il livello ottimale di scambi di potenza tra i componenti, in funzione di determinati obiettivi, attraverso molteplici procedure che portano in conto di condizioni specifiche legate ai veicoli elettrici e alle relative stazioni di ricarica, all'accumulo di energia e alle fonti rinnovabili. Analogamente, l'integrazione dei veicoli elettrici in contesti più ampi, come le comunità energetiche e le reti di distri-

buzione, richiede adeguate funzioni di gestione dell'energia che affrontino le sfide tecniche ed economiche durante l'interazione con i sistemi di gestione dell'energia a livello di microrete o con le stazioni di ricarica. In questo contesto, l'obiettivo del presente lavoro è quello di sviluppare strategie di gestione dell'energia, basate su procedure di ottimizzazione, per gestire le problematiche di integrazione dei veicoli elettrici a diversi livelli. In particolare, una prima analisi riguarda la procedura di pianificazione day-ahead per le microreti che integrano stazioni di ricarica per veicoli elettrici, basata su ipotesi e previsioni, con focus sulla possibilità di fornitura di riserva interna e sull'integrazione delle stazioni di ricarica fast-charge. I sistemi di monitoraggio e misurazione svolgono un ruolo centrale in una microrete, poiché forniscono dati dal campo al sistema di gestione. In questo quadro, un altro tema di ricerca è l'analisi di un'architettura di monitoraggio per l'acquisizione dei dati e la comunicazione dei comandi di controllo tra il sistema di gestione dell'energia e i dispositivi di campo. La possibilità di aggregazione di microreti in comunità energetiche è affrontata attraverso una strategia di programmazione day-ahead per la gestione delle risorse di una comunità energetica che comprende microreti in corrente continua, al fine di garantire la coerenza degli scambi di potenza delle microreti rispetto a una pianificazione a più livelli, garantendo anche livelli di riserva interna per tener conto di errori di previsione di produzione fotovoltaica.

Inoltre, gli effetti dell'integrazione delle stazioni di ricarica dei veicoli elettrici sulle reti di distribuzione sono valutati definendo metodologie e strumenti di simulazione per la gestione della ricarica dei veicoli elettrici. In particolare, l'impatto economico e ambientale dell'operatività dei veicoli elettrici nelle stazioni di ricarica, anche installate in modalità aggregata sui singoli nodi, e il ruolo dell'integrazione dei sistemi di accumulo stazionario nel raggiungimento di benefici economici ed ambientali è valutato attraverso strategie di ottimizzazione con obiettivi tecnici ed economici. Infine, lo sviluppo di strategie multi-obiettivo, sulla base delle metodologie di programmazione delle microreti e delle reti di distribuzione, permette di

valutare gli effetti dell'integrazione di questi sistemi all'interno delle reti di distribuzione, ponendo le basi per lo studio del ruolo delle comunità energetiche all'interno di esse.

Il lavoro di tesi è inquadrato nelle attività sviluppate dal gruppo di Sistemi Elettrici del Politecnico di Bari nell'ambito dei progetti europei H2020 (CONNECT e PROGRESSUS) culminati con la realizzazione di una microrete in corrente continua per l'alimentazione di veicoli elettrici come caso d'uso dei progetti.

"To strive, to seek, to find, and not to yield."

A. Tennyson, *Ulysses*

Acknowledgments

With the conclusion of this challenging journey, I feel obliged to thank all those who contributed to the achievement of this milestone. First and foremost, I would like to thank my Ph.D. supervisor, Prof. Maria Dicorato. Her constant support, guidance, and encouragement have been invaluable throughout the entire process. I am profoundly grateful to Dr. Giuseppe Forte for the all immeasurable contributions during these years, from the initial stages of my research to the final submission of the thesis. I would like to thank Prof. Liana Cipcigan, along with all the researchers of the A-HIVE Lab of Cardiff University, for warmly welcoming me during my staying in Cardiff, and for sharing knowledge and experiences in an open-minded research environment. A special thanks to SEPE and LabZERO collegues, whose support has been a constant source of motivation. Our lunch breaks and informal chats lightened even the most difficult days. I also deeply thank my lifelong friends, for our spontaneity and for what binds us together after all these years. Finally, I would like to thank my parents and my brother. I will never thank you enough for always believing in me, and for constantly supporting me. I hope you are aware of and proud of the significant role you have played in shaping my path.

Contents

List of Figures

List of Tables

Acronyms

AC Alternate Current. 6, 12, 17, 27, 28, 62, 64, 66, 76–78, 86, 126

AFIR Alternative Fuels Infrastructure Regulation. 5, 6

ARERA Regulatory Authority for Energy Networks and Environment. 15, 36, 65

BESS Battery Energy Storage System. 11, 12, 16–20, 24, 27, 29–33, 35, 36, 41–43, 45–52, 54–61, 64, 65, 68, 75, 82, 83, 85–90, 92, 93, 96, 97, 99–102, 104–107, 109–111, 113–116, 118, 160, 162–164, 166, 169–171, 177–181

CDS Closed Distribution Systems. 14

CEC Citizen Energy Community. 14

DC Direct Current. 6, 11, 12, 17–20, 24–28, 30, 36, 41, 42, 47, 58, 59, 62, 64–67, 69, 70, 73, 75–78, 82, 83, 86, 95, 104, 125, 126, 159, 160, 162–164, 166, 169–171, 177, 178, 180, 181

EMS Energy Management System. 16, 84, 177

EV Electric Vehicle. 2–5, 7–14, 17–20, 24–26, 28–36, 39–47, 49–52, 54–69, 71, 75, 76, 78, 80–83, 85–90, 92, 93, 95, 96, 98–102, 104–109, 112–122, 126, 127, 129–131, 134, 135, 138–142, 144–147, 149, 151–157, 159, 160, 162–171, 177–181

EVSI Electric Vehicle Supply Infrastructure. 11, 18, 19, 28, 33, 36, 47, 55, 62, 65, 70, 82, 86, 91, 105, 177, 180

HPC High Power Charging. 78–81

HV High Voltage. 124, 175

LEC Local Energy Community. 13–15, 17–19, 83, 85–88, 91, 92, 95, 101, 175–178, 180, 181

LV Low Voltage. 8–10, 15, 20, 104, 151, 179

MV Medium Voltage. 10, 15, 19, 20, 104, 124, 134, 151, 159, 160, 175, 179, 180

PCC Point of Common Coupling. 71

PHEV Plug-in Hybrid Electric Vehicle. 2

PV Photovoltaic. 11–13, 16, 17, 24, 29, 30, 33, 36, 39–43, 47, 52, 55–61, 65, 67–69, 71, 72, 75, 76, 83, 86, 89, 90, 92, 96, 98, 100–103, 164, 168–170, 177, 178

REC Renewable Energy Community. 14–16

RES Renewable Energy Sources. 17, 82

SC Smart Charging. 114, 117

SOC State of Charge. 29–31, 41, 42, 49–52, 54, 55, 57, 66, 68, 75, 81, 82, 85, 90, 96, 99, 100, 107, 108, 111, 120, 121, 126, 135–137, 140–142, 144, 160, 163, 164, 170

SSPC Simple Systems of Production and Consumption. 15

TEN-T Trans-European Network Transport. 5

V2G Vehicle-to-Grid. 9, 10, 12, 17–19, 24, 27, 41–43, 46, 48, 50, 52, 59, 61, 66, 67, 76, 79, 84–86, 90–93, 118–120, 122, 126, 130, 131, 133–135, 140, 144–146, 149, 150, 152–155, 157, 162, 165, 169–171, 177–180

ZLEV Zero and Low Emission Vehicle. 2

Chapter 1

Electric Mobility: Diffusion and Integration

1.1 Transport electrification

The transport sector is the fourth largest sector when accounting for CO_2 emission, responsible in 2022 for 8.1 Gte (corresponding to 14% of the total CO_2 emissions), after the energy supply sector with 20.9 Gte (36%), the industry with 14.4 Gte (25%) and agricultural one (10.3 Gte, 18%), according to the Emission Gap Report 2023 data reported in Fig. 1.1 [1].

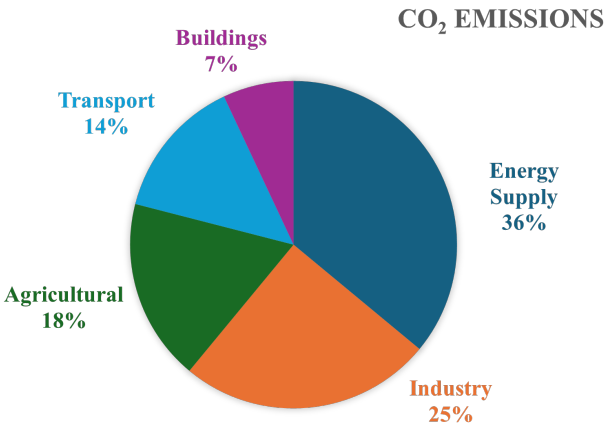

Figure 1.1: CO_2 emissions split into the major economic sectors. Data source in [1].

Transport electrification represents a promising solution for CO_2 reduction and many

countries are promoting supportive regulatory framework for the adoption of electric vehicles (EVs). In particular, the Fit-for-55 package of the European Union focuses also on transport sector initiatives. As part of Fit-for-55, Directive RED III of the European Commission sets binding targets on shared renewable energy in final consumption and on the reduction of greenhouse gas intensity by 2030 [2].

The European Commission actions to strengthen the emission limits for new passenger cars and light commercial vehicles registered in the European Union are carried out by the update of Regulation (EU) 2019/631 [3]. This regulation sets specific CO_2 emission limits that apply to the entire new vehicle fleet of each manufacturer registered in a given year in Europe. The new objectives include:

- maintaining the existing 2025 targets for passenger cars and vans, which require a 15% reduction in specific CO_2 emissions compared to 2021,
- increasing the required reductions from 2030 to 55% for passenger cars (previously 37.5%) and 50% for vans (previously 31%),
- introduction of a new 100% emission reduction requirement for both categories from 2035, implying zero emissions,
- removal of the Zero and Low Emission Vehicle (ZLEV) incentive scheme from 2030.

These measures put the basis for zero-emission transport by 2035, thus implying the use of EVs, hydrogen-powered vehicles or, in the case of internal combustion engines or plug-in hybrid vehicles (PHEVs), by using carbon neutral renewable fuels.

1.2 EV diffusion: European and Italian context

According to the Global EV Outlook 2023 [4], EV sales hit a new record year in 2022, with 10 million EV sold worldwide (see Fig. 1.2). A total of 14% of all new cars sold were electric in 2022, up from around 9% in 2021 and less than 5% in 2020. China still dominate the global sale market, accounting for around 60% of global EV sales, allowing to exceed its 2025 target for new energy vehicle sales. Europe is the second largest market, where EV

sales increased by over 15% in 2022. EV sales in the United States, the third largest market, increased 55% in 2022, reaching a sales share of 8%. Data reported for 2023 confirms the increase of sales, and 14 million sales are expected by the end of 2023, representing a 35% year-on-year increase.

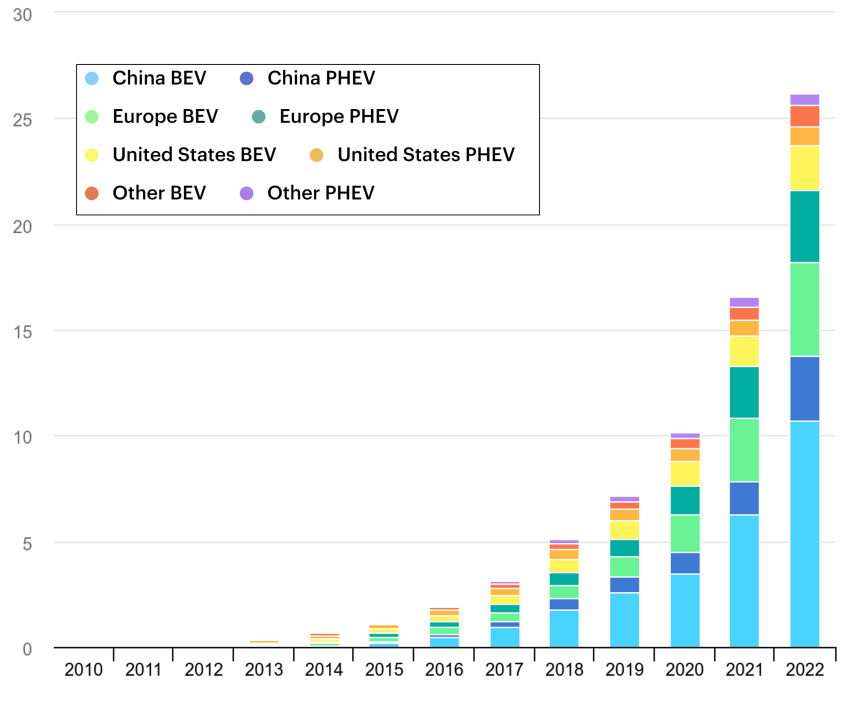

Figure 1.2: Global EV stock, 2010-2022. Data source in [4].

Regarding the Italian EV diffusion, considerable divergences are detected in car registrations with respect to the other European countries [5]. In particular, in 2022 the percentage of EV of the total number of registrations was just under 9%, below the European average. The maximum percentage has been reached by Norway with 90% of EVs on the total new registration.

The diffusion of EV charging infrastructures is linked to the EV diffusion in order to guarantee same levels of accessibility as for refuelling conventional vehicles. In particular, more than 600000 public slow charging points (up to 22 kW) were installed in 2022, 360000 of them were in China. Europe total charging points are 460000 slow chargers in 2022, with a 50% increase from the previous year. The Netherlands leads in Europe with 117000, followed by around 74000 in France and 64000 in Germany.

Public fast-charging stations increased reaching 330000 globally in 2022, half of slow chargers, where almost 90% of the growth came from China. The deployment of fast charging is due to the lack of private chargers in densely populated cities and supports China's goals for rapid EV deployment. Europe reached 70000 fast chargers by the end of 2022, 55% more than 2021. Countries with the largest fast charger stock are Germany (over 12000), France (9700) and Norway (9000).

Fig. 1.3 shows the average public charging power capacity per EV, which is globally around 2.4 kW per EV. In the European countries, the ratio is lower, with an average around 1.2 kW per EV. Korea has the highest ratio at 7 kW per EV, even with most public chargers (90%) being slow chargers [4].

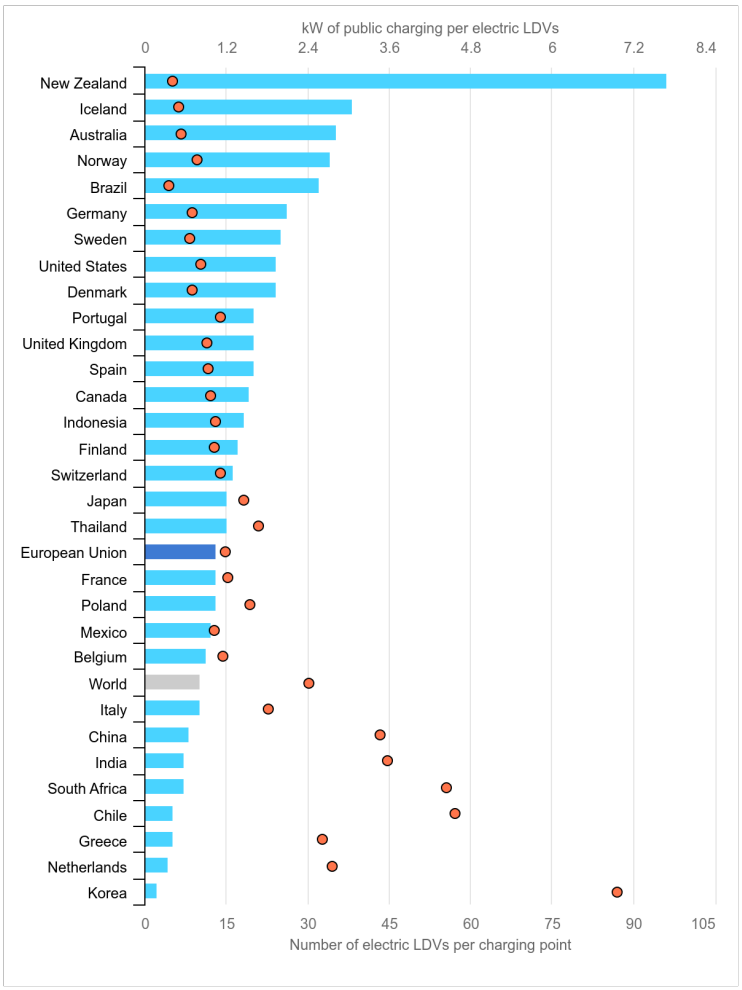

Figure 1.3: Number of electric EV per public charging point and power [kW] per EV, 2022 [4].

As aforementioned, European Union aim is to further develop the public charging infrastructure, as indicated by the deployment of Alternative Fuels Infrastructure Regulation (AFIR) [6], which set electric charging coverage requirements across the trans-European network-transport (TEN-T). This regulation not only sets specific targets, but also common technical standards for information provided to users, infrastructure-related data, and payment methods. In addition, it regulates the national strategic frameworks that Member States are required to develop, which include the planning and implementation of alternative fuel infrastructures in areas where obligations have not been established at the European level and require reporting on progress in the implementation of these infrastructures. In addition, the Regulation 2023/1804 [7] of European Parliament establishes a series of targets to be achieved by European countries regarding EV charging stations across the TEN-T, thus substituting Directive 2014/94/UE on Deployment of Alternative Fuel Infrastructure (DAFI). In particular, the measure determines that Member States shall ensure along the core and comprehensive TEN-T network, in each direction of travel, groups of publicly accessible charging stations for light electric vehicles at a maximum distance of 60 km from each other. At least 400 kW of output power should be provided by each group of stations (including also a charging point of at least 150 kW) by the end of 2025 and of at least 600 kW (with two 150 kW points) by the end of 2027, whereas along the TEN-T comprehensive network, each group of EV stations will have to provide at least 300 kW and include a 150 kW point by the end of 2030, rising to at least 600 kW with two 150 kW points in each group by 2035. The regulation also sets the minimum number of charging stations for heavy-duty vehicles.

The report [5] assesses that the Italian growth of public charging points is in line with the European trend. It is also estimated that private access charging points have increased even faster, mainly due to the Superbonus effect. In particular, by the end of 2022 almost 30000 public access charging points are installed in Italy. Approximately 80% of these are slow charger while the remaining are fast ones [8]. By 2022, installations of private access charging points in Italy increased 170% compared to 2021, bringing total installations total installations to 370000 [5]. Figg. 1.4 and 1.5 report the total number of EV charging points

and the number of AC and DC points considering all AFIR charging rate classification.

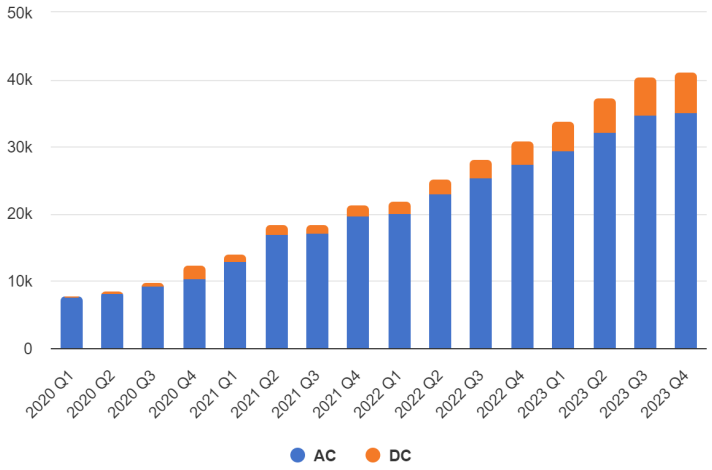

Figure 1.4: Total number of EV charging points, according to the AFIR classification [8].

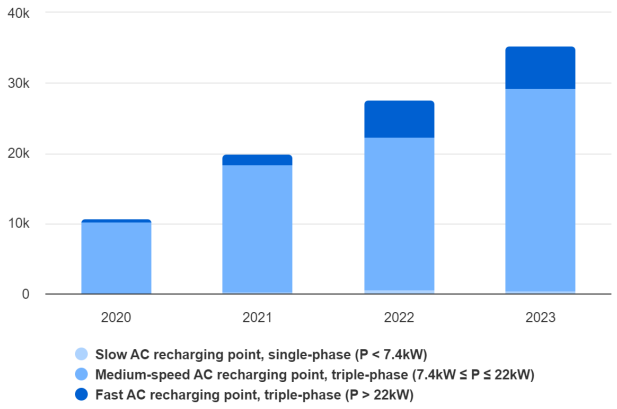

(a)

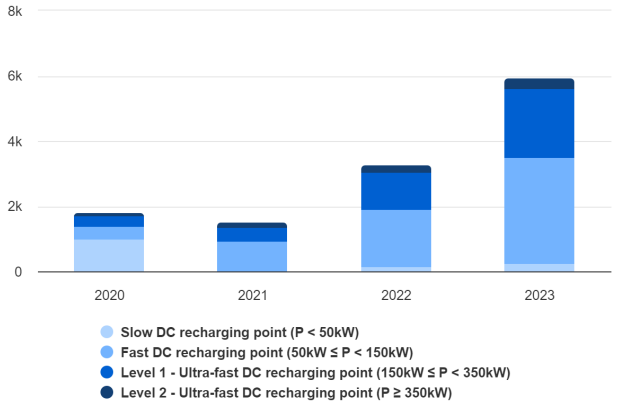

(b)

Figure 1.5: Total number of publicly accessible AC (a) and DC (b) EV charging points, according to AFIR categorization [8].

1.3 Impact of EVs on the grid

The transport electrification contributes to energy demand increase, as reported in [9] and in Fig. 1.6 for the Italian case. Energy demand grew up to 2008, with a contraction during the economic crises of 2009 and 2012, and until they remained more or less constant from 2017 to the present, net of today, net of 2020 where measures to contain the Covid-19 pandemic have resulted in reduced electricity demand. In the horizon years of the scenarios, the electrification process leads to a substantial increase in the electricity demand. In the case of the Distributed Energy (DE) scenario, that considers the highest penetration of the electric carrier for the Italian scenarios, a value of 418 TWh is envisaged by 2040. Moreover, the most electrified European scenario, the 2030 DE, has a higher electricity demand than the Policy Fit-for-55 (FF55), that considers a penetration of 8 million EVs, implying a 12 TWh demand increase. In 2040, on the other hand, both Italian scenarios, 2040 DE IT and 2040 GA IT (EV penetration respectively set to 14 and 12.5 million), have lower demand values than those identified in Policy FF55.

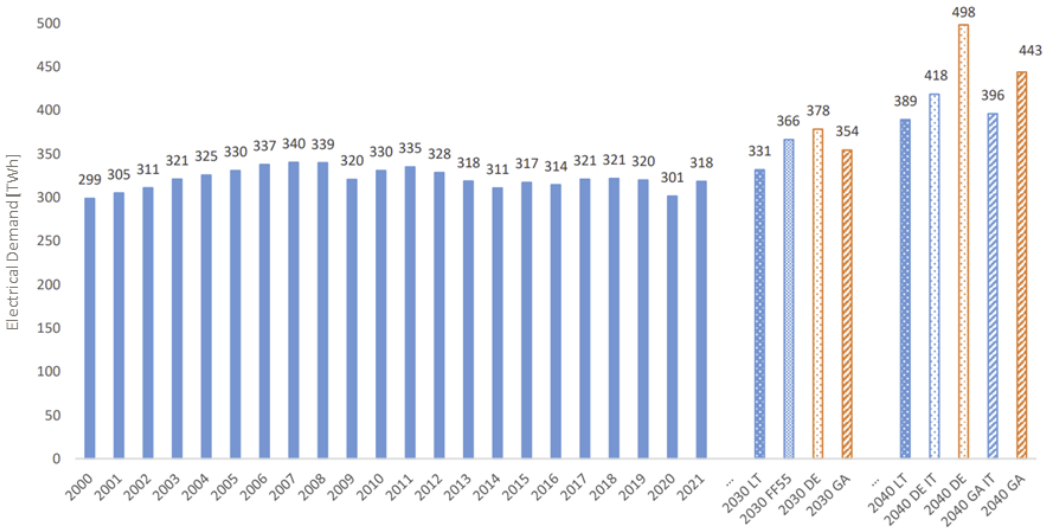

Figure 1.6: Total Italian energy demand in all scenarios [9].

1.3.1 Technical impact on grid operation

The increasing number of integrated charging stations could affect the distribution grid operation, since connected EV charging demand modifies grid global load profiles, according to

charging management procedure adopted. Although the procedure of uncontrolled charging is considered the easiest way to integrate EVs, since they are charged at maximum power until they are completely charged, it leads to several grid issues due to high load increase on the grid (see Table 1.1 [10]) . Several studies focused on the effects of EV integration into power grids, in terms of load profile, voltage profile and harmonic distortion [11]. Another potential effect is registered in [12] on transformer performances, especially considering EV uncoordinated charging, as well as issues concerning transformer performances with high penetration levels that can lead to grid upgrades [13]. This demonstrates that EV charging requirements can cause load and voltage unbalancing, leading to unsafe operation of the grid [14].

Table 1.1: EV charging approaches [10].

Charging mode	Load profile	Advantages	Disadvantages
Uncontrolled charging	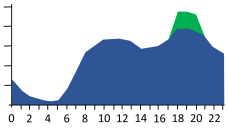	Easy for implementing and for EV owners	Overloading in transformers and distribution feeders Grid issues
Off-peak charging	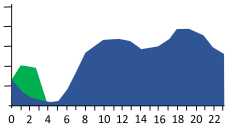	Flattening the load profile Integration of renewables at off-peak hours	Unbalance of load demand Voltage deviations
Valley filling charging	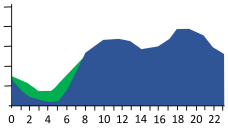	Flattening the load profile Integration of renewables Ancillary service provision	Complex implementation Data exchange infrastructure
Peak-shaving charging	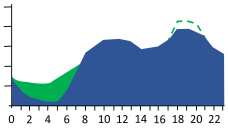	Integration of renewables Ancillary service provision Peak load reduction	Complex implementation Data exchange infrastructure Battery degradation for V2G

Several studies focus on the analysis of EV charging effects on the distribution and low voltage (LV) grid, highlighting the possibility of grid congestions and over/under compensations when uncoordinated charging occur [15]. A sensitivity study carried out in [16]

shows that EV number, charger power rating [14] and modelling of driving pattern are the factors that most influence transformer and line loading in LV distribution networks, considering urban context. Level of EV penetration also affects the safe operation of networks: the assessment study in [13] on a radial residential LV grid reveals that for a 60% penetration of EVs thermal and loading violations on distribution transformer and feeder occur. For higher integration rates, voltage drops and loss increases are detected in [17] and a distribution feeder reconfiguration is studied to reduce negative impacts of EV uncontrolled charging. In addition, suburban grids are found as the most vulnerable to massive EV integration, as higher congestion events arise [18]. In [19] the impact of EV integration on a low voltage distribution network is evaluated considering different EV penetration levels and showing that the uncoordinated charging implies the infrastructure upgrade, with respect to the case of EV coordinated charging. The possibility to control EV charging, in order to minimize total energy losses, has also effects on reducing negative impacts into distribution networks [20]. Off-peak charging and valley filling charging are examples of controlled procedures (Table 1.1). Furthermore, in [21] EV charging stations are integrated into the optimization model of economic dispatch as flexible loads with price elasticity, confirming that the control of charging loads is able to avoid grid congestion, as in [22], where EV charging is scheduled during off-peak demand times to sustain load balance, verifying the possibility to fill the valley of the load profile [13], although this approach could still lead to voltage instabilities and load imbalance. Moreover, controlled charging strategies, based on limitation of power supply at primary distribution transformers and minimization of EV aggregator costs, show positive effects on grid voltage profile, energy losses and transformer loss of life [23] as compared to uncontrolled charging effects.

The possibility for EVs and charging stations to exploit vehicle-to grid (V2G) technology [24] is advantageous for EV owners, since EV discharging could support distribution network, providing ancillary services [25]. According to [26], V2G mode could support voltage control regulating bidirectionally reactive power and providing spinning reserve in the context of isolated networks. As a matter of fact, the study in [27] proposes a coordinated EV management system for a LV residential network for grid support, encouraging

V2G exploitation in order to reduce EV owner costs. In [28] the problem of EV charging station allocation in distribution grid is investigated minimizing power losses. Moreover, in [29] voltage analyses on MV /LV grid with integrated fast charging station enabling V2G show that V2G can achieve a voltage improvement and a current reduction at the point of charging.

In the presence of an EV fleet, the role of the aggregator is significant in managing all the EVs towards the distributor system operator and the electricity market, for providing an optimized power scheduling [30]. In general, two control schemes could be implemented, centralized and decentralized ones. The first one has the advantage of better performances on service provision and network capacity, whereas the second is more scalable and requires less communication infrastructures [31]. The methodology proposed in [27] demonstrates that instead of curtailing the charging demand of EVs responsible for grid constraints violations, the flexibility of neighborhood aggregated EVs is exploited to address these issues. In the framework of optimal programming, EV user behaviour constitutes an aleatory variable, as well as plug-in times and energy required for the charging [17], that are taken into account by means of stochastic technique.

1.3.2 Environmental impact of EV integration

As discussed in Section 1.3.1, smart charging strategies along with V2G exploitation have shown the possibility to shift clustered EV charging load to achieve economic and technical targets.

However, the environmental impact of EVs is still under discussion, in terms of emissions produced during EV charging. The study presented in [32] deals with the evaluation of electricity generation emissions produced due to EV charging, highlighting that smart charging technologies could unintentionally lead to an increase in emissions production, as marginal emissions could have different patterns from average emission, as shown also in [33]. In this context, the study in [34] investigates possible optimal EV charging/discharging strategies for minimizing carbon emissions, underlying the advantage of V2G exploitation in CO_2 reduction, not in all scenarios though, as energy efficiency rating

can widely influence emission evaluations. The strategy proposed in [35] based on both the time-of-use price and marginal emission factors reveals that the smart charging strategy can reduce the cost and carbon emissions by up to 27% and 16% compared with uncontrolled charging, respectively. The study in [36] aims to address the trade-off between cost and emission minimization of EV charging using multi-objective optimization framework. Moreover, the assessment of cost and emission benefit from system perspective for grid reinforcing is proposed. Costs and emissions of grid reinforcements outweigh the benefits in costs and emissions in EV charging optimization resulting from increased grid capacity. However, substantial reductions in EV charging costs and emissions can be achieved under the current transformer capacity.

The inclusion of renewable energy sources, such as photovoltaic (PV), in dedicated infrastructures for EV charging represents an important aspect of the safe integration of charging stations into the distribution networks, as reported in [37] where a technical-economic-environmental assessment methodology is implemented for photovoltaic-powered charging stations, which is demonstrated to produce less emissions with respect to power-connected charging stations, and [38], where a bidding model of a power grid involving PV and EVs is proposed in order to reach low-carbon grid operation. Moreover, battery energy storage system (BESS) could be involved in optimal scheduling procedures, as in [39], allowing the minimization of annual equivalent carbon emissions, especially considering second-life batteries. Off-grid PV -BESS system for EV charging is shown to be a profitable project to deal with carbon emissions reduction [40].

1.4 Microgrids and energy communities: new concepts for EV integration

In order to promote the integration of charging station, renewable energy sources, such as PV [41], and BESS could be installed, thus constituting a microgrid-based electric vehicle supply infrastructure (EVSI). It should be pointed out that PV , BESS, and EVs are based on DC technologies, therefore the integration in DC microgrids is advisable, considering

that DC connection enables the V2G operation [42], [43]. In DC architectures there is not the need of frequency synchronization in island-mode operation [44], and reactive power control [45]. Furthermore, it should be remarked that PV , BESS and EVs are based on DC technologies, therefore the integration in DC microgrids connected to the AC network represents a field of expansion of DC distribution concept, considering that V2G is usually enabled by DC connection [46–48]. In Fig. 1.7 an example of DC architecture is proposed.

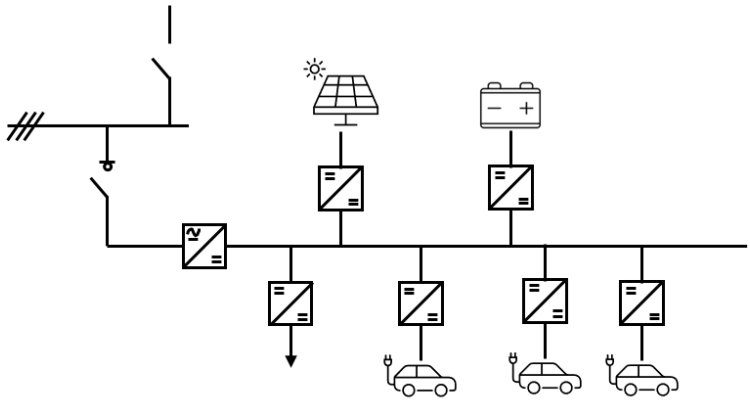

Figure 1.7: DC architecture scheme.

The optimal power planning can achieve economic and technical targets [49], [50], considering that the life cycle of storage components of the microgrid is affected by several charging and discharging cycles [51].

The multi-objective optimization is often used for energy management of microgrids. For instance, in [52], the optimization problem consists of the minimization of the daily purchasing costs (economic goal) and the circulation energy of storage batteries (technical goal). In [53], the objective functions are the O&M costs and exchanging cost of AC grid and loss of power supply probability of the system. The robust multi-objective optimization carried out in [54] aims to minimizing the cost function, including fuel cost, maintenance cost, purchasing and selling electricity cost, battery depreciation cost, penalty cost, and carbon emission. Three objective functions are formulated in [55]: life-cycle cost, self-balancing rate, and converter power loss. In [56], a cost operation-based method with considerations on power losses is investigated, for a DC microgrid. An example of opti-

mization problem reaching exclusively a technical goal as the reduction of the peak demand of the EV solar parking lot may be found in [57]. The economic and technical functions may be also linearly combined into one objective function for the optimal dispatch of EV charging stations, as investigated in [58].

Deterministic programming is based on the hypothesis of perfect determination of some values. This makes programming results idealistic compared to the real values found in systems. The intermittency of some renewable generation sources (such as PV) further emphasizes the limitations of this type of programming. Studies [59], [60] are now moving towards stochastic optimization since it considers the uncertainties and probabilities of some variables or parameters as input, in order to assess their influence on the system output data. In [61], several techniques for stochastic optimization are presented, e.g., recourse method, chance-constrained optimization, risk averse optimization, and sample average approximation. Stochastic optimization offers a range of possible solutions that can approach real-world situations providing benefit operators and/or consumers in assessing the risks associated with the uncertainties of renewable energy generation sources.

1.4.1 European Legislative framework of energy communities

In the context of the spread renewable distributed generation and EVs, according to European targets to achieve net-zero greenhouse gas emissions by 2050, the transition of power systems towards a decentralized framework involves a change in the role of consumers and prosumers, which are called to actively participate both individually and collectively in this transformation, investing in new technologies and new pathways for local generation and consumption. The Local Energy Community (LEC) initiative allows different users to jointly act in order to provide energy services to each other, whit the possibility of economic savings.

As a matter of fact, in 2015 the European Commission launched the ”European Energy Union Strategy” [62], with the aim of creating an Energy Union for market reforming and renewable energy supporting, that could empower the role of customers. This strategy, along with the commitments after the Paris Agreement, put the premises for the package

of proposal called ”Clean Energy for all Europeans Package” or ”Clean Energy Package” (CEP) [63] in 2016, in which eight legislative acts of 2018 and 2019 are collected in order to promote a regulatory framework for the energy transition. The main directives and regulations for LEC are here listed:

- Directive 2018/2001: The recast Renewable Energy Directive (REDII) [64],
- Directive 2019/944: Electricity Market Directive (IEMD) [65].

The CEP highlights the necessity of adopting sustainable energy sources, while giving the costumers an active role as individuals or collectively gathered. Directives REDII and IEMD play a fundamental role in the formal recognition for the first time of LEC, in particular defining Renewable Energy Community (REC) and Citizen Energy Community (CEC).

The REC concept is firstly introduced in the Directive REDII, where it is defined in Art. 2 as a legal entity based on: i) open and voluntary participation of members, and controlled by members located in the proximity of community project developed by the entity, ii) participation open to natural people, small and medium enterprises, and local authorities and iii) main purpose of providing environmental, social and economic benefits for the whole community, without pursuing any financial profit. Moreover, RECs are enabled to produce, sell, and consume energy from their plants, with the possibility also to share that among members or to provide grid services in the electricity markets.

The Directive IEMD defines the CEC entity quite similarly to a REC, with the main difference that large enterprises cannot take the control of the CEC. Moreover, it can be aggregated to provide energy services to members or stakeholders, as energy efficiency or EV charging. Furthermore, there is not a limitation in geographical area or in type of energy source.

1.4.2 Italian Laws for energy communities

The Italian regulatory framework allowed self-consumption schemes as a primary legislative and technical form of LEC, which are the Closed Distribution Systems (CDS) and

Simple Systems of Production and Consumption (SSPC) [66]. The first ones are private geographically-limited systems, that generally do not supply household users, whereas the second ones refers to systems involving generation plants and consumption connected to the public grid but still ensuring a self-consumption scheme. These schemes require the presence of one production site and one final costumer, differently from the multiple configurations of LECs.

With the Law 8/2020 [67] a partial transposition of the REDII directive has started, in order to promote the activation of the collective self-consumption schemes and RECs in the Italian energy context. Some constraints and features are defined for these configurations:

- renewable energy plants owned by RECs or self-consumption schemes must have started their operation after March 1^{st} 2020,
- the capacity of each plant may not exceed 200 kW of installed power,
- plants and consumers (members, partners or participants in the scheme) must be subject to the same MV /LV transformer substation for RECs and belong to the same building in the case ofcollective self-consumption schemes.

Moreover, the Italian Regulatory Authority for Energy Networks and Environment (ARERA) and Ministry for Economic Development have defined regulatory model and tariff components to be applied to members of the RECs and participants in collective self-consumption schemes, along with the incentives to be granted to the two schemes. Concerning regulation model, ARERA Deliberation 318/2020 [68] grants RECs the refund of certain grid components of electricity tariff amounting to approximately 8 €/MWh (10 €/MWh for self-consumption schemes) in relation to the energy produced by the plant owned by the RECs and consumed in the same time frame by its members. In addition, the incentive (feed-in premium) identified by the Ministerial Decree of September 16^{th} 2020 [69] corresponds to 100 €/MWh for energy shared by participants in self-consumption schemes collective, and 110 €/MWh for energy shared by members of RECs. Recently, on 24^{th} January 2024, the decree of Ministry for the Environment and Energy Security promoting the development of REC and widespread self-consumption in Italy has been published and

came into full effect, having been previously approved by the European Commission [70]. The text identifies two ways to promote the development of RECs in the country: a contribution of up to 40% of eligible costs, for communities whose plants are built in municipalities with less than 5000 inhabitants, which will support the development of 2 GW in total, and an incentive tariff on renewable energy produced and shared throughout the country. The two incentives are cumulative. Through the measure, the development of a total of 5 GW of renewable energy production plants is thus supported. Moreover, the decree determines that the feed-in tariff to be applied to shared energy should not exceed:

- 120 €/MWh for plants with installed power lower than 200 kW,
- 110 €/MWh for plants with installed power within 200 kW and 600 kW,
- 100 €/MWh for plants with installed power greater than 600 kW.

1.4.3 Rules for optimal scheduling of communities

In this context of shared energy promotion, the optimal scheduling of the community energy resources by a specifically developed EMS is important. Distributed approaches may be preferred with respect to centralized ones, as they have less communication requirements and better guarantee prosumers' independence [71] [72].

The microgrid structure allows prosumers to coordinate their internal resources, as PV and BESS units, to match local load demand and to reach reliability and economic goals. Moreover, grid-connected microgrids can support the external grid by providing ancillary services, such as frequency control, voltage control and load curtailment operation [73] [74]. In the procedures presented in the literature, multi-microgrid energy management strategies are often based on hierarchical and distributed approaches [75] [76], which usually consist of multiple optimization stages. Bi-level optimal procedures are proposed in e.g. [77] for systems of microgrids integrated in the distribution network: in one level, daily costs [78] or profits of distribution network company [79] are optimized, while the second level optimizes the microgrid costs. A data-driven multi-agent deep reinforcement learning approach is investigated in [80] to calculate the Stackelberg equilibrium for the bi-level optimization

problem. The integration of EV charging stations in DC microgrids [81] can be addressed by, e.g., hierarchical distributed procedures, where they are modeled as independent players [82], or by multi-agent deep reinforcement learning methods [83] with the aim of minimizing total costs. The presence of BESS and PV units in the microgrids leads to a better performance in terms of cost reduction, particularly when V2G is exploited [84] [85].

The LEC framework that optimally exploits PV and BESS units, represents a promising solution for EV integration [86]. The integration of intermittent energy resources in microgrids [87], as wind and PV generation, as well as the integration of EVs, implies the need to address the management of the associated uncertainties. Therefore, in optimal scheduling procedures, deterministic programming approaches, based on the assumption of perfect forecasts, are replaced by stochastic programming techniques [61]. Monte Carlo and stochastic scenario models are used in [88] to simulate RES generation, load and prices variations, and in [89] to account for driving behavior of EVs. Chance-constrained programming techniques, that imply a mathematical program model containing constraints to be satisfied with a suitable probability level, are used to account for uncertainties in renewable generation in a community integrated system, as in [90], and levels of energy outputs of a hybrid AC-DC microgrid [91]. Recurse optimization is adopted in [92] for a day-ahead multistage stochastic scheduling of a LEC that provides a multi-stage decision tree to a receding horizon intra-day optimization procedure. In [93] a scenario tree generation and fast forward scenario reduction is adopted to account for RES generation uncertainties in a 15-bus microgrid test system. Moreover, robust optimization is proposed in [94] for the optimal charging and frequency reserve scheduling of EVs and in [95] for the microgrid reserve scheduling considering uncertainties associated to load, price, and renewable production. Information gap decision theory is used for the representation of reserve probabilities in [96] and [97] in the presence of fluctuations in RES generation and electricity prices. For large-scale systems, distributionally robust optimization procedures are adopted to represent fluctuations of load demand and renewable generation, as in [98] and [99].

Regarding the type of systems under study, chance-constrained programming is implemented in small and medium systems, as microgrids or communities of microgrids, while

robust and distributionally robust optimal programming is implemented in larger networks, such as multiple-area grids. Most of procedures included in this comparative analysis do not significantly consider the role of EVs (as in [93], [96], and [97]) or only their charging processes are involved. Further exploitation of V2G functionalities is not investigated, with the exception of [95].

1.5 Description of Ph.D. activity

The activities carried out during Ph.D. period focus primarily on the achievements of CONNECT and PROGRESSUS project objectives, regarding the energy management strategies of EVSI in the framework of DC microgrid, starting from problem evaluation, leading to development and test into simulative environment and then to preliminary implementation into the physical system by means of interfaces with cloud-based software. Furthermore, preliminary analyses concerning decentralized power regulation approach is presented for converters operating in DC microgrids. The impact of V2G-enabled EVs integrated in distribution grids is also assessed by means of optimal procedures. In the same project context, the collaboration with University of Bologna (Italian cluster partner of the projects) aims at exploring the possibility of DC microgrids to cooperate in a LEC with the aim of achieving economic benefits.

In addition, studies carried out during a six-month research period at the School of Engineering of Cardiff University (UK), under the supervision of Prof. Liana Cipcigan, regard preliminary degradation of small-size battery tests under different temperature conditions, and environmental and economic impacts of BESS for EV charging.

Further activities involve performance analysis of a set of network development projects, including zonal market framework and load flow analysis, and a time-series hosting capacity assessment of maximum distributed resources production. Moreover, an ongoing research field is represented by the impact of fast-charge EV infrastructures in motorways on the transmission network scenarios, in collaboration with Terna S.p.A. (Italian transmission system operator).

Research results have been disseminated by means of journal and conference papers presented in Section 1.7, along with poster presentations at the attended Ph.D. Schools.

1.6 Contributions of the work and Thesis strucure

The thesis is focused at presenting the developed research activies concerning optimal programming strategies for EV integration in DC microgrids, taking into account the possibility of providing internal reserve to cope with uncertainties related to intermittent renewable generation and EV usage exploiting V2G features and BESS discharge, and to assess technical and economic benefits of aggregated DC microgrid systems in a LEC perspective by means a two-stage optimal procedure.

Environmental, economic and technical impacts of EVs and EV clusters integration into distribution networks are evaluated for different EV penetration levels on the grid and V2G exploitation condition to ensure grid support. Furthermore, multi-objective optimal procedure is exploited with the aim of studying EV-based DC microgrid integrated in MV grids, and derived economic benefits from the aggregation of microgrids in LEC.

The thesis is organized as follows.

- Chapter 2 focuses on the optimal energy management strategies for a DC-based EVSI, proposing deterministic and stochastic approaches with the aim of taking into account uncertainties related to renewable generation and EV usage pattern through the provision of proper reserve levels, while assessing the influence of economic and technical targets on the microgrid operation. Moreover, the impact of an additional fast-charging station on the systems is studied and the integration of procedure into a cloud-based platform for smart grid energy management is then described.

- A two-stage optimal procedure applied to a LEC including DC microgrids is proposed in Chapter 3, considering both deterministic and stochastic approaches for internal reserve provision in order to inspect further different asset exploitation in a coordinated community context. The study has been carried out within the collaboration of University of Bologna, in the framework of the PROGRESSUS project,

- Chapter 4 discusses about optimal procedures for EV charging infrastructure integration in distribution networks. In particular, environmental and economic impact of interaction between BESS and EV station on EV parking lots operation are studied considering different charging rates. This activity has been carried out with the cooperation of the School of Engineering of Cardiff University. Moreover, technical impacts of both EV stations and EV clusters integration in MV and LV grids at different penetration levels on daily operation are assessed through techno-economic optimization procedures from network operator viewpoint. Furthermore, the study is then expanded proposing an optimal procedure for the EV-based DC microgrids integration in the MV distribution network, investigating energy community perspectives.

- The main conclusions and perspectives for future works are drawn in the final chapter.

1.7 List of publications

During the three years, 4 articles have been published on international journals, and 10 articles published in international conference proceedings. They are listed as follows.

1.7.1 Journals

1. F. Marasciuolo, C. Orozco, M. Dicorato, A. Borghetti and G. Forte, "Chance - Constrained Calculation of the Reserve Service Provided by EV Charging Station Clusters in Energy Communities," in IEEE Transactions on Industry Applications, vol. 59, no. 4, pp. 4700-4709, July-Aug. 2023, doi: 10.1109/TIA.2023.3264965.

2. P. Montegiglio, G. Acciani, M. Dicorato, G. Forte and F. Marasciuolo, "A Decentralized Power and Bus Voltage Regulation Approach for DC Microgrids," in IEEE Transactions on Industry Applications, vol. 59, no. 4, pp. 4773-4785, July-Aug. 2023, doi: 10.1109/TIA.2023.3258422.

3. F. Marasciuolo, M. Dicorato, G. Tricarico, P. Montegiglio, G. Forte and M. Trovato, "The Influence of EV Usage Scenarios on DC Microgrid Techno-Economic Operation," in IEEE Transactions on Industry Applications, vol. 58, no. 3, pp. 3957-3966, May-June 2022, doi: 10.1109/TIA.2022.3159298.

4. M. Dicorato, G. Tricarico, G. Forte, and F. Marasciuolo, "Technical Indicators for the Comparison of Power Network Development in Scenario Evaluations," Energies, vol. 14, no. 14, p. 4179, Jul. 2021, doi: 10.3390/en14144179. [Online].

1.7.2 Conference proceedings

1. F. Marasciuolo, M. Dicorato and G. Forte, "A stochastic approach for power and reserve programming in EV-based DC microgrid," 2023 8th IEEE Workshop on the Electronic Grid (eGRID), Karlsruhe, Germany, 2023, pp. 1-6,
doi: 10.1109/eGrid58358.2023.10380867.

2. M. Dicorato, F. Marasciuolo and G. Forte, "Optimal Operation of a Semi-urban Network Integrating Electric Vehicles," 2023 AEIT International Annual Conference (AEIT), Rome, Italy, 2023, pp. 1-6,
   doi: 10.23919/AEIT60520.2023.10330332.

3. F. Marasciuolo, G. Forte and M. Dicorato, "Distribution network optimal operation with electric vehicles," 7th E-Mobility Power System Integration Symposium (EMOB 2023), Copenhagen, Denmark, 2023, pp. 169-175,
   doi: 10.1049/icp.2023.2700.

4. M. Dicorato, G. Forte, F. Marasciuolo, M. C. Cavarretta and D. De Michino, "Enabling optimal vehicle-to-grid operation in a DC microgrid," 2023 IEEE International Conference on Environment and Electrical Engineering and 2023 IEEE Industrial and Commercial Power Systems Europe (EEEIC / I&CPS Europe), Madrid, Spain, 2023, pp. 1-5, doi: 10.1109/EEEIC/ICPSEurope57605.2023.10194813.

5. G. Tricarico, F. Gonzalez-Longatt, F. Marasciuolo, O. Ishchenko, M. Dicorato and G. Forte, "A Time-series Hosting Capacity Assessment of the Maximum Distributed Energy Resource Production," 2023 EEEIC / I&CPS Europe, Madrid, Spain, 2023, pp. 1-6, doi: 10.1109/EEEIC/ICPSEurope57605.2023.10194869.

6. F. Marasciuolo, M. Dicorato, G. Forte and P. Montegiglio, "The influence of electric vehicle position on technical operation of a distribution grid," 2022 IEEE International Conference on Environment and Electrical Engineering and 2022 IEEE Industrial and Commercial Power Systems Europe (EEEIC / I&CPS Europe), Prague, Czech Republic, 2022, pp. 1-6,
   doi: 10.1109/EEEIC/ICPSEurope54979.2022.9854633.

7. F. Marasciuolo, M. Dicorato, G. Forte and P. Montegiglio, "Effect of V2G Technology Integration on MV Distribution Grids," 2022 IEEE 21st Mediterranean Electrotechnical Conference (MELECON), Palermo, Italy, 2022, pp. 366-371,
   doi: 10.1109/MELECON53508.2022.9842981.

8. P. Montegiglio, G. Acciani, M. Dicorato, G. Forte and F. Marasciuolo, ”A Decentralized Power Regulation Approach for DC Microgrids,” 2021 IEEE International Conference on Environment and Electrical Engineering and 2021 IEEE Industrial and Commercial Power Systems Europe (EEEIC / I&CPS Europe), Bari, Italy, 2021, pp. 1-6, doi: 10.1109/EEEIC/ICPSEurope51590.2021.9584653.

9. F. Marasciuolo, C. Orozco, M. Dicorato, A. Borghetti and G. Forte, ”Two-stage Scheduling of Electrical Vehicle Charging Station Clusters in a Community of DC Microgrids,” 2021 IEEE International Conference on Environment and Electrical Engineering and 2021 IEEE Industrial and Commercial Power Systems Europe (EEEIC / I&CPS Europe), Bari, Italy, 2021, pp. 1-6,
doi: 10.1109/EEEIC/ICPSEurope51590.2021.9584584.

10. M. Dicorato, G. Tricarico, F. Marasciuolo, G. Forte and M. Trovato, ”Performance analysis of EV stations optimal operation in DC microgrid configurations,” 2020 IEEE International Conference on Environment and Electrical Engineering and 2020 IEEE Industrial and Commercial Power Systems Europe (EEEIC / I&CPS Europe), Madrid, Spain, 2020, pp. 1-6,
doi: 10.1109/EEEIC/ICPSEurope49358.2020.9160758.

Chapter 2

Energy management of DC-based EVSI

The inclusion of EV stations in microgrids can allow to exploit source controllability to obtain a safer network integration and hence sustain electric mobility diffusion. The integration of PV systems and electric storage in DC microgrid can easily enable V2G functionality. This chapter describes the procedure adopted for the energy management of a DC-based EV charging infrastructures that involves PV generation, stationary storage and EV charging stations. The system is also the italian demonstrator for the European project PROGRESSUS, whose framework is proposed in Section 2.1. Then, a deterministic approach for optimal day-ahead procedure is introduced with its formulation, implementation to the system and result discussions in Section 2.2. In the same framework, a study focused on system price variation influence on V2G exploitation is presented and discussed in Section 2.3. The chance-constrained programming technique is then implemented in the optimal procedure in order to determine reserve levels provided by BESS to cope with uncertainties related to renewable generation and EV usage pattern, by defining probabilistic constraints and probability distribution functions. The effect of the inclusion of a fast charging station on the system operation is evaluated in Section 2.5 considering different scenario of PV availability. Furthermore, the problem is linearized by means of Big-M method and power loss evaluation is carried out in order to asses the influence of fast charging station

within the system.

The last Section 2.6 focuses on the description of a cloud-based platform for energy management of the system, based on signal exchanges between optimal set points (output of the procedures) and field devices. The Section provides also the discussion of tests of the real demonstrator carried out on the field.

2.1 PROGRESSUS Project and DC microgrid framework

The DC microgrid constitutes the Use Case of the projects CONNECT (from 2017 to 2020) and PROGRESSUS (from 2020 to 2023). In particular, PROGRESSUS is a project funded under the H2020-ECSEL-2019-2-RIA call, with 22 European partners from academia and industry. PROGRESSUS contributes to the European Union's 2030 climate targets by proposing a next-generation smart grid, as demonstrated by the application example "smart charging infrastructure" which integrates seamlessly into pre-existing concepts of smart-grid architectures while requiring minimal additional investment. Intelligent charge infrastructure design and establishment face unique issues due to the anticipated high power needs of ultra rapid charging stations. The efficient utilization of charging infrastructure is still in its infancy, much like the concepts of emission-free driving are still relatively new to the economy. The objectives of the PROGRESSUS project cover three main themes [100]:

- power conversion, whose objectives concern power converter design and implementation for DCcharging stations and ultra-fast charging towards the modularization of rapid chargers and various power converters;
- energy management in microgrids (charging infrastructure), to develop smart management algorithms that could lead to reduce the power losses, increase the efficiency. In particular, design optimal energy management algorithms for DC microgrids and low voltage DSO networks, by also taking into account EVs and EV charging stations;

- measurement, monitoring and communication infrastructure for the development of advanced current sensors, metrology and monitoring solutions as well as novel network management approaches to support secure management of decentralized infrastructure and services and to enable smart and secure energy management.

Furthermore, four use cases (UC) are implemented and demonstrated in PROGRESSUS project:

- UC 1 that combines solutions for highly efficient power conversion including storage, hardware security supporting blockchain, decentralized data management, distributed energy management to maximize grid utilization and efficient power line networks for high speed communication;
- UC 2 refers to the integration of various sub-systems, such as a protective interface between local grid and connected power processing converters, a cloud based smart charging framework, where different inputs can be used and where different algorithms can easily be applied and configured.
- UC 3 aims at demonstrating the effectiveness of a cooperative energy management scheme when applied to multiple self-organised microgrids, that allows to maximize the utilization of the energy generated by renewable sources, while minimizing the energy storage losses and the dependency on the main grid.
- UC 4 that focuses on the energy management strategies for a DC microgrid with the objectives of proving specific local services to the grid and promoting new infrastructures supporting electromobility and modular fast charging enabling long-distance drive with EVs.

The activities of the research group of the Politecnico di Bari, within the PROGRESSUS project, focus on the development of methodologies and algorithms for energy management in the DC microgrid (already being designed within the CONNECT project), for different control time intervals. In addition, activities aim at defining the regulation services to be provided to the electric distribution grid, in the presence of electric vehicle charging stations

in fast and conventional modes. In collaboration with Enel X Way, project partner for UC 4 realization, a further contribution consists in the modification of the demonstrator (of previous CONNECT Project at the port of Bari, see Fig. 2.1b) to integrate fast charging stations for electric vehicles into the DC microgrid, with related control and communication, and operational tests are devoted to the implementation of the developed optimal management strategies. The expected objectives aim at: i) 20% reduction in losses for internal power distribution in DC systems, compared to AC systems; ii) 10% reduction in grid exchange levels and voltage variations; iii) 10% increase in energy exchanges between DC microgrids, aiming at validating the applicability of the concept of energy communities based on modular DC microgrids. Therefore UC 4 provides a testbed for:

- the development of technologies for the integration of fast charging stations on a DC grid, in the presence of other components (photovoltaics, batteries, conventional charging stations);
- the definition of regulatory services to be provided to the distribution network to encourage active user participation in grid management;
- the synthesis of solutions for the implementation of energy communities based on modular microgrids integrating renewable sources and electric mobility systems.

(a) (b)

Figure 2.1: Bari Port location (a) and DC microgrid of UC 4 (b).

The DC microgrid structure consists of a photovoltaic plant (PV), located on the parking rooftop, a BESS, and a set of 5 charging stations that allow charging and V2G processes and a fast charging station. In Fig. 2.2 the layout of the structure is represented. All components

are connected to the DC bus through a DC/DC converter, in order to control the power exchange levels. The DC microgrid is connected to the distribution network through a bidirectional AC/DC converter, with an internal voltage control. The DC microgrid has been already field for sizing, planning and reliability studies. The inclusion of a cloud-based supervision system for energy management allows to control all the assets and to manage anomalies through remote connection.

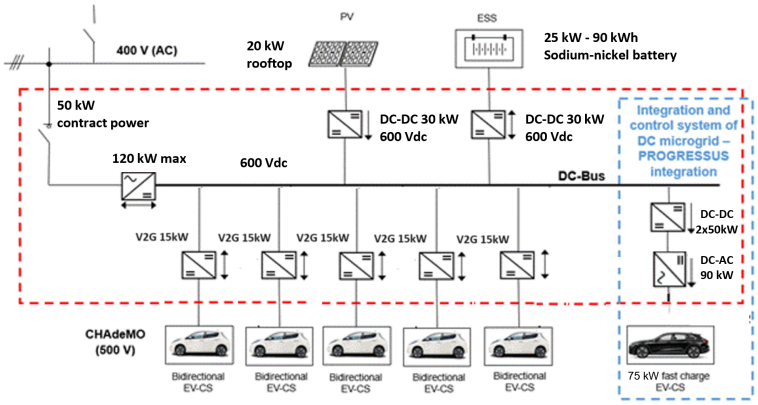

Figure 2.2: DC microgrid architecture.

2.2 Deterministic approach for day-ahead optimal operation

This section focuses on the performances of day-ahead optimal planning algorithms, proposing in order to manage the DC-based EVSI. The main contributions of this work are resumed in the following:

- a methodology for energy management of the system is proposed, aiming at minimizing total daily costs,
- additional optimization functions, targeting a technical goal, and successively a combined techno-economic goal are proposed,
- simulations involve different scenarios, generated through EV usage historical data

statistical analyses, which lay the basis for a stochastic approach to the day-ahead procedure, presented in the next sections.

A detailed description of the mathemathical formulation of the proposed methodology is reported in the following.

2.2.1 Mixed-integer linear programming for daily cost minimization

In order to carry out optimal operation planning of the system in the day-ahead time window, the set of EV should be defined along with relevant mobility usage pattern (represented by departure time, arrival time, route length, energy consumption), and the PV availability should be properly forecast. Therefore, a mixed integer linear programming problem should be solved as reported in (2.1):

$$\min_{\mathbf{x}} OF(\mathbf{x}) \quad s.t. \begin{cases} \mathbf{A} \cdot \mathbf{x} \leq \mathbf{b} \\ \mathbf{A_{eq}} \cdot \mathbf{x} = \mathbf{b_{eq}} \\ \mathbf{lb} \leq \mathbf{x} \leq \mathbf{ub} \end{cases} \tag{2.1}$$

where the state variable vector **x** includes, for each time step t of the daily time window, the following variables:

- Active power withdrawn from / delivered to the distribution network, named $P_g^{in}(t)$ and $P_g^{out}(t)$ respectively;
- Charge power, discharge power and State of Charge (SOC) of the BESS, named $P_B^c(t)$, $P_B^d(t)$ and $S_B(t)$ respectively;
- Charge power, discharge power and SOC of the j–th EV, named $P_{EV,j}^c(t)$, $P_{EV,j}^d(t)$ and $S_j(t)$ respectively;
- Integer variables for grid connection $v_g(t)$, for BESS $v_B(t)$, and for each j–th EV

$v_j(t)$, equal to 1 if the power exchange is towards the DC common bus and 0 otherwise.

In order to achieve optimized operation, a first formulation of the problem involves the minimization of the total cost of system operation, hence the objective function $OF1$ has the following form in (2.2):

$$\begin{aligned} OF1 =& \Delta t \cdot \sum_t \Bigg\{ c_g(t) \cdot P_g^{in}(t) - r_g(t) \cdot P_g^{out}(t) + w_B \cdot [P_B^c(t) + P_B^d(t)] + \\ &+ \sum_j [w_j + c_{EV}(t)] \cdot P_{EV,j}^c(t) + [w_j - r_g(t)] \cdot P_{EV,j}^d(t) \Bigg\} \end{aligned} \tag{2.2}$$

In particular, the first two terms represent the cost for energy exchange at grid connection point, where a tariff $c_g(t)$ is applied at power purchase, and a unit revenue $r_g(t)$ is linked to power delivery. The third term represents wearing cost of BESS, incurred during charge and discharge, and the last two terms represent cost for EV charge and revenue for EV discharge, considering the presence of an aggregator accounting for EV wearing cost w_j as well.

2.2.2 Problem constraints

The optimization problem is subject to a set of constraints (2.1) that account for component technical limitations and power balance. the active power balance at common DC busbar at timestep t is ensured by constraint (2.3),

$$\begin{aligned} &\alpha_g \cdot P_g^{in}(t) - \frac{1}{\alpha_g} \cdot P_g^{out}(t) + \alpha_B \cdot P_B^c(t) - \frac{1}{\alpha_B} \cdot P_B^d(t) + \\ &+ \sum_j \left[\alpha_j \cdot P_{EV,j}^c(t) - \frac{1}{\alpha_j} \cdot P_{EV,j}^d(t) \right] + \alpha_{PV} \cdot P_{PV}(t) = 0 \end{aligned} \tag{2.3}$$

where $P_{PV}(t)$ is PV production forecast and the coefficients α_x account for converter efficiencies and cable losses.

Moreover, SOC update for BESS and EVs ($S_B(t)$ and $S_j(t)$) is taken into account in

(2.4) and (2.5),

$$S_B(t) = S_B(t-1) + \Delta t \cdot \left[\eta_B^c \cdot P_B^c(t) - \left(\frac{1}{\eta_B^d}\right) \cdot P_B^d(t)\right] - sd_B \tag{2.4}$$

$$S_j(t) = S_j(t-1) + \Delta t \cdot \left[\eta_j^c \cdot P_{EV,j}^c(t) - \left(\frac{1}{\eta_j^d}\right) \cdot P_{EV,j}^d(t)\right] - sd_B - \Delta E_j^{tr}(t) \tag{2.5}$$

where η_B^c and η_j^c are charging efficiencies, while η_B^d and η_j^d are discharge at efficiencies. Furthermore, sd_B and sd_j account for self-discharge rate, whereas $\Delta E_j^{tr}(t)$ is the energy amount required to cover the distance of envisaged trips, different from zero only in traveling timesteps and estimated according to unit consumption depending on average speed. In constraints (2.6a) and (2.6b) the initial and final SOC levels $S_j(0)$ and $S_j(N_T)$ are kept at 90% of nominal storage capacity, whereas in each time interval the state of charge should be between 20% and 100% of capacity.

$$S_j(0) = 0.9 \cdot H_j \;\; \forall j \in [1, .., n_{EV}] \tag{2.6a}$$

$$S_j(N_T) = 0.9 \cdot H_j \;\; \forall j \in [1, .., n_{EV}] \tag{2.6b}$$

Inequality constraints (2.7) and (2.8) are set with the aim of avoiding contemporaneous bidirectional power exchange at grid connection,

$$P_g^{in}(t) \leq v_g(t) \cdot P_{g,MAX}^{in} \tag{2.7}$$

$$P_g^{out}(t) \leq \Big(1 - v_g(t)\Big) \cdot P_{g,MAX}^{out} \tag{2.8}$$

where $P_{g,MAX}^{in}$ and $P_{g,MAX}^{out}$ represent maximum levels of power withdrawal/delivery, respectively. Analogous relations can be written for BESS and EVs.

Furthermore, each state variable is limited by lower and upper bounds, as reported in (2.9a)-(2.9i).

$$P_g^{in,min} \leq P_g^{in}(t) \leq P_g^{in,MAX} \;\; \forall t \in [1, .., N_T] \tag{2.9a}$$

$$P_g^{out,min} \leq P_g^{out}(t) \leq P_g^{out,MAX} \;\; \forall t \in [1, .., N_T] \tag{2.9b}$$

$$P_B^{c,min} \leq P_B^c(t) \leq P_B^{c,MAX} \ \ \forall t \in [1,..,N_T] \tag{2.9c}$$

$$P_B^{d,min} \leq P_B^d(t) \leq P_B^{d,MAX} \ \ \forall t \in [1,..,N_T] \tag{2.9d}$$

$$S_B^{min} \leq S_B(t) \leq S_B^{MAX} \ \ \forall t \in [1,..,N_T] \tag{2.9e}$$

$$P_{EV,j}^{c,min} \leq P_{EV,j}^c(t) \leq P_{EV,j}^{c,MAX} \ \ \forall t \in [1,..,N_T], \forall j \in [1,..,n_{EV}] \tag{2.9f}$$

$$P_{EV,j}^{d,min} \leq P_{EV,j}^d(t) \leq P_{EV,j}^{d,MAX} \ \ \forall t \in [1,..,N_T], \forall j \in [1,..,n_{EV}] \tag{2.9g}$$

$$S_j^{min} \leq S_j(t) \leq S_j^{MAX} \ \ \forall t \in [1,..,N_T], \forall j \in [1,..,n_{EV}] \tag{2.9h}$$

$$0 \leq v_x(t) \leq 1 \ \ \forall t \in [1,..,N_T], \forall x \in [g,B,j] \tag{2.9i}$$

2.2.3 Technical target

In order to reduce impacts on the connected distribution network, a second objective is proposed to minimize power exchange levels at grid connection point. To this purpose, the objective function $OF2$ is defined in (2.10):

$$OF2 = \Delta t \cdot \sum_t [P_g^{in}(t) + P_g^{out}(t)] \tag{2.10}$$

Technical constraints (2.1) follow the aforementioned formulation. Furthermore, in order to avoid unnecessary oscillations in EV state of charge and to prevent excessive wearing when the objective is $OF2$, a proper limit on daily discharge should be considered in this case. In particular, the daily horizon the total energy discharged from EV battery over the daily horizon, including discharge when connected and the energy consumption for trips $\Delta E_j^{tr}(t)$, should not exceed a cycle of charge/discharge (2.11). This is related to EV battery energy capacity H_j by means of target depth-of-discharge d_j. The BESS relation (2.12) is formulated analogously, without energy consumption for travels. These relations are valid for a daily planning interval, where it is assumed that the state of charge at the end of the

horizon returns to defined target values.

$$\sum_t \left[\frac{1}{\eta_j^d} \cdot \Delta T \cdot P_{EV,j}^d(t) + \Delta E_j^{tr}(t) \right] \leq H_j \cdot d_j \tag{2.11}$$

$$\sum_t \left[\frac{1}{\eta_B^d} \cdot \Delta T \cdot P_B^d(t) \right] \leq H_B \cdot d_B \tag{2.12}$$

2.2.4 Economic target neglecting storage wearing costs

The application of penalties to EV and BESS wearing could hinder their exploitation in the procedure considering a plain economic target. Therefore, a third formulation of the problem, named $OF3$, is here considered, where the minimization of the total daily system operation cost does not take into account the wearing costs of the storage devices, as expressed in (2.13). This formulation is intended to inspect maximum technical exploitation of storage devices, removing the penalties in the economic optimization goal, giving out a techno-economic trade-off. For instance, in a framework where the EV aggregator is different from the EVSI owner, degradation costs of EVs could be neglected [101].

$$\begin{aligned} OF3 = &\Delta t \cdot \sum_t c_g(t) \cdot P_g^{in}(t) - r_g(t) \cdot P_g^{out}(t) + \\ &+ \sum_j c_{EV}(t) \cdot P_{EV,j}^c(t) - r_{EV}(t) \cdot P_{EV,j}^d(t) \end{aligned} \tag{2.13}$$

As already described in Section 2.2.3, constraints (2.11) and (2.12) are included in the general formulation of the procedure in order to avoid unnecessary oscillations in storage systems (BESS and EVs).

2.2.5 Probabilistic approach for EV usage pattern generation

Since input data of the optimization problem, the forecast PV production and EV usage information (e.g., departure and arrival times, route length and energy consumption) are affected by uncertainties, a probabilistic approach is exploited to address EV usage scenario generation: starting from historical data about the number of daily routes and length of routes for each EV over a year, probability distribution functions are estimated and vali-

dated, in order to randomly generate samples of EV usage. Three distributions are considered, Normal, Poisson and Weibull, whose probability density functions are expressed in (2.14)-(2.16):

$$f_N(x) = \frac{1}{\sigma \cdot \sqrt{2\pi}} \cdot e^{-\frac{(x-\mu)}{2\sigma^2}} \tag{2.14}$$

$$f_P(x) = \frac{\lambda}{x!} \cdot e^{-\lambda} \tag{2.15}$$

$$f_W(x) = \frac{k}{c} \cdot \left(\frac{x}{c}\right)^{k-1} \cdot e^{-\left(\frac{x}{c}\right)^k} \tag{2.16}$$

The estimation of the parameters (μ, σ, λ, k and c) for each distribution is carried out using the MATLAB Distribution Fitter tool, whose input and output are reported in the flowchart of Fig. 2.3 along with statistical analysis steps. The validation is therefore carried out through the χ^2 goodness-of-fit test. For the test computation, data are divided into m classes and χ^2 is calculated as in (2.17), where O_i and E_i are respectively the observed and expected frequency for each class. Given a significance level α, which defines a critical value CV for χ^2, the goodness of the theoretical probability function under test can be assumed if the inequality in (2.18) is verified. If condition (2.18) is true, the proposed distribution function (either f_N, f_P, or f_W) is acceptable, and it is defined as "not rejected" (NR). Otherwise, the function is "rejected" (R) since it does not properly fit experimental observations. The reader is referred to [102] for full description of the goodness-of-fit test.

$$\chi^2 = \sum_{i=1}^{m} \frac{(O_i - E_i)^2}{E_i} \tag{2.17}$$

$$\chi^2 < CV(\alpha) \tag{2.18}$$

2.2.6 Economic and technical indicators

A comparison among results, derived by applying separately each of the three objective functions, is carried out by means of economic and technical indicators with the aim of evaluating operation costs and technical performances of batteries. Concerning the economic indicator, the total operation cost is evaluated using (2.2), since it takes into account

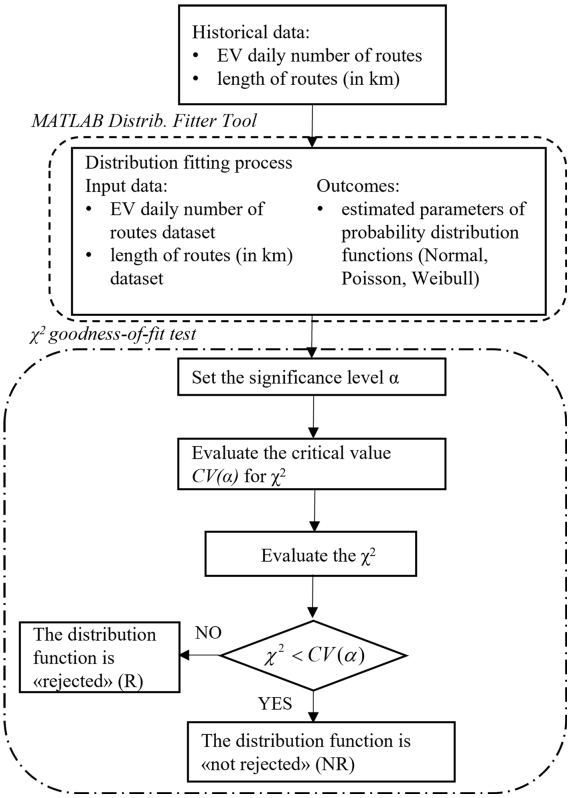

Figure 2.3: Flowchart of the statistical procedure applied to EV usage datasets.

wearing costs of batteries. Technical indicators are power peak values at grid connection, $P_g^{in}(t)$ and $P_g^{out}(t)$, easily evaluated finding the maximum value of the vectors, and the number of the discharge cycles of EV and BESS over the daily horizon calculated as in (2.19),

$$n_x^d = \sum_j \frac{S_j(t_{d,i}) - S_j(t_{d,f})}{\eta_x^d \cdot H_x} \tag{2.19}$$

where j is the generic interval when a discharge occurs, $t_{d,i}$ and $t_{d,f}$ are the initial and final time-step of the discharge process, η_x^d is the discharge efficiency of the storage system x, while H_x is the capacity of the battery. This expression is used for both EVs and BESS batteries.

2.2.7 Case study and EV usage pattern generation

The optimal procedures are implemented and tested in Matlab environment. Results are evaluated by means of the economic and technical indicators, taking as reference the pres-

ence of EV uncoordinated charge. The DC microgrid is expected to be realized for an EVSI framework. The basic layout [103] involves a 12.96 kW PV system, a 30 kW / 65.2 kWh BESS and five EV stations with maximum power exchange of 10 kW. The cost of electricity withdrawal from the grid $c_g(t)$ varies for hours and scenarios, in the range 0.14÷0.19 €/kWh, whereas unit revenue for electric energy delivery $r_g(t)$ is in the range 0.025÷0.055 €/kWh, according to data from ARERA [104]. EV charging cost $c_{EV}(t)$ is modeled considering a surplus to be added to $c_g(t)$, as well as $r_{EV}(t)$ considering a surplus on the $c_{EV}(t)$. Wearing costs associated to BESS and EV batteries are respectively fixed at 1.8 c€/kWh and 6.7 c€/kWh.

The expected application is represented by Bari Port Authority, where EV mobility data for service matters are assumed corresponding to current exploitation of 5 fuel-based service cars, replaced by a suitable EV model. Identifying the five vehicles as EV1-EV5, information is collected for a whole year of usage, then the probability distribution functions are estimated, following the procedure in Section 2.2.5. It should be remarked that travels mostly occur in between 07:00 and 20:00.

The following Figg. 2.4, 2.5 and 2.6 collect the inputs and outcomes of the Distribution Fitter Tool. In each figure, bar plot represents historical data and curves represent fitted distribution functions.

As represented in Fig. 2.4, EV1 and EV3 perform, on average, more than one travel per day. EV2 and EV5 more frequently accomplish one travel per day, while EV4 does not usually travel. In Table 2.1 the estimated parameters for the Normal and Poisson distributions are collected for each EV.

In Fig. 2.5 the distributions for the length of a single travel for each EV are reported in kilometers. EV1, EV2 and EV3 generally have short travels, with respect to EV4 and EV5. Merging the information of number of daily travels and length, it can be argued that EV1, EV2 and EV3 take several short travels a day (on average 10 km). The opposite situation regards EV4 and EV5, experiencing a lower number of travels with higher length (about 60-130 km) in comparison to the others. The estimated parameters for the variable related to the length of a single travel for each EV are reported in Table 2.2.

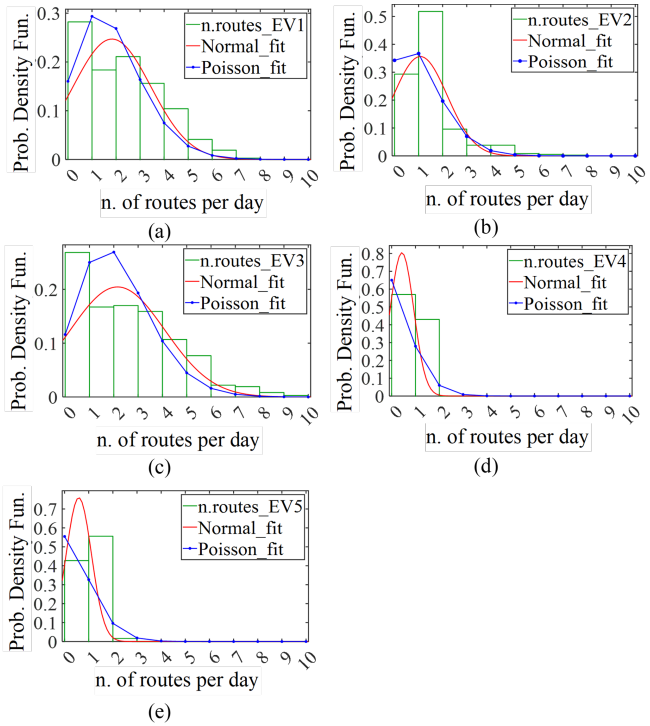

Figure 2.4: Probability distribution functions fitted from EVs number of routes data.

Table 2.1: Distribution fitting of the number of daily travels.

	Normal Distribution		Poisson Distribution	
	μ	σ	λ	cov
EV1	1.83	1.62	1.83	0.005
EV2	1.07	1.12	1.07	0.054
EV3	2.15	1.95	2.15	0.0059
EV4	0.43	0.25	0.43	0.0012
EV5	0.59	0.53	0.59	0.0016

Table 2.2: Distribution fitting of the length of single travels.

	D. Normal		D. Poisson		D. Weibull	
	μ	σ	λ	cov	k	c
EV1	9.62	14.48	9.62	0.014	9.79	1.03
EV2	29.76	35.98	29.76	0.076	27.17	0.85
EV3	8.94	14.29	8.94	0.014	9.09	1.03
EV4	120.1	23.34	120.2	0.765	128.0	6.96
EV5	58.46	81.54	60.14	0.2877	59.68	1.041

As can be inferred from the Figures, not all the analyzed distributions are acceptable, regards the goodness of fit. Concerning the length of single routes, it could be noted that

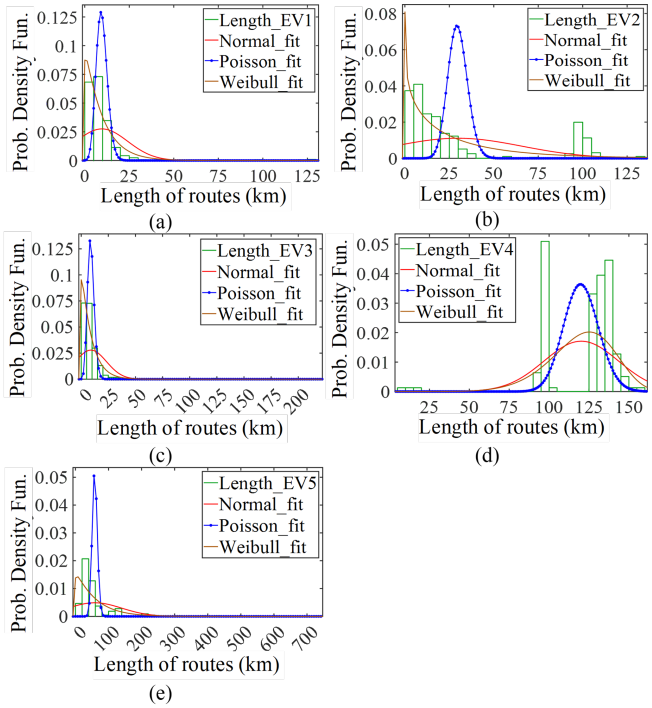

Figure 2.5: Probability distribution functions fitted from EVs' route length data.

the test also accepts Poisson distribution, but only for EV1, EV3 and EV5. The reason is related to the fact that both EV2 and EV4 show different behaviors during the observation period (one year): in the first half of the year, route length of both vehicles is quite short; on the contrary, in the second half, the frequency of longer routes increases. Considering the different behaviors, a distinction in categories could be carried out. Data of EV2 could be divided into two categories: routes with length shorter than 70 km, and routes with length longer than 70 km. For EV4, a division between routes longer/shorter than 110 km could be done. Distribution fitted are presented in Fig. 2.6.

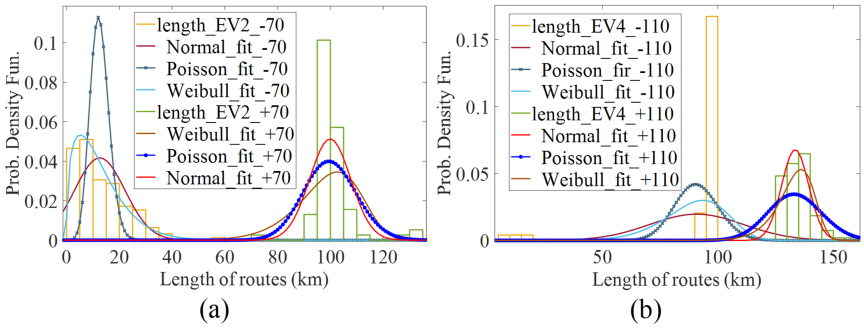

Figure 2.6: Probability distribution functions fitted from EV2 (a) and EV4 (b) route length data.

In MATLAB environment, the χ^2-test described in Section 2.2.5 is carried out through the *chi2gof* function, giving as an outcome indication of the distribution function condition, that can be rejected (R) or not rejected (NR). For the statistical analysis of number of routes, three significance levels α are set, in order to evaluate which distribution better fits data. In Table 2.3 the results of the tests are shown. The Normal distribution is always rejected, for all the EVs, while Poisson distribution is not rejected, only for the routes of EV1 (when α is lower than 20%), EV3 (when α is 0.5%), EV4 (for all values of α) and EV5 (when α is lower than 20%). Therefore, it can be affirmed that the best distribution fitting is obtained with data from EV4, with a good fitting for EV1 and EV5 as well. The variable related to EV2 cannot be fitted neither with a Normal nor a Poisson distribution.

As regards the route length, the results of the χ^2-goodness of fit test are shown in Table 2.4. The results refer to a value of α equal to 5%. As it can be observed, the Normal and Weibull distributions do not fit data of all EVs, in contrast to the Poisson distribution, that fits data from EV1, EV3 and EV5. Since EV2 and EV4 data never fit a distribution, the test is carried out also for the divided data groups pointed out in Fig. 2.6. Table 2.5 gathers the results. It can be seen that with this assumption the Poisson distribution fit is always rejected, whereas a Weibull distribution fits data of EV2 route length shorter than 70 km, and a Normal Distribution fit is good for EV4 route length longer than 110 km. According to the statistical analysis outcome, the random generation of the routes of vehicles is carried out in the following by considering for each EV the not rejected distribution and extending the use of Poisson distribution where all the hypotheses are rejected.

Table 2.3: χ^2-test results for number of routes.

	$\alpha = 0.5\%$		$\alpha = 5\%$		$\alpha = 20\%$	
	Normal	**Poisson**	**Normal**	**Poisson**	**Normal**	**Poisson**
routes EV1	*R*	*NR*	*R*	*NR*	*R*	*R*
routes EV2	*R*	*R*	*R*	*R*	*R*	*R*
routes EV3	*R*	*NR*	*R*	*R*	*R*	*R*
routes EV4	*R*	*NR*	*R*	*NR*	*R*	*R*
routes EV5	*R*	*NR*	*R*	*NR*	*R*	*R*

Regarding input data of the problem, the daily horizon is split into 15 minutes intervals, according to available data for PV production and in order to catch short travel time of EVs.

Table 2.4: χ^2-test results for length of routes ($\alpha = 5\%$).

	Normal	**Poisson**	**Weibull**
length EV1	*R*	*NR*	*R*
length EV2	*R*	*R*	*R*
length EV3	*R*	*NR*	*R*
length EV4	*R*	*R*	*R*
length EV5	*R*	*NR*	*R*

Table 2.5: χ^2-test results for length of routes EV2 and EV4 ($\alpha = 5\%$).

	Normal	**Poisson**	**Weibull**
length EV2>70	*R*	*R*	*R*
length EV2<70	*R*	*R*	*NR*
length EV4>110	*NR*	*R*	*R*
length EV4<110	*R*	*R*	*R*

In Fig. 2.7, two scenarios for EV exploitation are shown, where plug-in times are reported. For each vehicle, the number of routes and the route length are randomly chosen from the probability distribution functions. In the first scenario, analogous to the one analyzed in [105], all the vehicles except EV4 take at least one route, with maximum duration 30 minutes. In the second scenario, both EV4 and EV5 take longer routes (maximum duration is 2 hours), while EV2 is not exploited for mobility. These scenarios are quite different one from the other, in order to evaluate the influence of EV plug-in times on their exploitation within the microgrid. An auxiliary routine is developed to determine the route lengths and the relevant amount of energy needed for each travel for each EV, equipped with 30-kWh capacity. Moreover, two different PV production curves are estimated, representing summer and winter PV availability. For the purpose of the study, PV production and EV usage scenarios are combined, simulating a total of 4 typical days. Two of the 5 Configurations already introduced in [105] are studied for each day and for the 3 optimization problems. In particular, the Configuration 1 represents the complete outline, while the Configuration 5 represent the EVs uncoordinated charge case.

2.2.8 Results of the deterministic procedure

In this section the simulation results are shown and divided into two main groups: the results referring to the summer day and the ones relating to the winter day. The application

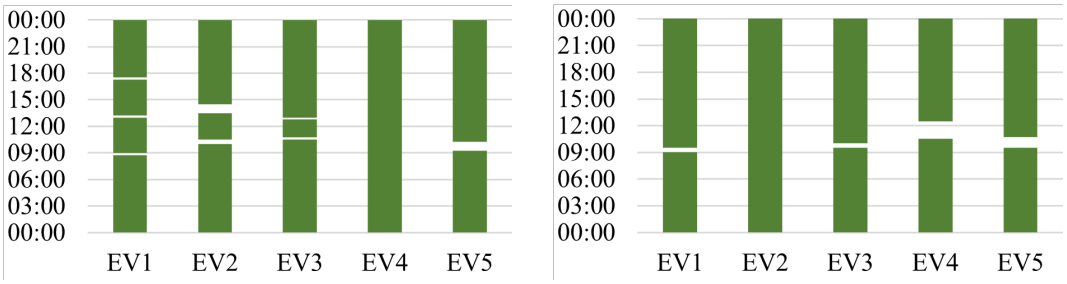

Figure 2.7: EV plug-in times in Scenario 1 (a) and Scenario 2 (b).

of OF3 to the DC microgrid (Configuration 1), considering a clear-sky summer day under EV Scenario 1, leads to power exchanges during the daily horizon shown in Fig. 2.9a. With respect to the application of OF1 in the same conditions reported in Fig. 2.8, the discharges of EVs during the day are more frequent, due to the absence of wearing costs linked to EVs and BESS. Moreover, from 00:00 to 02:00 power exchanges among the vehicles (V2V) are present, while in the time interval between 08:30-08:45 EVs discharge, added to the PV production, is delivered to the grid (V2G). Furthermore, PV availability is mostly used to charge the vehicles. The BESS also exploits discharging (after 04:00 and 13:00) and charging processes.

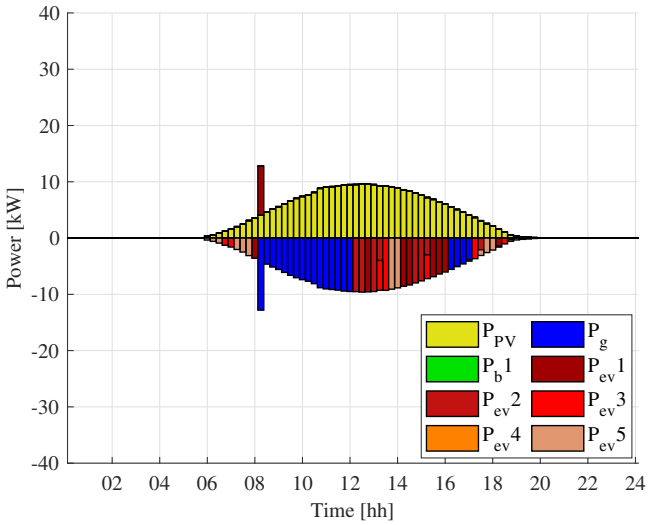

Figure 2.8: Application of OF1 to Configuration 1 in a summer day, considering EV Scenario 1.

The evolution of SOC for EVs and BESS is reported in Fig. 2.9b. The BESS is dis-

charged down to 48% from 04:00 to 05:00 to charge mostly EV4. Moreover, both EV1 and EV2 have SOC values often greater than 70%, due to frequent though short routes during the day.

In case of considering the application of EV Scenario 2, with less intense use of EVs, results of OF1 are reported in Fig. 2.10a, where a longer V2G session is pointed out from 08:15 to 08:45. Moreover, the availability of PV guarantees the charge of EVs and the selling to the grid. No grid power purchase is observed, and the BESS is not called to exchange power, due to the presence of wearing costs. Results of OF2 application are reported in Fig. 2.10b. With respect to OF1, a more distributed exploitation of EVs and BESS is observed. The absence of economic targets frees out the power exchanges, especially in the interval 01:00-03:00, when some V2V and V2G exchanges are observed, in addition to power exchanges among EVs and BESS. This behavior is frequent even during the daylight hours when the PV is available. No grid purchases from the external grid are spotted.

In Fig. 2.11 the power balance and SOC trends are reported, applying OF3 to Configuration 1 and the EV usage Scenario 2. The reduced mobility of EVs does not affect consistently the power exchanges profile (quite similar to the previous case), but a more intense V2G exploitation is observed in the time interval 08:00-10:00. As a matter of fact, at 08:00 all EVs discharge at maximum power (10 kW) to sell power to the grid and also to charge the BESS. Furthermore, the intense use of EV4 and EV5, because of their long routes, is marked by the SOC level under the 50%. For this reason, most of the PV power production is dedicated to the charge of these two EVs, until they are fully charged (from 15:00 to 18:00). During a winter day, the reduced PV availability affects the operation of the DC microgrid. The peak of PV production is nearly 6 kW, with 28.4 kWh daily generation that cannot provide the EVs power requests, so it is necessary for the system to purchase energy from the distribution grid, in order to charge the EVs before their departures (Fig. 2.12) and after their arrivals. Considering the application of the technical target OF2, power purchases are distributed during the time interval 05:00-18:00 (Fig. 2.12b). The general behavior does not change, with respect to the previous case. The application of OF3 (Fig. 2.12c) leads to a different conduct of the system, due to the presence of only techni-

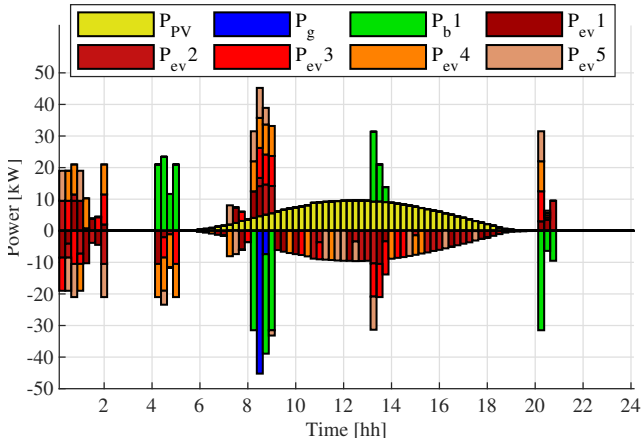

(a)

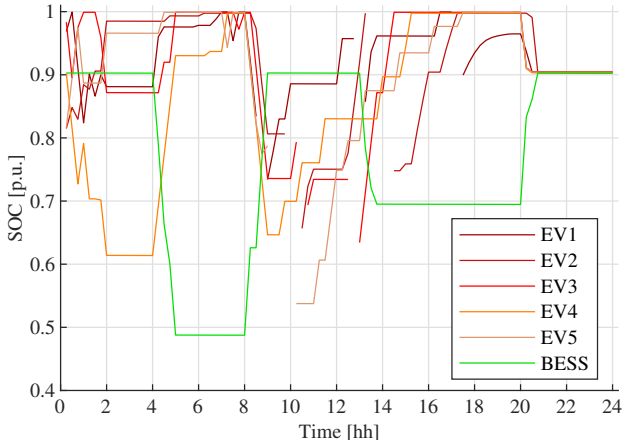

(b)

Figure 2.9: Application of OF3 to Configuration 1 in a summer day, considering EV Scenario 1. Power exchanges (a) and trends of EVs and BESS state of charge (b).

cal constraints on BESS discharge. In particular, from 00:00 to 03:00 EVs exchange small power quantities among them. In interval 05:00-06:00 the microgrid purchases energy from the external grid and all the PV power is dedicated to charge EVs. Other V2V processes can be noted before 20:00. In the winter day, no BESS exploitation is detected in Scenario 1. This is ascribable to the lack of excess PV power able to charge battery, and to higher wearing costs of BESS with respect to EV ones. Furthermore, EVs never operate in V2G mode, regardless of the considered target. Considering the EV Scenario 2, a quite similar operation can be seen in OF1 and OF2. In Fig. 2.12d the application of OF3 is represented. Differently from the Scenario 1, a small operation of BESS is detected in order to sustain intense EV charge. Subsequently, after 19:00, BESS is recharged by EV2 and EV5.

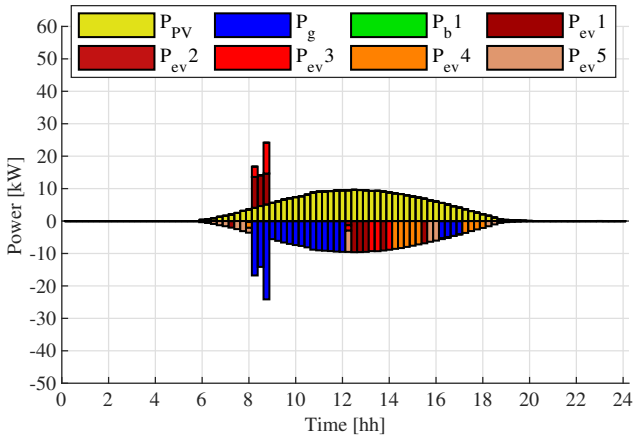

(a)

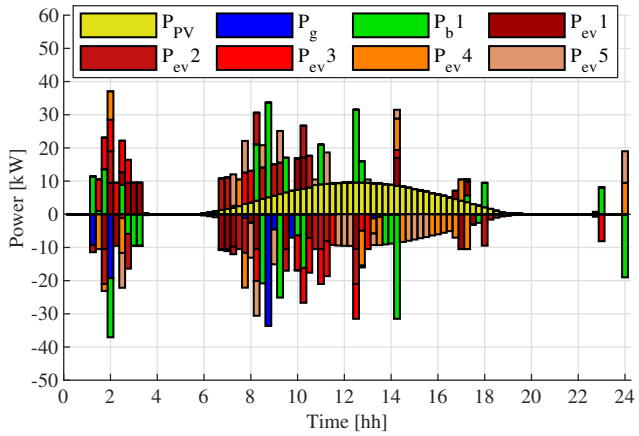

(b)

Figure 2.10: Application of OF1 (a) and OF2 (b) to Configuration 1 in a summer day, considering EV Scenario 2. Power exchanges.

2.2.9 Indicator evaluations

Total daily costs for both summer and winter days are reported in Table 2.6. It can be observed that the application of OF3 in summer day leads to lower economic efforts than OF2 and slightly higher than OF1. In the winter day the application of OF3 implies the highest costs, while the OF2 is the most convenient. The reason is that the application of OF3 leads to numerous power exchanges among EVs, affecting the total cost. The reduced EV mobility considered in the Scenario 2 leads to lower daily costs, and to a bigger saving, in comparison to the uncontrolled charging (Configuration 5): the registered saving is about 57% in summer day, and 38% during winter day.

The peak values of power exchange with the grid for both summer and winter days, referring

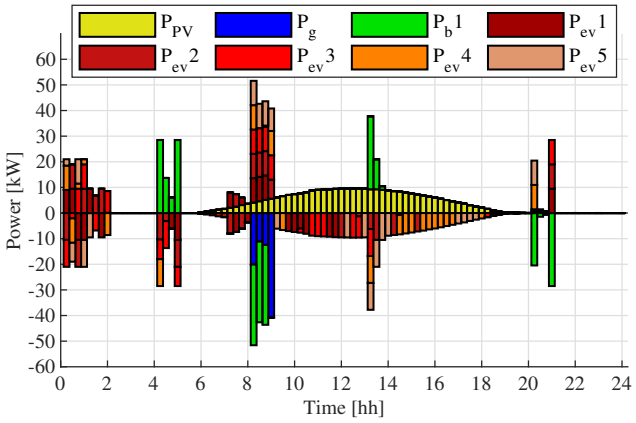

(a)

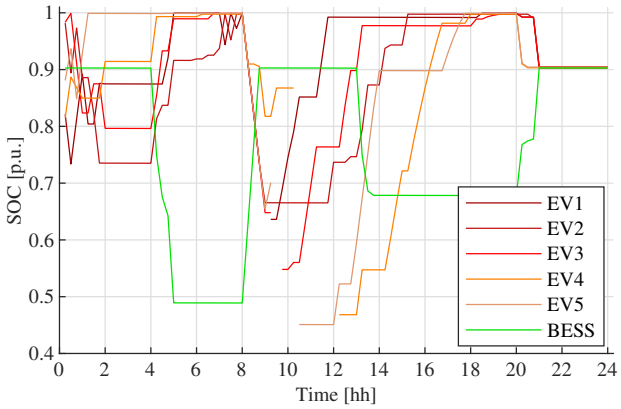

(b)

Figure 2.11: Application of OF3 to Configuration 1 in a summer day, considering EV Scenario 2. Power exchanges (a) and trends of EVs and BESS state of charge (b).

to the EV Scenario 1, are reported in Table 2.7. As expected, the lower peaks (10.57 kW sold in summer and 11.94 kW purchased in winter) are registered when OF2 is simulated. The peak power demand in Configuration 5 (uncontrollable EV charge) is lower than the one from Configuration 1, in winter day. However, the total daily costs is higher, confirming that the Configuration 5 is not optimized. Furthermore, for each day and configuration, it is observed that the targets of objective functions imply that grid power exchanges are oriented in only one direction, as reported in previous figures. In the presence of excess energy production, power exchange flows only from microgrid to the distribution grid (and the power P_g^{out} is always null, see in Table 2.7 summer day in Configuration 1), otherwise power is only withdrawn from the external grid (while P_g^{in} is always null).

In Table 2.8, the number of daily equivalent cycles for EVs and BESS in Configuration 1 is

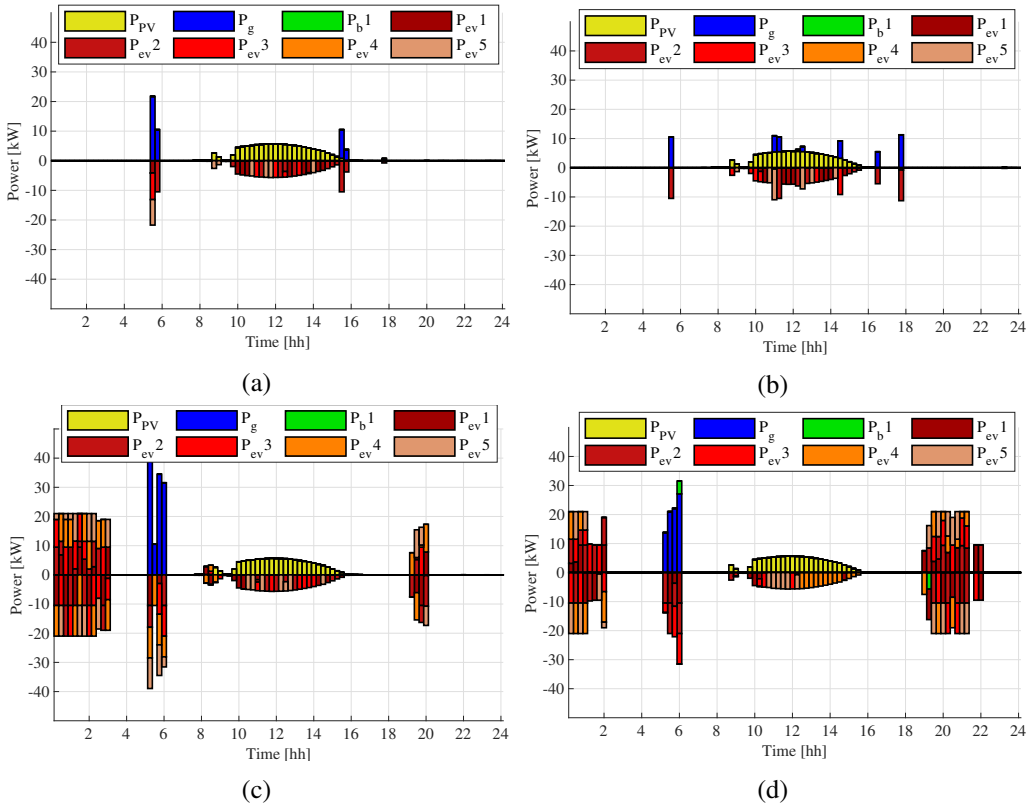

Figure 2.12: Application of OF1 (a), OF2 (b) to Configuration 1 in a winter day, considering EV Scenario 1, and OF3 to Configuration 1 in a winter day, considering EV Scenario 1 (c) and 2 (d). Power exchanges.

reported for the three objective functions in summer and winter days, for both EV Scenarios. For what concerns the summer day of the Scenario 1 of EVs, discharge due to mobility – a parameter for the optimization problem – is roughly 50% for EV2, and less for the other vehicles. The results of OF2 and OF3 show that all EVs experience nearly 1 full equivalent discharge cycle, considering the sum of mobility and additional discharging (EV4 with OF3 is exploited at 99% in Scenario 1). BESS experiences a full discharge cycle when OF2 is simulated. A completely different situation (no exploitation) is revealed in winter day. From the application of OF1 and OF2, EVs do not experience additional discharges, while BESS never operates. The application of OF3 implies additional discharges for vehicles. As a matter of fact, in Scenario 1, EV5 is exploited at 92% (the sum of 32% from mobility and 60% from additional discharging), while other EVs at nearly 80%. Regarding the EV Scenario 2, the EV4 usage affects its exploitation in V2G mode: the vehicle amount of further discharge is about 36% in summer, and 25% during the winter day (considering objective

function OF3). Moreover, EV2 discharges reach the 99% of a full discharge equivalent cycle (considering both OF2 and OF3 in summer), as well as BESS, that gets to the maximum number of equivalent discharge cycles, only minimizing the technical objective function (OF2). During winter, optimizing with OF3 leads to a reduced exploitation of BESS (3% of equivalent discharge cycle), and to an intense use of EVs, except for EV4.

Table 2.6: Total daily cost [€].

		EV Scenario 1			**EV Scenario 2**		
		OF1	**OF2**	**OF3**	**OF1**	**OF2**	**OF3**
Summer	Config. 1	8.65	12.07	10.70	5.41	8.89	7.49
	Config. 5	18.30	18.30	18.30	12.45	12.45	12.45
Winter	Config. 1	13.04	11.03	16.25	8.49	8.23	12.07
	Config. 5	17.81	17.81	17.81	13.22	13.22	13.22

Table 2.7: Grid power exchange peak value [kW] in Scenario 1.

		OF1		**OF2**		**OF3**	
		P_g^{in}	P_g^{out}	P_g^{in}	P_g^{out}	P_g^{in}	P_g^{out}
Summer	Config. 1	0	12.14	0	10.57	0	42.87
	Config. 5	20.00	0	20.00	0	20.00	0
Winter	Config. 1	23.00	0	11.94	0	41.22	0
	Config. 5	20.00	0	20.00	0	20.00	0

2.3 Influence of price variations on V2G exploitation

It could be pointed out that, although electricity pricing has been investigated in different aspects of EV integration even including PV systems, the effect of different buying/selling prices is seldom analyzed along with bidirectional energy exchange with EVs. In addition, aspects concerning the interactions in microgrid energy management procedures between energy pricing schemes and wearing costs of energy storage and EVs need to be investigated in order to individuate the most suitable strategies.

In this section, the day-ahead energy management of the DC-based EVSI proposed in Section 2.2.1 is carried out, considering different scenarios based on a set of structural, operating, and economic conditions. The layout of the DC-based EVSI differs only for BESS size, considered in these analyses with 15 kW maximum charging/discharging power and

Table 2.8: EV and BESS equivalent discharge cycles in Configuration 1, for both Summer and WInter days, for all EV scenarios.

	SUMMER							
	EV Scenario 1				EV Scenario 2			
	Mobility	OF1	OF2	OF3	Mobility	OF1	OF2	OF3
EV1	0.38	0.10	0.62	0.56	0.13	0.33	0.85	0.73
EV2	0.50	0	0.50	0.38	0	0	0.99	0.99
EV3	0.25	0	0.66	0.72	0.13	0.15	0.85	0.78
EV4	0	0	0.91	0.99	0.50	0	0.49	0.36
EV5	0.32	0	0.58	0.56	0.31	0	0.63	0.65
BESS	—	0	1.00	0.80	—	0	1.0	0.82
	WINTER							
	EV Scenario 1				EV Scenario 2			
	Mobility	OF1	OF2	OF3	Mobility	OF1	OF2	OF3
EV1	0.38	0	0	0.47	0.13	0	0	0.84
EV2	0.50	0	0	0.30	0	0	0	0.90
EV3	0.25	0	0	0.62	0.13	0	0	0.87
EV4	0	0	0	0.88	0.50	0	0	0.25
EV5	0.32	0	0	0.60	0.31	0	0	0.69
BESS	—	0	0	0	—	0	0	0.03

30 kWh capacity. This approach aims at investigating how the system deals with different scenarios, in terms of exchanged power within the microgrid and with the distribution grid, in order to point out possible influences on microgrid day-ahead operation planning of autonomous management strategies (e.g. devices under maintenance, availability of higher energy levels). Moreover, the presence of different price schemes, related to actual energy market and tariff behaviour, can reflect the possibility to promote energy service provision by microgrid involving V2G technologies. The consideration of a real-sized installation allows to inspect possible applications to single users in the framework of energy communities.

2.3.1 Definition of scenarios

The definition of scenarios involves the combination of structural and operating conditions, defined in the following:

- Structural condition regards the inclusion or the exclusion of BESS with the aim of investigating its influence within the microgrid, affecting the investment decision or

the maintenance plans,

- operation conditions, regarding initial and final SOC (at 00:00 and 24:00) of BESS - whenever present - that are set to 10 kWh, which means that BESS is discharged at the beginning and at the end of the simulation time window (roughly 0.26 p.u.). Differently, EV initial and final SOC are set to 27 kWh (at 0.9 p.u.) in order to be ready for possible mobility needs.

As previously reported in Section 2.2.8, where BESS is charged to 0.9 p.u. at the beginning of the simulation, its exploitation is not significant with respect to the other components (as EV charging stations). Therefore, the analyses are aimed at fostering a different exploitation of BESS.

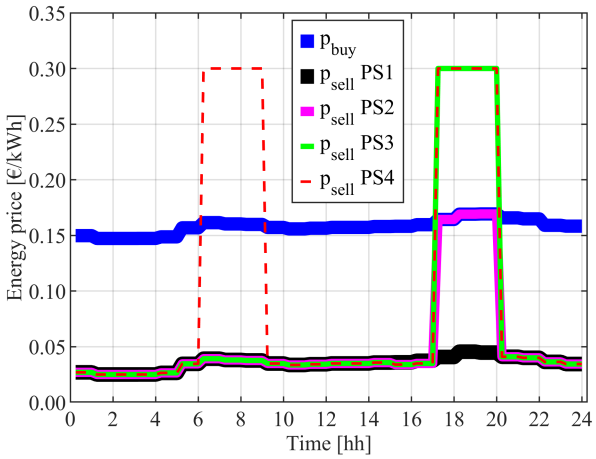

Figure 2.13: Adopted price schemes.

The microgrid is simulated also considering different price schemes, where buying price profile is the same for all schemes and selling price is properly modified. In Fig. 2.13 all price schemes are reported. The blue line represents buying price profile. Price scheme 1 (PS1) includes and . In Price Scheme 2 (PS2) selling price profile is modified introducing a spike variation during the interval 17:00-20:00, with a peak equal to the buying prices in that time interval, while in Price Scheme 3 (PS3) the peak is increased to 0.30 €/kWh with the aim of stressing the system to sell energy to the grid. Moreover, a fourth price scheme scenario (Price Scheme 4 – PS4) is studied, adding a second spike variation of 0.30 €/kWh

in selling price profile. The additional peak is set in the interval 07:00-10:00, with the same duration of 3 hours of the second one. Furthermore, EV battery wearing costs is set to 0.033 €/kWh while 0.03 €/kWh for BESS, in line with moderate depth-of-discharge estimation in [106], in order to catch technology evolution and to avoid the possible hindering of V2G functionalities. EV usage pattern is the one shown in Fig. 2.7a.

Eight simulation scenarios are divided into two sets A and B. Scenarios A do not involve BESS in the operation scheduling, while scenarios B include BESS optimal operation. Table 2.9 synthetizes scenario characteristics. Relevant simulation outcomes are compared with reference scenario (presence of BESS with high initial SOC and Price Scheme PS1) in terms of total daily cost (i.e. the value of objective function (2.2)) and equivalent cycle number, as defined in (2.19).

Table 2.9: Scenario definition

Scenario	Operating Conditions	
	BESS	Price Scheme
A.1	NO	PS1
A.2	NO	PS2
A.3	NO	PS3
A.4	NO	PS4
B.1	YES	PS1
B.2	YES	PS2
B.3	YES	PS3
B.4	YES	PS4

2.3.2 Results and indicators

Fig. 2.14 shows power exchanges within the system and SOC levels of EV batteries in Scenario A.1. Solar generation is used to charge EVs when they need, while the excess is sold to the utility grid when selling price is convenient. No V2G exploitation is detected in this scenario.

Introducing a spike price variation in Scenario A.2, power exchanges are reported in Fig. 2.15a, while SOC levels in Fig. 2.15b. It can be seen that the system reacts with EV discharge at maximum rate (10 kW) in order to take economic advantage by selling the

maximum amount of power to the grid. Since the price variation occurs in the evening when all EVs are connected to the microgrid, the required EV SOC level at the end of the day – to cover the energy needs of next journeys – is reached because EVs are charged during the day by PV. Same consideration could be made for Scenario A.3, whose results are not showed for purpose of brevity. Results for Scenario A.4 are reported in Fig. 2.16. The additional spike price during the morning hours implies an additional discharge of EVs from 06:00 to 07:15. In order to deal with energy required by EVs for mobility, charging processes occur from 02:00 to 03:30.

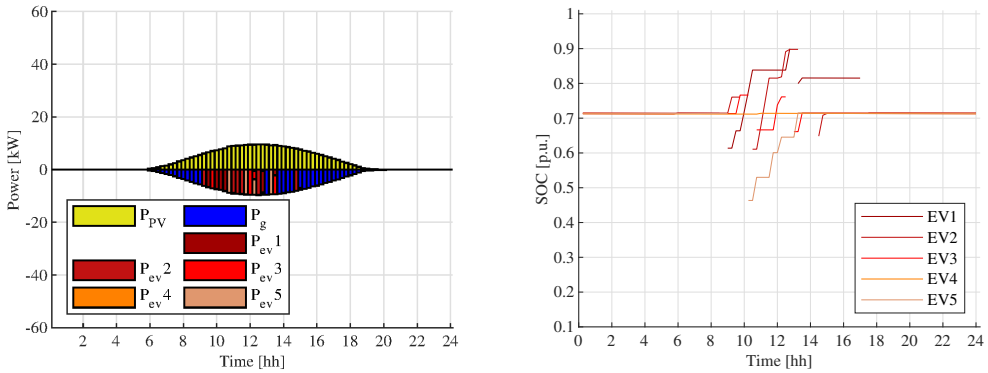

(a) (b)

Figure 2.14: Scenario A.1. Power exchanges (a) and EV SOC levels (b).

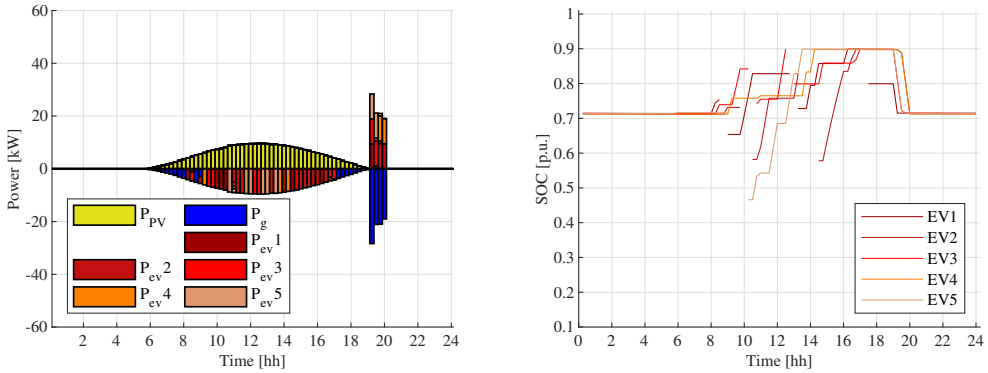

(a) (b)

Figure 2.15: Scenario A.2. Power exchanges (a) and EV SOC levels (b).

Considering the inclusion of BESS system in the optimal operation strategies, in Scenario B.1 (i.e. with the same price scheme PS1), power exchanges and SOC levels are similar to ones presented in Scenario A.1, since BESS wearing costs hinder its possible

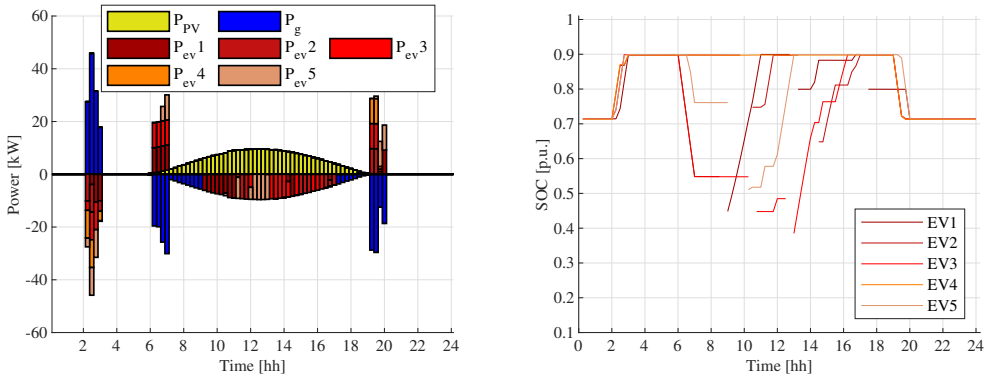

(a) (b)

Figure 2.16: Scenario A.4. Power exchanges (a) and EV SOC levels (b).

exploitation. In Scenario B.2 BESS is called to participate in selling energy, discharging together with EVs during the interval when the spike price occurs, as in Fig. 2.17a. Since initial SOC level of BESS is 0.26 p.u., it is charged by PV production (from 06:00 and 15:00) before its discharge. In Scenario B.3, a more intense use of EVs is seen and BESS discharging is anticipated with respect to Scenario B.2 (Fig. 2.17b). V2G exploitation for EVs is consistent, while EV charge occurs at 02:00, purchasing energy from the distribution grid because of its advantageous buying price. With the second price spike in Scenario B.4 (Fig. 2.17c) BESS and EVs take economic advantage in discharging in the morning and in the evening, after an intense charging that takes place from 02:00 to nearly 03:30.

Fig. 2.18 collects BESS SOC levels in the Scenarios B. BESS exploitation in Scenarios B.2 and B.3 is similar, in terms of energy, however charging and discharging in B.3 are anticipated with respect to B.2 due to the further exploitation of EV discharge. Furthermore, two events of almost full charging and discharging are detected for Scenario B.4.

Daily costs for all scenarios evaluated as in (2.2) are reported in Table 2.10. It can be seen that Scenarios A.1 and B.1 leads to the same daily cost, as BESS operation is not consistent. The assumptions of different price schemes imply lower daily costs, as expected for cost minimization procedure. Scenario B.4 reaches a daily microgrid cost near to 0 € exploiting the spike of selling price.

The number of equivalent discharge cycles for EVs and BESS is reported in Table 2.11. For EVs, the evaluation of this indicator does not include the discharge related to mobility. It

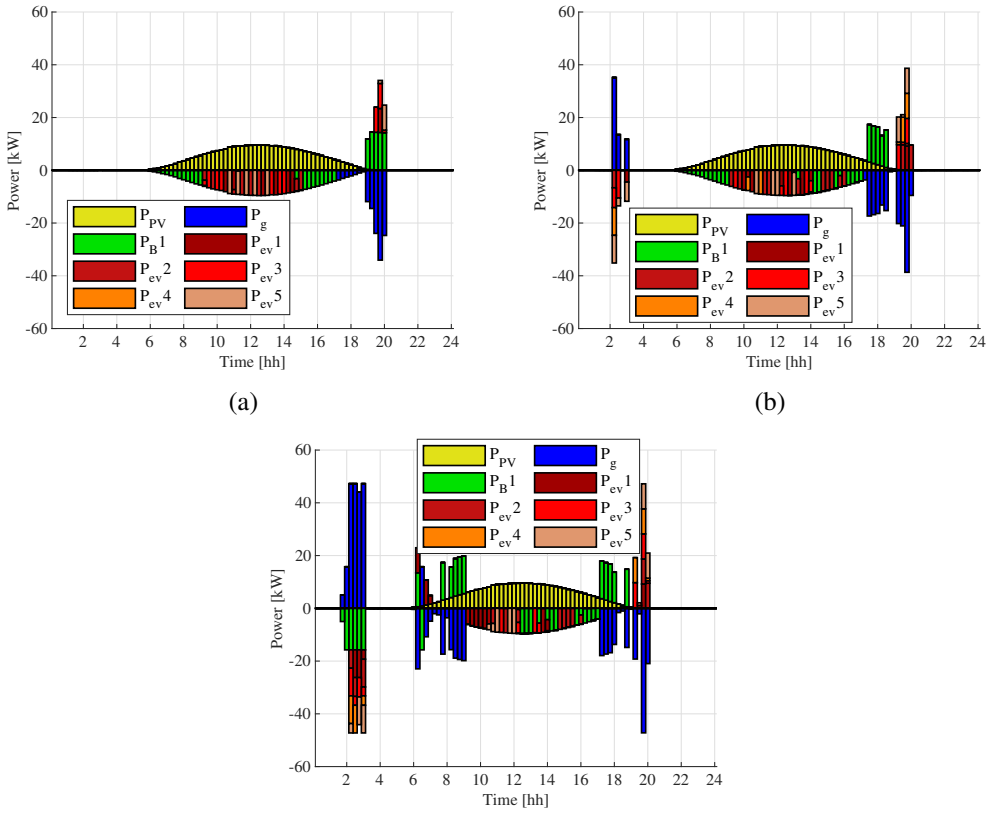

Figure 2.17: Power exchanges in Scenarios B2 (a), B3 (b), B4 (c).

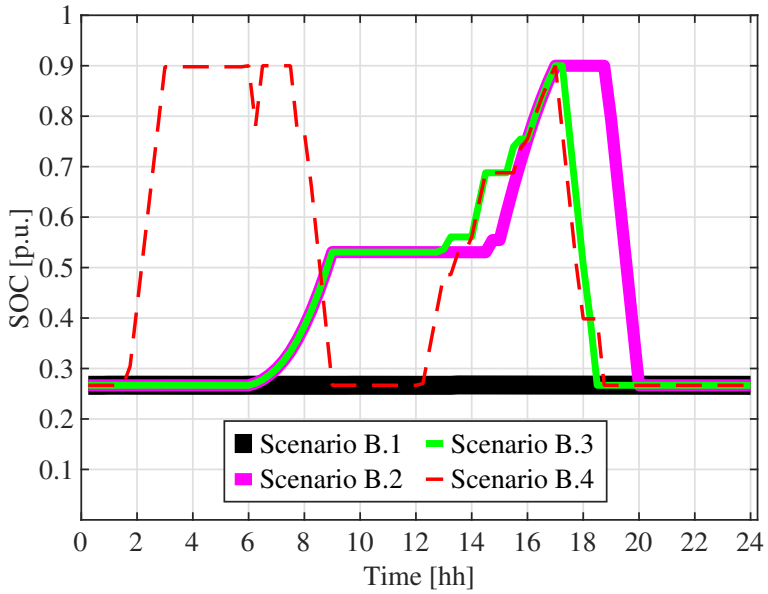

Figure 2.18: BESS SOC levels in Scenarios B.1-4.

can be seen that adopting PS2 and PS3 the discharge of EVs reaches 0.2 cycle, with respect to Scenario A.4 where discharge cycles of EV1, EV3 and EV5 are respectively 0.46, 0.56 and 0.34. In scenarios B.2, B.3 and B.4 BESS contribution in energy selling is significant, as 0.67 discharge cycle is reached in B.2 and B.3, while more than 1 cycle (1.45) occurs in B.4. Assuming low level of initial and final BESS SOC leads to a significant exploitation in Scenarios B.2-4, whereas has not any influence in Scenario B.1.

The analysis of power trends and of indicators points out that the spikes in selling price, if high enough to compensate wearing costs, represent a powerful mean to drive the behaviour of BESS and EV discharge. When BESS is available, the economic goal implies a preference for BESS discharge with respect to EVs, therefore the need for specific advancement of EV technology and information flow arises in order to push bidirectional energy exchanges while providing energy for the mobility.

Table 2.10: Total daily cost.

Scenario	**Daily cost [€]**
A.1	7.50
A.2	6.32
A.3	3.07
A.4	0.93
B.1	7.50
B.2	5.84
B.3	1.75
B.4	0.005

Table 2.11: Equivalent discharge cycle number.

Scenario	**BESS**	**EV1**	**EV2**	**EV3**	**EV4**	**EV5**
A.1	-	0	0	0	0	0
A.2	-	0.09	0.19	0.19	0.19	0.19
A.3	-	0.004	0.19	0.19	0.19	0.19
A.4	-	0.46	0.20	0.56	0.20	0.34
B.1	0	0	0	0	0	0
B.2	0.67	0.09	0	0.20	0	0.10
B.3	0.67	0.09	0.20	0.20	0.20	0.20
B.4	1.45	0.30	0.20	0.20	0.20	0.20

2.4 Stochastic approach for power and reserve programming

In this section, the day-ahead energy management procedure proposed in Section 2.2 is enriched embedding the reserve provision by EVs and BESS to cope with uncertainties in PV generation and EV mobility forecasts. The methodology is based on chance-constrained mixed-integer linear programming (MILP) approach of Section 2.1 and integrating errors on EV arrival state. The procedure is implemented in Matlab environment, to determine exchanged power with the distribution grid and within the EVSI, and local up and down reserve levels, minimizing the daily total costs of the microgrid.

The procedure includes: i) internal reserve provision scheduling by BESS and EVs to deal with fluctuations in PV generation and EV mobility, ii) PV production and EV SOC uncertainty, modelled through forecast error probability, and included in chance-constrained MILP strategy, iii) different strategies for reserve provision in terms of target subdivision among BESS and EVs and total economic effort.

2.4.1 Chance-constrained programming for BESS reserve provision

The proposed stochastic approach is aimed to ensure the balance of generation and demand and proper usage of sources in the presence of uncertainties related to PV generation and EV usage. The procedure is based on the definition of forecasting errors for the PV generation and the arrival SOC of a defined subset of EVs affected by uncertainty $\Omega_{EV,unc}$. The actual values of PV production and arrival SOC depend on the forecast errors $\epsilon_{PV}(t)$ and $\epsilon_S(t^{arr}_{EV,j})$, as in (2.20) and (2.21).

$$P^{act}_{PV}(t) = P_{PV}(t) + \epsilon_{PV}(t)\ \forall t \in [1, N_T] \tag{2.20}$$

$$S^{arr,act}_{EV,j}(t^{arr}_{EV,j}) = S^{arr}_{EV,j}(t^{arr}_{EV,j}) + \epsilon_S(t^{arr}_{EV,j}) \tag{2.21}$$

Negative values of $\epsilon_{PV}(t)$ and $\epsilon_S(t^{arr}_{EV,j})$ imply that the system requires additional generation. On the contrary, positive values of errors report the case of the network requiring a decrease in generation. Assuming that the forecasts are independent each other, the worst case is present when the two errors have the same sign. Hence, maximum positive and negative aggregated error are defined in (2.22a) and (2.22b).

$$\epsilon^{-}(t) = \epsilon_{PV}(t) + \epsilon_S(t) \; \forall t \in [1, N_T] \tag{2.22a}$$

$$\epsilon^{+}(t) = -\epsilon_{PV}(t) - \epsilon_S(t) \; \forall t \in [1, n_t] \tag{2.22b}$$

The chance-constrained approach is adopted to define the level of positive (up) and negative (down) reserves provided by BESS, $R^{+}_{B}(t)$ and $R^{-}_{B}(t)$, which represent additional state variables of the procedures, needed to compensate the forecasting error of PV power production and EV SoC with proper confidence levels $\alpha^{+}_{x}(t)$ and $\alpha^{-}_{x}(t)$ in each time step, where subscript x represents the general uncertainty source. Therefore, the following constraints (2.23a) and (2.23b) are included in the optimal day-ahead programming problem:

$$\mathbb{P}\left(\epsilon^{-}(t) \leq R^{-}_{B}(t)\right) \geq 1 - \alpha^{-}_{x}(t) \tag{2.23a}$$

$$\mathbb{P}\left(\epsilon^{+}(t) \leq R^{+}_{B}(t)\right) \geq 1 - \alpha^{+}_{x}(t) \tag{2.23b}$$

With the assumption that errors $\epsilon_{PV}(t)$ and $\epsilon_S(t^{arr}_{EV,j})$ can be described by distinct normal distributions, with respective mean values $\mu_{\epsilon,PV}(t)$ and $\mu_{\epsilon,S,j}(t^{arr}_{EV,j})$ and standard deviations $\sigma_{\epsilon,PV}(t)$, $\sigma_{\epsilon,S,j}(t^{arr}_{EV,j})$, the stochastic relations (2.23a) and (2.23b) can be linearized and included in the microgrid programming problem in order to ensure that positive and negative reserve levels should be at least equal to the $(1-\alpha^{+}_{x})$-th and $(1-\alpha^{-}_{x})$-th quantile of probability distributions associated to the x uncertain input:

$$R^{-}_{B}(t) \geq q^{PV,-}_{1-\alpha^{-}}(t) + \sum_{k \in \Omega_{EV,unc}} \frac{q^{S,k,-}_{1-\alpha^{-}}(t)}{n_{\epsilon,S,k} \cdot \Delta t} \tag{2.24a}$$

$$R^{+}_{B}(t) \geq q^{PV,+}_{1-\alpha^{+}}(t) + \sum_{k \in \Omega_{EV,unc}} \frac{q^{S,k,+}_{1-\alpha^{+}}(t)}{n_{\epsilon,S,k} \cdot \Delta t} \tag{2.24b}$$

$$q^{PV,-}_{1-\alpha^-}(t) = +\mu_{\epsilon,PV}(t) - \text{erf}^{-1}\left(\alpha^-_{PV}(t) - 1\right) \cdot \sigma_{\epsilon,PV}(t) \tag{2.25a}$$

$$q^{PV,+}_{1-\alpha^+}(t) = -\mu_{\epsilon,PV}(t) + \text{erf}^{-1}\left(1 - \alpha^+_{PV}(t)\right) \cdot \sigma_{\epsilon,PV}(t) \tag{2.25b}$$

$$q^{S,k,-}_{1-\alpha^-}(t) = -\text{erf}^{-1}\left(\alpha^-_{S,k}(t) - 1\right) \cdot \sigma_{\epsilon,S,k}(t^{arr}_{EV,k}) + \mu_{\epsilon,S,k}\left(t^{arr}_{EV,k}\right) \tag{2.25c}$$

$$q^{S,k,+}_{1-\alpha^+}(t) = \text{erf}^{-1}\left(1 - \alpha^+_{S,k}(t)\right) \cdot \sigma_{\epsilon,S,k}\left(t^{arr}_{EV,k}\right) - \mu_{\epsilon,S,k}\left(t^{arr}_{EV,k}\right) \tag{2.25d}$$

As in (2.24a) and (2.24b), quantiles related to arrival SoC uncertainty are expressed in kWh, while quantiles of PV production are in kW. Therefore, the energy quantities are spread through $n_{\epsilon,S,j}$ time intervals after the forecast arrival time $t^{arr}_{EV,j}$. Moreover, quantiles depend on the distribution parameters, as in (2.25a)-(2.25d), where erf^{-1} is the inverse error function for a specific probability level.

The reserves that can be provided the BESS unit at time t are limited by the actual available energy stored and the maximum charging/discharging power, assuming that forecast error and subsequent reserve provision are not affected by previous conditions and accounting for charge/discharge efficiencies (2.26a)-(2.26d):

$$R^+_B(t) \leq \frac{S_B(t) - S^{MIN}_B}{\eta^d_B \cdot \Delta t} \tag{2.26a}$$

$$R^+_B(t) \leq P^{d,MAX}_B - P^d_B(t) \tag{2.26b}$$

$$R^-_B(t) \leq \eta^c_B \cdot \frac{S^{MAX}_B - S_B(t)}{\Delta t} \tag{2.26c}$$

$$R^-_B(t) \leq P^{c,MAX}_B - P^c_B(t) \tag{2.26d}$$

2.4.2 Reserve provision by BESS and a cluster of EVs

Assuming that one of the EVs is affected by uncertainty in SOC at arrival time, i.e. $\Omega_{EV,unc} = \{1\}$, the reserve provision of $n_{EV} - 1$ EVs, when connected to the charging stations, requires the inclusion of positive and negative reserves in the state vector, adding $R^+_{EV,j}(t)$ and $R^-_{EV,j}(t)$. For each EV $j \in \{2, \ldots, n_{EV}\}$ enabled to provide reserve and for each time

t, further relations analogous to (2.26a)-(2.26d) are considered as well.

$$\sum_{k=2}^{n_{EV}} R^{-}_{EV,k}(t) + R^{-}_{B}(t) \geq q^{PV,-}_{1-\alpha^{-}}(t) + \frac{q^{S,k,-}_{1-\alpha^{-}}(t)}{n_{\epsilon,S,k} \cdot \Delta t}\bigg|_{k=1} \tag{2.27a}$$

$$\sum_{k=2}^{n_{EV}} R^{+}_{EV,k}(t) + R^{+}_{B}(t) \geq q^{PV,+}_{1-\alpha^{+}}(t) + \frac{q^{S,k,+}_{1-\alpha^{+}}(t)}{n_{\epsilon,S,k} \cdot \Delta t}\bigg|_{k=1} \tag{2.27b}$$

In order to evaluate the distribution of BESS and EV power reserve during the day, operational constraints are defined for BESS exploitation. In particular, (2.28a) and (2.28b) impose that total negative and positive reserves by BESS cover at least the 25% of the total required reserves, while (2.28c) refers to the BESS daily operation, forcing daily charging energy to be at least the 50% of BESS capacity H_B.

$$\sum_{t} R^{-}_{B}(t) \geq 0.25 \cdot \left[q^{PV,-}_{1-\alpha^{-}}(t) + \frac{q^{S,k,-}_{1-\alpha^{-}}(t)}{n_{\epsilon,S,k} \cdot \Delta t}\bigg|_{k=1} \right] \tag{2.28a}$$

$$\sum_{t} R^{+}_{B}(t) \geq 0.25 \cdot \left[q^{PV,+}_{1-\alpha^{+}}(t) + \frac{q^{S,k,+}_{1-\alpha^{+}}(t)}{n_{\epsilon,S,k} \cdot \Delta t}\bigg|_{k=1} \right] \tag{2.28b}$$

$$\Delta t \cdot \sum_{t} P^{c}_{B}(t) \geq 0.5 \cdot H_B \tag{2.28c}$$

2.4.3 Case study and results

The proposed methodology requires the modelling of uncertainties by means of probability distributions. Error of PV generation is modelled as Normal distribution with mean $\mu_{\epsilon,PV}(t) = 0$ and standard deviation $\sigma_{\epsilon,PV}(t)$ corresponding to 10% of the forecasted value of $P_{PV}(t)$ in each timestep (PV production curve considered is the one representing a summer day in Section 2.2.7). Since EV1 is the vehicle with the highest number of journeys during the day (see Scenario 1 in Fig. 2.7) – arriving at the DC microgrid at timesteps 36, 53 and 70 – the SoC uncertainty is associated to it, and the distribution is defined with mean value $\mu_{\epsilon,S,j}\left(t^{arr}_{EV,j}\right)$ set to 0 and standard deviation $\sigma_{\epsilon,S,j}\left(t^{arr}_{EV,j}\right)$ set to 20% of EV capacity $C_{EV,j}$, according to the studies in [egrid6] and [egrid8]. Constraint violation probabilities $\alpha^{+}_{x}(t)$ and $\alpha^{-}_{x}(t)$ are both set equal to 0.5% for each time-step for PV uncertainty, while they are set to 5% for EV SoC uncertainty, that is spread in terms of power over

one hour, therefore in $n_{\epsilon,S,j} = 4$ timesteps (keeping 15-min duration as in Section 2.2.1). Probability distribution function parameters and relevant quantiles used in the procedure are summarized in Table 2.12.

Table 2.12: Probability function parameters and quantiles.

Uncertainty	μ_ϵ	σ_ϵ	α_x^+	α_x^-
$\epsilon_{PV}(t)$	0	$0.1 \cdot P_{PV}(t)$	0.005	0.005
$\epsilon_S(t_{EV,k}^{arr})$	0	$0.2 \cdot C_{EV,k}$	0.05	0.05

Simulations are carried out considering three cases:

- Case 1: reserve provided only by BESS,
- Case 2: reserve provided by BESS and EV batteries,
- Case 3: reserve provided by BESS and EV batteries including the constraints (2.28a)-(2.28c).

Fig. 2.19a shows up and down reserve profiles for BESS in Case 1. As it can be seen about 8 kWh reserve for arrival SoC variations is spread over 1 hour operation after each arrival time of EV1. This amount of reserve is added to the bell-shaped one related to PV fluctuations. However, the installed battery size is able to fully comply with the required internal reserve. In Fig. 2.19b daily optimal schedule of DC microgrid is reported, where PV production is used for energy selling to the distribution grid and successively for EV charging. EV1 exploitation in V2G mode occurs at 08:15. It could be observed that the wearing cost contribution implies that BESS remains unexploited for power balance, although useful for reserve tasks.

When EV batteries are included in the reserve provision schedule in Case 2, most of reserve is provided by EVs, as shown in Fig. 2.20a, where EV4 and EV5 cover most part of reserve energy, since the first does not take any trip while the second takes only one travel during the day. EVs provide most of reserve in the central hours of the day, with some contributions by EV3 after 14:00. Between these intervals, when the reserve requirement exceeds 10 kW, EV5 alone is not able to cover the reserve, therefore some help from other

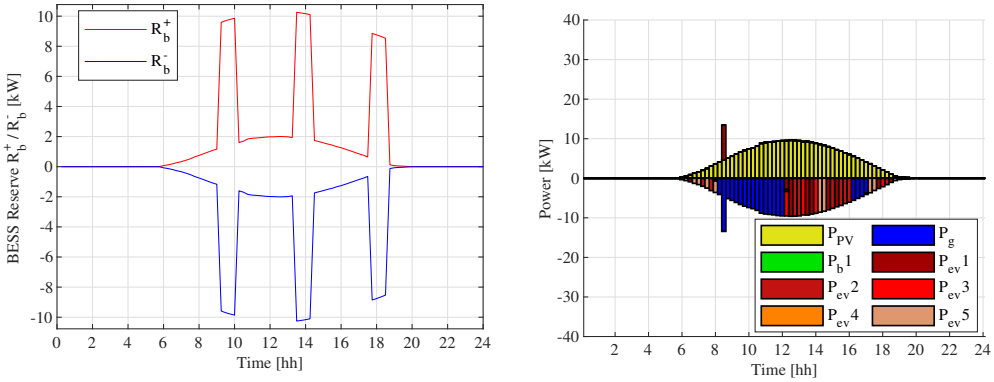

(a) (b)

Figure 2.19: Reserve levels (a) and power exchanges (b) in Case 1.

EVs is present. The provision of reserve by BESS is concentrated at the beginning and at the end of PV production interval, only to absorb negative errors. Power exchanges within microgrid (Fig. 2.20b) occur during central hours of the day, since PV production is delivered to the distribution network in the morning and then exploited for EV charging in the afternoon, with little contribution by BESS due to higher wearing cost and lower efficiency with respect to EVs. Moreover, EV5 has changed the charging plan, in order to avoid high power exchange when providing reserve.

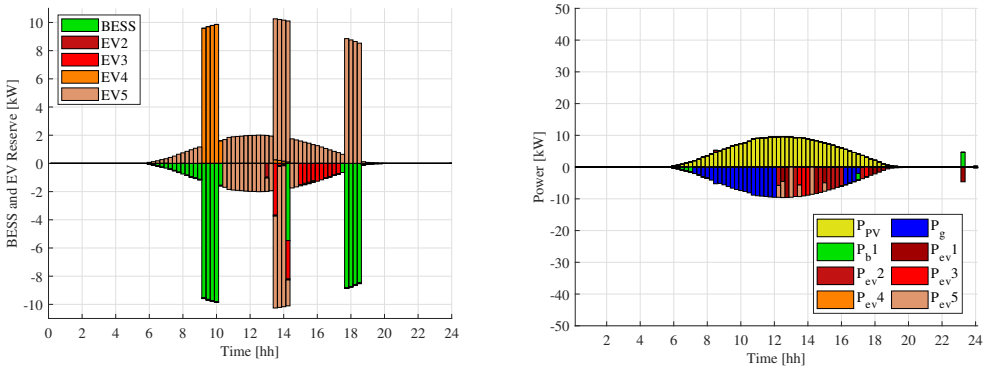

(a) (b)

Figure 2.20: Reserve levels (a) and power exchanges (b) in Case 2.

Different daily operation is depicted in Case 3. In Fig. 2.21a, the distribution of internal reserve shows that EV3 partly replaces BESS reserve provision (between 09:00 and 10:00 and after 18:30). This reveals that the amount of power that BESS could provide is reduced, since its operation is forced to comply a minimum level of energy. In fact, a more significant

BESS exploitation for power provision can be noted in Fig. 2.21b, since a discharge at maximum power occurs at 08:00, when also EV1 and EV2 operate in V2G mode to sell energy to the grid, according to advantageous energy selling price. BESS is charged by PV when EVs are absent, replacing grid connection exchanges, and again discharged in the last intervals in order to charge EV1 and EV2.

A comparison of daily microgrid costs observed in the three Cases, corresponding to the objective function (2.2) values, is carried out in Table 2.13. Slight cost differences can be noted, since no revenues are associated to internal reserve energy provision. The increase of costs when BESS is forced to operate is due to the presence of wearing cost in the objective function of the optimization problem.

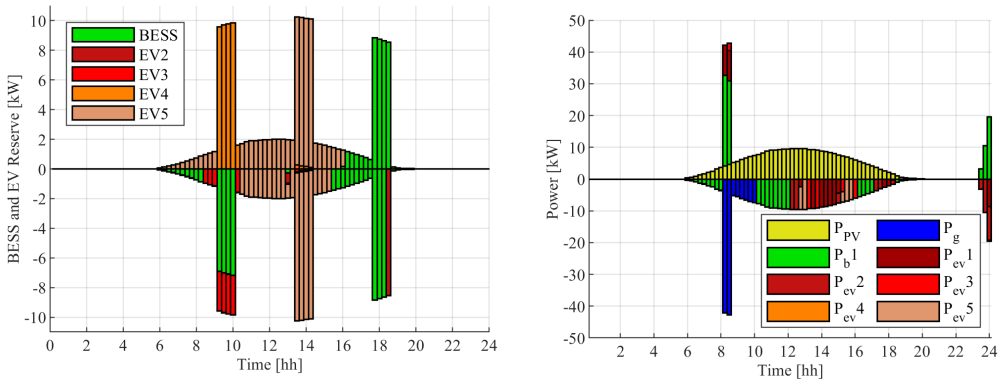

(a) (b)

Figure 2.21: Reserve levels (a) and power exchanges (b) in Case 3.

Table 2.13: Microgrid daily costs.

Case study	Daily cost [€]
Case 1) reserve only by BESS	8.65
Case 2) reserve by BESS and EVs	8.72
Case 3) reserve by BESS and EVs with BESS use	9.60

2.5 Fast charging station integration into DC-based EVSI

In this section, the integration of fast charging station within the DC-based EVSI is further investigated. Taking the cue from the methodology already presented in Section 2.2, the problem is reformulated taking into account an additional fast charging station, with particular focus on cable losses. In particular, same objective functions (2.2) and (2.10) are separately considered, while the equality constraint (2.3) representing the active power balance at DC common bus is modified as in (2.29)

$$\begin{aligned}\eta_{inv}^{in}\cdot P_g^{in}(t)-\frac{1}{\eta_{inv}^{out}}\cdot P_g^{out}(t)+\eta_B^d\cdot P_B^d(t)-\frac{1}{\eta_B^c}\cdot P_B^c(t)+\\ +\sum_j\left[\left(\eta_{EV,j}^d\cdot P_{EV,j}^d(t)-\frac{R_j}{V^2}\cdot P_{EV,j}^d(t)^2\right)-\right.\\ \left.\left(\frac{1}{\eta_{EV,j}^c}\cdot P_{EV,j}^c(t)-\frac{R_j}{V^2}\cdot P_{EV,j}^c(t)^2\right)\right]=-\eta_{PV}\cdot P_{PV}(t)\end{aligned} \tag{2.29}$$

where η_{inv}^{in} and η_{inv}^{out} are AC/DC converter efficiencies, while R_j is the cable resistance value of the j-th charging station. Moreover, EV station cable losses are expressed in (2.30a) and (2.30b) for charging and discharging processes. The value of cable resistance is calculated as in (2.31),

$$P_{EV,j}^{loss,c}(t)=R_j\cdot I_{EV,j}^c(t)^2=R_j\cdot\left(\frac{P_{EV,j}^c(t)}{V}\right)^2\ \forall t\in[1,N_T],\ \forall j\in[1,n_{EV}] \tag{2.30a}$$

$$P_{EV,j}^{loss,d}(t)=R_j\cdot I_{EV,j}^d(t)^2=R_j\cdot\left(\frac{P_{EV,j}^d(t)}{V}\right)^2\ \forall t\in[1,N_T],\ \forall j\in[1,n_{EV}] \tag{2.30b}$$

$$R_j=\rho_j\cdot\frac{l_j}{S_j}\ \forall j\in[1,n_{EV}] \tag{2.31}$$

where ρ_j, l_j and S_j are respectively cable resistivity, length and section.

2.5.1 Big-M method for problem linearization

Power balance constraint (2.29), as formulated, is not linear, hence it is not possible to include it in the mixed-integer linear problem. Big-M method is therefore used to linearize the constraint [107]. The aim of the linearization is to approximate quadratic functions to linear ones: in the specific application, the auxiliary variables $y^c_{EV,j}(t)$ and $y^d_{EV,j}(t)$ linearly approximate quadratic values of EV charging and discharging powers $P^c_{EV,j}(t)$ and $P^d_{EV,j}(t)$, as in (2.32a) and (2.32b). Therefore, a set of constraints reported below ensure the linearization of the problem by means of auxiliary continuous variables $\delta^{c,m}_{EV,j}$, $\delta^{d,m}_{EV,j}$, and integer variables $\lambda^{c,m}_{EV,j} \in [-1;1]$ and $\lambda^{d,m}_{EV,j} \in [-1;1]$, both for charging (2.33a)-(2.33d) and discharging power (2.34a)-(2.34d). Moreover, in the following equations, m is the number of branches for linearization, while M is a big constant value.

$$y^c_{EV,j}(t) = P^c_{EV,j}(t)^2 \tag{2.32a}$$

$$y^d_{EV,j}(t) = P^d_{EV,j}(t)^2 \tag{2.32b}$$

$$P^{c,MIN}_{EV,j} - \Delta P \cdot (m-1) \geq \lambda^{c,m}_{EV,j} \cdot M \tag{2.33a}$$

$$\lambda^{c,m}_{EV,j} + 1 \geq \delta^{c,m}_{EV,j} \geq \lambda^{c,m}_{EV,j} + 1 \tag{2.33b}$$

$$y^c_{EV,j}(t) = P^c_{EV,j}(t)^2 + \sum_{m>1} \delta^{c,m}_{EV,j} \cdot \left(\left(Y^{c,m}_{EV,j} \right)^2 - \left(Y^{c,m-1}_{EV,j} \right)^2 \right) \tag{2.33c}$$

$$P^c_{EV,j}(t) = P^{c,MIN}_{EV,j} + \sum_{m>1} \delta^{c,m}_{EV,j} \cdot \left(Y^{c,m}_{EV,j} - Y^{c,m-1}_{EV,j} \right) \tag{2.33d}$$

$$P^{d,MIN}_{EV,j} - \Delta P \cdot (m-1) \geq \lambda^{d,m}_{EV,j} \cdot M \tag{2.34a}$$

$$\lambda^{d,m}_{EV,j} + 1 \geq \delta^{d,m}_{EV,j} \geq \lambda^{d,m}_{EV,j} + 1 \tag{2.34b}$$

$$y^d_{EV,j}(t) = P^d_{EV,j}(t)^2 + \sum_{m>1} \delta^{d,m}_{EV,j} \cdot \left(\left(Y^{d,m}_{EV,j} \right)^2 - \left(Y^{d,m-1}_{EV,j} \right)^2 \right) \tag{2.34c}$$

$$P^d_{EV,j}(t) = P^{d,MIN}_{EV,j} + \sum_{m>1} \delta^{d,m}_{EV,j} \cdot \left(Y^{d,m}_{EV,j} - Y^{d,m-1}_{EV,j} \right) \tag{2.34d}$$

Then, (2.32a) and (2.32b) are substituted in (2.29), obtaining a linear equality constraint for active power balance, as in the following (2.35):

$$\begin{aligned}&\eta_{inv}^{in}\cdot P_g^{in}(t)-\frac{1}{\eta_{inv}^{out}}\cdot P_g^{out}(t)+\eta_B^d\cdot P_B^d(t)-\frac{1}{\eta_B^c}\cdot P_B^c(t)+\\&+\sum_j\left[\left(\eta_{EV,j}^d\cdot P_{EV,j}^d(t)-\frac{R_j}{V^2}\cdot y_{EV,j}^d(t)\right)+\right.\\&\left.-\left(\frac{1}{\eta_{EV,j}^c}\cdot P_{EV,j}^c(t)-\frac{R_j}{V^2}\cdot y_{EV,j}^c(t)\right)\right]=-\eta_{PV}\cdot P_{PV}(t)\end{aligned}\tag{2.35}$$

With respect to the formulation in Section 2.2.1, $m\cdot N_T\cdot n_{EV}\cdot 4$ additional variables are added, along with $2\cdot(2\cdot n_{EV}\cdot m+2\cdot n_{EV}\cdot N_T)$ further constraints.

2.5.2 Indicators

As for studies in Section 2.2, a comparison of results is carried out by means of technical and economic indicators, such as daily cost evaluated as in (2.2) and maximum values of imported and exported power at AC/DC converter, namely $E_g^{in,tot}$ and $E_g^{out,tot}$. Furthermore, converter losses L_{conv}^{tot} and cable losses $L_{EV,j}^{joule,tot}$ are evaluated respectively in (2.36a) and (2.36b), whereas energy stored in BESS E_B and EVs $E_{EV,j}$ (when plugged-in) are evaluated in (2.37a) and (2.37b).

$$\begin{aligned}L_{conv}^{tot}=\sum_t\Bigg[&\left(1-\eta_{inv}^{in}\right)\cdot P_g^{in}(t)+\left(1-\frac{1}{\eta_{inv}^{out}}\right)\cdot P_g^{out}(t)+\left(1-\eta_B^d\right)\cdot P_B^d(t)+\\&+\left(1-\frac{1}{\eta_B^c}\right)\cdot P_B^c(t)+\sum_j\left(1-\eta_{EV,j}^d\right)\cdot P_{EV,j}^d(t)+\left(1-\frac{1}{\eta_{EV,j}^c}\right)\cdot P_{EV,j}^c(t)\\&+\left(1-\eta_{PV}\right)\cdot P_{PV}(t)\Bigg]\end{aligned}\tag{2.36a}$$

$$L_{EV,j}^{joule,tot}=\sum_t\left[\frac{R_j}{V^2}\cdot y_{EV,j}^d(t)+\frac{R_j}{V^2}\cdot y_{EV,j}^c(t)\right]\tag{2.36b}$$

$$E_B=\Delta t\cdot\sum_t\left[P_B^c(t)-P_B^d(t)\right]\cdot\frac{1}{H_B}\tag{2.37a}$$

$$E_{EV,j} = \Delta t \cdot \sum_{t} \left[P^{c}_{EV,j}(t) - P^{d}_{EV,j}(t) \right] \cdot \frac{1}{H_{EV,j}} \tag{2.37b}$$

2.5.3 Case study

The DC microgrid layout has been already introduced in the previous Section 2.2.7, with component features as well. Some variations are here introduced, in order to approach the implementation of the day-ahead programming procedure in the energy management system of an EVSI (see Section 2.6 for completion). In particular, the Sodium-Nickel BESS is characterized by nominal capacity of 90 kWh and 25 kW charging/dischargin power, whereas PV has 20 kW installed power and bidirectional EV charging stations have 15 kW nominal power.

The input data concerning solar irradiance for PV production is taken from Solcast [108], considering two different scenarios: typical summer days with high PV production (characterized by peak power of 16.83 kW and 207 kWh generated) and low PV production (characterized by peak power of 11.26 kW with 100 kWh daily production). Moreover, buying and selling prices are taken respectively from ARERA authority [109] and National Single Prices [110]. For the standard charging stations the EV usage pattern is not modified, while the EV connected to the additional fast charging station has the characteristics reported in Table 2.14 and a usage configuration reported in Fig. 2.22. EV6 shorter plug-in times (comparing to the other 5 EV times) are chosen in order to push the fast charging station to operate at maximum of its potentiality. Moreover, the fast charging station does not allow EV discharge.

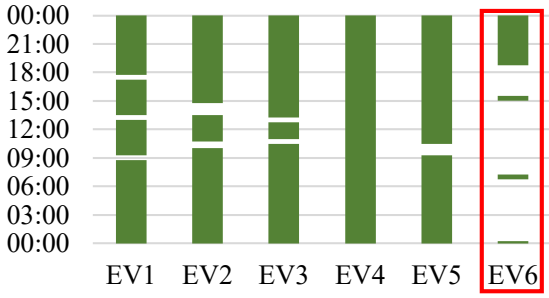

Figure 2.22: EV plug-in times including EV6 at the fast charging station.

Table 2.14: EV6 station features.

	EV6
Autonomy [km]	250
η_{EV}^{c}	0.95
η_{EV}^{d}	0.95
$P_{EV}^{c,MIN}$ [kW]	0
$P_{EV}^{c,MAX}$ [kW]	75
$P_{EV}^{d,MIN}$ [kW]	0
$P_{EV}^{d,MAX}$ [kW]	0
Cap [kWh]	76.6
S_{EV}^{MIN} [kWh]	15

2.5.4 Results with high PV production

Fig. 2.23a shows the exchanged powers within microgrid assets. It can be noted that EV6, which is enabled only for charging and not for V2G mode, is charged from 06:45 to 07:15 with a 75 kW peak around 07:00, according to the routes shown in Fig. 2.22. As a matter of fact, due to long routes and short plug-in times (30 minutes), EV6 exploits the fast station up to its maximum power of 75 kW, requesting power from other connected EVs and either from the grid or the ESS, since maximum power of AC/DC converter at the point of connection is lower than the power requested by the fast charging station. One more charging process occurs from 14:45 to 15:30, with a peak power of 64.79 kW at 15 p.m., taking advantage of the stored energy from the other EVs, and another one with a peak power of 36.72 kW at about 19:15, due to power contribution of EV4 and EV5. It can be observed from Fig. 2.23a, that in the case of cost minimization, EV1-5, while performing some discharges to support EV6, do not have an incentive to perform many operations, as battery degradation costs hinder their exploitation.

EV SOC levels are shown in Fig. 2.23b. It can be seen that EV6 charge is more intense than other EVs in p.u. value of its capacity as well, according to its energy need and usage. EV6 SOC goes from 58% to 100% during the first charge from 06:45 to 07:15, from 53% to 89% during the second charge from 15:00 to 15:30, and from 69% to 96% during the third charging process. Thus, EV6 SOC variation is contained within 45%. In contrast, SOC variation of EVs 1,2,3,5 is contained within 30%-35%, the SOC variation of EV4 is

larger within 40-45%, since its longer plug-in time allows it to contribute more for balancing power flows.

Implementing the power exchange minimization problem (see Fig. 2.24), a different EV exploitation is depicted, as EVs actively participate in power exchange with the DC bus. They are encouraged to exchange more power due to the absence of degradation costs, compared to the case of cost minimization. Moreover, several V2G and V2V processes take place, even in the early hours of the day when there is no PV production. EV6, connected to the fast charging station, is charged similarly to the cost minimization scenario (except for last two charging processes in the early evening), with contribution of other EV discharges.

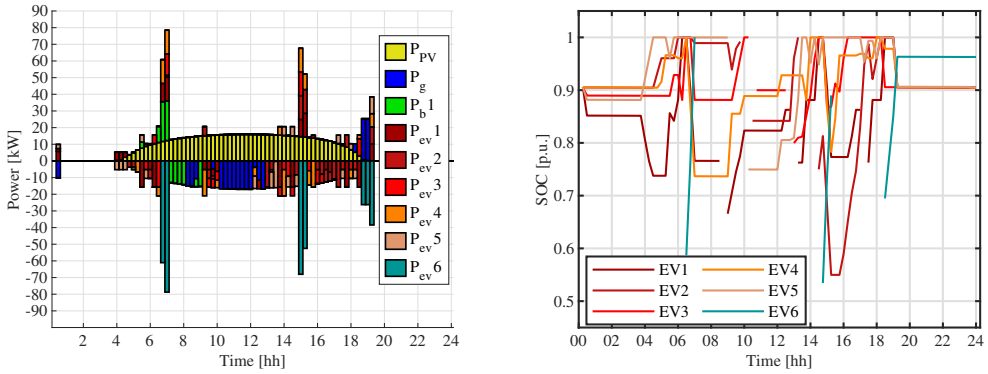

(a) (b)

Figure 2.23: Cost minimization with high PV production. Power exchanges (a) and EV SOC levels (b).

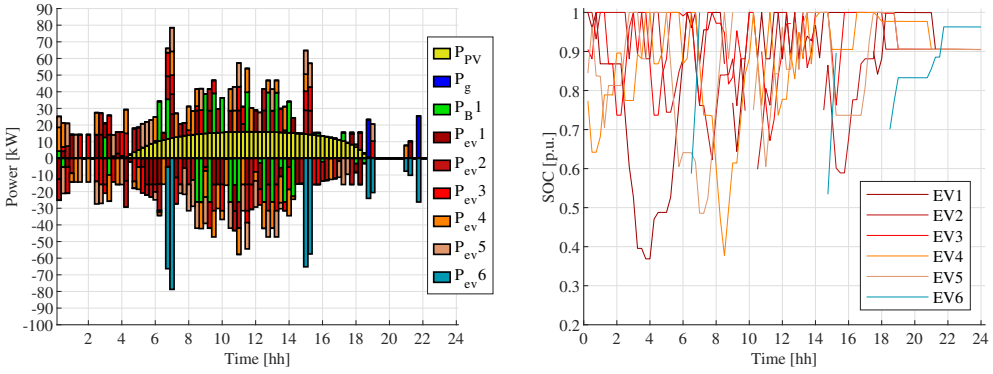

(a) (b)

Figure 2.24: Exchange minimization with high PV production. Power exchanges (a) and EV SOC levels (b).

2.5.5 Results with low PV production

Power exchanges within the microgrid considering low PV production and cost minimization procedure are shown in Fig. 2.25a. At 03:45 BESS discharges providing energy to EV5. Subsequently, at 05:00 it discharges again to provide power to EV4. Moreover, at 07:00, EV6 charges by taking advantage of PV availability, purchased power from the grid and discharge of BESS and other EVs previously charged. In case of low PV production, it is necessary to buy energy from the grid because PV production is not sufficient to guarantee energy required by EV6. At 15:00 power from the grid, with a peak of 45 kW, is requested to recharge EV6, since EV1-4 discharging powers are not sufficient, and it is not economically convenient to discharge the BESS again. It can be observed from Figure 2.25b that EV6 SOC variation range is 58%-100% of capacity during the first charge from 06:45 to 07:15, from 53% to 87% during the second charge from 15:00 to 15:30, and from 68% to 96% during the third charge from 18:45 onwards. In contrast, the SOC variation for EV1-5 is contained within 25-30% of their capacity.

Considering power exchange minimization strategy, same considerations of cost minimization scenario could be done, as more V2V processes are detected by EVs to charge EV6, and more energy from the grid is required due to low PV availability.

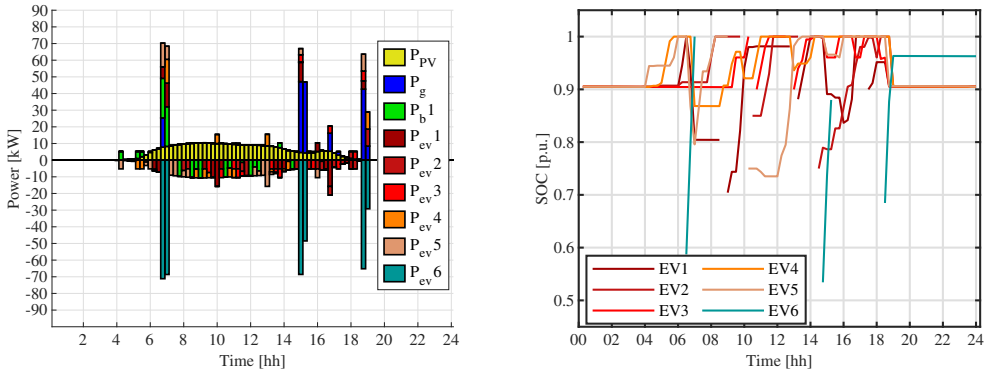

(a) (b)

Figure 2.25: Cost minimization with low PV production. Power exchanges (a) and EV SOC levels (b).

2.5.6 Indicator evaluation

Losses within the system are evaluated in order to depict any differences for each of the case. Data related to the basic layout of the DC microgrid (Base MG) are evaluated simulated considering the procedure with Big-M method and the updated characteristics of the devices. Table 2.15 collects the results for EV5 and EV6 charging stations. It can be pointed out that with technical objective OF2 EVs are more actively involved in power exchanges, and this leads to a reduction of energy losses in the presence of economic goals OF1 by 20-40%, whereas the use of fast charging station involves remarkable losses slightly different among scenarios since the charging needs are concentrated in the same short intervals and are covered by analogous power levels. The PV production level has low influence in base microgrid (less than 10% variation of losses among cases) whereas with fast charging the high PV production implies higher exchanges.

Table 2.15: Losses evaluation [kWh] in all scenarios at EV charging stations.

		OF1		**OF2**	
		$L_{EV,5}$	$L_{EV,6}$	$L_{EV,5}$	$L_{EV,6}$
Base MG	High PV prod.	0.204	-	0.285	-
	Low PV prod.	0.221	-	0.278	-
MG with fast charging	High PV prod.	1.491	1.092	2.077	1.092
	Low PV prod.	0.041	1.011	0.059	0.982

Table 2.16 collects technical and economic indicators used to assess the impact of fast charge integration within the DC microgrid. Higher costs are depicted when PV production is low applying cost minimization procedure, due to additional energy purchasing for the utility grid. The application of economic goal OF1 involves a reduction of daily procurement cost between 20% and 30%, or an increase of energy exchange revenue when present, with the exception of low PV production periods in the presence of EV fast charge posing challenging targets of internal production exploitation. Moreover, total energy exchanged with the grid in OF2 is always lower than in OF1, where the energy import is nullified or reduced by 10%, and with a reduction of energy export ranging from 15% to 70% in the presence of high PV production. Moreover, with low PV production and fast charge, the

energy needs imply the absence of excess power delivery to the external grid.

Table 2.16: Daily indicators of the microgrid in all scenario.

		OF1			OF2		
		Costs [€]	$E_g^{in,tot}$ [kWh]	$E_g^{out,tot}$ [kWh]	Costs [€]	$E_g^{in,tot}$ [kWh]	$E_g^{out,tot}$ [kWh]
Base	High PV	-23.46	6.23	132.00	-15.00	0.00	114.38
MG	Low PV	9.74	8.53	46.19	15.36	0.00	28.08
MG with	High PV	69.45	14.50	53.11	88.45	23.43	6.54
fast charge	Low PV	88.68	48.86	0.00	88.80	44.10	0.00

2.6 Implementation of developed procedure in energy management platform

In order to implement optimal strategies proposed in the previous sections within the DC microgrid EVSI, it is necessary to have a robust data exchange infrastructure that can ensure the information flow to and from the field and visualization of measured data from the field devices. For the PROGRESSUS Use Case realization, DEOP, a cloud platform provided by Siemens, was identified for supplying energy management of the DC microgrid demonstrator. DEOP is a cloud-based software that provides a complete and comprehensive view of all the plants, allowing the operator to benchmark and govern all assets thanks to the support of the data generated almost in real time, through the setting of optimal planning algorithms. Data amount generated in a microgrid is large and varied: energy and resource monitoring, information on failures or malfunctions, and historical databse of energy generation or consumption, and forecasts as well. The reading and interpretation of these data is often carried out by different parties, depending on relation to their task in microgrid management and control operations. DEOP allows all data to be available in a cloud environment. This means that measurements from sensors deployed in the plant, as well as data imported via APIs (Application Programming Interface) and other systems, are available in a single ”source” for all users. The main uses of DEOP are [111]: i) monitoring and trans-

parency: the software collects real-time data from all the sensors connected to devices in the field and displays it in an intuitive interface. It allows the creation of reports in standard or custom formats depending on the intended use of the same, ii) operation planning: DEOP makes it possible to visualize in a defined way the consumption levels in each controlled area at any time of the day. An identification of trends in the pattern of flows of energy in a given area is possible, developing strategies for maximizing efficiency, e.g., by maximizing self-consumption.
In the following sections a description of the data exchange framework and preliminary on-field test results are presented and discussed.

2.6.1 Development of interfaces

The definition of a suitable interface on the cloud-based platform of the energy management system is developed to manage all the assets of the use case during operation. In particular, the following activities have been carried out:

- Asset modelling and property definition,
- Report section creation,
- Event alert definition.

The assets modelled for the use case are: i) point of common coupling (PCC), ii) Energy storage systems, iii) PV shelter, iv) EV charging station (one asset for each of five EV stations - it should be noted that the EV fast charge inclusion in the interface is under realization -). Each asset collects feeds (power and energy set points, status info, etc.) optimized by the procedure, presented in the previous sections - details are provided in Section 2.6.2, and to be sent to the physical assets of the use case (see Fig. 2.26). A reporting section is also configured in order to create a control panel for graphic visualization of the most representative variables of the system (see Fig. 2.27), such as:

- EV state of charge comparison,
- EV power exchange comparison,

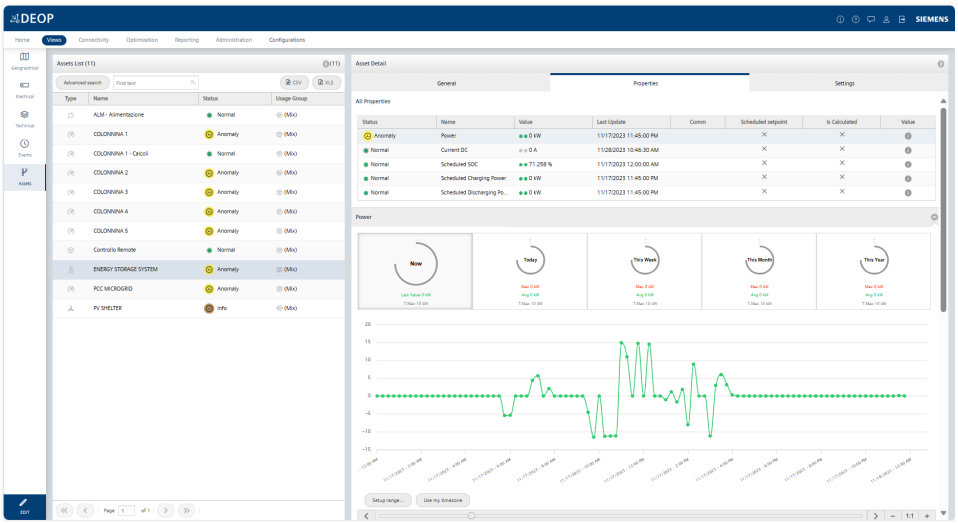

Figure 2.26: Properties and feeds associated to BESS asset.

- Energy storage system power,
- Energy storage system state of charge,
- PV power production,
- PCC power exchanges.

In DEOP, data are collected and shown as average values over 5-minute period, and instant maximum and minimum values.

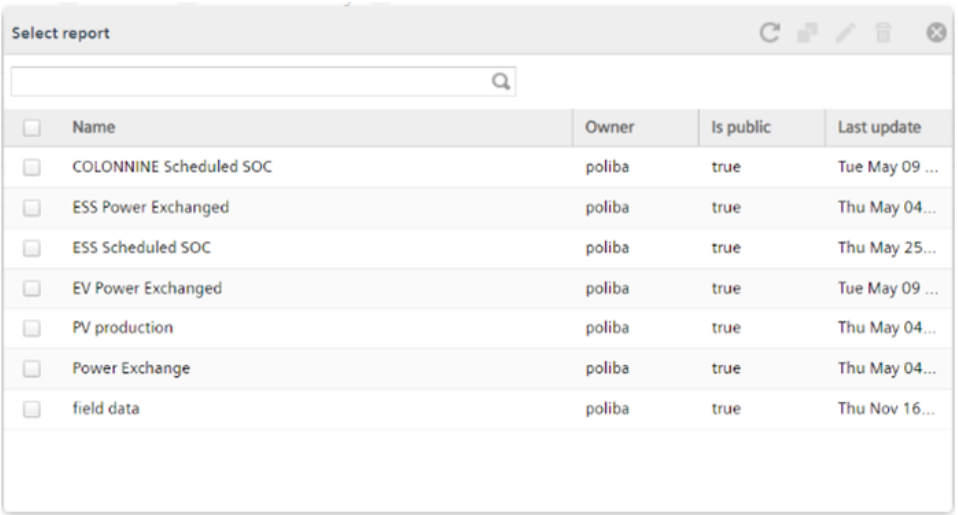

Figure 2.27: Visualized reports.

Furthermore, the possibility of configuring specific events related to anomalies that may

occur in the various components of the microgrid is evaluated. This configuration allows timely alarm notifications to be received and prompt action to be taken if necessary.

The configuration of events associated with faults is an important measure to ensure the proper functioning of the microgrid. Events can be set to monitor a wide range of parameters and conditions, e.g. component disconnections. Alarm notifications allow the responsible personnel to be promptly informed of the presence of anomalies, enabling them to take the necessary actions to resolve the problem. The first implemented alert is a reminder that sends appropriate notifications at the beginning of each trimester in order to keep energy prices updated. Thus, the implementation of four "Properties" associated events is considered:

- First trimester
- Second trimester
- Third trimester
- Fourth trimester

Trigger values are then chosen for the assets for practice purposes to test other anomaly events. As expected, all the assets for which a trigger is set have generated the configured event, reported in Fig. 2.28. Fig. 2.29 reports the interface created to have a general overview of the microgrid operation through the report sections and to notify possible event occurring, as in Fig. 2.30.

2.6.2 Data acquisition from developed optimal procedure and external sources

The preliminary implementation of Matlab algorithm in DEOP environment is carried out by automatically exporting output files for each optimized variable of the problem and importing them from DEOP as the set point for field assets, as shown in Fig. 2.31.

The implementation is tested exchanging data from the cost optimization of the DC microgrid, confirming its validity, since data shown in DEOP are corrispondent to MATLAB

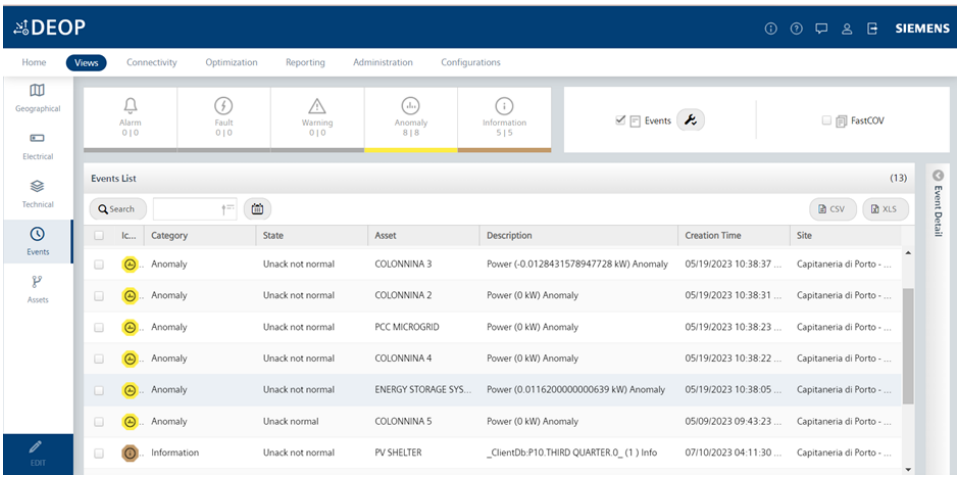

Figure 2.28: Configuration of alert event.

Figure 2.29: Creation of the dashboard for data visualization.

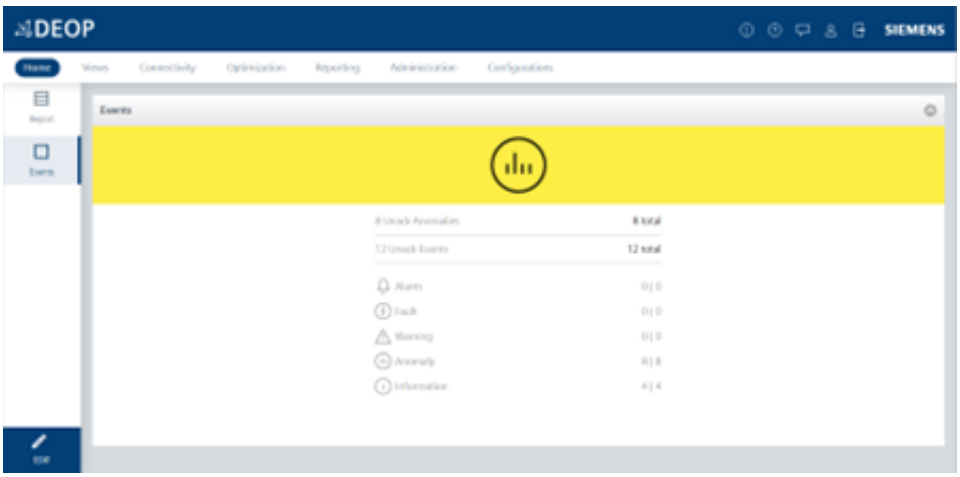

Figure 2.30: Creation of the dashboard for alert visualization.

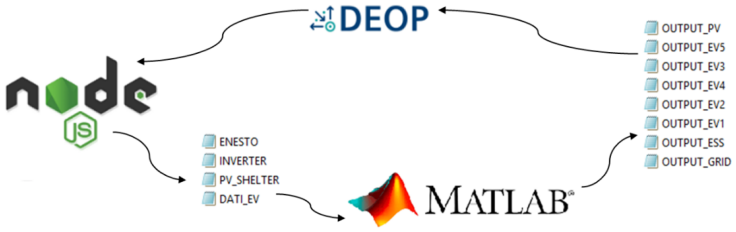

Figure 2.31: Data acquisition procedure.

ones. Fig. 2.32 shows EV SOC optimized levels considering high PV production and cost minimization problem of Section 2.5, exchanged between Matlab and DEOP environment and visualised in DEOP dashboard.

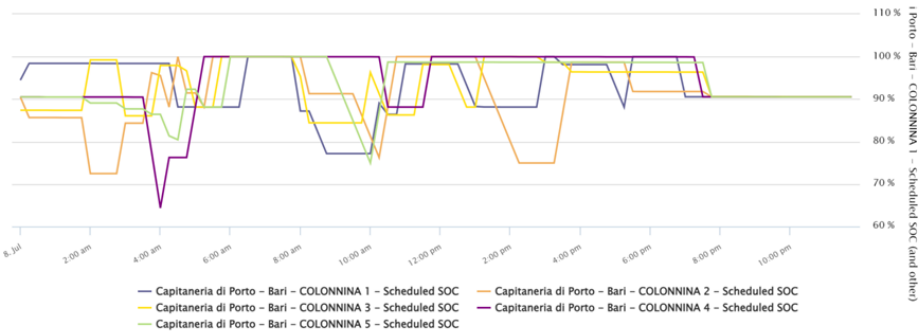

Figure 2.32: Visualization of scheduled EV SOC in DEOP dashboard.

The cloud based control system is interfaced with the field by means of a gateway-switch combination where a set of PLCs are connected, with the taks of managing the different protocols used by the devices (Profinet for battery energy storage BMS and for photovoltaic converter, Modbus for EV charging stations), according to the scheme reported in the Fig.2.33. Therefore, proper interface pages have been designed by system integrator (Politecnico di Bari subcontractor in CONNECT Project with further activity in PROGRESSUS Project), with focus on the network configuration, alarms, and specific converters for BESS and PV systems, as reported in Fig. 2.34. Moreover, the DC microgrid is equipped with an industrial wireless router, in order to make internet connection available in the demonstrator area, enabling data exchange with the cloud-based energy management system (DEOP) and with the Enel group EV backend system (EVOS), called to supervise EV charging processes, and to be implemented for API exchange.

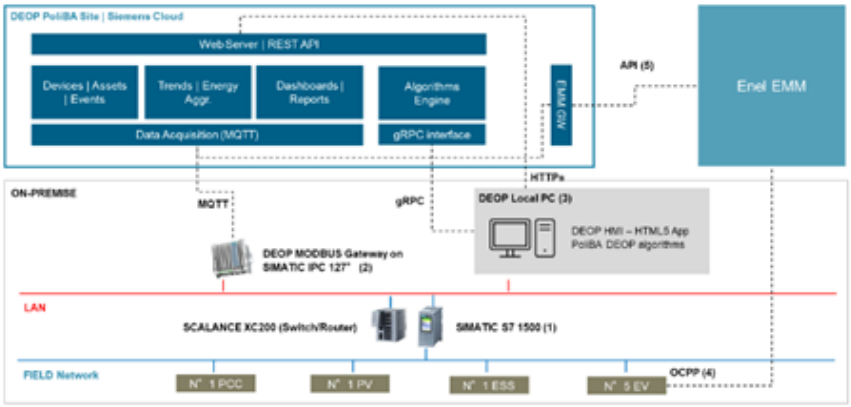

Figure 2.33: Schematization of the communication devices in the DC microgrid testbed.

2.6.3 Preliminary functionality test of DC microgrid devices

The devices integrated in the microgrid (converters for PV and batteries, DC common bus, grid connection converter) have been assembled by system integrator at its premises before final installation on field. In this stage, preliminary functionality of the DC microgrid connection (without connecting any load or generator) has been performed. As reported in Fig. 2.35, where the HMI interface page is shown, it can be seen that the AC/DC converter connecting the DC microgrid to the distribution network is able to light up the DC bus and to take it within the required operation level, that ranges between 550 V and 600 V according to the operation range required for the devices to be connected on field. This commitment test has been repeated on field, proving the grid to be put on in operation.

Additional tests on site concern the operation of components. In particular, the function test of a single V2G charging station is carried out, thanks to the availability of a suitable EV by Politecnico di Bari fleet. Due to the limitation of the passive temporary connection, and to the absence of further EVs as loads, the test is carried out only in charging mode, providing a proper local modulation of the charging power up to 15 kW, as can be seen in real time in the local interface in Fig. 2.36 and registered in the developed energy management interface for field data acquisition reported in Fig. 2.37 (it should be remarked that the energy management system acquires positive power for loads and negative for generators, on the contrary of the operation programming strategy output). Moreover, an islanding test is performed, connecting the sole photovoltaic system and the battery energy storage

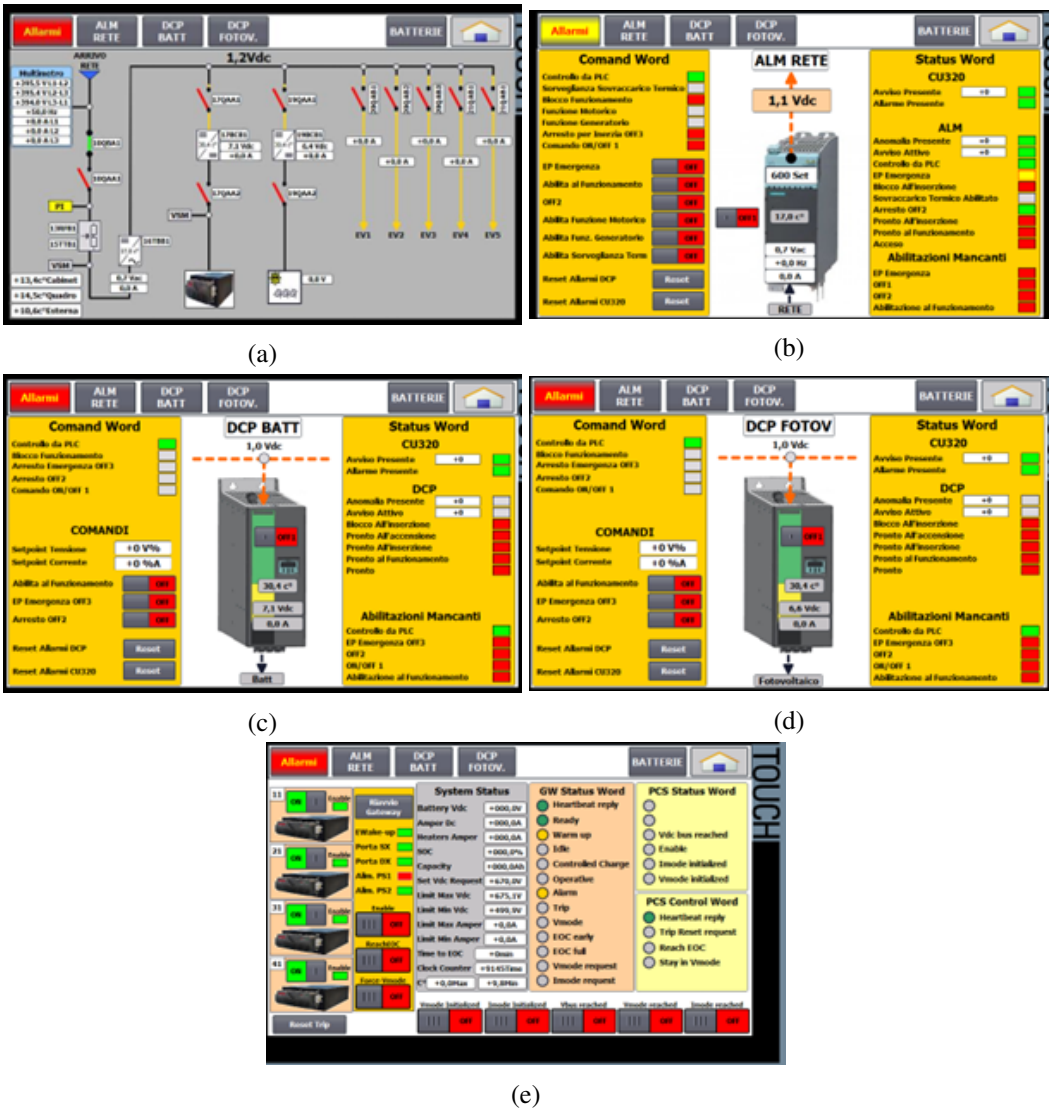

(a) (b) (c) (d) (e)

Figure 2.34: HMI pages for the local communication system of the DC microgrid testbed: grid layout (a), alarms (b), battery converter (c), photovoltaic converter (d), BESS management system (e).

in the early pre-heating stage, deactivating the AC/DC grid connection converter, for a 15-min test. The registered trends in the energy management system interface are reported in Fig. 2.38, where it can be seen that the photovoltaic converter can modulate the active power generation (below the MPPT forecast production level) to cover an uncontrollable load as the battery pre-heating.

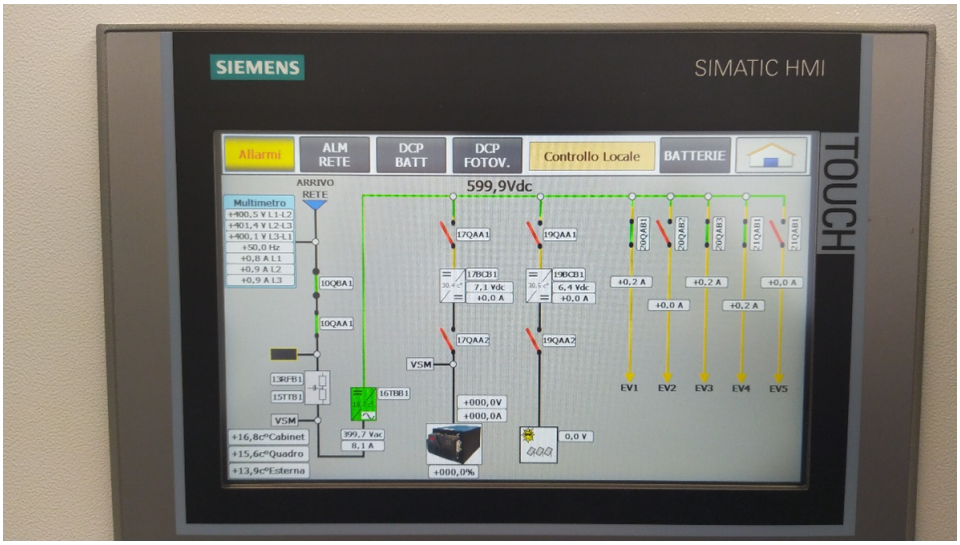

Figure 2.35: DC microgrid interface for preliminary functionality test of DC bus and connections.

Figure 2.36: DC microgrid interface during charging test of EV1 at a V2G charging point.

2.6.4 Preliminary tests of the fast-charging station

The 75 kW EV fast charging station – defined HPC, has been installed within the DC microgrid demonstrator area, occupying the last parking slot below the photovoltaic canopy, as shown in Fig. 2.39. It is provisionally connected at the AC level of the demonstrator area, prior to the DC microgrid interfacing AC/DC converter, in order to prove the effectiveness of the connection with Enel group backend EVOS and the modulation of charging process via the power setpoints provided by Politecnico di Bari procedures and with the realization

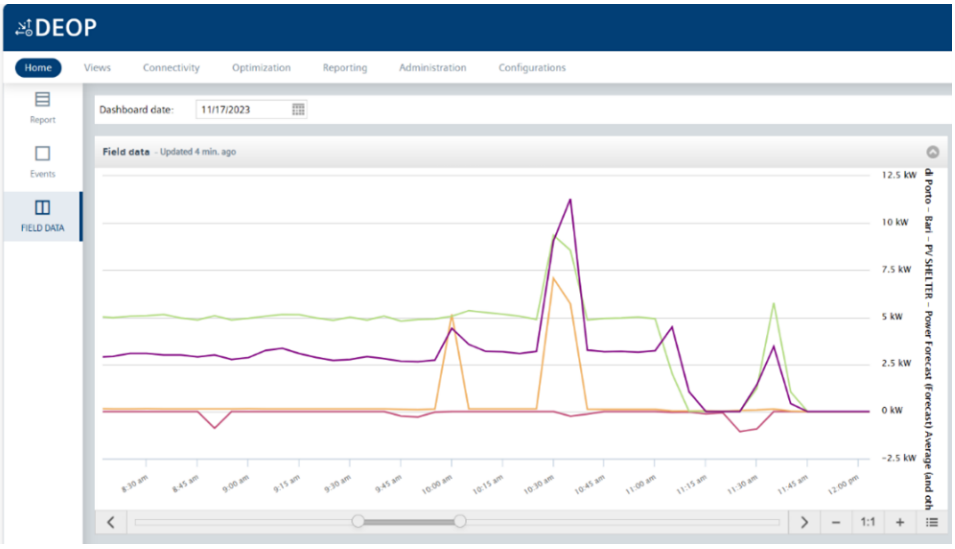

Figure 2.37: DC microgrid energy management system interface during charging test of EV1 at a V2G charging point (red: photovoltaic, orange: V2G station, green: total power at DC side including auxiliaries, purple: total power at AC converter side).

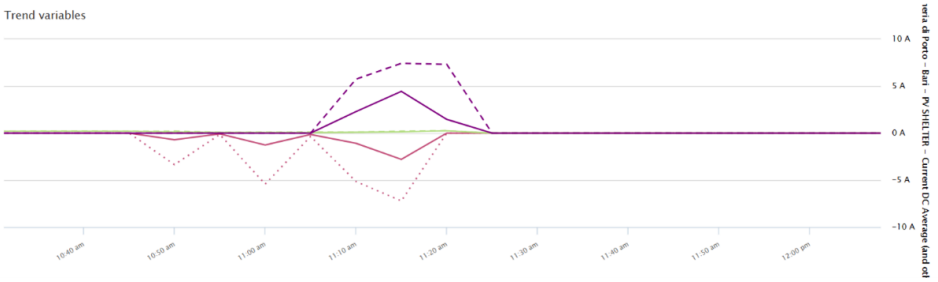

Figure 2.38: DC microgrid energy management system interface during island tests (solid: average values every 5 minutes, dashed/dotted: maximum values every 5 minutes; red: photovoltaic, green: total power at DC side including auxiliaries, purple: battery storage).

of a "load control area" in EVOS backend in order to directly control the charging process of the HPC station and of the V2G stations.

As a preliminary test, a session for the power modulation is accomplished using chargers in Enel laboratories, connected to EVOS platform, and to Energy Services Platform for the setpoint during charging and so the power modulation. The communication between EVOS and Energy Services platform is not based on same APIs shared with Politecnico di Bari, but is an internal communication. Third party backend platforms usually gather the properly details and information from EVOS database by means of interoperability services using specific APIs. On the other hand, this kind of test is useful to make sure all setpoints scenario, shared by Politecnico di Bari, can be reached by the chargers involved. In this re-

gard, extensive testing is performed with unidirectional HPC 75 kW, such as remote starting and charging stations power output modulation following the setpoints scenario scheduled. Tests are performed using either EV Volkswagen ID.3 or a battery simulator. In Table 2.17 setpoints for preliminary tests of fast-charging station are reported. The test duration is 22 minute, and power setpoints are sent with at least 1-minute time-step.

(a) (b)

Figure 2.39: HPC fast charging station ready to operate (a) and operation panel of the station (b).

Table 2.17: Setpoints for the preliminary test of fast charging station

Time	Output power [kW]
11:13	7.3706
11:15	58.157
11:19	9.7053
11:24	0
11:25	25
11:30	58.157
11:31	75
11:32	0
11:33	62.083
11:34	54.75
11:35	0

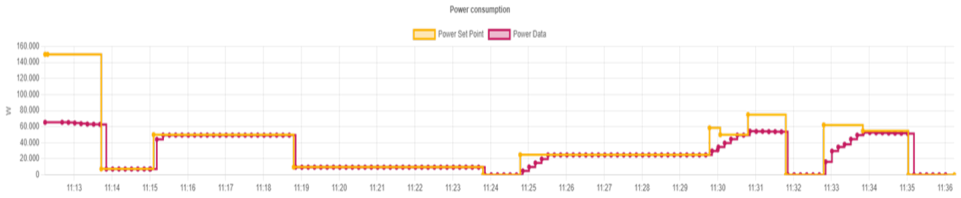

(a)

(b)

Figure 2.40: Comparison of power setpoint (a) and power output (b) by HPC fast charging station in the test.

From the test, it results that the HPC follows the setpoint got from Enel X Way platform, and the modulation works properly (see Fig. 2.40). In general, smart charging is more visible for low level of SOC where the EV can also charge at maximum power, otherwise due to the intrinsic nature of the battery, the power during charging decreases accordingly to the increasing of the SOC.

Chapter 3

Energy management strategies for a LEC of DC microgrids

The inclusion of EVSI in a energy community can be of particular interest expecially when bidirectional units are present. To this purpose, the combination of microgrids differently equipped with RES, BESS and EV charging stations, even in a DC configuration is addressed in this chapter. A two-stage approach to deal with the day-ahead scheduling problem associated with the operation of an energy community with the presence of clusters of EV charging stations is proposed in Section 3.1. In Section 3.1.1 the first stage, an ADMM-based procedure that minimizes the total energy procurement cost of the community is presented. In this stage, all the EV batteries connected to the same microgrid are represented by an aggregate storage unit with variable capacity and SOC, depending on EV arrivals and departures. In the second stage introduced in Section 3.1.2, local optimization algorithms provide the detailed scheduling for each component and charging station inside each microgrid. The second-stage optimization has been conceived to preserve the energy transactions with other participants and the external utility grid according to the first-stage solution.

Section 3.2 aims at extending the deterministic two-stage optimal procedure introducing the possibility for BESS and EV batteries to provide the reserve needed to cope with the uncertainties due to the fluctuations of solar generation. The main contributions of the procedure

are listed and discussed below:

- chance-constrained programming technique is implemented to EV-based DC microgrids in a LEC to model BESS and EV reserves by means of a set of probabilistic constraints in order to counterbalance the uncertainty associated with PV production within the microgrid (as proposed in Section 2.4). The application of the chance constrained approach is focused on the internal source of uncertainty. The effectiveness of chance-constrained method is further assessed through a comparison with simulation results of Monte-Carlo stochastic scenarios;
- the flexibility of EV charging stations and BESS to provide both up and down reserve is used to compensate the PV forecast uncertainties, accounting for specific technical constraints.

3.1 Deterministic two-stage approach for LEC operation planning

The day-ahead scheduling of an energy community of microgrids with the presence of EV charging stations is addressed by the two-stage scheduling approach illustrated in Fig. 3.1. In the first stage, an ADMM-based optimization approach is employed to define the scheduling of the resources for all the hours of the next day, following the procedure proposed in [112]. The community includes microgrids equipped with clusters of bidirectional EV charging stations and other prosumers (in the figure indicated as conventional) equipped with PV systems, storage units, and local loads. According to the ADMM procedure, the solution of the global optimization problem is distributed among the prosumers and microgrids that iteratively solve a local problem. The local optimization of each microgrid equipped with a cluster of bidirectional charging stations employs an aggregate representation of the connected EVs' batteries, like the one presented in [85]. The iterations are stopped when the equilibrium of the energy sold and bought between each couple of community participants is reached. The energy transactions between the prosumers and with

the external utility grid calculated by the first stage are provided to the second-stage local optimizations. For each EV-based microgrid, the second-stage optimization defines the individual scheduling of each charging stations whilst keeping the feasibility of the global solution of the energy community. The second-stage optimization can fully exploit V2G services provided by each connected EV.

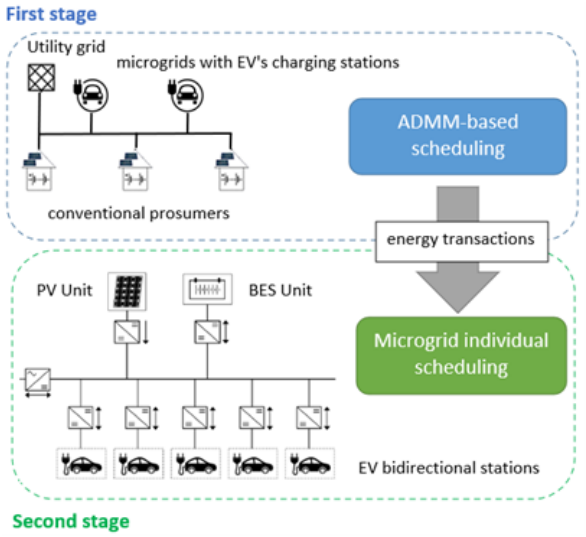

Figure 3.1: Scheme of the two-stage scheduling approach.

3.1.1 First Stage: scheduling of the transactions among the microgrid

The objective of the community EMS is the minimization of the total energy procurement cost during the next day. In the ADMM-based approach, the optimization is iteratively carried out by each participant. For each member i belonging to set Ω of the community participants, the local objective function is given by (3.1)

$$\begin{aligned} OF_i = \sum_{t \in T} \Big[& \pi_{buy}(t) \cdot P_{buy,i}(t) \cdot \Delta t - \pi_{sell}(t) \cdot P_{sell,i}(t) \cdot \Delta t + \\ & + \sum_{j \in \Omega, j \neq i} \lambda_j(t) \cdot P_{buyi,j}(t) \cdot \Delta t - \sum_{j \in \Omega, j \neq i} \lambda_i(t) \cdot P_{selli,j}(t) \cdot \Delta t + \\ & + l_i(t) + C_S(t) + w_{BES} \cdot (P^c_{BES,i}(t) + P^d_{BES,i}(t)) \Big] \end{aligned} \tag{3.1}$$

$$
\begin{aligned}
l_i(t) = & m \cdot \rho \cdot \Bigg[\sum_{j \in \Omega, j \neq i} \left(\hat{P}_{buy,ji}(t) - P_{sell,ji}(t) \right)^2 + \\
& + \sum_{j \in \Omega, j \neq i} \left(P_{buy,ij}(t) - \hat{P}_{sell,ji}(t) \right)^2 \Bigg]
\end{aligned}
\tag{3.2}
$$

$$
C_S(t) \geq \begin{cases} w_{EV} \cdot P_{clustEV}(t) \cdot \Delta t \quad if \ P_{clustEV}(t) \geq 0 \\ -w_{EV} \cdot P_{clustEV}(t) \cdot \Delta t \quad if \ P_{clustEV}(t) < 0 \end{cases} \tag{3.3}
$$

where $P_{buy,i}(t)$ and $P_{sell,i}(t)$ are the power exchanged with the external utility grid (considered as the energy provider for all the community participants) at each period t (when buying and selling, respectively). Prices $\pi_{buy}(t)$ and $\pi_{sell}(t)$ are the tariffs when buying and selling energy from and to the utility grid, respectively. Δt is the duration of each period t. $P_{buy,ij}(t)$ and $P_{sell,ij}(t)$ correspond to the power bought and sold by i-th LEC member from/to j-th member at time t. Lagrangian multipliers $\lambda_i(t)$ and $\lambda_j(t)$ are associated to the equilibrium between energy sold and bought in each power exchange inside the community. Term $l_i(t)$ uses scale factor m and parameter ρ to penalize the imbalances in the exchanges between i and every other participant at each time t, as in (3.2). Parameters $\hat{P}_{buy,ji}(t)$ and $\hat{P}_{sell,ji}(t)$ correspond to the most updated available optimization results of participant j. Both cost $C_S(t)$, associated with the operation of the charging stations, and wearing cost w_{BES}, associated with the charging and discharging processes of the BESS unit, are considered in (3.1). $P^c_{BES,i}(t)$ and $P^d_{BES,i}(t)$ are the charging and discharging power of the BESS unit, respectively. In (3.3), $P_{clustEV}(t)$ is the power output of the cluster of EVs' stations, assumed negative when charging and positive when exporting energy (i.e., providing V2G services). Cost w_{EV} corresponds to the average value of the wearing costs associated with charging and discharging processes of the EV batteries.

A forecast of the EV trips provides the time of departure and arrival for each EV together with the corresponding decrease in the energy stored in the EV's battery during each trip. Based on this information and the setting of the desired SOC at the departure of each EV, the proposed procedure calculates the total new available stored energy in the microgrid due

to EV arrivals at time t (E_{S+}) and the total stored energy subtracted to the microgrid due to EVs' departures at time t (E_{S-}), which are inputs of the optimization model. The total energy stored in the EVs' batteries at the end of period t (E_S) is given by (3.4)

$$E_S(t) = E_S(t-1) + E_{S+}(t) - E_{S-}(t) - \delta \cdot E_{RatedEV}(t) \tag{3.4}$$

where parameter δ is the self-discharge rate and $E_{RatedEV}(t)$ is the rated total capacity of the EVsconnected at the charging stations at each time t. Additional local constraints, i.e., the ones described in [112] for conventional prosumers, and in [85] for microgrids with the presence of charging stations, are included in the optimization model. The representation of the batteries considers efficiencies in charging and discharging processes of the BESS units, respectively. Analogously, average efficiencies are adopted in the model of EV clusters. Typical constraints are included to bound the operational values within maximum and minimum values. Moreover, constraints to avoid that the same participant simultaneously acts as producer and consumer are posed in the LEC model.

Once the ADMM procedure reaches the convergence, each LEC participant identifies the optimal scheduling of energy transactions with the external energy provider, energy transactions with other participants inside the LEC, the operation of the own BESS unit and, in the case of microgrids equipped with cluster of EV charging stations, the total power outputs of the EV cluster. The price for each energy transaction inside the community is also obtained.

3.1.2 Second Stage: Scheduling of EV-based microgrids

The layout of each parking lot includes a PV plant, a BESS and a set of bidirectional EV stations, enabled to exploit charging and V2G functionality, as described in Chapter 2. All internal sources are connected to the DC bus by mean of DC/DC bidirectional converters, except for the PV plant, whose converter is unidirectional. The EV-based microgrid is connected to the distribution grid through an AC/DC converter. The sold and bought power profiles for each EV-based microgrid (EVSI) are provided by the first stage optimization.

On this basis, the power allocation among the internal resources is scheduled to provide the same sold and bought power, the optimization problem for each microgrid with EVsaims to minimize an objective function that includes both the sum of quadratic deviations of bought and sold power in each time-step and the operating costs of the parking lot:

$$\begin{aligned} OF_{EVSI} = \sum_{t \in N_T} \Big\{ & \Delta t \cdot \left(P^{in}_{LEC}(t) - P^{in}_{g}(t)\right)^2 + \left(P^{out}_{LEC}(t) - P^{out}_{g}(t)\right)^2 + \\ & + \gamma \cdot \Delta t \cdot \Big[w_{BES} \cdot (P^{c}_{BES}(t) + P^{d}_{BES}(t)) + \\ & + \sum_{k}^{n_{EV}} (c_{EV,k} + w_{EV,k}) \cdot P^{c}_{EV,k}(t) + (-r_{EV,k} + w_{EV,k}) \cdot P^{d}_{EV,k}(t) \Big] \Big\} \end{aligned} \tag{3.5}$$

where $P^{in}_{g}(t)$, $P^{out}_{g}(t)$, $P^{c}_{BES}(t)$, $P^{d}_{BES}(t)$, $P^{c}_{EV,k}(t)$ and $P^{d}_{EV,k}(t)$ are the injected and withdrawn power, charging and discharging power of the BESS, and charging and discharging power of the k–th EV, respectively; γ is a penalty constant; w_{BES} and $w_{EV,k}$ are BESS and EV battery wearing costs, respectively; $c_{EV,k}$ and $r_{EV,k}$ represent the cost for the EV charge and the revenue for EV energy discharge. $P^{in}_{LEC}(t)$ and $P^{out}_{LEC}(t)$ are the injected and withdrawn power profiles evaluated as the sum of power purchased from the utility grid and from the other prosumers of the LEC as provided by the first stage optimization. The relations are reported in (3.6a)-(3.6b).

$$P^{in}_{LEC}(t) = P_{buy,i}(t) + \sum_{j \in \Omega, j \neq i} P_{buy,ij}(t) \tag{3.6a}$$

$$P^{out}_{LEC}(t) = P_{sell,i}(t) + \sum_{j \in \Omega, j \neq i} P_{sell,ij}(t) \tag{3.6b}$$

Since the objective function is quadratic, a piecewise linearization of the quadratic terms is carried out, in order to reformulate the model as a mixed-integer linear problem (MILP). In this study, two affine functions are evaluated for each quadratic term. Following the procedure in [113] and [114], the MILP reformulation is achieved introducing binary variables $\delta_{y,q}$, and auxiliary variables $z_{y,q}$ and $\tilde{z}_q$, as in (3.7a)-(3.7c).

$$\delta_{y,q} = \begin{cases} 0 \;\; if \;\; x \leq u_{y,q} \\ 1 \;\; if \;\; x \geq u_{y,q} \end{cases} \tag{3.7a}$$

$$z_{y,q} = \begin{cases} a_{y+1,q} \cdot x_q + b_{y+1,q} \quad if \;\; \delta_{y,q} = 1 \\ a_{y,q} \cdot x_q + b_{y,q} \quad if \;\; \delta_{y,q} = 0 \end{cases} \tag{3.7b}$$

$$\tilde{z}_q = \sum_{y}^{Y-1} z_{y,q} \tag{3.7c}$$

The indices y and q respectively represent the number of the strokes and the total number of quadratic linearized functions. Suitable inequality constraints are set in order to ensure proper relation among original and new variables, in a number of $(n_T \cdot 2 \cdot 8)$, with N_T number of time-steps, Y equal to 2 and q equal to 8. The MILP formulation of the problem is obtained by the linearizing the objective function in (3.5) - see (3.8), and the constraints regarding the operation of components of the microgrids (described in Section 2.2.1) and linearization variables, described in [114] and reported in (3.7a)-(3.7c). In order to evaluate if costs influence storage exploitation, a second objective function (3.9) is considered, that only involves BESS and EV wearing costs (i.e., $c_{EV,k}$ and $r_{EV,k}$ are null):

$$\begin{aligned} OF_{EVSI}^{lin} = & \sum_{q \in Q} \tilde{z}_q + \gamma \cdot \Delta t \cdot \sum_{t}^{N_T} \Big\{ w_{BES} \cdot \Big[P_{BES}^{c}(t) + P_{BES}^{d}(t) \Big] + \\ & + \sum_{k}^{n_{EV}} (c_{EV,k} + w_{EV,k}) \cdot P_{EV,k}^{c}(t) + \\ & + (-r_{EV,k} + w_{EV,k}) \cdot P_{EV,k}^{d}(t) \Big] \Big\} \end{aligned} \tag{3.8}$$

$$\begin{aligned} OF_{EVSI}^{lin,wear} = & \sum_{q \in Q} \tilde{z}_q + \gamma \cdot \Delta t \cdot \sum_{t \in T} \Big\{ w_{BES} \cdot \Big[P_{BES}^{c}(t) + P_{BES}^{d}(t) \Big] + \\ & + \sum_{k}^{n_{EV}} w_{EV,k} \Big[P_{EV,k}^{c}(t) + P_{EV,k}^{d}(t) \Big] \Big\} \end{aligned} \tag{3.9}$$

where Q is the set of quadratic terms, subject to the constraints described in [114] and in Section 2.2.1.

3.1.3 Description of the test case

The considered LEC corresponds to a set of five participants organized in one feeder and connected to the same low voltage network. Three of them (prosumer 1, 3 and 5) correspond

to prosumers equipped with a generating unit (e.g., PV unit), a BESS unit and local loads. The rest of participants (prosumer 2, indicated as EV-based microgrid 1, and prosumer 4, indicated as EV-based microgrid 2) correspond to two microgrids, each equipped with a cluster of bidirectional charging stations for EVs, a PV generating unit and a BESS. The optimization horizon corresponds to one day divided into 96 periods (Δt equal to 0.25 h). The price profile of buying ($\pi_{buy}(t)$) and selling ($\pi_{sell}(t)$) energy from and to the grid, and the profile of the PV power generation per installed area of PV unit are reported in Fig. 3.2. Fig. 3.3 shows the load profile of each prosumer in the community, adapted from [112].

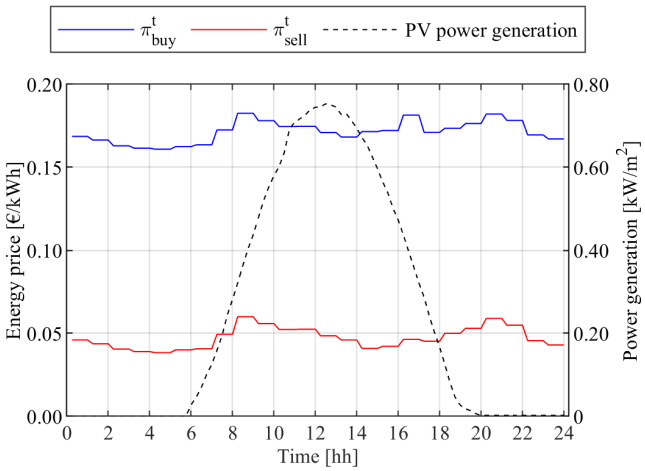

Figure 3.2: Price profile of the grid (buying and selling) and profile PV power generation per m^2 of panel surface.

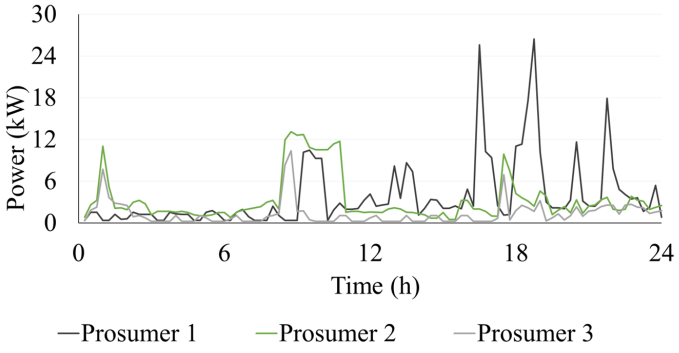

Figure 3.3: Load profile of each prosumer.

Each one of the prosumers is equipped with a PV -BESS system with the following characteristics: i) prosumer 1 with a 4-kW PV unit and a 5-kWh/5-kW BESS unit; ii) prosumer

2 with a 2.6-kW PV unit and a 4-kWh/4-kW BESS unit; iii) prosumer 3 with a 3.5-kW PV unit and a 3-kWh/3-kW BESS unit. For the prosumer BESS units, the minimum and maximum SOC are equal to 10% and 100% of the maximum capacity, respectively. The prosumers batteries have been assumed fully charged at the beginning and at the end of the day. Efficiencies $\eta^{c}_{BES,i}$ and $\eta^{d}_{BES,i}$ are equal to 0.96.

Each one of the microgrids is equipped with a 12.96-kW PV unit, a 50-kWh/30-kW BESS unit and 5 bidirectional charging stations. Efficiencies η^{c}_{BES} and η^{d}_{BES} are equal to 0.95. In this case, the minimum and maximum SOC are equal to 23% and 93% of the maximum capacity, respectively. The wearing costs are equal to 0.02 €/kWh. The EVs' capacity $E_{RatedEV}$ is equal to 30 kWh with a rated power equal to 10 kW. The wearing cots of EV is equal to 0.06 €/kWh. Average efficiencies $\eta^{c}_{EV,k}$ and $\eta^{d}_{EV,k}$ are equal to 0.95. Unit costs and EV discharge revenues are assumed as in Section 2.2.7. Revenue prices are chosen higher than charging costs, in order to promote V2G exploitation. The scheduling of arrivals and departures for the EVsin the microgrids are the same shown in Fig. 2.7a for microgrid 1 and Fig. 2.7b for microgrid 2. In microgrid 1 EV travels are frequent and short, while in microgrid 2 EVstake at least one long travel (especially EV4 and EV5). Full occupancy of the charging stations is assumed at the beginning and at the end of the day. The total energy stored in EVsat the beginning and at the end of the day is equal to 90% of the EV rated capacity ($E_{RatedEV}$). The EV SOC at every departure is assumed equal to 80% of $E_{RatedEV}$. The energy reduction in the EV battery during each Δt due to a scheduled trip is, on average, equal to 1.5 kWh [103]. In this study, γ is equal to 10 kWh^2/€.

3.1.4 Results: Day-ahead community scheduling

The first-stage optimization procedure has been implemented in AIMMS Developer and tested by using the Cplex V20.10 MILQP solver on 2-GHz processors with 8 GB of RAM, running 64-bit Windows. The ADMM convergence tolerance ϵ has been set equal to 25 W for the case study. The time employed to solve the day-ahead scheduling problem of five participants is around 300 s. Fig. 3.4 shows the obtained profile of the power exchanged

between the community and the external energy provider (positive if imported by the community and negative if exported by the community). Fig. 3.5 shows the power exchanged by each participant inside the community (positive if absorbed and negative if injected). It can be noted that EVSI mostly export energy to the other prosumers of the LEC. In particular, in the morning (from 00:00 to 10:45) EVSI microgrid 1 and 2 provide energy for prosumers 2 and 3, while only at 18:00 EVSI microgrid 1 buys energy from EVSI microgrid 2. Moreover, from 09:00 to 12:00 all LEC members sell energy to the distribution network. Table 3.1 shows the energy procurement cost for each community participant (negative values indicate revenues). The total cost calculation considers the energy transactions between each participant and the external energy provider and every other participant with the corresponding prices. Table 3.1 also shows the energy procurement cost obtained when energy transactions among community members are not allowed (i.e., without community). The distributed approach employed by the first stage of the approach allows an economic benefit for each participant with respect to the results without community.

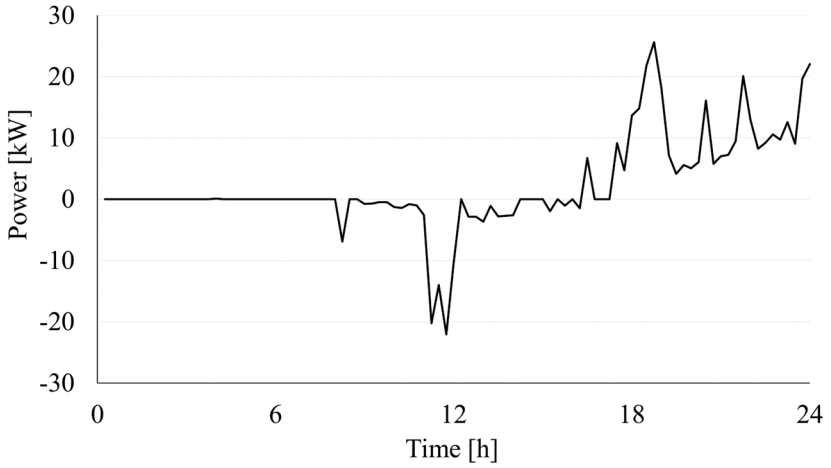

Figure 3.4: Total power exchanged by the community with the external energy provider.

3.1.5 Results: Day-ahead EV-based microgrid scheduling

The second stage optimization procedure is implemented in MATLAB environment, using *intlinprog* function. In Fig. 3.6, power exchanges in parking lot 1 are shown. It can be noted that EV1 operates in V2G mode from 00:15 to 03:15 to sell energy to the other

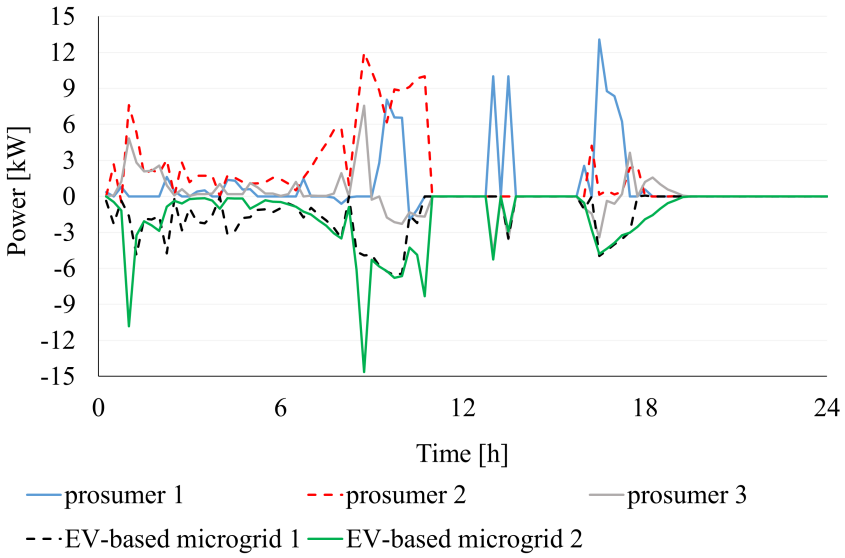

Figure 3.5: Power exchanged by each participant inside the community (positive if absorbed and negative if injected).

Table 3.1: Stage 1: Energy procurement cost in € for each community participant.

Participant	Community	Without community
prosumer 1	9.81	11.18
prosumer 2	6.92	11.11
prosumer 3	2.36	3.34
EV-based microgrid 1	-2.62	-1.39
EV-based microgrid 2	-3.53	-2.30

prosumers of the community. From 03:30 to 05:15 BESS discharging occurs to provide energy to the community. PV plant production is mostly sold to the LEC and distribution grid from 08:00 to 12:00. In the second part of the day EV charging is provided always by PV plant. Only at the end of day energy from the distribution grid is bought to charge EV1. Similar considerations could be made for power exchanges in microgrid 2 (Fig. 3.7). In the early hours of the day all the discharging power from EVsand BESS is sold to the community. During the central hours the availability of PV plant is partly used to charge EVs(particularly for EV4 that comes back from a 2-hours travel) and to exchange energy with community prosumers and distribution grid (Fig. 3.5). In these two systems, BESS exploitation is limited with respect to EVs. The reason is that revenues associated to the EV discharge encourage V2G exploitation. As a matter of fact, considering only wearing costs

of batteries, as in objective function (3.9), the different optimal solution for both microgrids of Fig. 3.8 shows a more intense BESS use. Similar behavior is found in the results relevant to microgrid 2.

Fig. 3.9 and Fig. 3.10 compare the parking lot aggregated power and the locally optimized power of the charging stations, showing the difference of EV exploitation depending on the presence or absence of revenues for V2G. It can be seen that more V2G exploitations occur in both EV-based microgrids when revenues are included in the objective functions, with respect to the only wearing cost inclusion. Local cost for EV-based microgrid 1 and 2 is calculated according to objective function (3.5). Local daily cost of microgrid 2 (7.93 €) is lower than microgrid 1 (10.71 €), because the amount of energy sold to distribution grid and prosumers is higher. Therefore, bigger revenue due to a more intense discharge of EV influences the final cost of the microgrid.

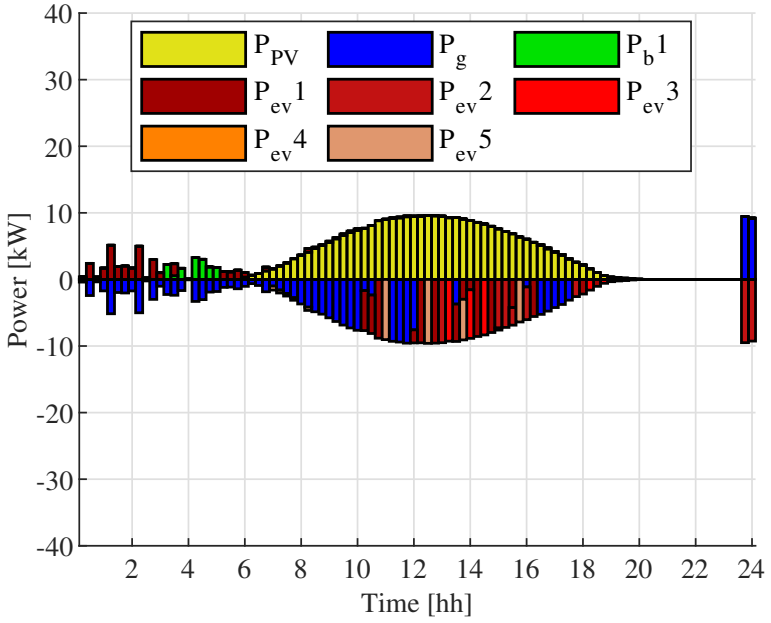

Figure 3.6: Power exchanges in EV-based microgrid 1.

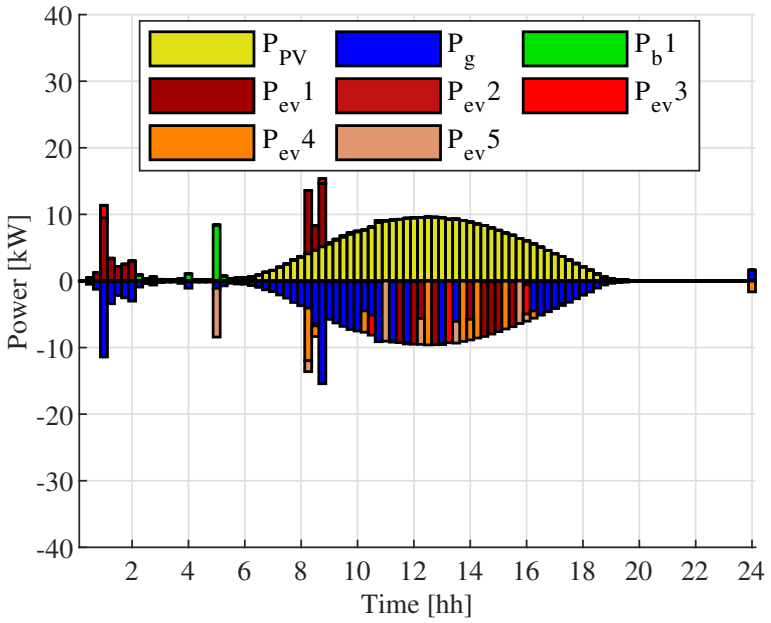

Figure 3.7: Power exchanges in EV-based microgrid 2.

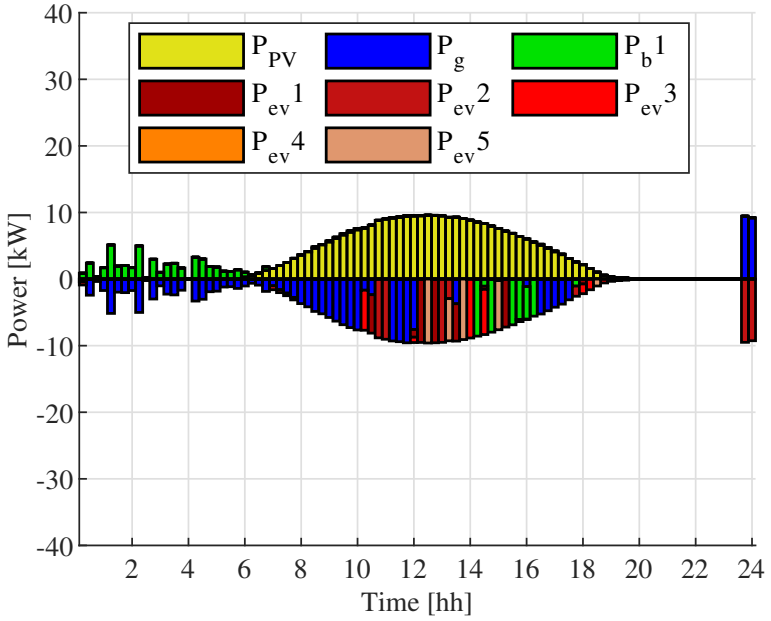

Figure 3.8: Power exchanges in EV-based microgrid 1, considering only wearing costs of batteries.

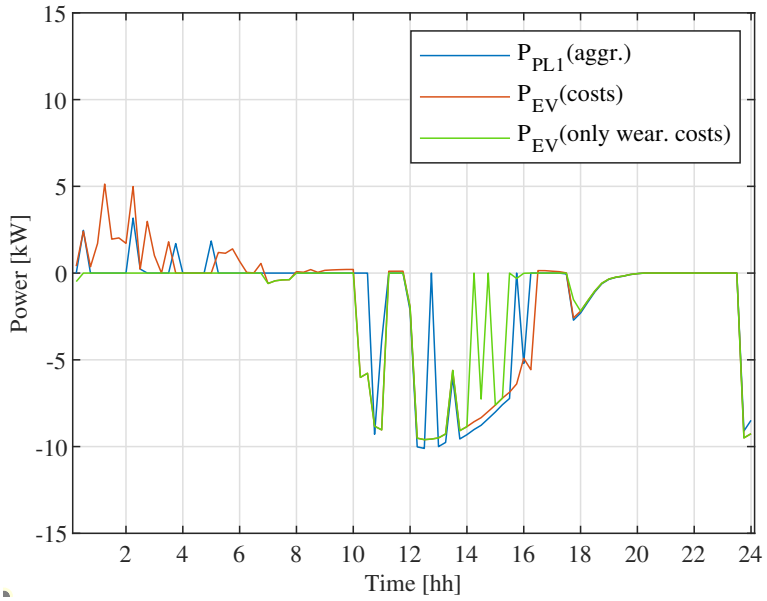

Figure 3.9: EV-based microgrid 1 aggregated power and the locally optimized power of the charging stations.

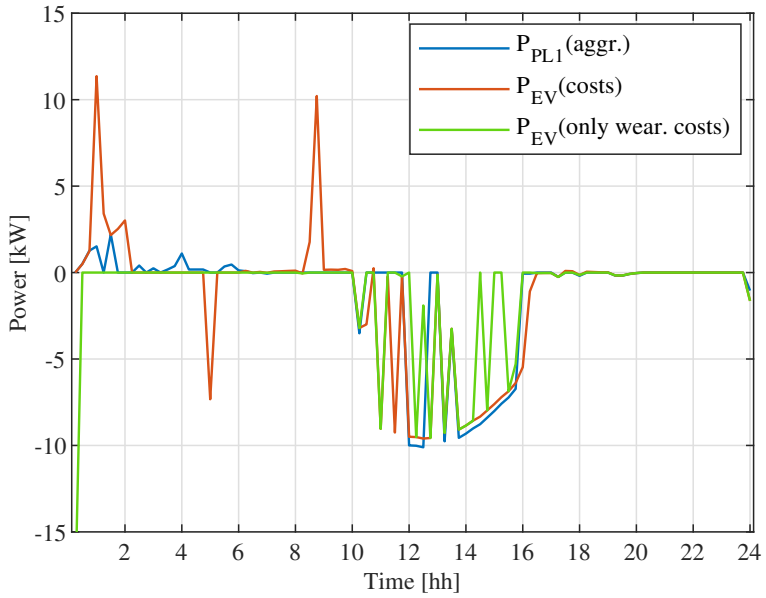

Figure 3.10: EV-based microgrid 2 aggregated power and the locally optimized power of the charging stations.

3.2 Stochastic approach for two-stage strategy for reserve provision within LEC

By extending the deterministic two-stage optimal procedure proposed in Section 3.1 for the day-ahead energy management of a LEC of DC microgrids with bidirectional EV charging

stations, this Section presents a procedure that calculates the optimal scheduling of the community considering also the possibility for BESS and EV batteries to provide the reserve needed to cope with the uncertainties due to the fluctuations in solar generation forecast. The procedure is applied in order to evaluate reserve provision from only BESS and then from BESS and EV batteries.

3.2.1 Chance-constrained methodology

The chance-constrained approach already presented in Section 2.4 is implemented in the second stage of the procedure introduced in Section 3.1.2, assuming uncertainties in solar production and neglecting EV SOC at plug-in time uncertainty. Therefore, $\epsilon_S(t^{arr}_{EV,k})$ in (2.21) is considered null in this case, implying that total positive and negative errors only depend on error in solar forecast. Moreover, quantiles of PV error distribution $q^{PV,+}_{1-\alpha^+}$ and $q^{PV,-}_{1-\alpha^-}$ are calculated as in (2.25a) and (2.25b), whereas $q^{S,k,+}_{1-\alpha^+}$ and $q^{S,k,-}_{1-\alpha^-}$ are considered null.

The objective function of the second stage is the one linearized in (3.8), considering all operating costs. Moreover, technical constraints for microgrid components as presented in Section 2.2.1 are added in the formulation, whereas for positive and negative reserve when provided only by BESS are the ones in (2.26a)-(2.26d), while constraints (2.27a) and (2.27b) are considered when reserve is both provided by BESS and EVs. Constraints related to auxiliary variables for the linearization of the quadratic terms (3.7a)-(3.7c) are included as well.

3.2.2 Case study and results

The case study considered is the one already presented in Section 3.1.3, while the error of solar forecast considered is reported in Table 2.12 for both PV systems (that follow the same configuration of the one in Section 2.4) in microgrid 1 and 2. Constraint violation probabilities α^+ and α^- are both set equal to 5% for each time-step. Fig. 3.11 shows the probability distribution functions of the error at specific times (namely, 9:00, 12:00 and 16:00) and the related positive quantile values. As expected, probability distribution at 12:00 is less steep

than others at 9:00 and 16:00 characterized by lower σ_ϵ values. Similar observations hold for negative error probability distribution functions. In Fig. 3.12 optimal power exchanges

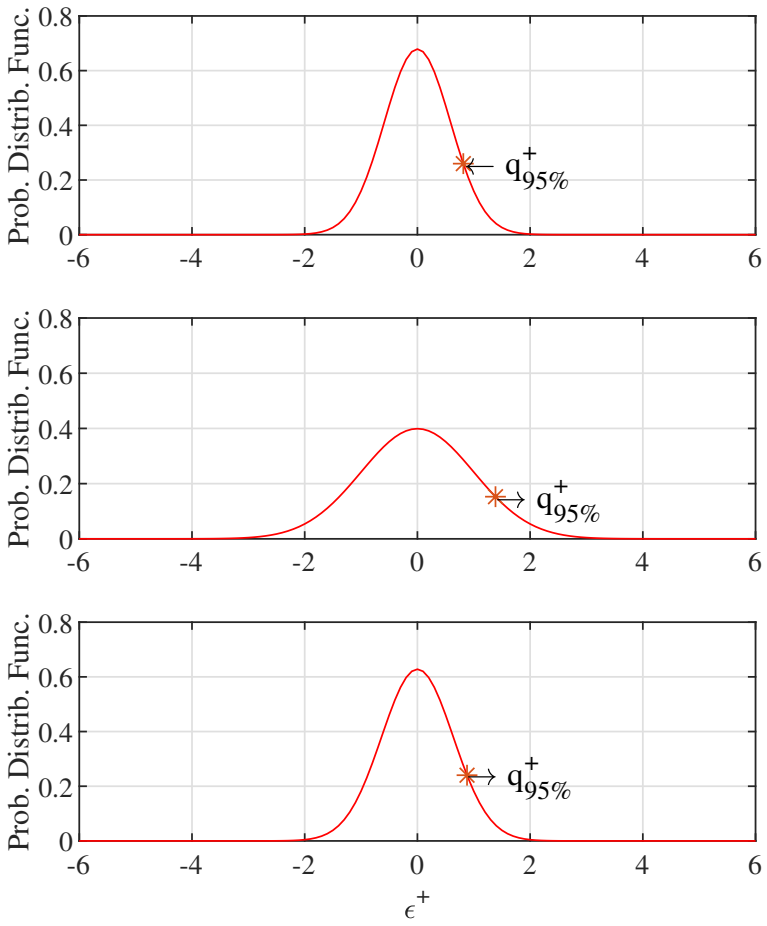

Figure 3.11: Error probability distributions and positive quantile values relevant to the PV generation forecast at 9:00 (top), 12:00 (middle) and 16:00 (bottom).

in microgrid 1 are shown, considering the reserve provided by the BESS unit. Comparing to the results in Fig. 3.6 without reserve provision, all units in the microgrid follow a similar behavior. Reserve guaranteed with a probability of 90% by the BESS unit (being α^+ and α^- equal to 5%, as mentioned) is shown in Fig. 3.13. The maximum value of reserve (both positive and negative) to be provided is 1.7 kW at 12:30. The value of reserve would increase considering lower values of α^+ and α^-. On the contrary, higher values of admitted violation probability would imply lower values of reserve to be guaranteed. EV-based microgrid 2 power exchanges shown in Fig. 3.14 are slightly different from Fig. 3.7 in terms

of EV exchange powers. Reserve provided is the same to microgrid 1 since the same error probability distribution is assumed on the same PV production curve.

The inclusion of EV batteries in the reserve provision procedure affects the power ex-

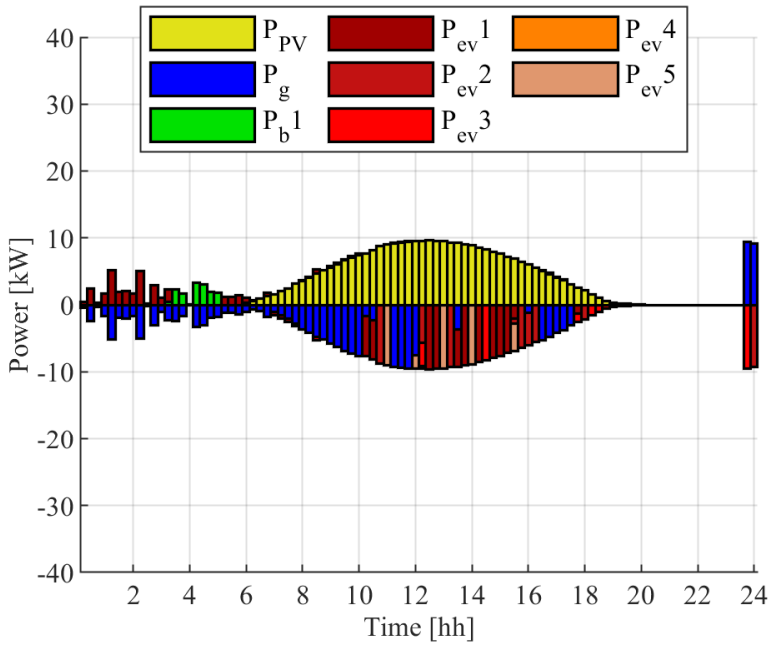

Figure 3.12: Power exchanges in microgrid 1, considering the reserve provided by the BESS unit.

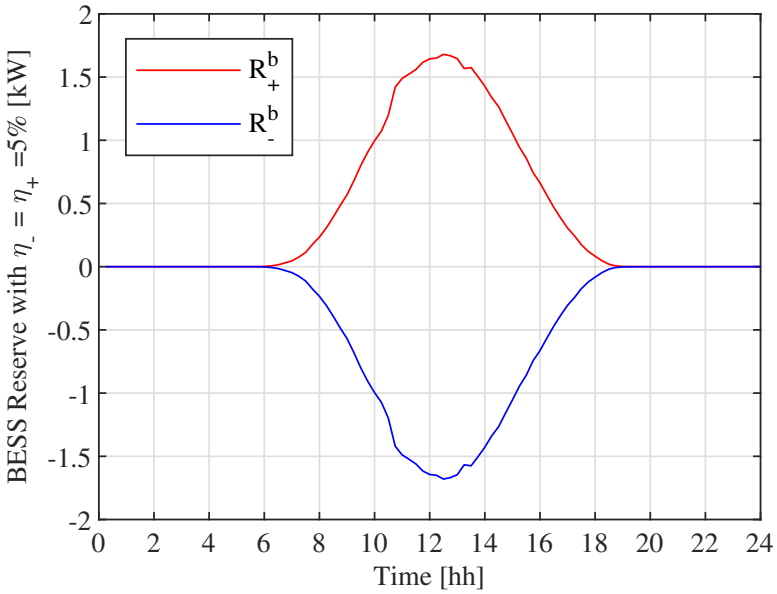

Figure 3.13: Positive and negative reserve in microgrid 1 provided by the BESS unit.

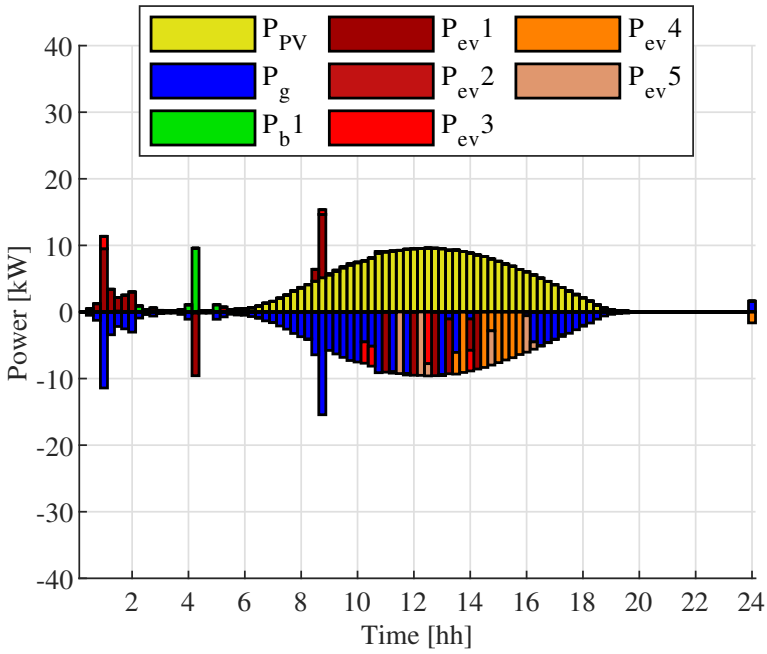

Figure 3.14: Power exchanges in microgrid 2, considering the reserve provided by the BESS unit.

changes within microgrids. In Fig. 3.15 the reserve levels and power exchanges in microgrid 1 are shown. From 00:00 to 06:00 BESS discharging occurs to provide energy externally with a grid exchange profile close to the previous case given by slight EV discharge (see Fig. 3.6 and Fig. 3.12), then EVs and BESS exchange energy among each other (see Fig. 3.15b). BESS charge is seen at 10:00-11:00, replacing EV charge of previous case and avoiding delivering powerr to the grid. Intense EV charge is detected in the afternoon, reached by means of BESS discharge without requiring power from the grid. Fig. 3.15a shows the total positive and negative reserve dispatched among storage devices. Most reserve energy is provided by BESS, since EV batteries cannot be available when EVs are not connected to the charging stations. Positive reserve corresponds to a discharging event, i.e., additional generation, while negative reserve represents a charging event of the storage, i.e., additional load.

Fig. 3.16 compares the SOC level profiles of the BESS unit and EV batteries of microgrid 1 for three cases: without reserve provision, when the reserve is provided only by the BESS unit, and when the reserve is provided by both the BESS unit and the EV batteries. No significant differences from the first case (no reserve provision operation) are shown in

the profiles when the reserve is provided by the BESS unit only. Different profiles are in general obtained, even for the SOC levels of the BESS unit, when the reserve is provided also by the EVs connected to the charging stations. In the considered scenario, the BESS unit experiences significant discharges during the first hours of the day, replacing the use of EV1 in order to provide upward reserve during first hours of PV production, and between 13:00 and 14:00, EV1 discharges at 20:00, EV3 discharges at 08:00. The different power exchanges in microgrid 2 and the corresponding reserve provisions are shown in Fig. 3.17. Negative reserve is mostly provided by EV batteries, as in Fig. 3.17a. Like microgrid 1, the BESS unit guarantees most of the positive reserve, especially in the first half of the daily PV production.

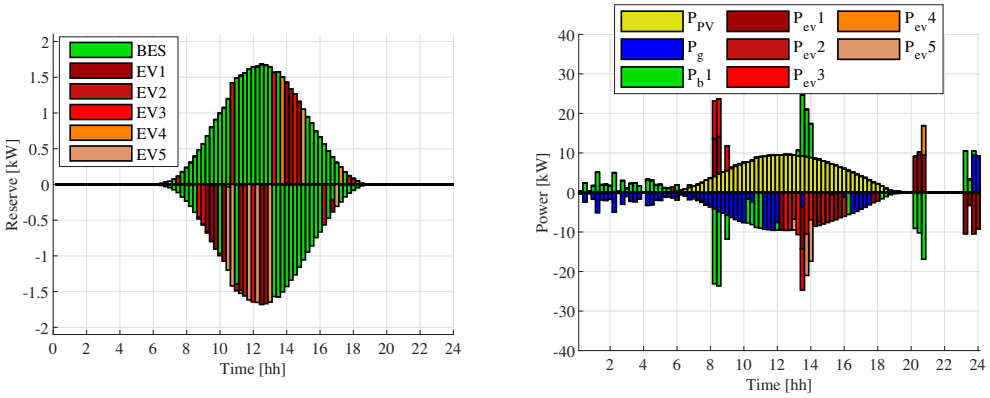

(a) (b)

Figure 3.15: Reserve levels (a) and power exchanges (b) in EV-based microgrid 1, when both BESS and EVs provide reserve.

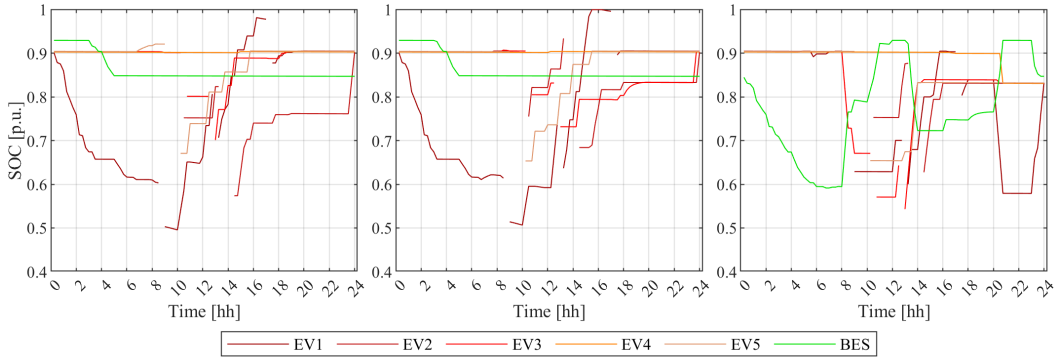

Figure 3.16: SOC levels of BESS unit and EV batteries in EV-based microgrid 1 considering no reserve provision (left), only reserve provided by BESS (middle) and reserve provided by BESS unit and EV batteries (right).

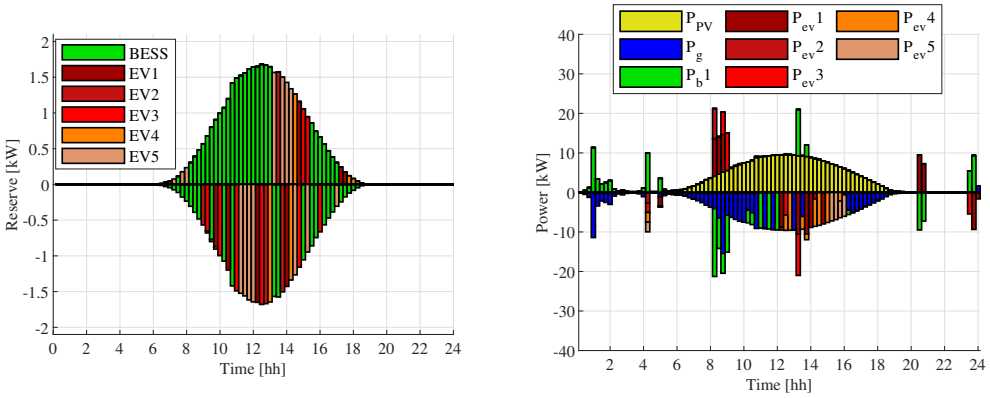

(a) (b)

Figure 3.17: Reserve levels (a) and power exchanges (b) in EV-based microgrid 2, when both BESS and EVs provide reserve.

In Table 3.2 a comparison of the operating costs of each microgrid with EV charging stations in the two cases is carried out: when the reserve is provided only by the BESS unit and when the reserve is provided by both the BESS units and the EV batteries. The costs are evaluated considering the forecasted PV profile and the economic part of objective function in (3.5), without additional costs or revenues related to reserve provision. The daily costs of both EV-based microgrid are lower in the case the reserve is provided by both BESS units and EV batteries. The benefit is expected to be lower when there is a significant uncertainty associated with the presence and state of charge of the EVs connected to the charging stations during the day. It should be remarked that for both the microgrids the daily operating cost of BESS reserve case is very close to the values obtained in the deterministic procedure provided in Section 3.1.5. From the analyses of the results, it is possible to assess that the optimal procedure guarantees the LEC operation plan of power exchange optimized in the first-stage, while providing internal reserve in the presence of forecasting errors.

Table 3.2: Daily operating costs of EV-based microgrids of the LEC

	BESS reserve	**BESS and EV batteries reserve**
EV-based microgrid 1	10.70 €	7.05 €
EV-based microgrid 2	7.92 €	5.17 €

3.2.3 Validation of the chance constrained procedure

In order to assess the advantages of the proposed chance constrained programming procedure, a comparison with the results of Monte-Carlo simulations is carried out. In particular, for microgrid 1, a set of 30 scenarios is considered, in which the PV production level at each daylight timestep is varied by a stochastic quantity deriving from the error probability distribution functions defined in Section 3.1.2, supposed independent from each other. The variations of PV production are depicted in Fig. 3.18, and compared with the total reserve levels, defined by (2.27a) and (2.27b) and illustrated in Fig. 3.13 and Fig. 3.15a. Roughly 10% of samples lay beyond the reserve amount, in agreement with the considered α^+ and α^- values. Each scenario is analyzed by means of the deterministic technique described in Section 3.1, with the same objective function involving operation costs and variations from community-level power exchanges at grid connection point. In this way, for each scenario, a different scheduling of the microgrid devices (EVs, BESS, grid connection) is obtained, representing the effective exploitation of the chance-constrained reserve amounts in each particular situation.

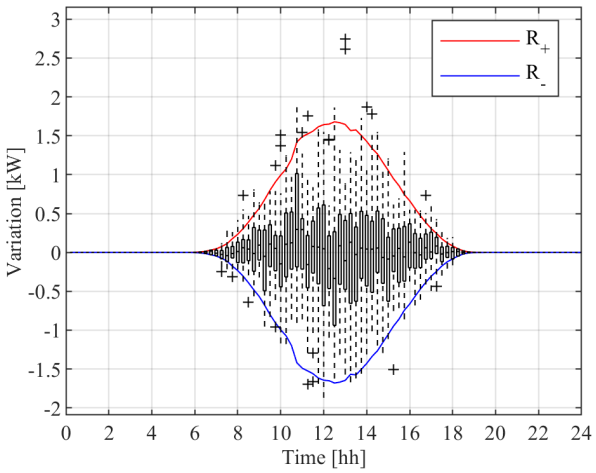

Figure 3.18: Distribution of samples for PV production Monte-Carlo scenarios and comparison with reserve levels according to quantiles for microgrid 1.

The obtained results are summarized in Fig. 3.19, that shows the variation of grid exchanges and costs with respect to chance-constrained procedure outcomes. It can be observed that Monte-Carlo stochastic scenarios do not reach solutions characterized by lower values of the objective function components than the corresponding ones in the chance-constrained formulation. In half of Monte-Carlo scenarios, grid power exchange levels are respected, whereas in other scenarios are slightly varied – by less than 1.1 kWh at most – increasing the total bought energy. The operating costs in all scenarios show a slight increase. The proposed comparative analysis shows that the chance-constrained procedure is able to find a feasible and more efficient solution representing the boundary of Monte-Carlo scenarios solutions, therefore it is able to schedule the internal reserve to cope with PV forecasting error within the defined quantile thresholds, while enabling community-level plan compliance and reasonably attaining lowest operation costs.

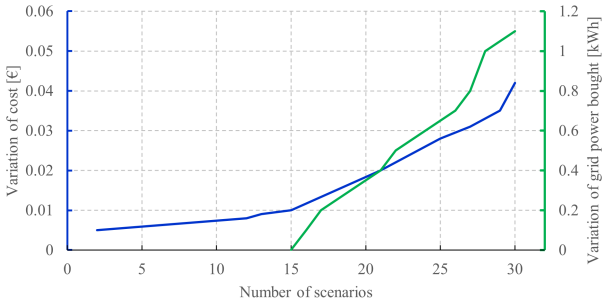

Figure 3.19: Cumulative distribution of variation of grid energy bought in the Monte-Carlo scenarios (blue – left axis) and of daily operation costs (green – right axis) with respect to chance-constrained solution of microgrid 1.

Chapter 4

EV charging infrastructure integration in distribution networks

In this chapter, the impact of EV charging infrastructure integration on the distribution network operation is assessed by firstly studying the environmental and economic system impact of the BESS and EV interaction in EV parking lot, implementing an optimal procedure to different scenarios. This activity is carried out with the collaboration of the School of Engineering of Cardiff University, and it is described in Section 4.1.

The EV integration is then evaluated by a technical grid point of view by reducing the detail of charging infrastructures within the distribution grid model. Section 4.2 provides an otimization procedure for the operation of the grid involving EVs, and the subsequent implementation in a MV grid is presented in Sections 4.3 and 4.4.

EV clusters integration into MV grid is also studied in Section 4.5, and in Section 4.6 for LV semi-urban grid. This activity put the basis for the techno-economic impact of DC microgrid integration into distribution grid, whose procedure and implementation are described in Section 4.7. Finally, an economic analysis concerning the perspective of aggregating microgrids into energy communities is carried out in the Section 4.8.

4.1 Carbon emission evaluation of assistant BESS in EV parking lots

The study presented in this section focuses on examining how the integration of stationary BESS into EVSI can contribute to the reduction of carbon emissions and enhance the overall sustainability of the energy system by exploring the potential synergies between BESS, type of EV charging and carbon intensity. For this aim, an optimal operation programming procedure is carried out on weekly time horizon, accounting for costs and emission objectives and considering technical operation features. The main contributions can be summarized as follows:

- the impact of BESS is assessed by means of optimal weekly scheduling procedure considering economic (cost minimization) and environmental (indirect carbon emission minimization) targets,
- different BESS sizes are examined for evaluating possible better exploitations, and different weeks of operation as well,
- slow and fast EV charging rates are considered, in order to assess the impact of dumb and smart fast charging stations on the operation of the system and on total carbon emissions.

Technical and economic indicators are defined and evaluated on weekly time frame in order to estimate them over a yearly time horizon.

4.1.1 Problem formulation considering uncoordinated EV charge

The proposed methodology employs a linear mixed-integer optimization problem to program the BESS discharging to provide energy for EV charging, while minimising the total daily CO_2 emissions. The assumptions underlying the procedure are described in the following:

- arrival times, charging durations and energy needs for each EV are determined generating samples from probability distributions,

- BESS optimal planning over the entire time horizon is carried out only for EV charging energy provision, not considering any further strategic behavior with respect to the external network.

The optimal procedure employs a MILP problem (see the structure in (2.1)) aiming at coordinating the exploitation of the BESS with EV uncontrolled (or dumb) charging, in order to obtain a power exchange with the external electric grid $P_g^{in}(t)$, for each time step t in the considered time horizon (with N_T timesteps), able to reach defined objective f subject to proper linear constraints. Two different objective functions are inspected, represented by total CO_2 emissions f^{CO_2} and total operation cost f^{Cost}, as defined in (4.1) and (4.2) respectively:

$$f^{CO_2} = \Delta T \cdot \sum_{t}^{N_T} CI(t) \cdot P_g^{in}(t) \tag{4.1}$$

$$f^{Cost} = \Delta T \cdot \sum_{t}^{N_T} P_{buy}(t) \cdot P_g^{in}(t) \tag{4.2}$$

where ΔT is the time-step duration in hours, $CI(t)$ is the carbon intensity expressed in gCO_2/kWh in the t-th time-step, $P_{buy}(t)$ is the purchase energy price from the grid in t-th time-step.

The problem is enriched with constraints related to the determination of power exchange with the grid, as in (4.3), where BESS active charging power ($P_{BESS}^c(t)$) and discharging power ($P_{BESS}^d(t)$) for each time step t represent further state variables, while $P_{EVs}^{dumb}(t)$ is the input referring to the total charging demand of EVs in the t-th time-step. In the procedure, the constraints are mainly related to technical limits of the BESS. In particular, constraints in (4.4) and (4.5) take into account technical limits of charge/discharge power of the BESS for each time-step. In order to make BESS discharge contribution available only for the charging of vehicles, $P_{BESS}^d(t)$ should have values lower or equal to EV demand at each time step, as in (4.6). Moreover, binary state variables $v_{BESS}^c(t)$ and $v_{BESS}^c(t)$ account for unidirectionality of BESS power exchanges, assuming value of 1 if the BESS is charging (or discharging), and 0 if not, as in (4.7). Constraints (4.8) and (4.9) limit charg-

ing/discharging power to the maximum values when binary variables are active. Equality constraint in (4.10) represents the evolution of BESS SOC $S_{BESS}(t)$ for each time-step, accounting for charge/discharge efficiencies ($\eta^c_{BESS}(t)$ and $\eta^d_{BESS}(t)$) as well, whereas (4.11) and (4.12) fix the initial and final SOC over the considered time horizon. Finally, in (4.13) proper limits on SOC evolution within feasible range for the considered BESS.

$$P^{in}_g(t) = P_{EVs}(t) - P^d_{BESS}(t) + P^c_{BESS}(t) \;\; \forall t \in [1, ..., N_T] \tag{4.3}$$

$$P^{c,min}_{BESS} \leq P^c_{BESS}(t) \leq P^{c,MAX}_{BESS} \;\; \forall t \in [1, ..., N_T] \tag{4.4}$$

$$P^{d,min}_{BESS} \leq P^d_{BESS}(t) \leq P^{d,MAX}_{BESS} \;\; \forall t \in [1, ..., N_T] \tag{4.5}$$

$$P^d_{BESS}(t) \leq P_{EVs}(t) \;\; \forall t \in [1, ..., N_T] \tag{4.6}$$

$$v^c_{BESS}(t) + v^d_{BESS}(t) \leq 1 \;\; \forall t \in [1, ..., N_T] \tag{4.7}$$

$$P^c_{BESS}(t) \leq P^{c,MAX}_{BESS} \cdot v^c_{BESS}(t) \;\; \forall t \in [1, ..., N_T] \tag{4.8}$$

$$P^d_{BESS}(t) \leq P^{d,MAX}_{BESS} \cdot v^d_{BESS}(t) \;\; \forall t \in [1, ..., N_T] \tag{4.9}$$

$$\begin{aligned} S_{BESS}(t) =& S_{BESS}(t-1) + \Delta T \cdot \eta^c_{BESS}(t) \cdot P^c_{BESS}(t) + \\ & - \Delta T \cdot \frac{1}{\eta^d_{BESS}(t)} \cdot P^d_{BESS}(t) \;\; \forall t \in [2, ..., N_T - 1] \end{aligned} \tag{4.10}$$

$$S_{BESS}(1) = S^i_{BESS} \tag{4.11}$$

$$S_{BESS}(N_T) = S^f_{BESS} \tag{4.12}$$

$$S^{min}_{BESS} \leq S_{BESS}(t) \leq S^{MAX}_{BESS} \;\; \forall t \in [1, ..., N_T] \tag{4.13}$$

The total number of state variables for the formulated problem with EV uncontrolled charging is $5 \times N_T$, the number of inequality constraints – including (4.4)-(4.5) and (4.7)-(4.9) – is $10 \cdot N_T$ and the number of equality constraints – including (4.3) and (4.10)-(4.12) – is $2 \times N_T + 2$. In particular, the quantity $P^{dumb}_{EVs}(t)$ represents the total charging demand in

t-th time step of a total number of n_{EV}, and under the assumption of uncontrolled charging, based on proper forecasts on EV maximum power rate P_{EVs}^{MAX} and arrival/departure time t_{in}^{v}, t_{out}^{v} and SOC, it is determined as follows:

$$P_{EVs}^{dumb}(t) = \sum_{v}^{n_{EV}} P_v(t) \;\; \forall t \in [1, ..., N_T] \tag{4.14}$$

$$P_v(t) = \begin{cases} 0 \;\; if \;\; t \notin [t_{in}^{v}; t_{out}^{v}] \\ \min(P_{v,M}; P_{EVs}^{MAX}) \;\; if \;\; t \in [t_{in}^{v}; t_{out}^{v}] \end{cases} \tag{4.15}$$

$$S_v(t) = S_v(t-1) + \Delta T \cdot \eta_v^c(t) \cdot P_v^c(t) \;\; \forall t \in [1, ..., N_T] \tag{4.16}$$

$$P_{v,M}(t) = \frac{S_v^{MAX} - S_v(t)}{\Delta T \cdot \eta_v^c(t)} \;\; \forall t \in [1, ..., N_T] \tag{4.17}$$

$$E_{EVs}^{target} = \Delta T \cdot \sum_{t}^{Ntd} P_{EVs}^{dumb}(t) \tag{4.18}$$

where $P_v(t)$ is the power required by the single EV in time-step t, which corresponds to the minimum between the maximum charging power and the modulated power $P_{v,M}$ for reaching maximum SOC (4.17). SOC levels $S_v(t)$ evaluation is reported in (4.16). Furthermore, the total daily energy required by EVs is calculated as in (4.18), where Ntd represents the number of time-step in each day.

4.1.2 Problem formulation considering EV smart charge

In order to investigate the effects of EV smart charging on CO_2 emissions and costs, the problem described in the Section 4.1.1 is slightly modified, considering as additional state variable $P_{EVs}(t)$, representing the aggregated power requested by EVs for each time step. This aggregated power is limited to a maximum value that depends both on the number of plugged-in EV for each time-step $N_{EVs}(t)$ and maximum power of the EV charging point P_{EVs}^{MAX} as reported in (4.19). Furthermore, the same daily charging energy (as in dumb-charging problem) is guaranteed by constraints in (4.20) for each day of the week.

$$0 \leq P_{EVs}(t) \leq N_{EVs}(t) \cdot P_{EVs}^{MAX} \quad \forall t \in [1, ..., N_T] \tag{4.19}$$

$$\sum_{t}^{Ntd} \Delta T \cdot P_{EVs}(t) = E_{EVs}^{target} \tag{4.20}$$

The aforementioned constraints are still included in the problem formulation. In particular, with EV smart charging $P_{EVs}(t)$ is considered as a state variable in (4.3) and (4.6) instead of the known value obtained for dumb charging as described before. Furthermore, some limitation are set to $P_g^{in}(t)$ in order to not exceed power peaks requested by EVs, compared to the case of uncontrolled charging.

The total number of state variables for the formulated problem with EV smart charging is $6 \times N_T$, the number of inequality constraints – including (4.4)-(4.5), (4.7)-(4.9) and (4.19) – is $12 \times N_T$ and the number of equality constraints – including (4.3), (4.10)-(4.12) and (4.20) – is $2 \times N_T + 7$.

4.1.3 Definition of indicators

The definition of proper economic and technical indicators is useful for comparing results, in order to assess which strategy achieves better performances as compared to the respective base case, represented by the EV dumb charging without the stationary BESS, e.g. considering $P_{BESS}^{d}(t) = P_{BESS}^{c}(t) = 0$, at the same EV charging rate of the optimised cases. Thus, for each weekly time horizon of the simulation the CO_2 emission variation of the optimized value reported in (4.1) with respect to the base case represents the technical indicator, and it is evaluated as in (4.21). Moreover, variation of costs for energy purchasing evaluated in (4.2) with respect to the base case represents the economic indicator, as reported in (4.22). The analysis is carried out on time horizons representing different weeks of the year, therefore the annual values of the indicators are derived as well in (4.23) and (4.24), being k the general period and W_k the number of weeks of the represented time horizon in each period. Furthermore, the usage of BESS is assessed by means of the equiv-

alent discharging cycle number n_{BESS}^{disch}, evaluated as in (4.25), where η_{BESS}^{d} is the BESS discharge efficiency, while H_{BESS} is the BESS capacity. Yearly evaluation of the indicator is reported in (4.26) as well.

$$\begin{aligned}\Delta CO_2 =& CO_2^{BESS} - CO_2^{noBESS} = \\ =& \Delta T \cdot \left(\sum_{t}^{N_T} CI(t) \cdot P_g^{in}(t) - \sum_{t}^{N_T} CI(t) \cdot P_{EVs}(t) \right)\end{aligned} \tag{4.21}$$

$$\begin{aligned}\Delta cost =& Cost^{BESS} - Cost^{noBESS} = \\ =& \Delta T \cdot \left(\sum_{t}^{N_T} P_{buy}(t) \cdot P_g^{in}(t) - \sum_{t}^{N_T} P_{buy}(t) \cdot P_{EVs}(t) \right)\end{aligned} \tag{4.22}$$

$$Y\Delta CO_2 = \sum_{k} W_k \cdot \Delta CO_{2,k} \tag{4.23}$$

$$Y\Delta cost = \sum_{k} W_k \cdot \Delta cost_k \tag{4.24}$$

$$n_{BESS}^{disch} = \sum_{t}^{N_T} \frac{\Delta T \cdot P_{BESS}^{d}(t)}{\eta_{BESS}^{d} \cdot H_{BESS}} \tag{4.25}$$

$$Y n_{BESS}^{disch} = \sum_{k} W_k \cdot n_{BESS,k}^{disch} \tag{4.26}$$

4.1.4 Case study description

The analyses are carried out considering a time horizon that spans 1 week, which is further divided into N_T =336 time steps with 30-minute duration (ΔT=0.5 h). The carbon intensity data utilized in the evaluation is sourced from [115] and pertains to the year 2022 for UK system. Fig. 4.1 shows the average CI evaluated monthly from 2018 to 2022. It can be seen that the overall trend is decreasing through years, with a minimum annual average in 2020 (due to the pandemic). In 2022 the average value is 27% lower than one in 2018 and 15% lower than one in 2019. Fig. 4.2 shows CI trends for each season used for the weekly analyses of the parking lot.

Regarding energy prices, Fig. 4.3 reports energy costs that are determined by elaborating 2022 UK price system analysis report data [116]. In particular, energy prices are eval-

uated considering average system price distinguished in values for short and long system, along with percentage of system length, reported by day of the season and by settlement period (30-minute period) over the season.

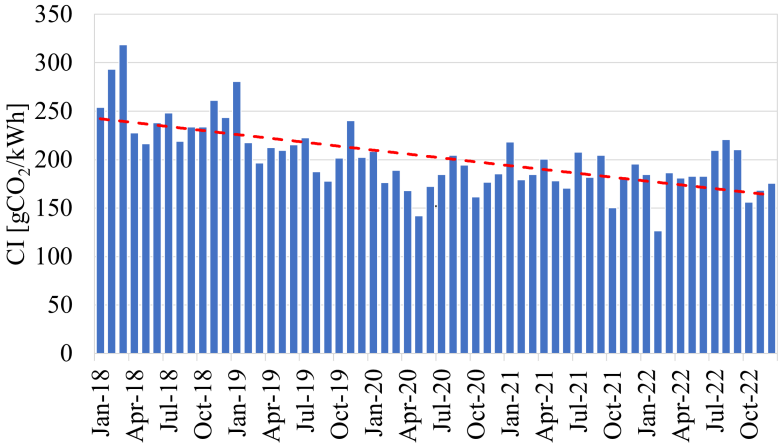

Figure 4.1: Monthly average CI from 2018 to 2022. Source [115].

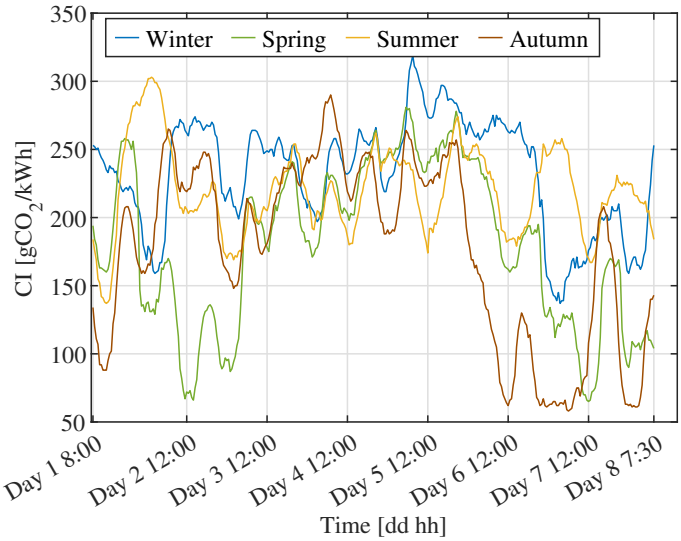

Figure 4.2: CI index over a week for each season over 2022. Source [115].

The inclusion of a $LiFePO_4$ stationary BESS in the system is evaluated through the simulation of two configurations, assuming charge/discharge efficiency of 0.95 initial and final SOC (S^i_{BESS} and S^f_{BESS}) at 90% of maximum capacity H_{BESS} and minimum/maximum SOC levels (S^{min}_{BESS} and S^{MAX}_{BESS}) of 20% and 90% of the capacity, respectively. The two configuration are reported in the following:

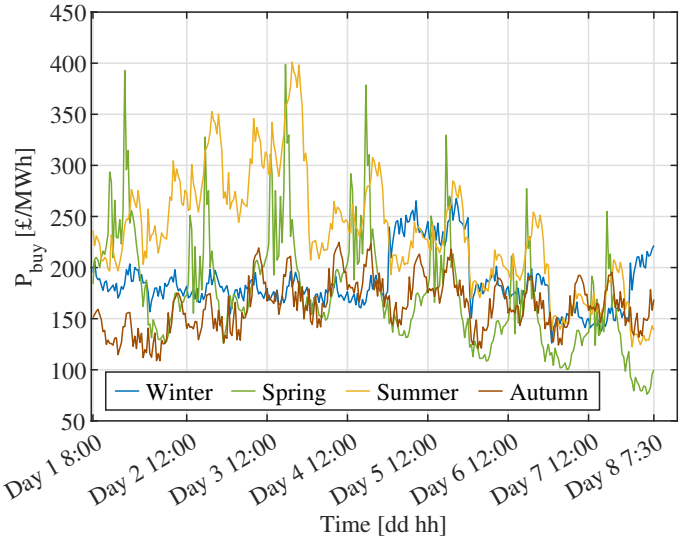

Figure 4.3: Energy prices over a week for each season over 2022. Source [116].

- BS 1: Capacity H_{BESS} of 1 MWh, with maximum charging/discharging power ($P_{BESS}^{c,MAX}$ and $P_{BESS}^{d,MAX}$) of 300 kW,
- BS 2: Capacity H_{BESS} of 4 MWh, with maximum charging and discharging power of namely 500 kW and 1.2 MW.

The case study refers to a parking lot of 83 EV charging stations. In order to construct an insightful case study reflecting practical scenarios, a survey of three distinct parking locations is conducted by physically observing and recording vehicle activities within the Cardiff area multiple times daily over a two-week period in two separate months. Among these sites, two were linked to workplaces, while the third served as a general-use parking facility primarily catering to individuals visiting the city center or engaging in shopping activities. Notably, the workplace parking areas exhibited substantial variability, attributed largely to the presence of contractors and visiting vehicles. According to the obtained data, the EV usage is modelled through a probabilistic approach that involves Normal distribution probabilities of plug-in start time and plug-in duration, whose parameters are reported in Table 4.1. Moreover, EVs are assumed to be charged considering separately a slow fixed rate of 7.4 kW, an accelerated 24 kW (over all the parking time), fast 50 kW and ultra-fast 150 kW (attaining a total energy amount of the charge E_{EVs}^{target} equal to a medium-speed

charge at 24 kW throughout the parking time interval).

System operation over a year is evaluated, in uncontrolled and smart charging, by the combination among one week per season (considering 4 seasons with average week number W_k=13.04), two BESS sizes, and four EV charging rates, and are simulated considering economic and technical targets. Therefore, the optimization problems described in Section 4.1.1 and 4.1.2 are run in 64 different combinations, respectively.

Table 4.1: Distribution probability parameters for EV usage.

Plug-in times	**Mean**	**Standard Deviation**
Start time [hh:mm]	12:15	02:45
Duration [h]	2.13	0.38

4.1.5 Results with EV uncoordinated charge

Concerning the operation with slow 7.4 kW charging rate, the power exchanges during winter week with technical objective (4.1) are shown in Fig. 4.4a-c, where it can be seen that BESS contribute to charge EVs when CO_2 minimization strategy is implemented, especially considering a 4 MWh capacity in BS 2 (Fig. 4.4c) where the BESS is able to cover most of EV charging energy requirements during the week, deferring power absorption from the external electric grid in most suitable time intervals. Lowest peak (485 kW, almost 79% of the EV installed power) is detected for 7.4 kW during winter week, as expected since it is the lowest charging rate considered. With the objective of energy cost minimization (4.2) the observed results are different: most of energy required for EV charging is purchased by the external grid in both BS 1 and BS 2 cases (see Fig. 4.4b-d). However, highest purchased power peaks are detected for CO_2 minimization in all scenarios, but especially for 24 kW charging rate and BS 2 configuration (nearly 1.4 MW peak due to BESS and EV charge, see Fig. 4.5, corresponding to 70% of total installed power), since energy from utility grid (requested when CI is low) is used for charging both EVs and BESS. The fast-charging rate of 150 kW leads to higher EV power peaks, in particular 1.7 MW peak (nearly 13.7% of total EV installed power) in BS 2 configuration in spring and summer weeks considering f^{Cost}, and winter weeks considering f^{Cost} is the results of required power by BESS and EVs.

Moreover higher energy requirements for EV charge cannot be fully provided by BESS, even considering BS 2 configuration, as reported in Fig. 4.6. With technical objective, charging events of BESS occur during night hours in winter season, according to low CI (Fig. 4.6a-c), while in summer the BESS is charged during the central hours of the day exploiting higher renewable contribution reducing carbon intensity. Considering economic target (Fig. 4.6b-d), BESS charging is always located in night hours, due to lower energy purchase costs. However, independently on configurations, BESS is not fully exploited when economic target is optimized, since the problem solution tends to reduce energy costs related to BESS recharge.

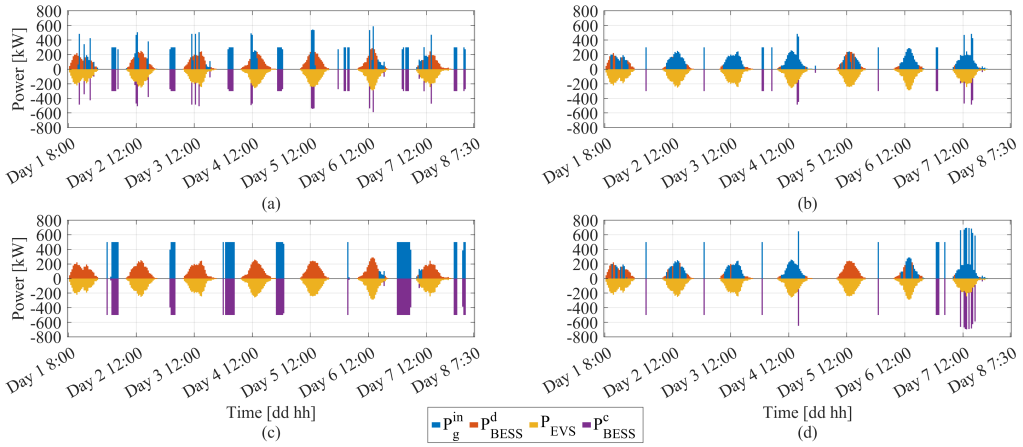

Figure 4.4: Power exchanges during winter for EV dumb charge at 7.4 kW charging rate, considering technical target with BS 1 (a) and BS 2 (c) configuration, and economic target with BS 1 (b) and BS 2 (d).

4.1.6 Results with EV smart charge

Results related to EV Smart Charging (SC) procedure considering economic and environmental targets are reported for BS 1 and BS 2 in Fig. 4.7, referring to winter week. It can be noted that EV smart charging profiles are different with respect to the dumb-charging cases. With BS 1, when optimizing f^{CO_2}, charging processes of EVs are concentrated during periods of low carbon intensity, around 12:00, as in Fig. 4.7a, while minimizing f^{Cost} it is concentrated in the early afternoon when energy costs are low as well, see Fig.4.7c. Configuration BS 2 shows significant exploitation for energy provision to the parking lot,

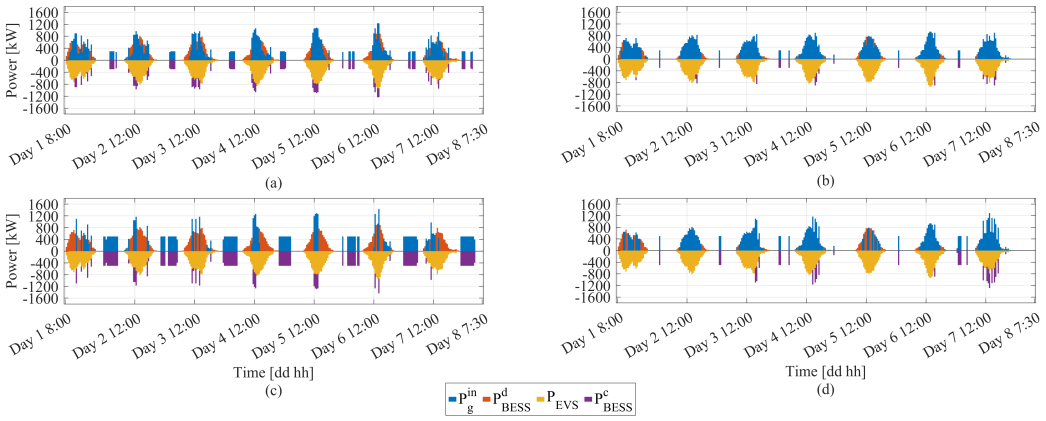

Figure 4.5: Power exchanges during winter for EV dumb charge at 24 kW charging rate, considering technical target with BS 1 (a) and BS 2 (c) configuration, and economic target with BS 1 (b) and BS 2 (d).

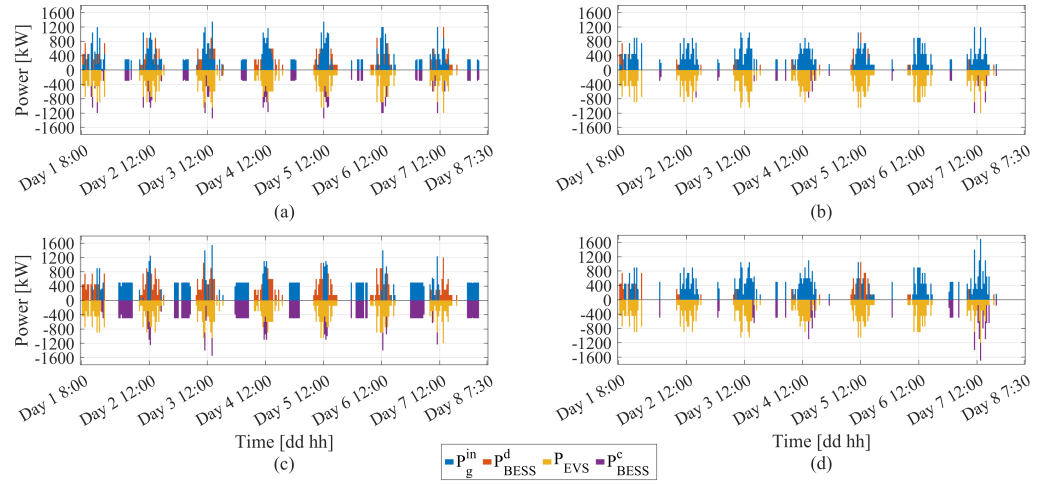

Figure 4.6: Power exchanges during winter for EV dumb charge at 150 kW charging rate, considering technical target with BS 1 (a) and BS 2 (c) configuration, and economic target with BS 1 (b) and BS 2 (d).

especially with f^{CO_2} minimization (Fig. 4.7b). BESS charging processes occur during night hour of the day, for both technical and economic targets. Power peaks registered do not exceed the value of 1.8 MW in all scenarios, nearly the 14.4% of the installed power considering the higher charging rate of 150 kW, similarly to the peaks depicted in the case of uncontrolled charging, thus avoiding line overloading conditions with higher peak values. However, the peak is reached for only EV charging in economic optimization, while by BESS and EV in the technical optimization, as in Fig. 4.7.

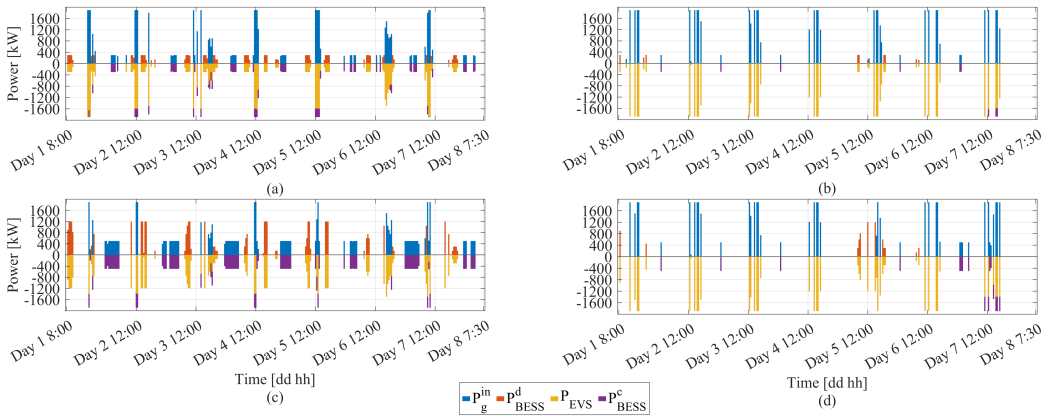

Figure 4.7: Power exchanges during winter for EV smart charge at 150 kW charging rate, considering technical target with BS 1 (a) and BS 2 (c) configuration, and economic target with BS 1 (b) and BS 2 (d).

4.1.7 Evaluation of indicators

The evaluation of indicators formulated in Section 4.1.3 is carried out and reported in Figg. 4.8-4.9 for a single example season and in Tables 4.2-4.3 for the yearly time frame.

Remarkable CO_2 reductions with respect to the base case are achieved with the environmental target and considering BS 2 configuration for all charging rates (Fig 4.8c), since the presence of stationary storage can provide energy to EVs when CI is high, whereas charging BESS during low levels of CI. However, the attainment of environmental target implies an increase of operation costs, that is more evident with fast charging rates (Fig. 4.8a). As regards smart charging the advantage is more evident with 150 kW size, whereas 50 kW smart charging does not perform well in the BS 2 configuration. When considering economic target, lower costs are obtained in all scenarios considering BS 2 with respect to BS 1 for each charging rate. The adoption of charging rates higher than 24 kW with dumb charging implies little improvement of the cost indicator. Moreover, the highest cost reductions with economic target are depicted considering EV smart charging with 150 kW rate (Fig. 4.8b), while CO_2 increase is detected especially for BS 2 and fast charging rate scenarios, except for winter season where CO_2 reduction is still detected for both sizes of storage and all charging rates (Fig. 4.8d), pointing out a combined optimal solution for both indicators.

As regards yearly evaluation, Table 4.2 illustrates the values of indicators for environmental

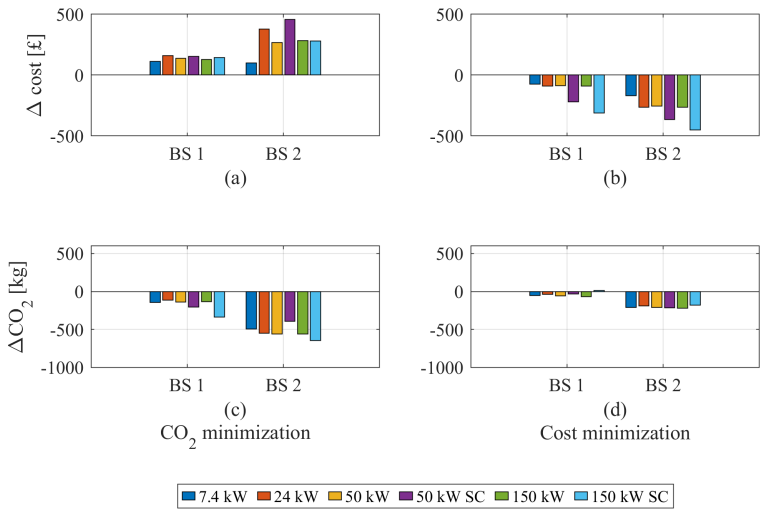

Figure 4.8: Winter week. Total daily cost variation (a)-(b) and CO_2 variations (c)-(d) for both BS configurations and optimal strategies.

target in all scenarios. It can be seen that BS 2 guarantees both cost and CO_2 reductions over the year, except for the case of 50 kW EV SC, whereas for BS 1 configuration and high charging rates (from 50 kW to 150 kW smart charging), an increase in operation costs is detected. It could be pointed out that EV smart charging procedure achieves higher CO_2 reduction already in BS 1 configuration (with respect to the uncontrolled charging), avoiding also the usage of bigger storage systems: as a matter of fact 26 958 kg CO_2 reduction with 150 kW SC rate with BS 1 are quite close to 31 438 kg CO_2 reduction with 150 kW uncontrolled-charging with BS 2 configuration. However, environmental target leads to higher number of equivalent discharging cycles, especially with 50 kW SC rate (483.4 cycles, more than one full cycle per day), whereas BS 2 configuration leads to lower discharge cycles over one year operation (44% average reduction).

Results of economic target are reported in Table 4.3, where it seems that significant cost reduction is achieved when stationary storage supports EV charge, especially considering BS 2 configuration. As for environmental target, EV smart charging procedure achieves higher cost reduction already in BS 1 configuration, avoiding also the usage of bigger storage systems: for instance, 32 302 £ reduction considering 150 kW SC rate and BS 1 is quite near to the 36 511 £ reduction with BS 2 and EV uncontrolled charging. Generally, CO_2 increase is depicted in the economic optimal procedure. However, smart charging mode

allows to achieve lower CO_2 increases with the respect to the uncontrolled charge in BS 2 configuration (for 50 kW and 150 kW). Furthermore, discharge cycle number are lower than in the case of environmental target, and smart charging mode for 50 kW and 150 kW leads to lower discharge cycles than uncontrolled charging at the same EV charging rate. Analogously to environmental target, BS 2 configuration allows even low discharging cycles (less than one cycle per day), avoiding excessive BESS wearing and life reduction.
Fig. 4.9 shows the number of BESS equivalent discharging cycles over a weekly operation for all the seasons and charging rates. It can be noted that, with CO_2 minimization target, higher cycles are reached in winter week, while in spring and autumn weeks higher cycles occur with economic target. Considering BS 1 configuration, cost minimization employs lower BESS discharge cycles with respect to the economic target, since lower exploitation is detected. Moreover, with cost minimization and BS 1, EV smart charging allows better exploitation of storage, with respect to the uncontrolled charging, with cycle numbers similar to the BS 2 ones. With cost minimization, BS 2 implies higher advantage on cycles in autumn and in summer.

Table 4.2: Indicator evaluation over a year - CO_2 minimization.

CO_2 MINIMIZATION							
		7.4 kW	24 kW	50 kW	50 kW SC	150 kW	150 kW SC
$\Delta cost$ [£]	BS 1	-132	-1 932	+906	+ 1 174	+1 128	+ 1 474
	BS 2	-3 790	-1 770	-1 228	+ 4 363	-641	-779
ΔCO_2 [kg]	BS 1	-9 317	-10 428	-9 928	-16 951	-9 628	-26 958
	BS 2	-25 186	-35 059	-30 849	-22 846	-31 438	-40 985
BS cycles	BS 1	344.3	476.5	337.9	483.4	450.0	384.1
	BS 2	127.4	262.4	223.0	305.3	241.7	225.6

4.2 Optimal EV operation for grid technical targets

In this section, a description of the methodology for EV integration in distribution grids is proposed, with the aim of investigating the impact of V2G technology on the grid operation.

The adopted methodology employs load-flow analyses to assess the impact of uncontrolled EV charging where the charge power is set at maximum level – according to EV bat-

Table 4.3: Indicator evaluation over a year - Cost minimization.

COST MINIMIZATION

		7.4 kW	24 kW	50 kW	50 kW SC	150 kW	150 kW SC
$\Delta cost$ [£]	BS 1	-12 082	-17 007	-14 558	-24 872	-14 414	-32 302
	BS 2	-22 494	-39 695	-33 783	-38 257	-36 511	-44 878
ΔCO_2 [kg]	BS 1	+2 608	+2 452	+2 999	+ 2 439	+2 809	+ 4 537
	BS 2	-718	+5 652	+7 446	+ 1 873	+8 135	+ 5 280
BS cycles	BS 1	241.6	351.7	283.2	202.8	285.9	173.5
	BS 2	107.9	190.3	177.8	133.1	184.1	126.4

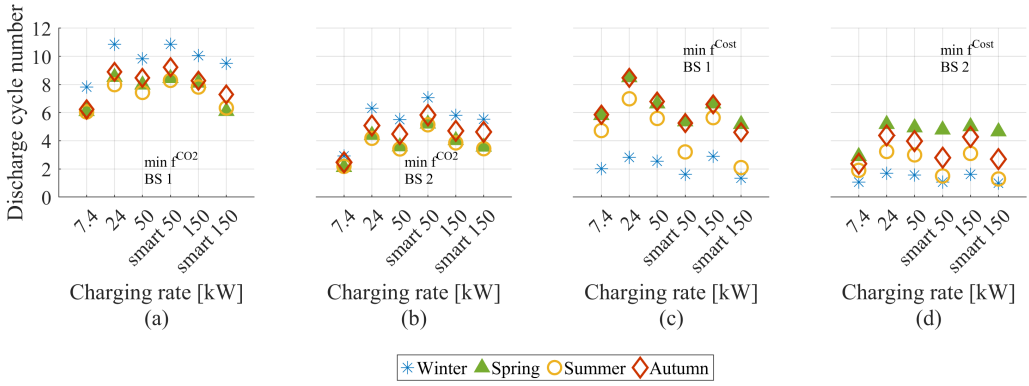

Figure 4.9: BESS equivalent discharging cycles, evaluated in all scenarios.

tery and station features – until the required energy amount of the EV is reached. Whereas, a MILP approach, whose structured is reported in (2.1), is adopted for investigating the grid behavior in both the controlled EV charging and V2G cases, considering a linearized load-flow model, as a constraint of the optimization, whose goal is to evaluate the charging/discharging powers of the considered EVs that minimize the system daily energy losses. Preliminary load-flow analyses (implemented, by means of the Matpower tool, in Matlab environment) are carried out to assess the most burdensome load profile in the absence of EVs. In this regard, different scenarios are investigated, sorted according to the type of loads (residential, industrial, etc.), day of the week (working day, weekend day), and season of the year. Once the number of stations (and EVs) is determined, MILP optimization is carried out (in Matlab environment) to evaluate the effects of controlled EV charging and V2G strategies. In this regard, a random EV users' behavior (i.e., departure and arrival stations, plug-in time intervals, energy consumption during trips, etc.) is assumed.

4.2.1 MILP problem for optimal day operation of the grid involving EVs

The optimal daily operation of the network integrating V2G features represents a complex problem that considers system non-linearities and discontinuities. In order to reduce the complexity of the problem and to facilitate the evaluation of the optimal solution for the network, taking into account the behavior of electric vehicles, a MILP technique is used for the system model linearization. The assumptions underlying the procedure are: i) EVs connected to the grid do not provide reactive power regulation, ii) radial configuration of the grid, considering one generation node and $n-1$ load nodes, iii) for all EVs, with aleatory behaviors, two charging events and one route between them are considered.

The state vector $\mathbf{x}$ includes for each time-step t of the daily horizon, the nodal voltage phases (in radians) and amplitudes (p.u.) - θ_i and V_i -,generated and withdrawn powers ($P_{G,i}$ and $P_{D,i}$), power levels of the installed EV stations ($P_{CS,i}$) at the i-th node of the grid; active and reactive power flows of the h-th network line ($P_{flow,h}$ and $Q_{flow,h}$), charge and discharge powers ($P^c_{EV,k}$ and $P^d_{EV,k}$), and SOC levels ($S_{EV,k}$) of the k-th EV.

The objective function represents the grid total energy losses, as expressed in (4.27), where $P_L(t)$ represents the grid active power losses in the generic time-step t, evaluated as the total difference between generated and withdrawn power at the n nodes of the network, whereas ΔT is the time interval between two consecutive steps expressed in hours.

$$f^{loss} = \sum_{t}^{N_T} \Delta T \cdot P_L(t) = \sum_{t}^{N_T} \Delta T \cdot \sum_{i}^{n} [P_{G,i}(t) - P_{D,i}(t)] \tag{4.27}$$

The problem involves constraints that take into account linearized load-flow equations (by means of sensitivity coefficients), reported in (4.28)-(4.32). In particular, $\hat{\theta}^0_i(t)$ and $\hat{V}^0_i(t)$ represent voltage phase and magnitude for each node i and time-step t during grid operation without EVs, whereas $\hat{P}^0_{flow,h}(t)$ and $\hat{Q}^0_{flow,h}(t)$ represent active and reactive power flows for each line h of the grid without EVs. Moreover, $\hat{P}^0_{G,1}(t)$ is the value of the assumed generated power at the slack node 1, in the absence of EVs, whereas $\hat{\sigma}_{\theta ji}(t)$, $\hat{\sigma}_{vji}(t)$, $\hat{\sigma}_{pjh}(t)$, $\hat{\sigma}_{qjh}(t)$ and $\hat{\sigma}_{pjG1}(t)$ represent the sensitivity coefficients of the network

variables for small variations of active power applied to each load node k, determined by repeated load flow simulations around working point in the absence of EVs.

$$\theta_i(t) = \hat{\theta}_i^0(t) + \sum_{k=2}^{n} \hat{\sigma}_{\theta ki}(t) \cdot P_{CS,k} \;\; \forall i \in [1; n], \; \forall t \in [1; N_T] \tag{4.28}$$

$$V_i(t) = \hat{V}_i^0(t) + \sum_{k=2}^{n} \hat{\sigma}_{vki}(t) \cdot P_{CS,k} \;\; \forall i \in [1; n], \; \forall t \in [1; N_T] \tag{4.29}$$

$$P_{flow,h}(t) = \hat{P}_{flow,h}^0(t) + \sum_{k=2}^{n} \hat{\sigma}_{pki}(t) \cdot P_{CS,k} \;\; \forall h \in [1; N_L], \; \forall t \in [1; N_T] \tag{4.30}$$

$$Q_{flow,h}(t) = \hat{Q}_{flow,h}^0(t) + \sum_{k=2}^{n} \hat{\sigma}_{qki}(t) \cdot P_{CS,k} \;\; \forall h \in [1; N_L], \; \forall t \in [1; N_T] \tag{4.31}$$

$$P_{G1}(t) = \hat{P}_{G1}^0(t) + \sum_{k=2}^{n} \hat{\sigma}_{pkG1}(t) \cdot P_{CS,k} \;\; \forall t \in [1; N_T] \tag{4.32}$$

For each j-th EV, the evaluation of SOC $S_{EV,j}$ is included in (4.33), where $\hat{S}_{EV,j}^{in,1}$ is the state of charge at the beginning of the first charging event, $\Delta S_{EV,j}^{trip}(t)$ is the SOC reduction during the trip between the two charging events, and $\eta_{EV,j}^{c}$ and $\eta_{EV,j}^{d}$ are charging and discharging efficiencies.

Moreover, the grid model includes constraints that avoid that the same charging station in acting simultaneously in charging and discharging modes. A binary parameter $\beta_{i,j}(t)$ assigns at each time step t the j-th EV to the EV station installed at i-th node, therefore $P_{CS,i}$ is determined as in (4.34).

$$S_{EV,j}(t) = \hat{S}_{EV,j}^{in,1} + \Delta T \cdot \eta_{EV,j}^{c} \cdot P_{EV,j}^{c}(t) - \Delta T \cdot \frac{1}{\eta_{EV,j}^{d}} \cdot P_{EV,j}^{d}(t) \qquad \forall j \in [1; n_{EV}], \; \forall t \in [1; N_T] \tag{4.33}$$

$$P_{CS,i}(t) = \sum_{j}^{n_{EV}} \beta_{i,j}(t) \cdot \left[P_{EV,j}^{c}(t) - P_{EV,j}^{d}(t) \right] \;\; \forall i \in [1; n], \; \forall t \in [1; N_T] \tag{4.34}$$

Finally, upper and lower bounds to the state variables are considered in order to obtain

feasible solutions, as reported in (4.35a)-(4.35j).

$$\theta_i^{min} \leq \theta_i(t) \leq \theta_i^{MAX} \ \ \forall i \in [1;n],\ \forall t \in [1;N_T] \tag{4.35a}$$

$$V_i^{min} \leq V_i(t) \leq V_i^{MAX} \ \ \forall i \in [1;n],\ \forall t \in [1;N_T] \tag{4.35b}$$

$$P_{flow,h}^{min} \leq P_{flow,h}(t) \leq P_{flow,h}^{MAX} \ \ \forall h \in [1;N_L],\ \forall t \in [1;N_T] \tag{4.35c}$$

$$Q_{flow,h}^{min} \leq Q_{flow,h}(t) \leq Q_{flow,h}^{MAX} \ \ \forall h \in [1;N_L],\ \forall t \in [1;N_T] \tag{4.35d}$$

$$P_{G,i}^{min} \leq P_{G,i}(t) \leq P_{G,i}^{MAX} \ \ \forall i \in [1],\ \forall t \in [1;N_T] \tag{4.35e}$$

$$P_{D,i}^{min} \leq P_{D,i}(t) \leq P_{D,i}^{MAX} \ \ \forall i \in [2;n],\ \forall t \in [1;N_T] \tag{4.35f}$$

$$P_{CS,i}^{min} \leq P_{CS,i}(t) \leq P_{CS,i}^{MAX} \ \ \forall i \in [2;n],\ \forall t \in [1;N_T] \tag{4.35g}$$

$$P_{EV,j}^{c,min} \leq P_{EV,j}^{c}(t) \leq P_{EV,j}^{c,MAX} \ \ \forall j \in [1;n_{EV}],\ \forall t \in [1;N_T] \tag{4.35h}$$

$$P_{EV,j}^{d,min} \leq P_{EV,j}^{d}(t) \leq P_{EV,j}^{d,MAX} \ \ \forall j \in [1;n_{EV}],\ \forall t \in [1;N_T] \tag{4.35i}$$

$$S_{EV,j}^{min} \leq S_{EV,j}(t) \leq S_{EV,j}^{MAX} \ \ \forall j \in [1;n_{EV}],\ \forall t \in [1;N_T] \tag{4.35j}$$

In order to consider the case of EV station integration with controlled charging mode, the optimization model is modified by removing state variables representing EV discharging in order to disable V2G functionality.

Nevertheless, a disadvantage of the model linearization consists of obtaining an approximated solution. Therefore, post-optimization analyses are proposed, whose purpose is to measure the effectiveness of the linear model, in terms of deviations from the real nonlinear network model.

4.2.2 Performance indicators and linear model accuracy test

The comparison among operational scenarios for a determined load condition is carried out by means of indicators, i.e., total daily energy losses, evaluated as in (4.27), active power losses for each time-step t and Load Voltage Deviation (LVD) value. In particular, the

LVD is a per unit indicator that measures deviations of the nodal voltages from the nominal voltage value, during grid operation. The indicator is evaluated as in (4.36), where $V_{nom,i}$ is the nominal voltage of the i-th node (set to 1 p.u.).

$$LVD(t) = \sum_{i}^{n} \left(\frac{V_i(t) - V_{nom,i}}{V_{nom,i}} \right)^2 \ \forall t \in [1; N_T] \tag{4.36}$$

In particular, the variation of LVD factor ($\Delta LVD(t)$) is evaluated as in (4.37), where $LVD^{bc}(t)$ represents the LVD factor of the grid in the base case (bc) in the t-th time-step, whereas $LVD^{nc}(t)$ is the one in the new case under evaluation in the t-th time-step.

$$\Delta LVD(t) = \frac{LVD^{nc}(t) - LVD^{bc}(t)}{LVD^{nc}(t)} \ \forall t \in [1; N_T] \tag{4.37}$$

Furthermore, the active power loss variation is evaluated as well in (4.38), following the same way of $\Delta LVD(t)$.

$$\Delta P_L(t) = \frac{P_L^{nc}(t) - P_L^{bc}(t)}{P_L^{nc}(t)} \ \forall t \in [1; N_T] \tag{4.38}$$

Moreover, a test is carried out in order to assess whether the linearized grid model accurately approximates the nonlinear one. The relative percentage error $e_{y,z}$ is calculated in (4.39) for each model variable y_z in the Z set, considering values obtained by nonlinear load flow analysis $y_z^{nonlin}(t)$ and obtained as results of MILP optimization $y_z^{opt}(t)$. If the error is lower than a determined level of tolerance γ then the linear model correctly approximates the nonlinear one. Otherwise, it is opportune to perform another sensitivity analysis and repeat the procedure until the condition for all the errors is verified.

$$e_{y,z}^{\%}(t) = \frac{|y_z^{nonlin}(t) - y_z^{opt}(t)|}{y_z^{nonlin}(t)} \cdot 100 \ \ \forall z \in \mathrm{Z}, \ \forall t \in [1; N_T] \tag{4.39}$$

4.3 EV station integration in IEEE-33 radial distribution grid

4.3.1 Grid characteristics and scenario definition

The integration study proposed in Section 4.2 is tested on the "IEEE-33 Radial Distribution System" radial test network [117], represented in Fig. 4.10. The operating voltage is assumed to be 15 kV. The tolerance on the grid voltage has been set to ± 10% of the nominal value. Therefore, a variation between 13.5 kV (0.9 p.u.) and 16.5 kV (1.1 p.u.) is allowed. In correspondence of node 1 the HV /MV substation is connected and the quantity of energy necessary to supply the loads present along the 5 branches of the network is withdrawn during the day. The whole system consists of 33 nodes and 32 three-phase lines.

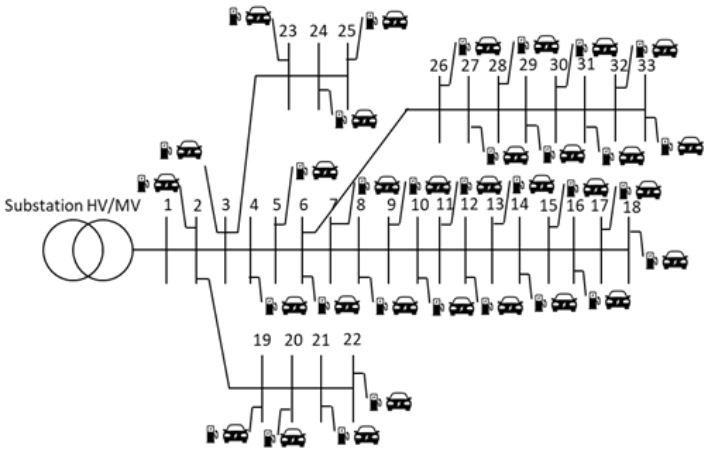

Figure 4.10: Integration of EV charging stations into the "IEEE-33 Radial Distribution System" radial test network.

Preliminary assumptions are made in order to carry out load flow analyses: i) the effect of load-side converters and transformers is neglected, ii) lines are represented using only the longitudinal impedance, neglecting shunt parameters, iii) node 1 is considered as the slack node in power flow analysis and iv) all the remaining nodes are considered as PQ load nodes (without any distributed generation units). Moreover, within the network a classification of the utilities has been performed: nodes from 2 to 6 and from 23 to 25 have been classified as industrial utilities, from 7 to 18 as residential ones and the remaining as commercial util-

ities.

In order to determine the daily load profile, 3 classes representing the utility categories (residential, industrial and commercial) are chosen and adapted from data collected by UK-ERC [118]. Residential utilities are characterized by peak power demands at 12:00 and during evening hours, whereas industrial and commercial utilities have power demand peak during the central hours of the day (except for a quasi-flat profile on Sundays). For all the 32 utilities load active power profiles have been calculated considering 5 periods of the year (Winter, Spring, Summer, High Summer and Autumn) and 3 categories of day (Weekdays, Saturday and Sunday). Reactive power profiles are evaluated considering a power factor equal to 0.9. The total load profile of the grid is shown in Fig. 4.11. It is noticeable that the highest load demand occurs during winter working days, between 17:00 and 18:00, laying between 4.8 MW and 4.9 MW. The lowest load demand occurs during summer Sundays, between 05:30 and 06:00 and it is roughly 1.65 MW.

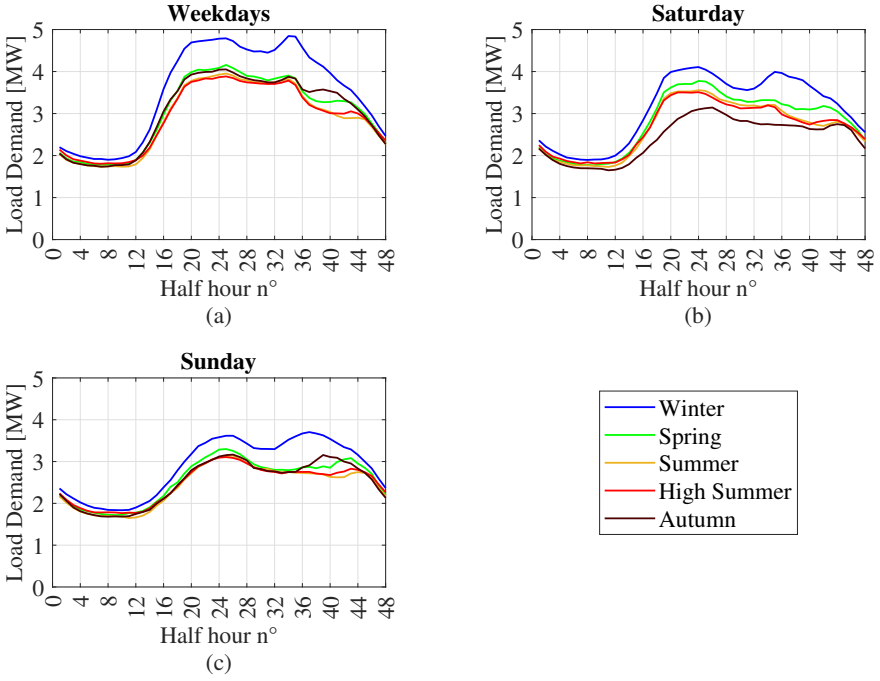

Figure 4.11: Network load demand on Weekdays (a), Saturday (b) and Sunday (c) in 5 different periods of the year.

In order to exploit integration studies on the test grid, 10 kW DC bi-directional charging stations are chosen. The use of identical recharging infrastructures simplifies the optimiza-

tion problem, since the conversion efficiency and the maximum power levels are identical for each position and for each time of day. Each CS is equipped with: static converter with a power factor close to 1 and nominal power 10 kW in AC/DC or DC/AC mode; a charging interface compatible with CHAdeMO and CCS COMBO standards; a three-phase AC input with active power factor correction; a Can-bus control/communication interface with the Battery Management System of the connected EV. The technical data are listed in [119]. Moreover, the maximum number of uncontrolled CSs that can be safely integrated in the distribution grid is determined by means of a stress-operation analysis. That is, load-flow analyses have been carried out by progressively increasing the number of considered uncontrolled CSs, with the aim of monitoring the closeness of the system to a critical operating condition. Therefore, a total of 60 stations have been integrated, 30 in correspondence of industrial (IND) and commercial (COMM) nodes and 30 in residential (RES) ones. The total installed power is 600 kW. Table 4.5 collects the number of CSs for each bus of the network.

For the purpose of the analyses, 30 EVs with 30 kWh nominal capacity and a 0.165 kWh/km average consumption factor are considered. Furthermore, a random EV users' behavior is assumed in order to generate 30 scenarios for each day category, supposing two daily charging events and one route between them. In particular, private EVs are considered, therefore a daylight charge is supposed at workplaces, in industrial/commercial district whereas a night-time charge occurs at residential premises. Table 4.4 collects position, initial SOC and energy required by all EVs integrated in the grid during their first and second discharging event. The integration study of EVs enabling controlled charging and V2G mode has been exploited solving the optimization problem formulated in Section 4.2 using the MATLAB function *intlinprog*. For the evaluation of indicators of Section 4.2.2, the base case is represented by the grid evaluated in the absence of integrated EV.

4.3.2 Results of EV station integration in uncontrolled charging

In order to simulate EV uncontrolled charging, load flow analysis is carried out using Matpower tool, increasing the daily load profiles by the power amount required to charge the

Table 4.4: EV usage configuration.

	I Charging event				II Charging event			
EV#	Grid Bus	Initial SOC [kWh]	Plug-in time [h]	Energy [kWh]	Grid Bus	Initial SOC [kWh]	Plug-in time [h]	Energy [kWh]
1	Bus 2	4.9	3.5	16.5	Bus 7	12.8	4.5	11.4
2	Bus 2	5.5	8.0	15.6	Bus 7	9.7	4.5	12.9
3	Bus 3	4.5	5.5	15.1	Bus 8	9.9	3.0	16.9
4	Bus 3	8.0	9.5	13.7	Bus 8	14.6	4.5	10.9
5	Bus 4	8.4	4.5	12.7	Bus 8	16.0	7.0	7.5
6	Bus 4	7.1	9.5	15.8	Bus 9	15.4	4.0	9.5
7	Bus 5	8.3	9.5	12.0	Bus 9	15.6	3.5	8.3
8	Bus 5	9.0	7.5	13.8	Bus 9	15.8	2.0	7.9
9	Bus 6	3.8	8.5	17.9	Bus 10	13.6	3.0	9.4
10	Bus 6	8.5	6.0	9.9	Bus 10	12.2	5.0	10.0
11	Bus 7	10.1	6.5	13.5	Bus 23	13.9	7.0	11.1
12	Bus 16	6.1	5.0	18.5	Bus 23	15.5	7.0	5.5
13	Bus 17	6.4	4.5	14.8	Bus 24	11.1	7.5	11.4
14	Bus 18	5.8	4.0	12.5	Bus 25	14.4	6.5	11.3
15	Bus 19	10.9	6.5	9.8	Bus 10	13.2	2.5	10.5
16	Bus 19	7.2	9.5	15.9	Bus 11	12.3	2.5	9.7
17	Bus 20	4.2	6.5	13.0	Bus 11	11.8	3.0	9.4
18	Bus 20	12.5	7.0	4.3	Bus 11	8.3	6.0	14.5
19	Bus 21	6.5	2.5	11.4	Bus 12	13.7	8.5	13.1
20	Bus 21	5.8	2.5	9.4	Bus 12	12.1	4.5	10.3
21	Bus 22	3.5	7.5	16.1	Bus 12	13.5	6.0	11.1
22	Bus 22	3.9	3.5	17.8	Bus 13	14.8	6.0	11.5
23	Bus 26	3.5	3.0	11.5	Bus 13	11.0	3.5	15.6
24	Bus 27	8.1	3.0	15.5	Bus 13	16.0	1.5	7.0
25	Bus 28	5.5	4.0	14.9	Bus 14	12.4	4.5	7.4
26	Bus 29	3.6	6.5	18.8	Bus 14	13.2	2.5	10.4
27	Bus 30	4.8	3.5	16.4	Bus 14	13.1	5.0	8.9
28	Bus 31	3.4	4.0	17.1	Bus 15	14.3	8.0	9.8
29	Bus 32	4.1	3.5	16.3	Bus 15	11.8	4.5	14.5
30	Bus 33	3.1	7.0	16.1	Bus 15	14.0	4.0	7.3

EVs in each time-step. In all the analyses a day as time horizon and 30 minutes time-step (a total of 48 time-steps) is considered. Table 4.6 shows the maximum percentage increases of load power and daily energy due to the integration of EVs and stations. The maximum increases are registered at 13:00 during Saturdays and weekdays. In particular, Summer and High Summer seasons register higher values of load active power increases (3.50% increase on High Summer Saturday). Furthermore, the highest value of daily load energy increase (1.22%) is recorded on a Summer Sunday.

Table 4.5: Charging station integration into the distribution grid.

Bus	Utility	n. EV stations	Bus	Utility	n. EV stations	Bus	Utility	n. EV stations
1	-	0	12	RES	3	23	IND	2
2	IND	2	13	RES	3	24	IND	1
3	IND	2	14	RES	3	25	IND	1
4	IND	2	15	RES	3	26	COMM	1
5	IND	2	16	RES	1	27	COMM	1
6	IND	2	17	RES	1	28	COMM	1
7	RES	3	18	RES	1	29	COMM	1
8	RES	3	19	COMM	2	30	COMM	1
9	RES	3	20	COMM	2	31	COMM	1
10	RES	3	21	COMM	2	32	COMM	1
11	RES	3	22	COMM	2	33	COMM	1

Fig. 4.12 reports the total amount of daily energy losses increase for all the 15 scenarios considered. The maximum increase occurs on weekdays in winter, where it reaches a value close to 70 kWh, while the minimum value is observed on days in high summer (about 46 kWh). From a technical point of view, this type of integration would therefore not be appropriate during high load demand periods, because it would not benefit the operation of the network.

Table 4.6: Maximum percentage increases of load instant power and energy due to EV CSs integration.

Day category	Season	Instant load power max increase (%)	Daily load energy increase (%)
Weekdays	Winter	2.46	0.93
	Spring	2.95	1.08
	Summer	3.14	1.13
	High Summer	3.17	1.12
	Autumn	2.95	1.08
Saturday	Winter	2.99	0.95
	Spring	3.22	1.06
	Summer	3.42	1.11
	High Summer	3.50	1.11
	Autumn	3.43	1.08
Sunday	Winter	2.24	1.04
	Spring	2.47	1.17
	Summer	2.62	1.22
	High Summer	2.60	1.20
	Autumn	2.56	1.19

In Fig. 4.13 the LVD values are reported and compared to the case of the grid without

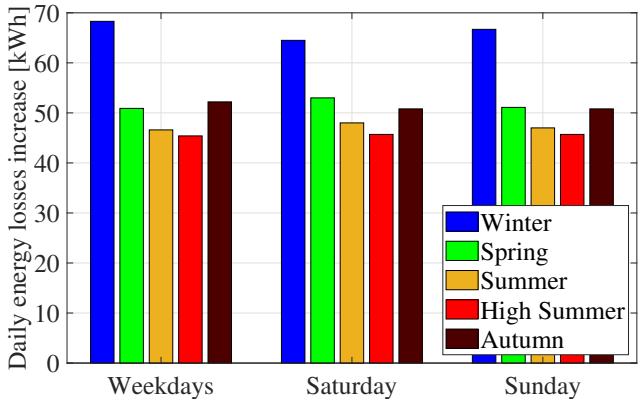

Figure 4.12: Daily energy losses increase of the grid with CSs in uncontrolled charging.

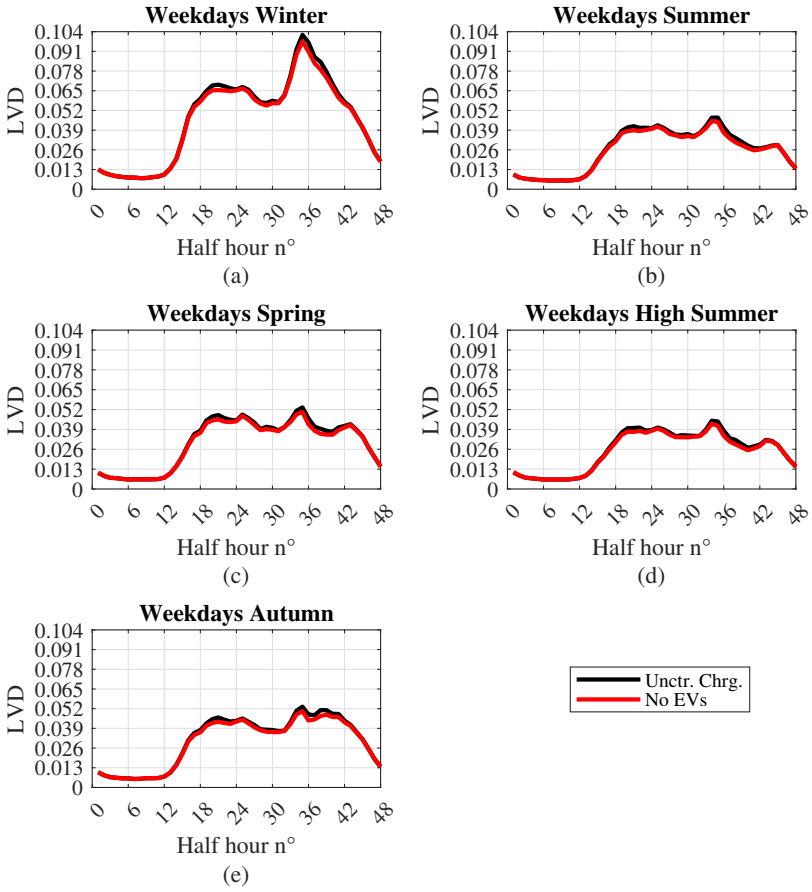

Figure 4.13: Daily LVD values of the grid considering EV uncontrolled charging and the same grid without EVs.

EVs. It can be seen that the uncontrolled charging leads to a reduction in voltage quality in the grid and an increase in losses. These effects are significant in the moments of the day when there is a greater load demand for EVs. Due to the uncontrolled load in the peak

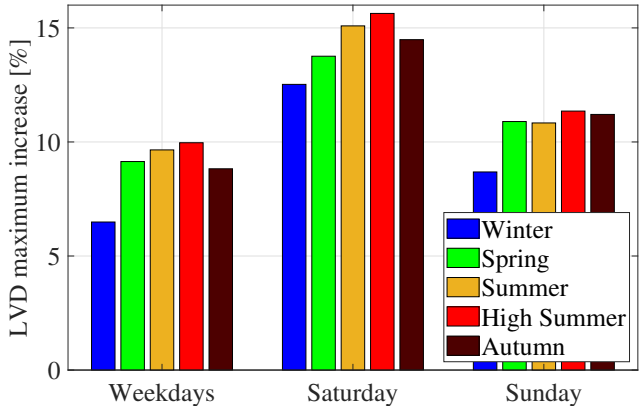

Figure 4.14: Daily LVD maximum increase considering EV uncontrolled charging (with respect to the same grid without EVs).

hour of winter weekdays, the LVD reaches a maximum value of 0.104, further lowering the voltage quality. Furthermore, percentage maximum increase of LVD for each scenario is reported in Fig. 4.14. The maximum increases are always registered during High Summer for each day category.

4.3.3 Results of EV station integration in controlled charging, and in V2G mode

The variation of power losses and LVD are respectively reported in Fig. 4.15 and Fig. 4.16, considering weekdays for all seasons comparing uncontrolled charging, controlled charging and V2G. It is possible to notice that EV exploitation in V2G mode allows to inject energy to the network when the load demand is high. Therefore, it is possible to minimize not only the losses (Fig. 4.15) in the instants of peak load demand, but also to improve the network voltage quality. It should be noted that the effect of V2G is most noticeable during winter when the load demand is the highest, and several EV discharges occur (Fig. 4.15a).

Furthermore, EV discharging events exploit peak shaving feature, thus reducing losses compared to the scenario without vehicles. The integration of the vehicles in controlled charge produces similar effects to the integration in V2G mode, in terms of temporal distribution (due to the control of charging processes) although with smaller amplitudes. In this case the index variations never assume negative values since EV discharge is not allowed.

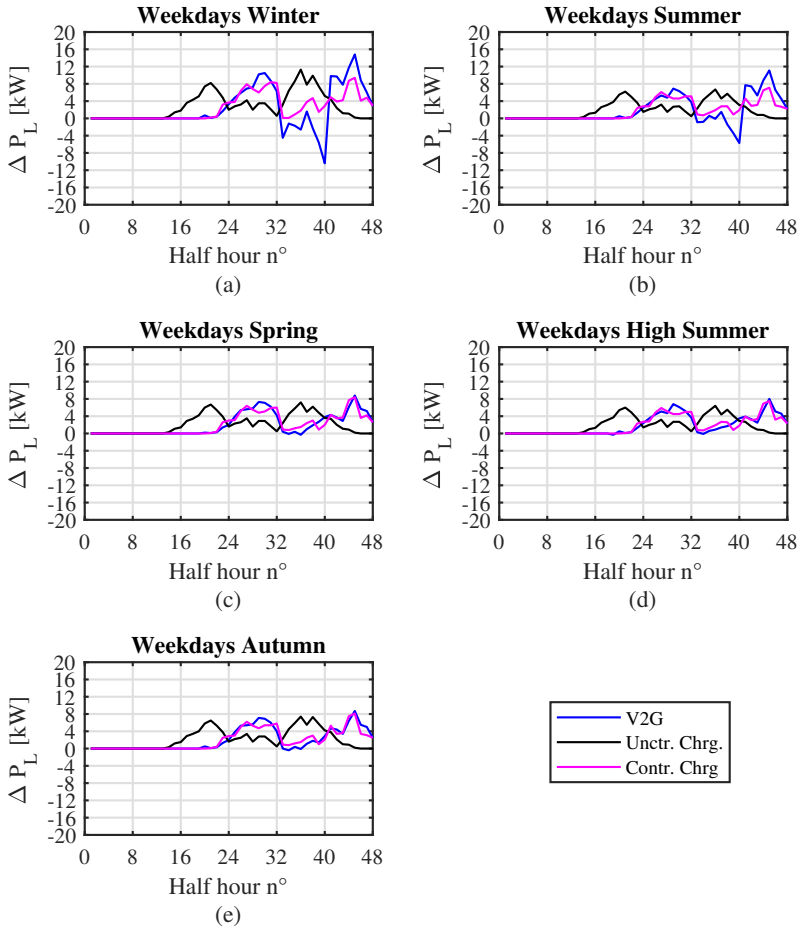

Figure 4.15: Active power losses absolute variation (ΔP_L) considering EVs enabling V2G.

Fig. 4.17 shows the percentage increases in total daily energy losses for all vehicle operating scenarios in Weekdays compared to the case without EVs. In each case energy losses increase, due to the increase of energy demand. The lowest increase occurs using V2G mode during winter weekdays, and it is equal to 1.81%. Despite the studied day, bi-directional charging still implies the best possible minimization of total daily energy losses, with respect to controlled and uncontrolled charging, although in High Summer weekdays quite similar percentage increases are registered both in V2G and controlled charging modes. On Saturday and Sunday analogous trends are observed for LVD and losses, although shifted in time according to load peak demand, and daily loss increase range between 2.2-3.2% on Saturday and 2.5-3.5% on Sunday, with higher values in Summer.

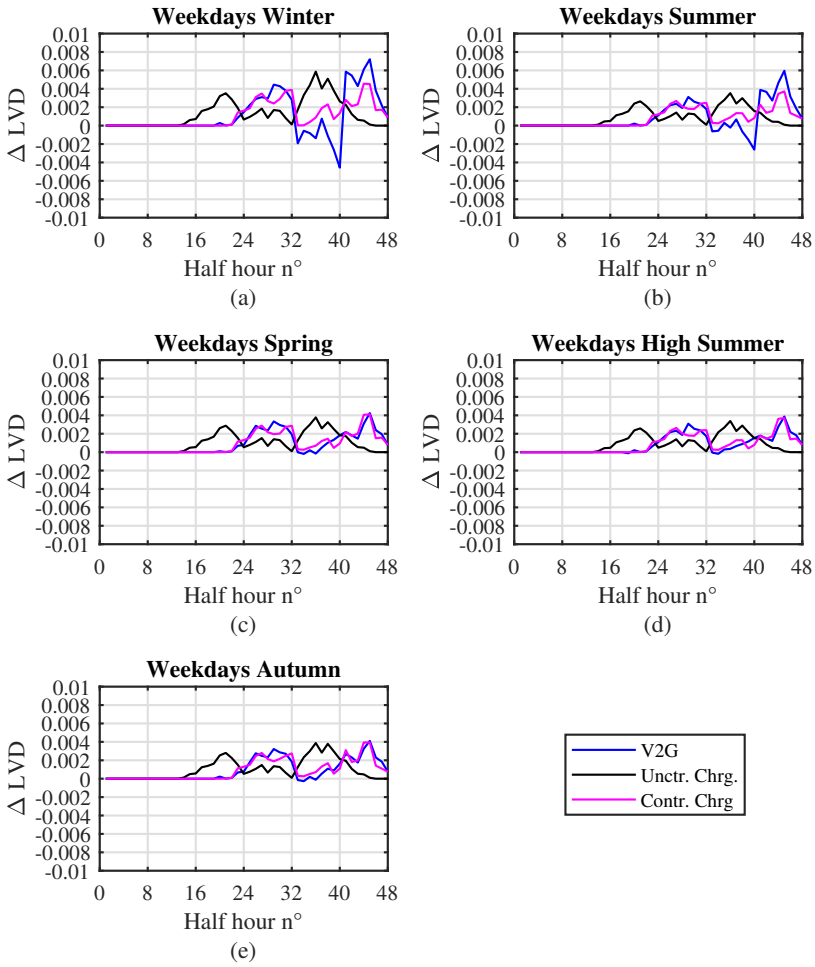

Figure 4.16: LVD values considering EV enabling V2G integrated into the network.

4.3.4 Accuracy test for grid model linearization

The accuracy of the linearized network model used in MILP optimization is tested performing daily load flow routines, using modified power demand data obtained in optimization problem solution. Successively, the percentage errors of hourly LVD, hourly active power losses, and total energy losses of linearized network model are compared to the full load flow algorithm for the 15 considered operating scenarios. Table 4.7 shows average and maximum values assumed by the hourly LVD and hourly active power losses, considering all simulated scenarios. Table 4.8 shows the percentage errors on the total daily energy losses. From collected data it is possible to demonstrate that the linear network model used in the MILP optimization is quite accurate, as the average percentage errors are always kept

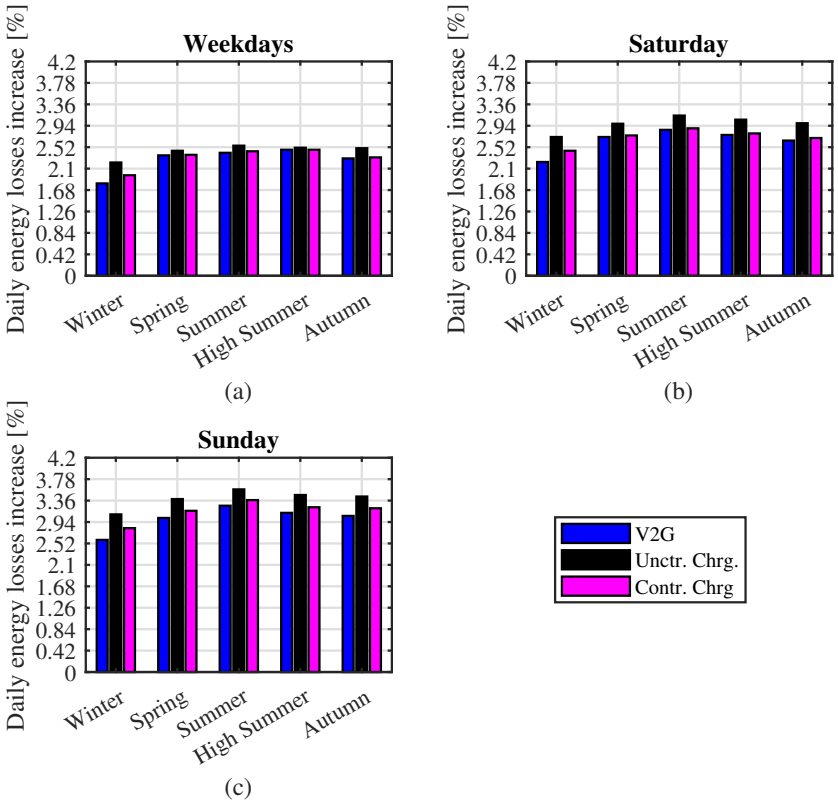

Figure 4.17: Percentage increases in total daily energy losses for all vehicle operating scenarios.

below 0.5% for LVD and daily losses and below 3% for losses in each timestep, which is lower than the tolerance limit equal to 5%. Therefore, optimization results represent with good approximation the real network operation in the presence of V2G.

Table 4.7: Percentage errors of hourly LVD and active power losses (P_L).

	Range of average values		**Range of maximum values**	
	e_{LVD} [%]	e_{P_L} [%]	e_{LVD} [%]	e_{P_L} [%]
Weekdays	0.016 - 0.032	0.156 - 0.253	0.159 - 0.260	1.566 - 2.489
Saturday	0.038 - 0.022	0.202 - 0.297	0.191 - 0.246	1.693 - 2.005
Sunday	0.032 - 0.061	0.378 - 0.594	0.212 - 0.378	3.365 - 4.666

Table 4.8: Percentage errors of daily energy losses.

	Weekdays	Saturday	Sunday
Winter	0.077%	0.220%	0.365%
Spring	0.029%	0.110%	0.203%
Summer	0.069%	0.174%	0.271%
High Summer	0.047%	0.214%	0.026%
Autumn	0.020%	0.208%	0.365%

4.4 The influence of EV position on technical operation of the IEEE-33 radial distribution grid

In this section, the influence of V2G-enabled EV plug-in positions on the MV grid operation on daily horizon is assessed by means of the optimal operation presented in Section 4.2. In particular, in order to establish which EVs should have their positions changed within the network, the evaluation of their daily discharge energy $E^d_{EV,j}$ is required, evaluated as in (4.40). In fact, the mobility needs require EV charge when connected, therefore the use of EV discharge highlights the need of reducing power flows to reach the goal of minimum losses in objective function (4.27). EVs that mostly discharge during the day are chosen to be positioned in a new configuration, keeping the parking times and the durations of the two charging events fixed.

$$E^d_{EV,j} = \sum_{t}^{N_T} \Delta T \cdot \frac{1}{\eta^d_{EV,j}} \cdot P^d_{EV,j}(t) \; \forall j \in [1; n_{EV}] \tag{4.40}$$

4.4.1 Case study definition and EV usage configurations

The study is carried out considering the grid already described in Section 4.3.1, with the same integrated EVs, while Winter Weekday load demand scenario is chosen. Starting from results considering the plug-in configuration (see Table 4.4), the discharge energy for each EV is evaluated as in (4.40) and the highest values of daily discharge energy are reached by EV4, EV12, EV19 and EV22, as reported below:

- EV4 with $E^d_{EV,4}$ of 11.25 kWh,

- EV12 with $E^d_{EV,12}$ of 12.08 kWh,
- EV19 with $E^d_{EV,19}$ of 23.02 kWh,
- EV22 with $E^d_{EV,22}$ of 11.40 kWh,

Therefore, EV4, EV12, EV19 and EV22 get their plug-in position changed, in both charging events. EV4 and EV22 first recharge at residential buses (12 and 16), differently from the first case (industrial and commercial buses). On the contrary, EV12 and EV19 change respectively to industrial (bus 3) and residential (bus 16). Residential and commercial buses are chosen for EV second charging event. Table 4.9 reports the updated configuration of the four EVs.

Table 4.9: EV new plug-in positions.

	I Charging event New position (Old position)	**II Charging event** New position (Old position)
EV4	Bus 12 (Bus 3)	Bus 26 (Bus 8)
EV12	Bus 22 (Bus 16)	Bus 13 (Bus 23)
EV19	Bus 3 (Bus 21)	Bus 18 (Bus 12)
EV22	Bus 16 (Bus 22)	Bus 30 (Bus 13)

For the evaluation of indicators of Section 4.2.2, LVD^{bc} and P^{bc}_L are respectively the LVD factor and active power losses of the grid evaluated in the presence of integrated EV in the first plug-in configuration analyzed in Section 4.3.

4.4.2 Results and discussion

Fig. 4.18 and Fig. 4.19 show power exchanges of the four EVs in the base case and in the "new position" case respectively. It can be seen that EV4 and EV12 trends show some difference, as with new positions EV4 provides a further discharge during the first charging event (red negative bar in Fig. 4.19) and EV12 experiences a more intense discharging during the second plug-in event (blue negative bars). Whereas, EV19 and EV22 show similar exploitation in the base case and in the new position case.

The evolution of the EV SOC $S_{EV,k}$ in both cases is reported in Fig. 4.20. As aforementioned, EV4 and EV12 V2G exploitation is more frequent with the respect to the first case.

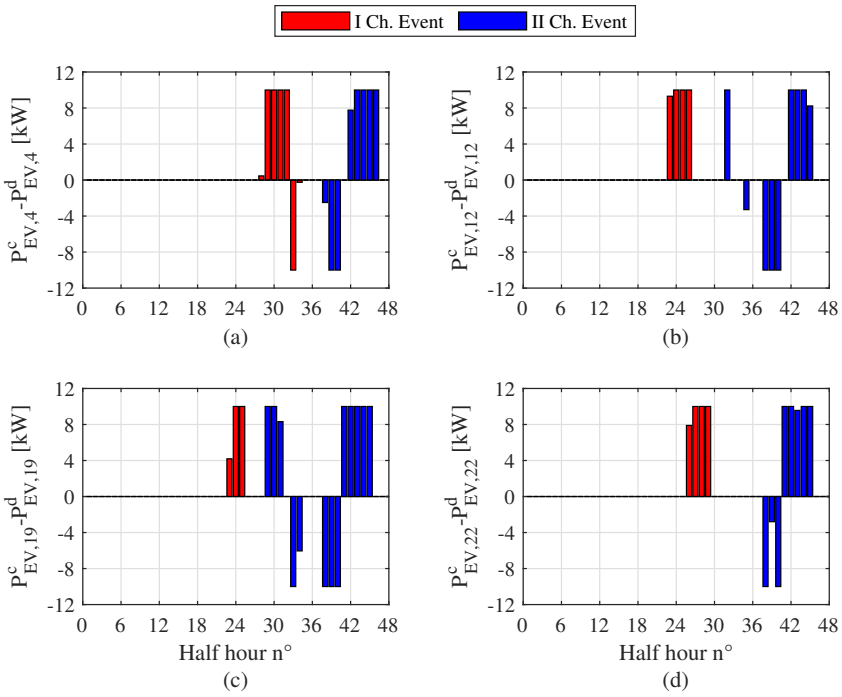

Figure 4.18: EV4, EV12, EV19 and EV22 power exchanges (base case).

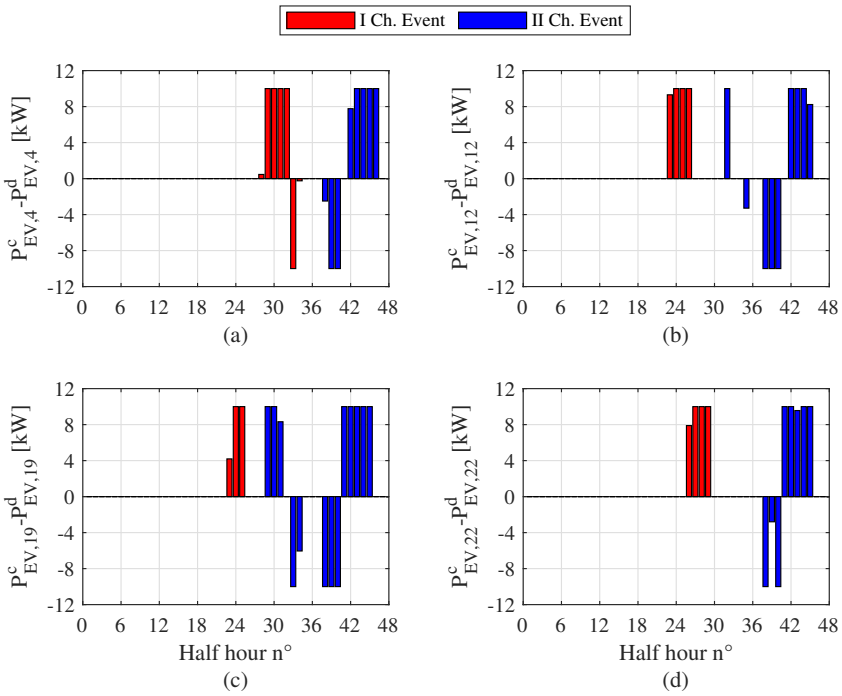

Figure 4.19: EV4, EV12, EV19 and EV22 power exchanges (new position case).

As a matter of fact, EV4 discharges at maximum power for one time-step, when connected at bus 12, with a SOC reduction of nearly 16%. A similar behavior is shown for EV12,

when connected at bus 13. During the second plug-in event, a 30 minute-charging event at maximum power occurs (at around 16:00), registering a SOC increase of 16%. Then at 17:00 3 kW discharging event leads to a EV12 battery SOC reduction of 8.3%. The position change of EV19 and EV22 changed positions does not remarkably affect their exploitation, as it can been seen from their SOC evolution during the day.

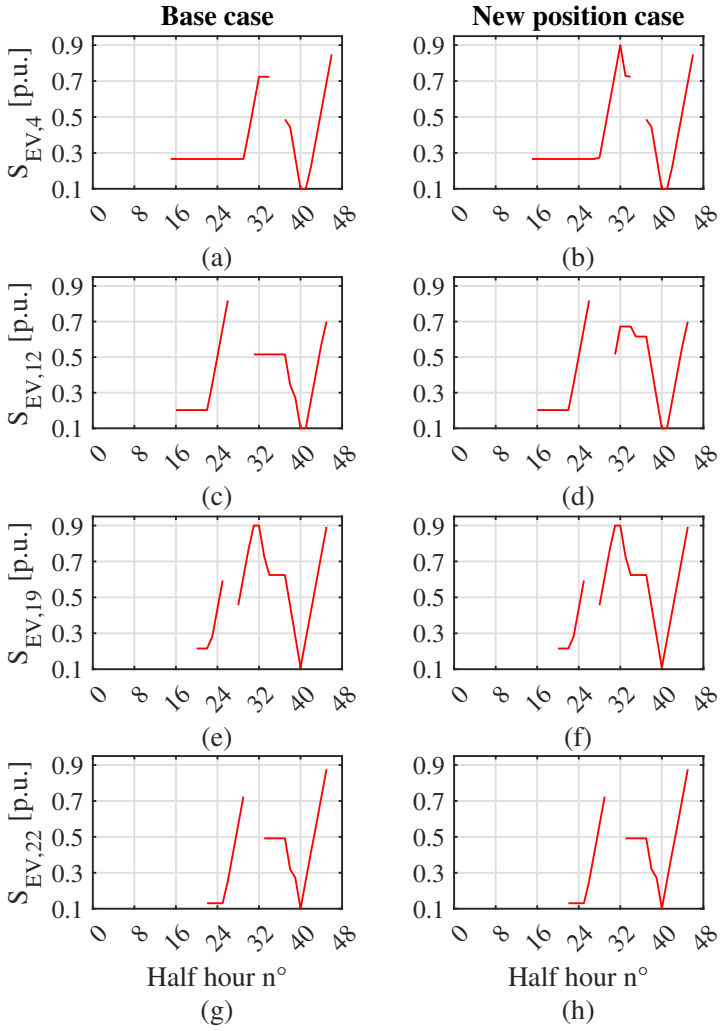

Figure 4.20: EV4, EV12, EV19 and EV22 state of charge (base case and new position case).

As it is depicted in Fig. 4.21, the new plug-in configuration does not affect the LVD during morning hours (until 11:00), while it leads to positive and negative variation during the following hours (Fig. 4.21a). The maximum increase is 2.39% at 14:30 (time-step 29), while the maximum reduction -1.28% is registered at 16:30 (time-step 33). This negative

value implies that the LVD evaluated considering the new EV positions is less than the one evaluated in the base case. Therefore, changes of EV position could have positive impact on the grid voltage quality. The evolution of active power losses follows the same behavior of the LVD, as in Fig 4.21b: negative LVD variations correspond to negative variation of power losses. A maximum increase of losses by 1.21% is observed at the same time-step of the maximum LVD variation. Analogously, the maximum losses reduction (-0.98%) is recorded in correspondence to the minimum LVD variation. Therefore, it can be affirmed that EV position change slightly affects power quality during optimal grid operation, implying lower voltage deviations and active power losses.

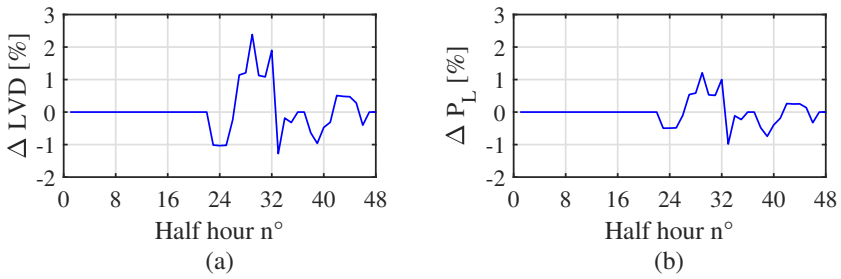

Figure 4.21: LVD and active power loss percentage variation for each time-step.

Figg. 4.22 and 4.23 show the grid nodal voltages expressed in p.u. considering respectively time-steps 29 and 33, that are the intervals when the maximum and minimum values of LVD and power loss variation occur, as just reported. In correspondence of a positive LVD variation, nodal voltages in base case are higher than the ones in the new position case (see nodes 12-18 in Fig. 4.22). The lowest values of voltages are reached for both cases at node 18 (with 0.94 p.u. in base case and 0.938 p.u. in new position case). At the time step 33 nodal voltages reach lower values in base case operation than in new position one, thus implying a negative variation of LVD factor. The lowest value (about 0.929 p.u.) is reached at bus 18 during base case operation, as in Fig. 4.23. All the analyzed conditions are well within the imposed voltage limits (0.9-1.1 p.u. of nominal voltage).

The loading percentage of representative grid branches is reported in Fig. 4.24 for time-steps 29 and 33. In both time-steps any significant difference between cases cannot be detected, except for a slight increase at Branch 1 and a decrease at Branch 18 during time-

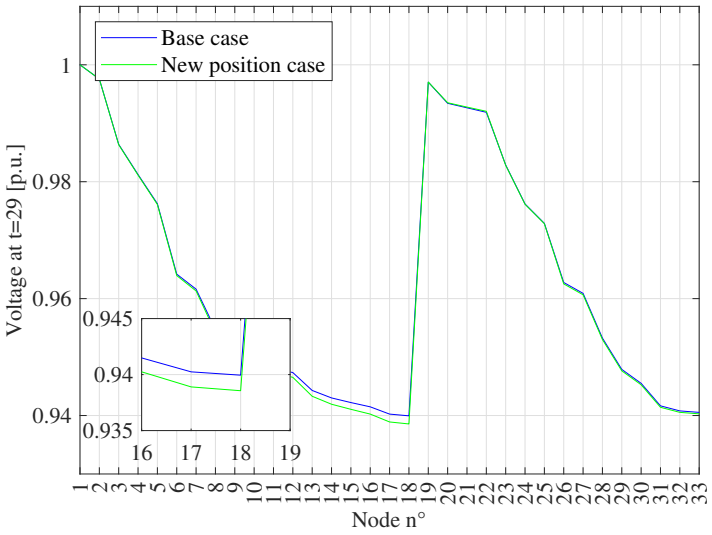

Figure 4.22: Nodal voltage at t =29 for old and new position cases.

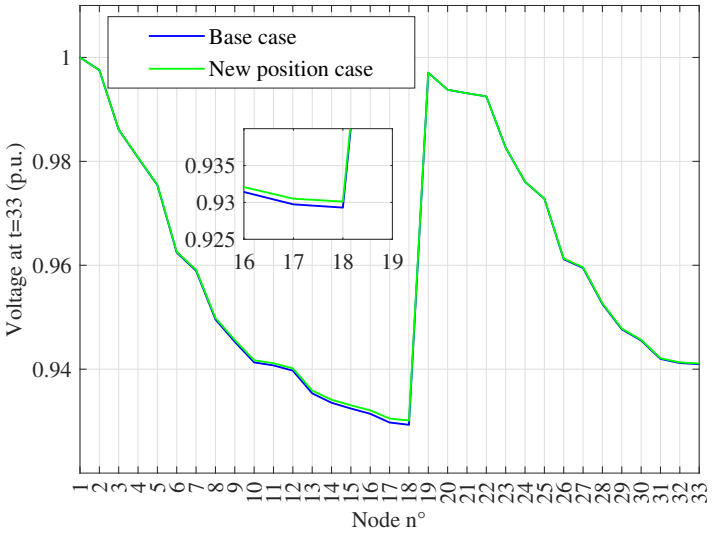

Figure 4.23: Nodal voltage at t =33 for old and new position cases.

step 29 (Fig 4.24a). Generally, Branch 1 is the most loaded one (at 80%), while Branch 18 is the less loaded (slightly less than 20%).

Finally, the daily energy losses are evaluated as in (4.27), obtaining 3126.146 kWh in the base case scenario, and 3126.084 in the new one. It can be seen that a slight reduction of energy losses is detected considering EV new positions. Compared to the grid without EVs (3070.4 kWh losses), an increase of energy losses of respectively 1.82% and 1.81% is detected.

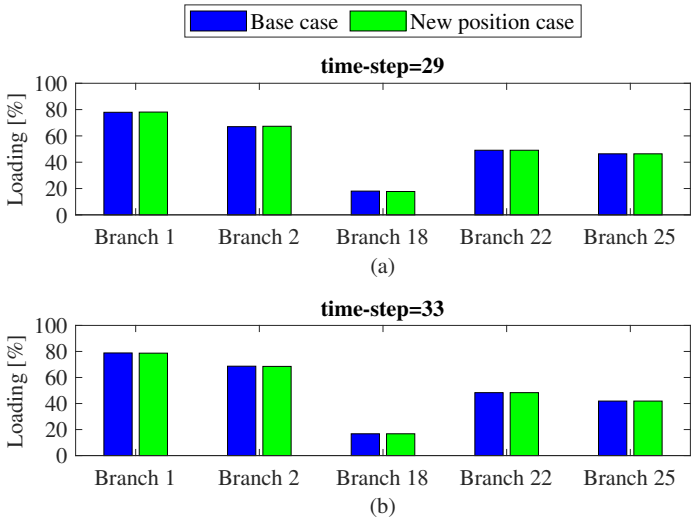

Figure 4.24: Loading percentage of the main grid branches at t =29 (a) and t =33 (b).

4.5 Integration of clusters of EV station in the IEEE-33 radial distribution grid

Taking the cue from the study presented in Section 4.3, the study proposed in this section focuses on the integration of clusters of EVs into the IEEE-33 radial distribution grid, which are here considered concentrated in few nodes of the grid. The analysis points out the interactions of electric vehicle smart charging and V2G processes on the network and among electric vehicles as well, individuating the possible interactions among clusters while dealing with distribution network operation and for further stressful conditions and relevant possible solutions for EV integration.

4.5.1 Modified MILP problem for daily optimal operation

Starting from the MILP problem of Section 4.2, some modifications are made in terms of state variables, objective function and constraints. In particular, the state variable vector $\mathbf{x}$ includes, for each time-step t of the daily horizon, the nodal voltage amplitudes (p.u.) - V_i -, generated powers ($P_{G,i}$), power levels of the installed EV stations ($P_{CS,i}$) of the i-th node of the grid; active power flows of the h-th network line ($P_{flow,h}$), charge and discharge powers ($P^c_{EV,j}$ and $P^d_{EV,j}$), and SOC levels ($S_{EV,j}$) of the j-th EV.

Then the objective function of grid energy losses in (4.27) is modified as in the following (4.41), accounting only losses for EV load and not considering energy losses due to grid load without EVs.

$$f'_{loss} = \sum_{t}^{N_T} \Delta T \cdot P_L(t) = \sum_{t}^{N_T} \Delta T \cdot \sum_{i}^{n} [P_{G,i}(t) - P_{CS,i}(t)] \tag{4.41}$$

Constraints (4.29), (4.30) and (4.32) are involved for grid linearization, while (4.33) and (4.34) take into account EV SOC evolution and EV station exchanged power. The total daily energy stored in EVs is also limited to a fixed maximum amount $S_{EV,j}^{MAX}$ (4.42), whereas the total EV charging energy in (4.43) should cover at least energy consumption due to the trip ($S_{EV,j}^{dep}$-$S_{EV,j}^{arr}$).

$$S_{EV,j}^{arr} + \Delta T \cdot \sum_{t}^{N_T} \eta_{EV,j}^{c} \cdot P_{EV,j}^{c}(t) \leq S_{EV,j}^{MAX} \;\; \forall j \in [1; n_{EV}] \tag{4.42}$$

$$\Delta T \cdot \sum_{t}^{N_T} \eta_{EV,j}^{c} \cdot P_{EV,j}^{c}(t) \geq S_{EV,j}^{dep} - S_{EV,j}^{arr} \;\; \forall j \in [1; n_{EV}] \tag{4.43}$$

Furthermore, upper and lower bounds (4.35b), (4.35c), (4.35e), (4.35g), (4.35i) and (4.35j) are included in the problem as well.

Indicators used in this study are the variation of grid active power losses with respect to the case of the grid without EVs (base case), that take into account also the existing load $P_{load,i}(t)$ for each i-th node of the grid, expressed in MWh in (4.38), the energy exchanged at EV charging stations calculated in (4.44) and line loading rate $F_h(t)$ defined for each h-th branch of the network as in (4.45).

$$E_{CS,i}(t) = \Delta T \cdot \sum_{tt}^{t} P_{CS,i}(tt) \;\; \forall i \in [2; n], \; \forall t \in [1; N_T] \tag{4.44}$$

$$F_h(t) = \frac{P_{flow,h}(t)}{P_{flow,h}^{MAX}} \;\; \forall h \in [1; n_L], \; \forall t \in [1; N_T] \tag{4.45}$$

4.5.2 EV cluster features and scenario description

The methodology is applied to the IEEE-33 radial distribution test grid, with the same features described in Section 4.3.1. Two grid load profiles are chosen representing a typical Summer Sunday and Autumn Weekday (see Fig. 4.11a and 4.11c), with 30-min time-step. Additional grid parameters are here provided:

- P_{G1}^{MAX} is set to 5.9 MW,
- $P_{flow,h}^{MAX}$ is set to 6.11 MVA for lines 1-2, 4.97 MVA for lines 3-5 and 2.76 MVA for all the others,
- V_i^{MAX} and V_i^{min} are respectively set to 1.1 and 0.9 p.u.

The EV model used in the study is BMW iX xdrive50, whose features are the following: i) capacity of 105.2 kWh, ii) minimum capacity of 31.56 kWh (assumed equal to 30% of capacity), iii) consumption rate of 20 km/kWh (taken from Worldwide Harmonized Light Vehicles Test Procedure [120]), and iv) maximum charging/discharging power of 11 kW.

As aforementioned, EV usage is affected by uncertainties, that are taken into account using a stochastic approach by generating samples from probability distributions as models of problem inputs like EV SOC at departure time $S_{EV,j}^{dep}$, arrival and departure times ($t_{EV,j}^{arr}$ and $t_{EV,j}^{dep}$), and travel distance $d_{EV,j}$.

The normal distribution is used for the first three inputs. In particular, departure and arrival times data are collected from a parking lot during opening hours (07:00-22:00) [121], while departure SOC $S_{EV,j}^{dep}$ is supposed to have mean of 90% of capacity $H_{EV,j}$ and 10% of capacity as 99.3% probability coverage. Travel distance is modelled using a Lognormal probability distribution, as [122]. Fig. 4.25 shows the probability functions and samples for all the stochastic inputs. Plug-in intervals are then determined and showed in Fig. 4.26, according to scenarios defined. Nodes 18, 22, 25 and 33 are chosen for placing EV charging stations with 9 EVs each, as they are the farthest node of the grid from the generation node, as reported in Fig. 4.27. Moreover, additional charging station is placed at node 7 when simulating higher EV integration, as better explained in the following.

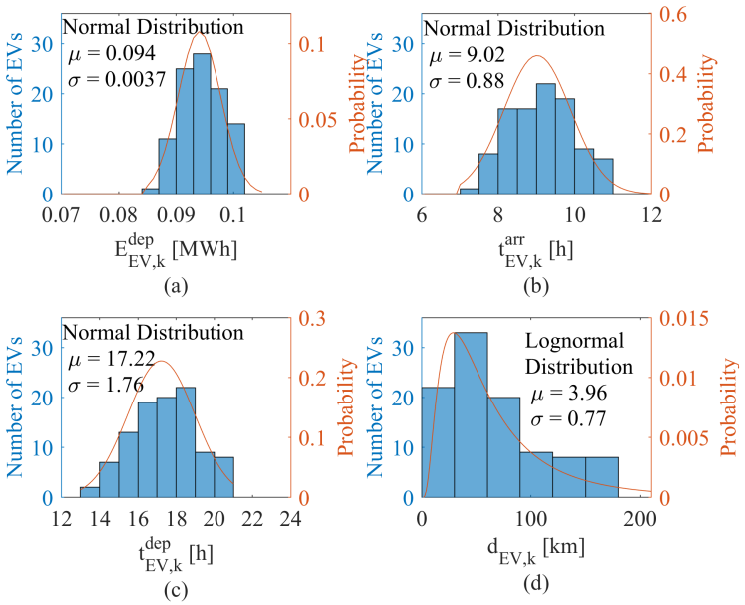

Figure 4.25: Probability function of EV departure energy (a), arrival times (b), departure times (c) and distance of routes (d).

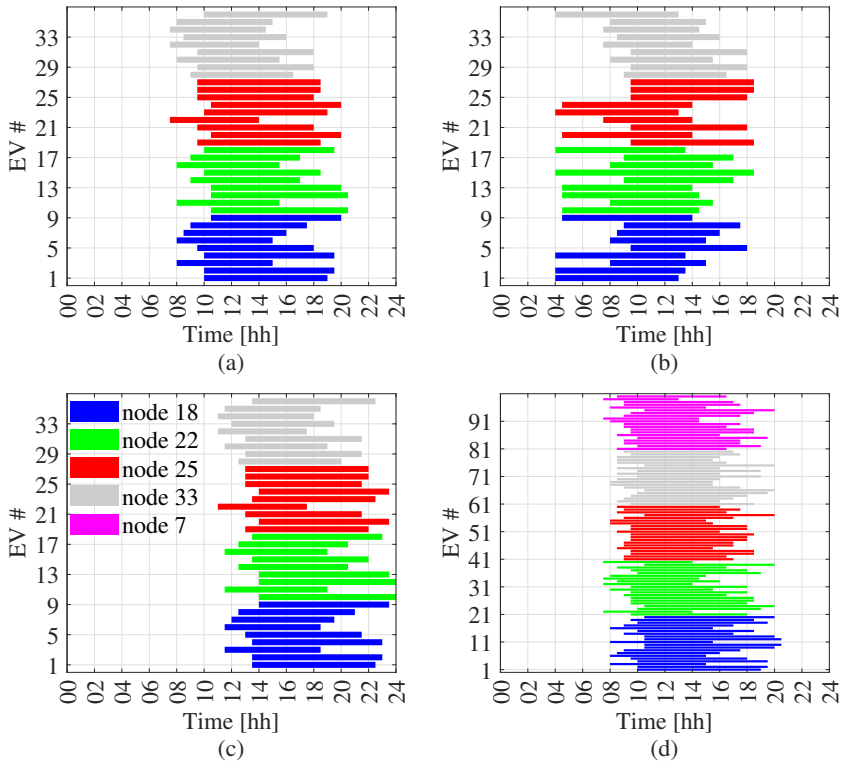

Figure 4.26: Plug-in intervals for scenarios 1-2 (a), scenarios 3-4 (b), scenarios 5-6 (c) and scenarios 7-9 (d).

Furthermore, arrival EV SOC $S^{arr}_{EV,j}$ is calculated as in (4.46), where $cr_{EV,j}$ is the EV consumption rate.

$$S^{arr}_{EV,j} = S^{dep}_{EV,j} - d_{EV,j} \cdot cr_{EV,j} \quad \forall j \in [1; n_{EV}] \tag{4.46}$$

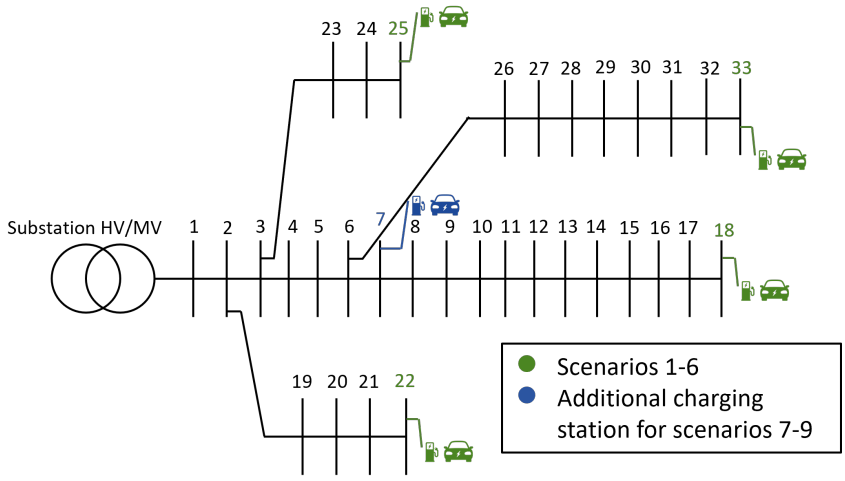

Figure 4.27: IEEE-33 Radial Distribution network topology integrating EV charging stations according to defined scenarios.

Simulations are carried out for several scenarios, that are obtained from the combinations, synthesized in Table 4.10, of the following factors:

- days (Summer Sunday – S – and Autumn Weekday – A), whose load profiles are already depicted in Fig. 4.11,
- number of integrated EVs (9 EVs for each of nodes 18, 22, 25, 33 in scenarios 1-6, and 20 for each of nodes 7, 18, 22, 25, 33 in Scenarios 7-9),
- the possibility to exploit V2G functionalities,
- the further limitation on nodal voltages,
- the plug-in time shifting during morning or night hours (see Fig. 4.26).

Moreover, for all scenario the value of $P^{MAX}_{CS,i}$ - see constratint (4.35g) - considered is equal to 0.1 MW, except for the cases of S8 and A8, where it is set to 0.2 MW.

Table 4.10: Simulated scenarios.

Scenario	EV number	V2G	Stringent voltage limit	EV park - night	EV park - morning
S1, A1	36	x	x	x	x
S2, A2	36	✓	x	x	x
S3, A3	36	✓	✓	x	x
S4, A4	36	✓	x	x	✓
S5, A5	36	✓	x	✓	x
S6, A6	36	✓	✓	✓	x
S7, A7	100	✓	x	x	x
S8, A8	100	✓*	x	x	x
S9, A9	100	✓	✓	x	x

*In this case the maximum power exchanged by all charging stations in each node is increased to 0.2 MW, while in the other scenarios is considered equal to 0.1 MW.

4.5.3 Results for the integration of 36 EVs

Results regarding 36 EVs integrated in the grid (Scenarios 1-6) are shown in Figg. 4.28, 4.29 and 4.30 for cumulated energy exchange at charging stations in Summer and in Autumn, and for loss variations, respectively - as evaluated with (4.44) and (4.38). When EVs are not enabled to exploit V2G functionality (in S1 and A1), grid losses increase due to load increase by EV charging, as shown in Fig. 4.30a, where the maximum increase of 99 kWh is reached at 16:00 for both summer and autumn scenarios (corresponding to 12.4% increase as compared to the network without EVs). Optimized charging energies in S1 and A1 do not occur in the same periods because of different grid operating conditions, as depicted in Fig. 4.28a for S1 and Fig. 4.29a for A1.

When V2G functionality is enabled, grid technical limits and EV energy requirements can hinder the possibility to discharge EVs, as in S2 in Fig. 4.28b, where only charging processes occur during the day, due to low differences of sensitivity coefficients during plug-in times that do not encourage EV discharging. However, higher grid load demand in autumn weekday in Fig. 4.29b could lead to V2G exploitation in node 22, that slightly contribute to EV charging in node 18. For both S2 and A2 scenarios, grid loss increases are depicted in Fig. 4.30b.

When stringent voltage limitations are imposed in S3 and A3, V2G exploitation is required by the network perspective from the EVs in order to avoid grid voltage to exceed

limits. In S3, EV discharging at nodes 18 and 33 occur, leading to peak shaving with a 0.63% total grid load reduction (Fig. 4.28c), while in A3 V2G functionality is not deeply exploited as in S3, due to grid demand (Fig. 4.29c). As a matter of fact, total load variation is 0.45%. This affects grid losses variations as well, that are negative for most of the day, as in Fig. 4.30c.

Anticipating plug-in intervals (S4, A4) leads to an increase of grid losses during early morning hours (Fig 4.30d), due to EV charging, while V2G operation is depicted in Fig 4.28d from 06:00 to 07:00 in nodes 18 and 33 in S4 and in Fig. 4.29d in node 22 in A4, because of significant variations of sensitivity coefficients in the times when EVs are available.

When plug-in times are shifted 3.5 h forward to cover evening-night period, the effect is the absence of V2G in S5 – Fig. 4.28e – since sensitivity variations are not enough significant to promote discharging events, while a significant discharge occurs at node 22 in A5 (Fig. 4.29e). Same considerations can be done on the loss variations during the day in Fig. 4.30e, that register an increase during evening and night hours, in correspondence of EV charging.

Introducing further voltage limitations in S6 leads to EV discharging during 11:30-12:30 for nodes 18, 22 and 33, and in the same period grid loss reduction is registered, as shown in positive variation in Fig. 4.30f. In addition, for the A6 it can be noted that in the period 12:30-16:00 EV discharging in node 22 support EV charging in node 18, thus realizing a principle of energy community among charging stations even considering a network objective without economic incentive of community configuration. Moreover, EV discharge occurs from 18:30 to 21:30 at node 18 for voltage supporting. EV power exchanges in this scenario are reported in Fig. 4.31.

It can be seen that in all scenarios, the upper limit $P_{CS,i}^{MAX}$ set to 0.1 allows EV simultaneous charging at maximum power.

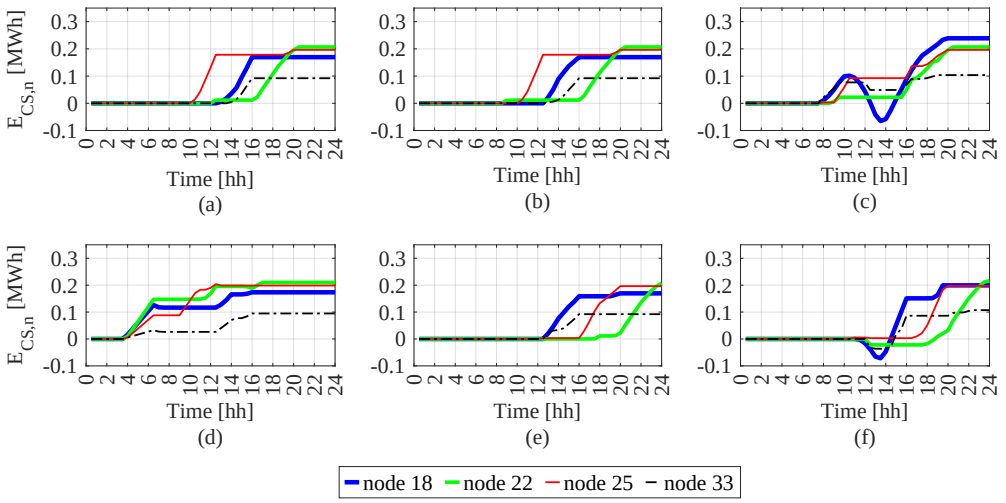

Figure 4.28: Charging station energy in S1 (a), S2 (b), S3 (c) S4 (d), S5 (e) and S6 (f).

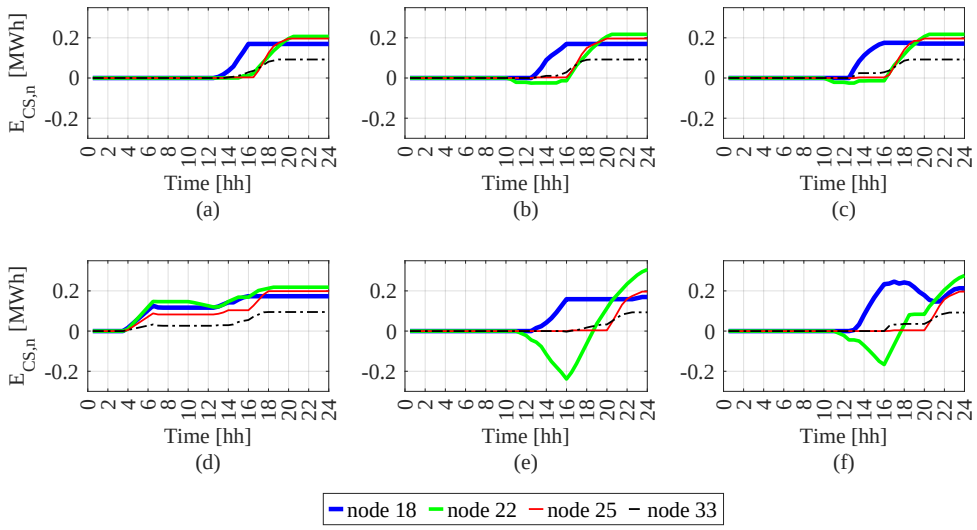

Figure 4.29: Charging station energy in A1 (a), A2 (b), A3 (c) A4 (d), A5 (e) and A6 (f).

4.5.4 Results for the integration of 100 EVs

The integration of 100 EVs grouped in 20 EVs at nodes 18, 22, 25, 33 and 7, leads to higher energy demand for charging and further concentration in critical nodes, along with an increase of grid losses with respect to the case where EVs are not integrated. In S7 not all EVs can not charge at the same time at maximum power, because the total maximum

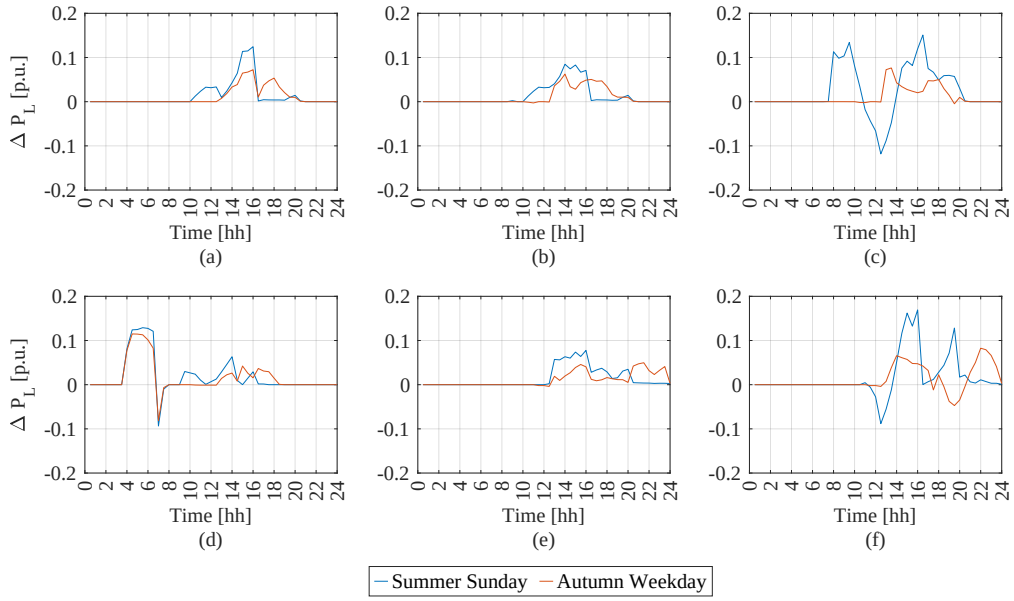

Figure 4.30: Delta energy losses considering 36 integrated EVs in scenarios S1 and A1 (a), S2 and A2 (b), S3 and A3 (c), S4 and A4 (d), S5 and A5 (e) and S6 and A6 (f).

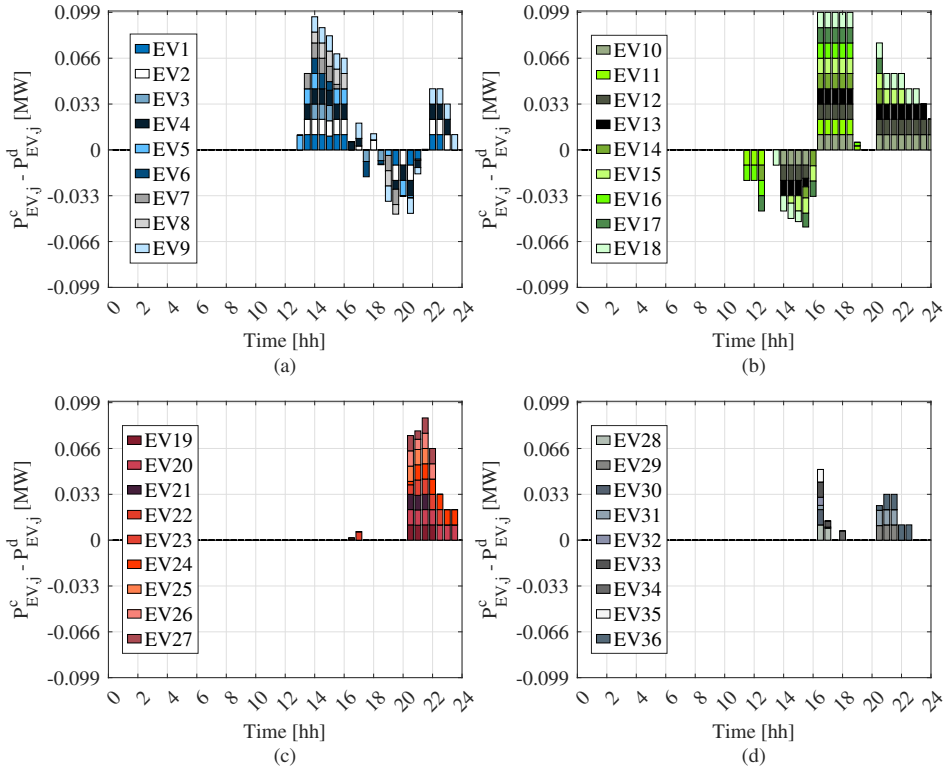

Figure 4.31: Power exchanged by 36 integrated EVs in scenario A6 grouped for node 18 (a), node 22 (b), node 25 (c) and node 33 (d).

charging power is set to 0.1 MW. Therefore, power modulation is necessary and no V2G is depicted, as well as in S8, where total charging power is increased to 0.2 MW and EVs can simultaneously charge (Fig. 4.32a-b). Consequently, grid loss variations reach higher negative peaks during charging events, as in Fig. 4.34b. Whereas, in S9 a reduction in grid losses is reached thanks to the discharge at nodes 18, 33 and 7 around 12:00. In autumn scenarios, more V2G events occur due to higher load demand that requires voltage support by the EVs. Deeper discharge occurs at node 22 in A8 around 10:30 for grid supporting. Same consideration could be done for scenario A9. Moreover, no power exchanges among EV clusters in different nodes occur, since grid operation is more stressed compared to the case of low EV penetration, thus prevailing on other actions not involved in the main target. All energy exchanged are reported in Fig. 4.33.

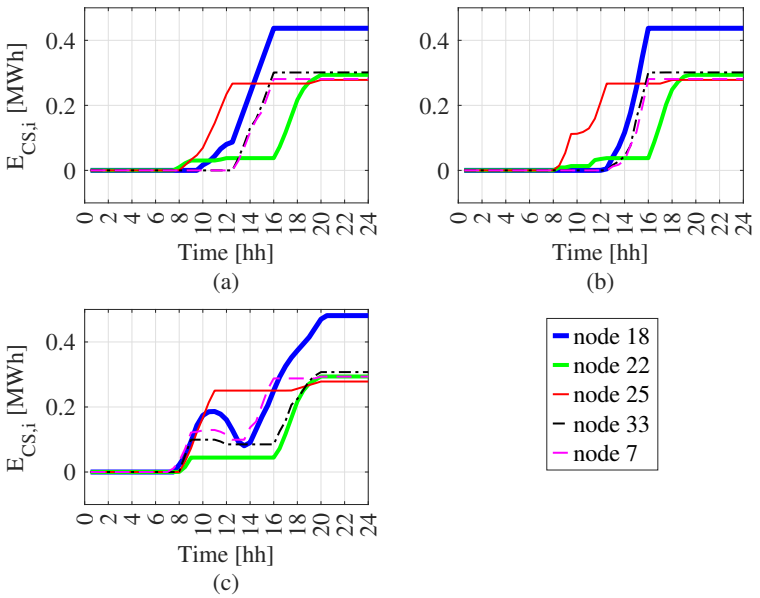

Figure 4.32: Charging station energy in S7 (a), S8 (b) and S9 (c).

Table 4.11 collects the daily energy losses for all simulated scenarios. Generally, the EV integration in the network leads to an increase of grid losses, especially when the number of EVs is high. However, exploiting V2G features could avoid high peaks of losses and load. The inclusion of EVs do not affect particularly the line loading, representing a slight increase (less than 5%) of total grid load requests, nor power flow inversion are observed during V2G exploitation. The activation of stringent nodal voltages in scenarios S3 (A3), S6

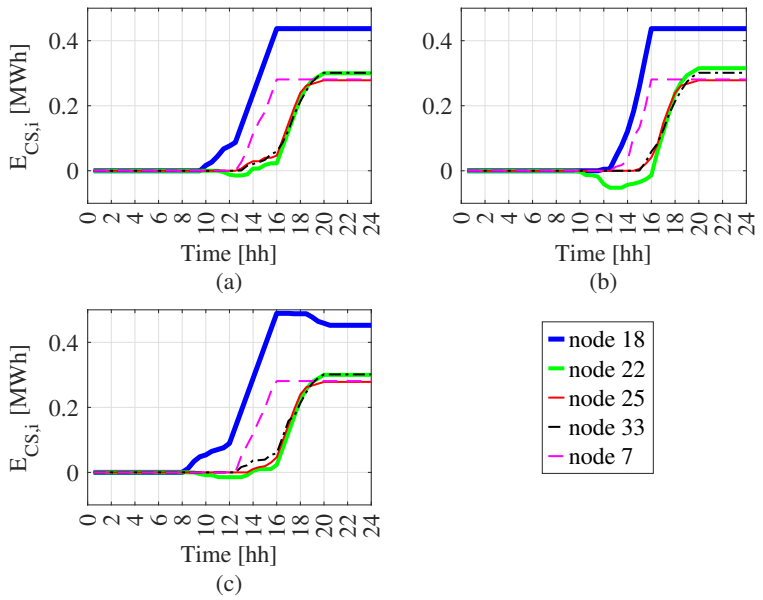

Figure 4.33: Charging station energy in A7 (a), A8 (b) and A9 (c).

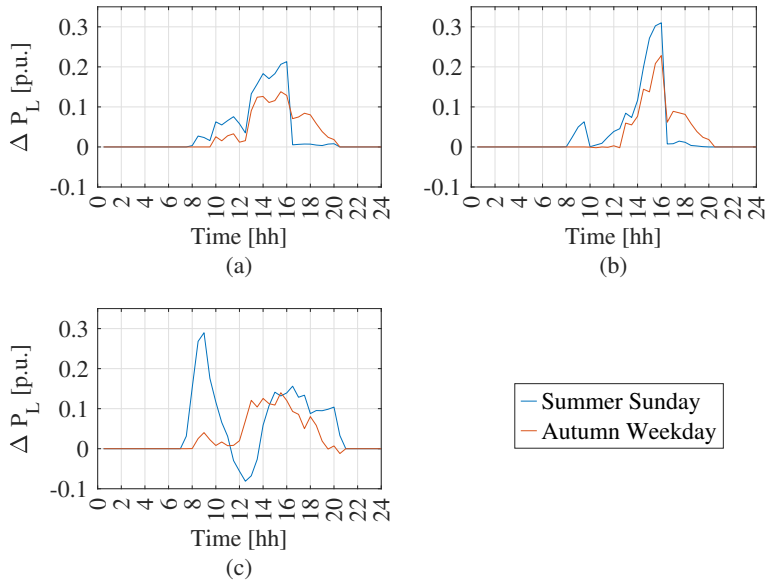

Figure 4.34: Delta energy losses considering 100 integrated EVs in scenarios S7 and A7 (a), S8 and A8 (b), and S9 and A9 (c).

(A6) and S9 (A9) forces the operation of V2G in order to limit voltage drops in the farthest node, such as node 18, where voltage reaches the minimum value imposed by constraints (see Fig. 4.35). Moreover, due to the presence of high load in autumn scenarios, minimum voltage limits are lower than the ones imposed in summer scenarios.

Table 4.11: Total daily losses [MWh] with and without EVs for all scenarios.

S without EVs	**S1**	**S2**	**S3**	**S4**	**S5**	**S6**	**S7**	**S8**	**S9**
1.31	1.34	1.34	1.35	1.33	1.34	1.34	1.39	1.39	1.40
A without EVs	**A1**	**A2**	**A3**	**A4**	**A5**	**A6**	**A7**	**A8**	**A9**
2.08	2.12	2.12	2.12	2.11	2.11	2.11	2.18	2.18	2.18

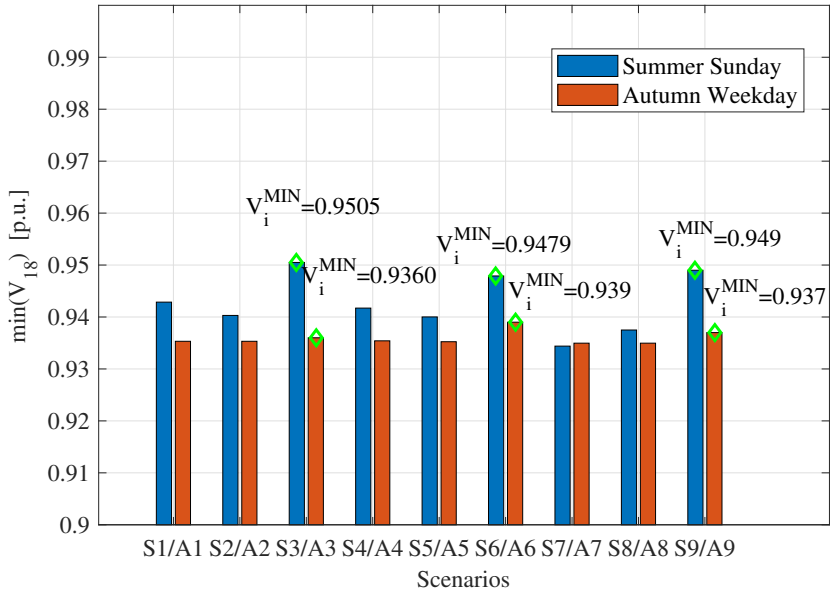

Figure 4.35: Minimum voltage registered at node 18 in all scenarios.

4.6 EV cluster integration into a semi-urban low voltage grid

The methodology presented in Section 4.5.1 is also applied to a semi-urban LV network, in order to inspect the impact of clusters EVs at different penetration level on grids with different features.

LV semi-urban network used is the one modelled by Distribution System Operator Observatory (DSOO) [123], whose scheme with EV station placed is reported in Fig. 4.36a. The grid consists of one MV /LV transformer at node one, 115 nodes and 114 branches organized in several radial feeders. The grid is characterized by total active load of 220 kW, maximum nodal power of 4 kW and load power factor of $cos\phi$ =0.957 [12]. Preliminary load flow analyses are carried out in Matlab (using Matpower tool) in order to inspect the safe operation of the grid under a possible uniform load variation. Two residential utility

load profiles are considered and adapted in the study, a typical autumn weekday and a typical summer Sunday, with 30-min timestep [118]. As shown in Fig. 4.36b, minimum load demand is reached during night hours, whereas peak loads are reached at around 12:00 in summer Sunday and in the interval 18:00 – 22:00 in autumn weekdays.

Additional grid parameters are set:

- P_{G1}^{MAX} is set to 0.4 MW,
- $P_{flow,h}^{MAX}$ is set to 0.29 MVA,
- V_i^{MAX} and V_i^{min} are respectively set to 1.06 and 0.95 p.u.

According to preliminary analysis on the grid, EV charging stations are placed at nodes 16, 66, 92 and 114, which are, respectively, the closest to the three network bifurcations and the farthest one from the transformer, as depicted in Fig. 4.36a. Each EV station includes two charging points. The number of EV stations is chosen in order to satisfy line maximum capacities. EV features are the same reported in Section 4.5.2, as well as distribution functions of stochastic inputs. Table 4.12 collects data generated for EV usage within the grid. Since the timestep granularity is 30 minutes, the samples for arrival/departure times are approximated accordingly.

Table 4.12: EV usage pattern.

node	EV	$t_{EV,j}^{arr}$ [h]	$t_{EV,j}^{dep}$ [h]	$S_{EV,j}^{arr}$ [kWh]	$S_{EV,j}^{dep}$ [kWh]
114	1	10:00	19:00	77.9	97.4
	2	10:00	19:30	73.2	98.9
66	3	08:00	15:00	85.6	89.9
	4	10:00	19:30	72.7	99.1
16	5	09:30	18:00	82.3	95.3
	6	08:00	15:00	85.5	89.3
92	7	08:30	16:00	85.4	91.9
	8	09:00	17:30	83.4	94.5

Several scenarios are simulated and compared by means of indicators defined in Section 4.2.2, combining operation modes of EVs (only coordinated charge or charge and V2G), technical limitation of nodal voltages, shift of arrival and departure times, and increase of the number of integrated EVs. A synthetic collection of scenarios is reported in

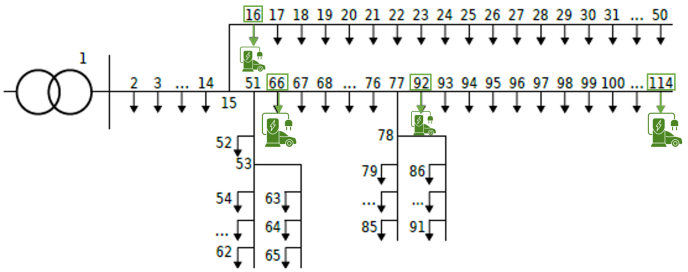

(a)

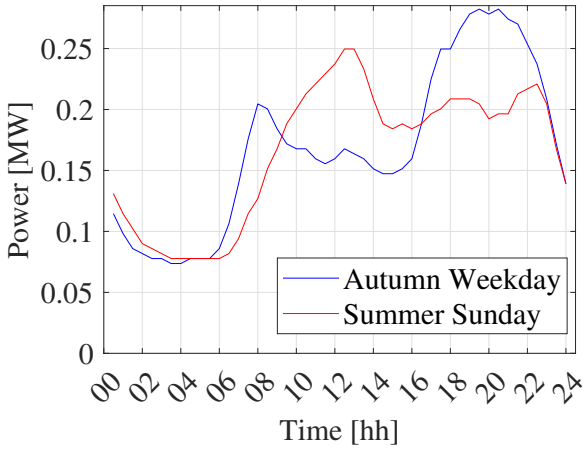

(b)

Figure 4.36: LV semi-urban network schematic integrating EVs [123] (a) and load data profiles in Autumn Weekday and Summer Sunday (b).

Table 4.13. Scenarios S1-4 are tested for summer Sunday, while Scenarios A1 and A2 are tested for autumn weekday.

Moreover, as can be inferred from Fig. 4.36b, maximum load in autumn is close to line loadability, therefore the presence of further EV charging with the arrival/departure time as in Table 4.12 is proved to imply line loading exceed the limits, hindering simulation convergence. Therefore, both autumn scenarios and S4 in summer include V2G functionality for EVs and shifted arrival and departure times during night hours for EV1-4: for EV1 plug-in interval is 17:30-05:00, for EV2 17:30-05:30, for EV3 17:00-06:00, and for EV4 17:00-08:00 – while keeping arrival/departure energies as in Table 4.12.

Table 4.13: Simulation scenarios.

Scenario	V2G	Stringent nodal voltage limit	EV park at night
S1	x	x	x
S2	✓	x	x
S3	✓	✓	x
S4	✓	x	✓
A1	✓	x	✓
A2	✓	✓	✓

4.6.1 Results in Summer scenarios

In scenario S1 EVs are considered as controllable loads. Energy losses are 0.186 MWh, nearly 6.89% higher than total energy losses in the absence of EVs. Fig. 4.37a reports the trends of ΔP_L calculated as in (4.38) during the day: it can be pointed out that losses increase when energy is requested by EVs (as in Fig. 4.37c), and especially in the interval 14:00-17:30 high values of losses are registered, with a maximum of 13.2 kWh (corresponding to 0.4 p.u. variation). EV charging events are optimally chosen during morning hours and afternoon, in order to avoid line overloading during the hours when grid load is high.

In scenario S2, daily energy losses are the same as S1, with a higher peak of 15.6 kWh at 15:00 (corresponding to nearly 0.5 variation, see Fig. 4.38a). The V2G functionality leads to peak shaving event, since EVs discharge when grid load reaches high values, around 12:00-13:00, as reported in Fig. 4.38c, where negative values represent discharging events.

Since the considered network is mainly passive, the voltage reduction is more challenging than voltage increase, therefore in S3 the value of V_i^{min} is increased up to the limit of procedure convergence. For a value of 0.986 p.u., a negative value of variation in the time 11:00-14:00 with respect to the case without EVs is observed, due to V2G exploitation (Fig. 4.39a-c) to cope with voltage constraint at the farthest node. The peak of losses is 12.1 kWh, lower than the ones in previous scenarios. From exchanged powers by EVs in Fig. 4.39c it can be seen that, during their plug-in time, EVs are first charged and then discharged to support the grid, and after that another charge is observed (as EV1 at node 114, see Fig. 4.39b).

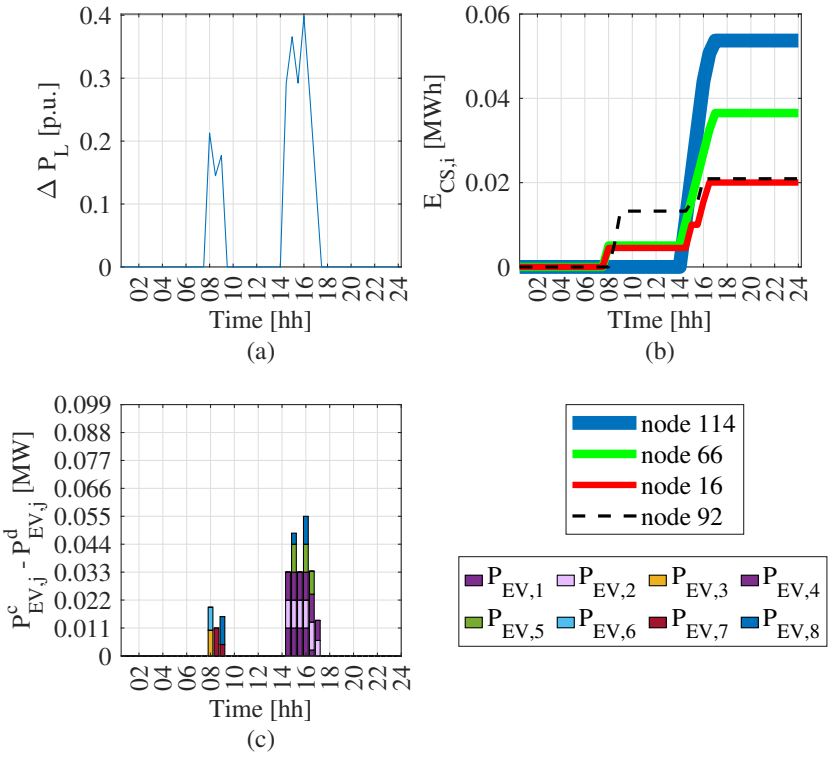

Figure 4.37: Variation of power losses ΔP_L (a), energy exchanged by CSs $E_{CS,i}$ (b), and exchanged powers by EVs (c) in Scenario S1.

Shifted plug-in times in S4 lead to an increase in energy losses during night hours (Fig. 4.40), due to EV charge, while during morning hours losses decrease due to EV5-8 discharge aiming to contribute to voltage support (Fig. 4.40c). Total losses are 0.176 MWh, 5.37% lower than ones in S2.

In Fig. 4.41 nodal voltage profiles are shown for all summer scenarios: as supposed, node 114 has the lowest voltage profile, reaching the minimum of 0.97 p.u. in S2 at 15:00. In S3 node 114 and the close ones reach the imposed minimum technical value. Line loading levels F_h are reported in Fig. 4.42. In S1 the maximum rate is 0.91 p.u. for line 1 at 12:30. However, line loading is affected by EV charging events during afternoon, while in S2 V2G functionality leads to flow inversion especially in line 63, as in Fig. 4.42b, as well as the flow inversion in the same line in S4 at 18:00, followed at 19:00 by line 112, and at 21:30 by line 108 and 112.

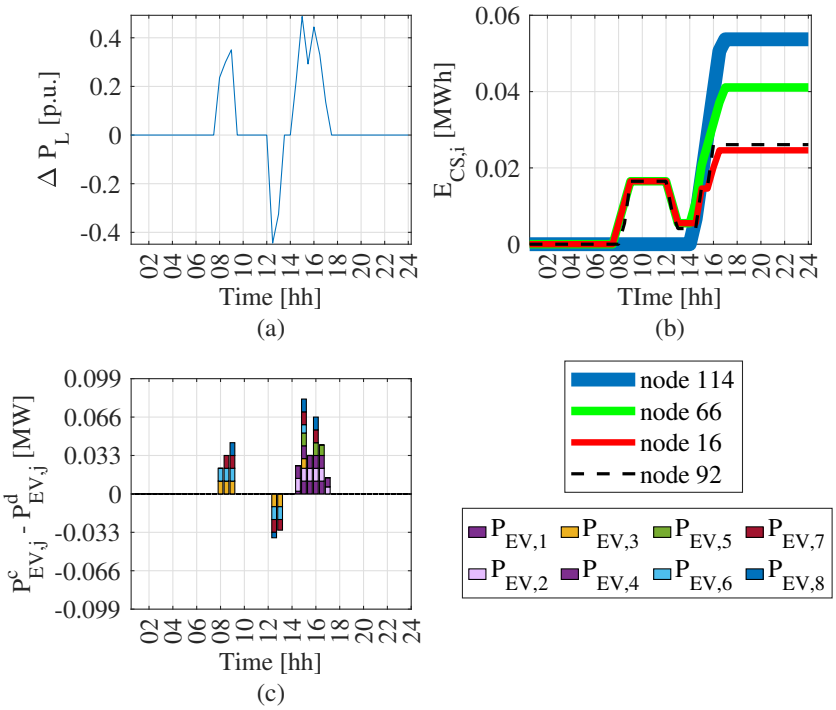

Figure 4.38: Variation of power losses ΔP_L (a), energy exchanged by CSs $E_{CS,i}$ (b), and exchanged powers by EVs (c) in Scenario S2.

4.6.2 Results in Autumn scenarios

In scenario A1 energy losses are 0.186 MWh, nearly 2.10% lower than the corresponding without EVs. As it can be seen in Fig. 4.43a, a decrease in losses is achieved during evening hours, when EVs can discharge. However, EV charging causes an increase in losses with a maximum of 8 kWh at 15:00, still lower than the ones in S2. In this scenario, EVs connected to nodes 114 and 66 discharge more frequently than ones in nodes 16 and 92 (Fig. 4.43c), due to variability of sensitivity coefficients during the evening that encourage discharging of EV1-4 to support grid voltage when load is higher. In A1, the minimum registered voltage value is 0.972 p.u. as shown in Fig. 4.45a.

In scenario A2 the minimum voltage limit is increased up to 0.979 p.u., representing the limit value for procedure convergence. Comparing losses in Fig. 4.44a it can be pointed out that same reduction in losses of A1 is reached during evening hours, as well as the loss peak at 15:00 due to EV charging. However, a lower peak of around 14 kWh at 18:30 is reached, which is 13% lower than the corresponding value in A1. Furthermore, the same

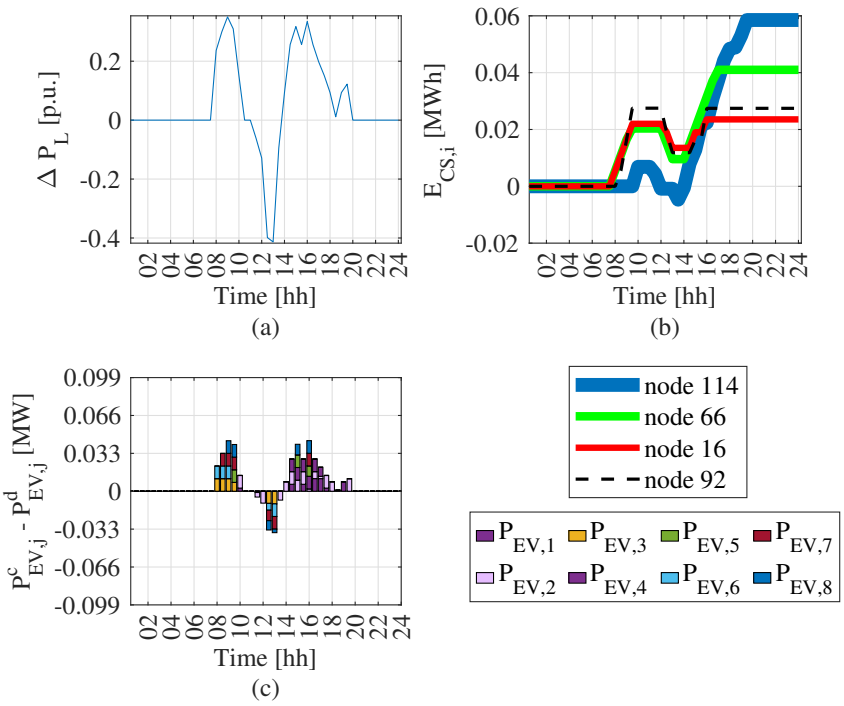

Figure 4.39: Variation of power losses ΔP_L (a), energy exchanged by CSs $E_{CS,i}$ (b), and exchanged powers by EVs (c) in Scenario S3.

amount of daily losses is registered. In order to satisfy the updated minimum voltage limit in A2 scenario, EV discharge occur to prevent limit violation at node 114 (as reported in Fig. 4.45b). Same considerations about EVs at nodes 114 and 66 that discharge at maximum power are still valid in scenario A2.

Table 4.14 collects the daily energy losses for all scenarios. It can be seen that the use of EV stations generally implies an increase of daily energy losses, except for the night-long parking scenarios, where the difference of sensitivity factors between night and other hours implies the possibility to reduce losses exploiting V2G. Line flow rates for both scenarios are shown in Fig. 4.46. Flow inversion due to V2G exploitation occurs in line 63 in both A1 and A2, in order to support nodal voltage.

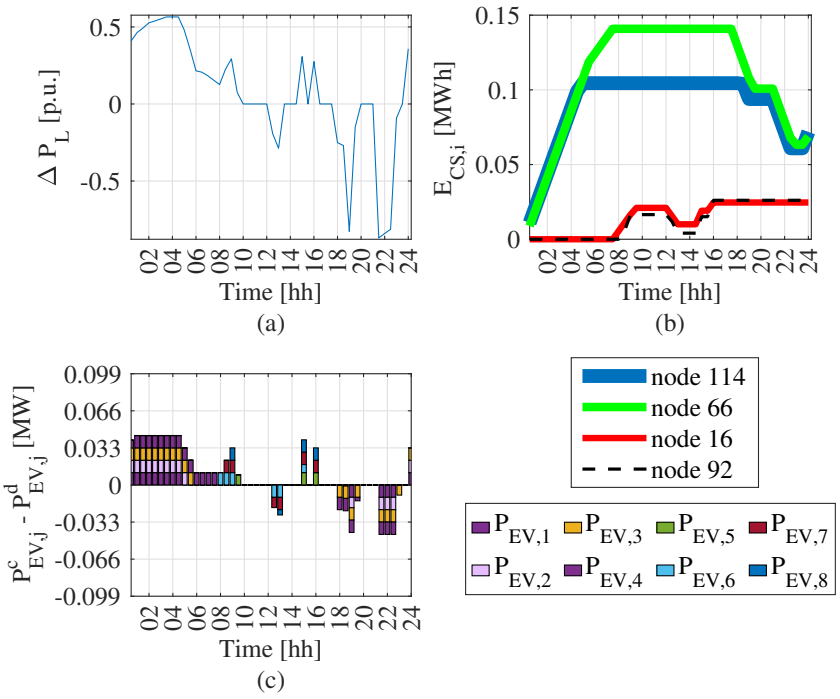

Figure 4.40: Delta energy losses ΔP_L (a), energy exchanged by CSs $E_{CS,i}$ (b), and exchanged powers by EVs (c) in Scenario S4.

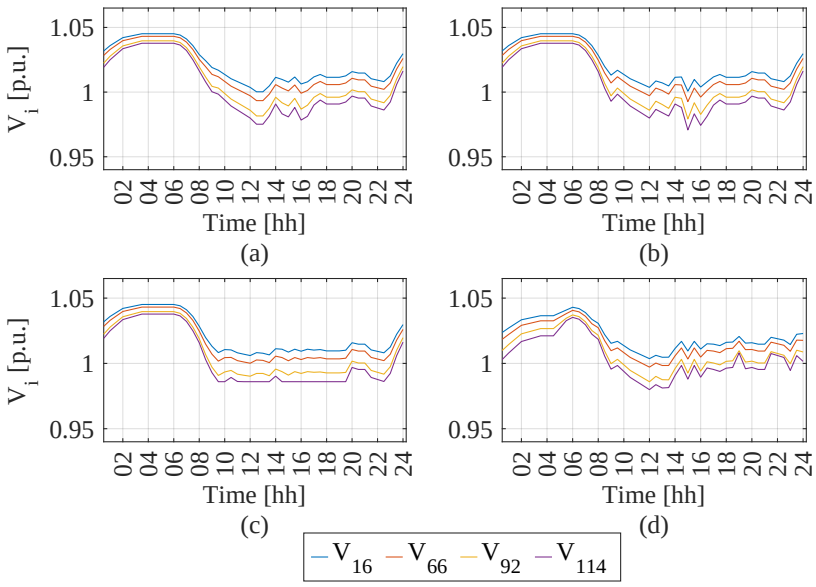

Figure 4.41: Voltage profile in nodes 16, 66, 92 and 114 in scenarios S1 (a), S2 (b), S3 (c) and S4 (d).

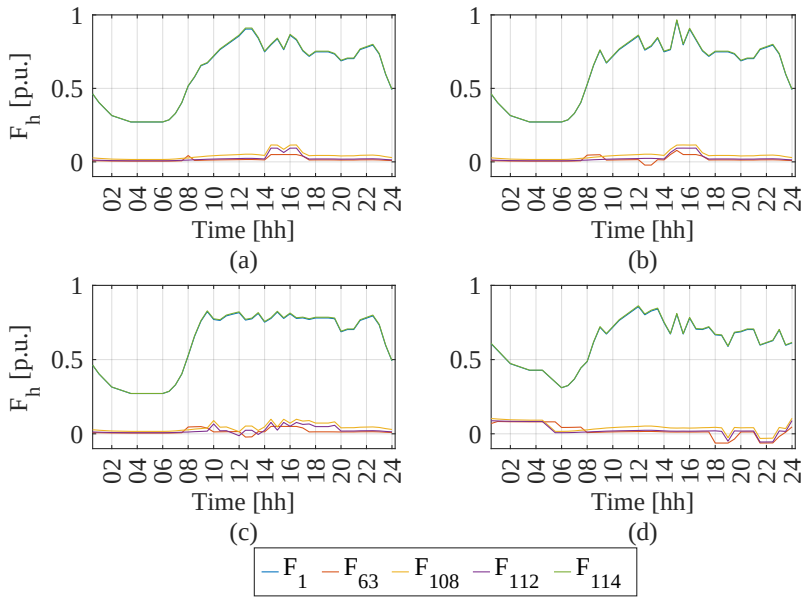

Figure 4.42: Loading profiles in lines 16, 66, 92 and 114 in scenarios S1 (a), S2 (b), S3 (c) and S4 (d).

Table 4.14: Daily energy losses in all scenarios.

Scenario	**w/o EVs [MWh]**	**With EVs [MWh]**
S1	0.174	0.186
S2	0.174	0.186
S3	0.174	0.187
S4	0.174	0.176
A1	0.190	0.186
A2	0.190	0.186

4.7 DC microgrid EVSI integration in MV distribution grid

In this section a multi-objective optimization is proposed for optimal programming of DC microgrids for EV supply integrated into MV distribution grid, with the aim of minimizing both utility grid and single microgrid targets. Starting from the methodologies described separately in Sections 2.2 and 4.5.1, a multi-objective problem is defined and tested on the realistic radial distribution grid integrating a set of 4 DC microgrids.

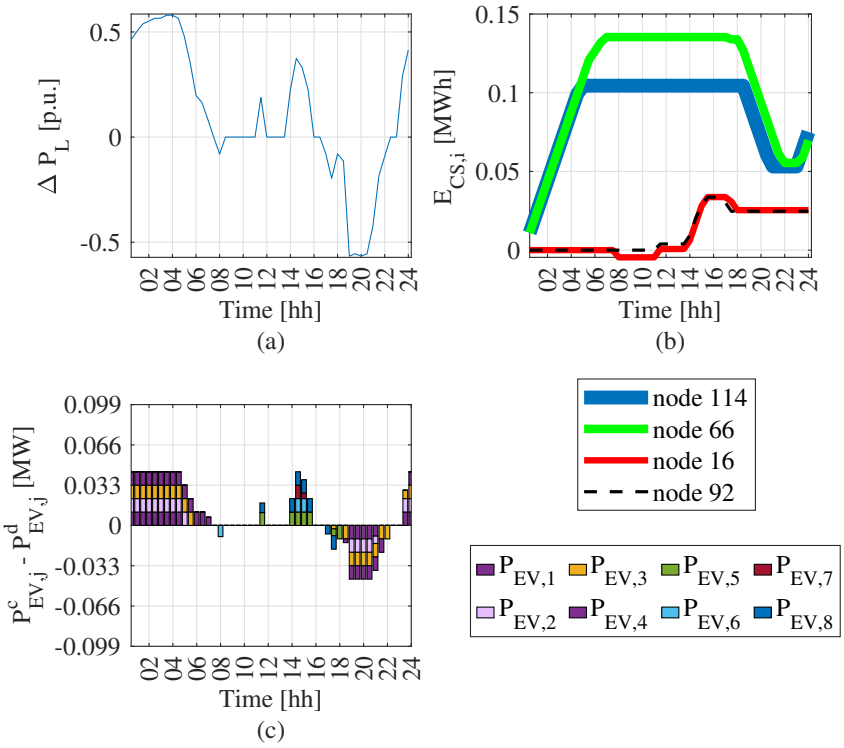

Figure 4.43: Delta energy losses ΔP_L (a), energy exchanged by CSs $E_{CS,i}$ (b), and exchanged powers by EVs (c) in Scenario A1.

4.7.1 Multi-objective MILP problem

The proposed procedure employs a MILP optimization problem for the integration of n_{MG} DC microgrids in a MV passive distribution grid consisting of n buses (1 generation node and $n-1$ load) and N_L lines. To this purpose, the grid state vector combines grid variables, such as the nodal voltage amplitudes (p.u.) - V_i -, generated powers ($P_{G,i}$), exchanged power of the integarted DC microgrid ($P_{MG,i}$), active power flows of the h-th network line ($P_{flow,h}$), and variables of each b-th DC microgrid, that are active power withdrawn from / delivered to the distribution network ($P^{in}_{g,b}(t)$ and $P^{out}_{g,b}(t)$), charge power, discharge power and SOC of the BESS ($P^{c}_{B,b}(t)$, $P^{d}_{B,b}(t)$ and $S_{B,b}(t)$), charge power, discharge power and SOC of each b–th EV microgrid - $P^{c}_{EV,b}(t)$, $P^{d}_{EV,b}(t)$ and $S_b(t)$ -, integer variables for grid connection $v_{g,b}(t)$, for BESS $v_{B,b}(t)$, and for each EV $v_b(t)$, equal to 1 if the power exchange is towards the DC common bus and 0 otherwise, for each time-step t (see Section 2.2).

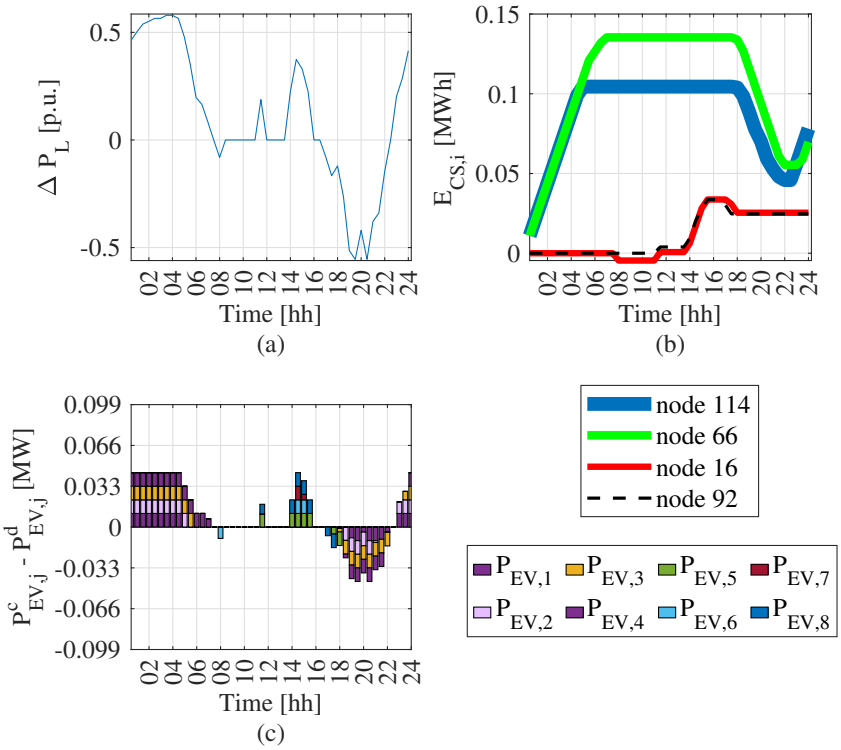

Figure 4.44: Delta energy losses ΔP_L (a), energy exchanged by CSs $E_{CS,i}$ (b), and exchanged powers by EVs (c) in Scenario A2.

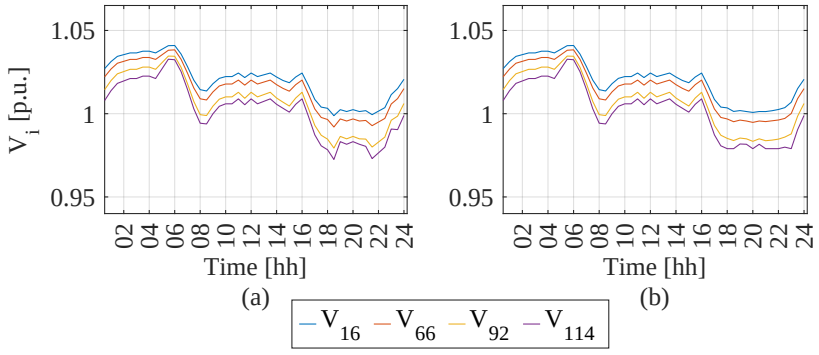

Figure 4.45: Voltage profiles in nodes 16, 66, 92 and 114 in scenarios A1 (a) and A2 (b).

Therefore, the state vector has dimensions $[(1+n+N_L+n_{MG})\times N_T+(3+5+5\times n_{EV})\times n_{MG}\times N_T]\times 1$.

The considered objective function aims at minimizing a technical target, represented by

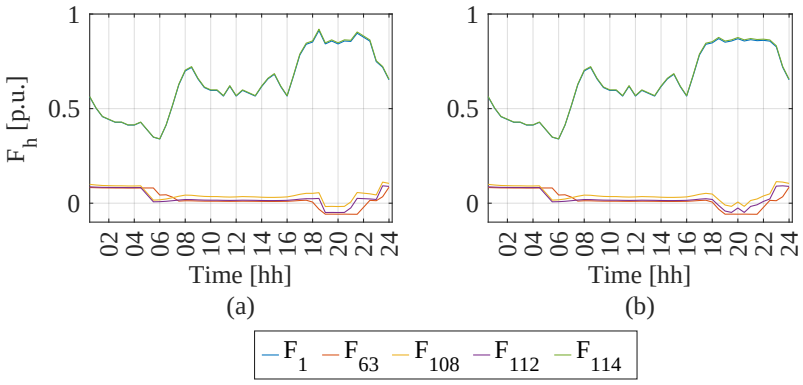

Figure 4.46: Power flow rate in lines 1, 63, 108, 112 and 114 in scenarios A1 (a) and A2 (b).

the total losses, and an economic one, given by the costs afforded by DC microgrids (4.47).

$$f^{comb} = \sum_{t}^{N_T} \left\{ \left[\frac{P_{G1}(t)}{P_{ref}} - \sum_{b}^{n_{MG}} \frac{P_{MG,b}(t)}{P_{ref}} \right] + \sum_{b}^{n_{MG}} \frac{Cost_{MG,b}(t)}{Cost_{ref}} \right\} \tag{4.47}$$

Daily costs for DC microgrid take into account costs for energy purchase, EV charging and for wearing of BESS and EVs, and revenues for power selling and EV V2G operation. The expression is the one defined in (2.2), adapted for each microgrid, and reported in (4.48).

$$\begin{aligned} Cost_{MG,b}(t) =& \Delta T \cdot \Big\{ c_g(t) \cdot P^{in}_{g,b}(t) - r_g(t) \cdot P^{out}_{g,b}(t) + w_B \cdot [P^c_{B,b}(t) + P^d_{B,b}(t)] + \\ &+ [w_b + c_{EV}(t)] \cdot P^c_{EV,b}(t) + [w_b - r_g(t)] \cdot P^d_{EV,b}(t) \Big\} \quad \forall b \in [1; n_{MG}] \end{aligned} \tag{4.48}$$

Equality constraints include grid load flow equations, linearized as in (4.29), (4.30) and (4.32), where $P_{MG,i}(t)$ is substituted to $P_{CS,i}(t)$. Moreover, the two levels are coupled by means of equality constraint (4.34) assigning microgrids to network node, which is modified as formulated in (4.49), considering active withdrawn power $P^{in}_{g,b}(t)$ and power delivered to the grid $P^{out}_{g,b}(t)$, where $\beta_{b,i}$ is a binary coefficient equal to 1 if the correspondence between b-th DC microgrid and the i-th load node is verified, 0 otherwise.

$$P_{MG,i}(t) = \sum_{b=1}^{n_{MG}} \beta_{b,i} \cdot \left[P_{g,b}^{in}(t) - P_{g,b}^{out}(t)\right] \quad \forall i \in [2; n],\ \forall t \in [1; N_T] \tag{4.49}$$

DC microgrid equality constraints regarding power balance at the DC bus (2.3), SOC evolution for BESS and EV batteries (2.4) and (2.5), and for setting initial and final SOC of BESS and EVs - (2.6a) and (2.6b) - are still included in the formulation. Inequality constraints for the grid regard the maximum and the minimum energy $E_{MG,b}^{MAX}$ and $E_{MG,b}^{min}$ that each microgrid could exchange in all daily horizon, as in (4.50a) and (4.50b).

$$\sum_{t}^{N_T} P_{MG,b}(t) \cdot \Delta T \leq E_{MG,b}^{MAX} \quad \forall b \in [1; n_{MG}] \tag{4.50a}$$

$$\sum_{t}^{N_T} P_{MG,b}(t) \cdot \Delta T \geq E_{MG,b}^{min} \quad \forall b \in [1; n_{MG}] \tag{4.50b}$$

For each DC microgrid inequality constraints (2.7) and (2.8) (also for BESS and EV powers), along with discharge limitations in (2.11) and (2.12) are still valid in this formulation. Finally, upper and lower bounds for each state variable are set in order to respect technical limits of the components - see (4.35a)-(4.35j) for the grid model and (2.9a)-(2.9i) for DC microgrid model.

4.7.2 Techno-economic indicators

Technical and economic indicators are defined in order to evaluated obtained results. In particular, active power loss variation with respect to the case of the grid without EVs (base case), that take into account also the existing load $P_{load,i}(t)$ for each i-th node of the grid, expressed in MWh in (4.38), the energy exchanged at DC microgrids calculated in (4.44) replacing $P_{CS,i}$ with $P_{MG,i}$, and line loading rate $F_h(t)$ defined for each h-th branch of the network as in (4.45). Moreover, the total cost evaluated in (4.48) is the economic indicator.

4.7.3 Grid features and DC microgrid architectures

The IEEE-33 radial distribution grid described in Section 4.3.1 with its characteristics is used for the implementation of the multi-objective procedure for the optimal daily programming of the grid integrating 4 DC microgrids (n_{MG} =4) at nodes 18, 22, 25 and 33, as in Fig. 4.47. Grid load profile is the one referring to a typical Summer Sunday, as shown in Fig. 4.11c.

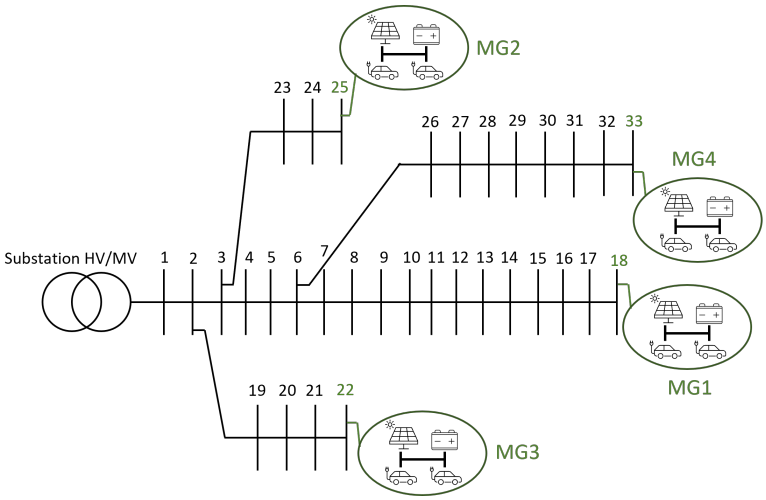

Figure 4.47: IEEE-33 grid topology with the integration of 4 DC microgrids.

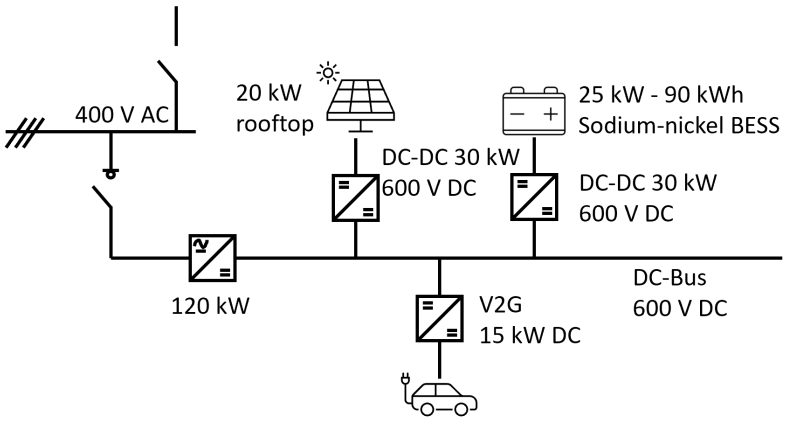

Figure 4.48: Layout of each DC microgrid integrated.

Each DC microgrid consists of a 20 kW PV generator, a 25 kW/ 90 kWh BESS and one 15 kW EV bidirectional charging station. Features of the BESS and EV station, along with BESS and EV initial SOC, are respectively collected in Table 4.15 and Table 4.16. The layout of the DC microgrid is shown in Fig. 4.48.

Table 4.15: BESS features.

	BESS
η_B^c	0.95
η_B^d	0.95
$P_B^{c,MIN}$ [kW]	0
$P_B^{c,MAX}$ [kW]	25
$P_B^{d,MIN}$ [kW]	0
$P_B^{d,MAX}$ [kW]	25
H_B [kWh]	90
S_B^{MIN} [kWh]	18
$S_B(t=1)$ [%]	60

Table 4.16: EV station features.

	EV station
$\eta_{EV,b}^c$	0.95
$\eta_{EV,b}^d$	0.95
$P_{EV,b}^{c,MIN}$ [kW]	0
$P_{EV,b}^{c,MAX}$ [kW]	15
$P_{EV,b}^{d,MIN}$ [kW]	0
$P_{EV,b}^{d,MAX}$ [kW]	15
Cap [kWh]	60
S_b^{MIN} [kWh]	6
$S_b(t=1)$ [%]	30

EV usage in each microgrid is generated according to the probabilistic approach reported in Section 2.2.5. Plug-in times are shown in Fig. 4.49, where it can be seen that the EV considered for microgrid 1 travels from 09:30 to 10:30 and from 12:00 to 13:30, the one of microgrid 2 from 08:00 to 10:00, the one connected to microgrid 3 from 10:30 to 12:00 and from 18:30 to 19:30, and the one connected to microgrid 4 from 13:30 to 15:30.

The energy buying and selling prices considered in (4.48) refer to a summer sunday in 2021, the year before the events of 2022 that brought a sharp increase in energy costs. Buying prices c_g are modeled by adding to the National Single Price values (taken in [110] from GME), the transportation costs and the system charges in the case of non-domestic loads, obtained from [109]. EV charging costs c_j are modeled by adding a surplus of 0.05 €/kWh to the energy buying prices, taking into account charging infrastructure charges, while revenues for V2G discharge r_j are assumed to be equal to costs of vehicle charging

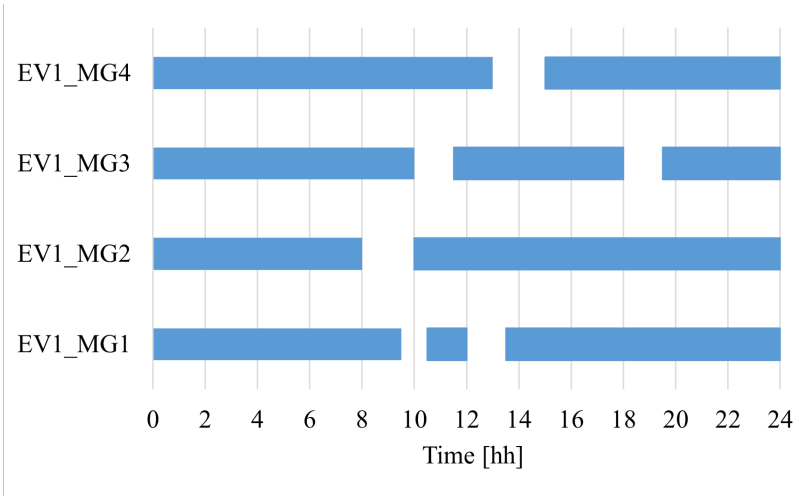

Figure 4.49: Plug-in times of EV1 in each microgrid integrated in the distribution network.

with a surplus of 0.16 €/kWh, corresponding to the remuneration to the vehicle owner for the service offered. Electric vehicle battery degradation cost and BESS degradation cost were assumed to be 2 € and 0.9 € per full discharge cycle, respectively. They represent plausible values for the two different battery technologies considered. Fig. 4.50 shows the trends over time of the unit costs used in the simulations. It can be seen that all the costs considered present the maximum value at 22:00. The minimum selling price is 0.072 €/kWh and it occurs from 11:00 to 12:00, while the minimum buying, charging, and discharging prices are respectively 0.11 €/kWh, 0.16 €/kWh, and 0.32 €/kWh, occurring at 07:00. In addition, the degradation costs of BESS (w_B) and EVs (w_j) are 0.01 €/kWh and 0.033 €/kWh.

P_{ref} considered in (4.47) is set to 0.1 MW, which corresponds to the power generated peak in the absence of microgrids, whereas C_{ref} is the reference cost for DC microgrids, evaluated as the sum of single cost for energy purchaising for EV charging assuming uncontrolled charge estimated at 17.53 €.

4.7.4 Results and indicator evaluation

In the scenario under investigation, total daily energy losses from the grid are 1.3002 MWh, 0.95 % lower than the 1.3126 MWh in the base case, in the absence of DC microgrids. Fig. 4.51 shows, all over the daily horizon, the power production by the generating node

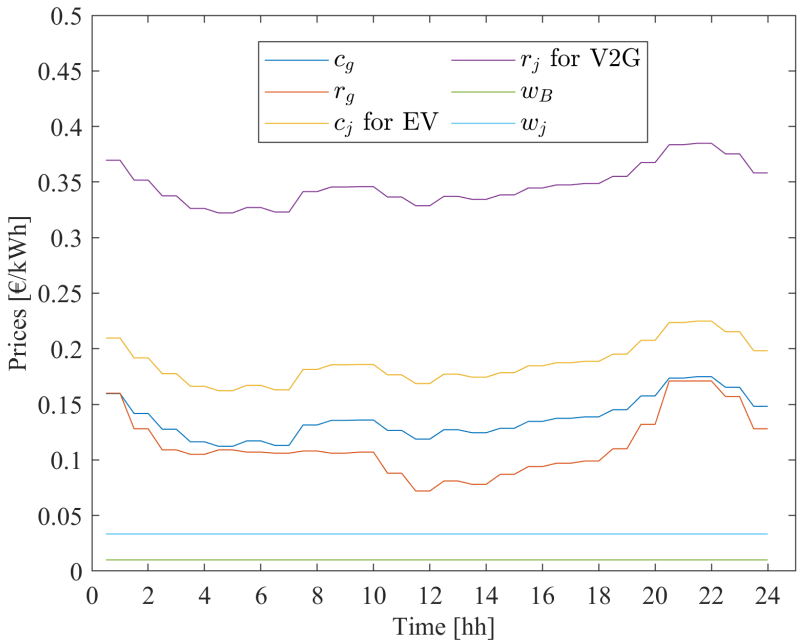

Figure 4.50: Unit costs used for economic evaluation.

P_{G1}, grid losses, power flow rates along the lines, nodal voltages, and power drawn totally from the microgrids. As shown in 4.51a, the generated power peak of 3.24 MW occurs at 13:00 (as in the case of no microgrids). Moreover, P_{G1} is decidedly reduced from 20:30 to 22:00, during the evening peak. A 1.7% increase of P_{G1} is detected at around 04:30, due to EV charging in each microgrid (see Fig. 4.52).

Losses and power flow rate show a decrease from 20:30 to 22:00 in Fig. 4.51b-c. Specifically, around 22:00, inversion of power flow occurs in load line 21 and 32 (terminal lines of the network), thus providing respectively 9.4 kW and 18.5 kW excess power to the grid over their maximum of 2.76 MW.

The nodal voltage amplitudes (Fig. 4.51d), especially the ones of farthest node from the generation, show a slight decrease around 04:30, in accordance to the increase of losses and power generation.

Referring to Fig. 4.51e, all microgrids absorb energy during the night, in order to provide it during the day. This is particularly intense for microgrid 1, up to 21.5 kWh at 06:30, due to its EV energy requirements for numerous trips. On the contrary, microgrid 3 has lower absorption, i.e. 6.10 kWh at 04:30, which is more similar to that obtained in micro-

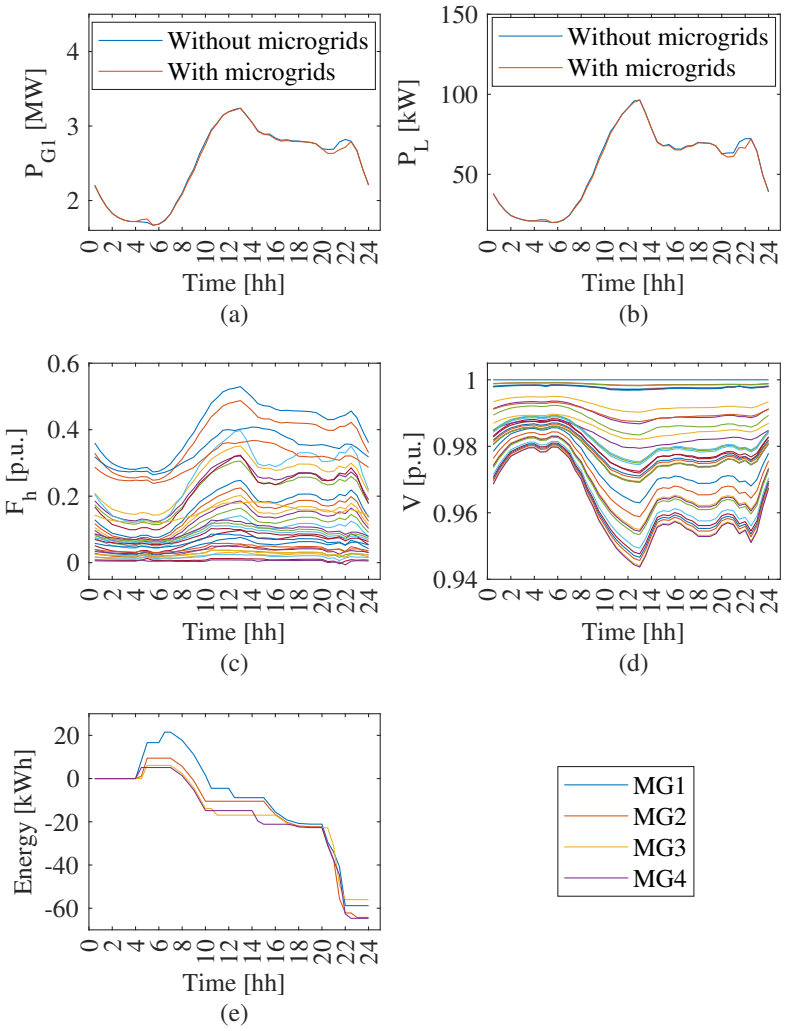

Figure 4.51: Power generated by the generating node P_{G1} (a), grid losses (b), power flow rates along the lines (c), nodal voltages (d), and power drawn totally from the microgrids (e).

grids 2 and 4 (that absorb 9.4 kWh at 05:00 and 5.1 kWh at 04:30, respectively). This is due to EV mobility of microgrid 3, where EV travels are long but spread out over time (with respect to EV in microgrid 1). Consequently, in microgrid 3, PV generator provides energy to the EV during the day (see Fig. 4.52c).

Furthermore, energy provided by microgrid 3 is lower than one by microgrid 1, because of the gap between the sensitivity coefficients of the power generated at the slack node between night and daytime hours is much greater for the node where microgrid 1 is connected

(node 18) than for the node to which microgrid 3 is connected (node 22). Moreover, the absorption occurs for all microgrids at night, as both cost of purchasing energy and sensitivity coefficients of power generation at the slack bus are lower during the night hours, thus implying lower increase of both the objective function terms.

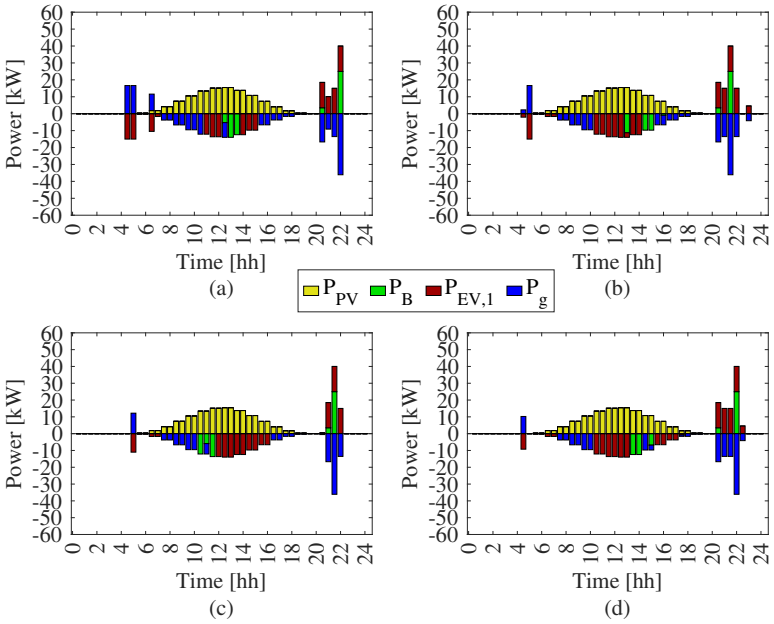

Figure 4.52: Power balance at the DC bus in microgrid 1 (a), 2 (b), 3 (c), and 4 (d).

Power exchanges inside each DC microgrid are reported in Fig. 4.52. Regarding powers in microgrid 1, it can be seen that 16.6 kWh energy import from the grid from 04:30 to 05:00 occurs, in order to charge EV at maximum power. Power generated by PV is delivered then to the distribution grid until 10:30 and then again from 15:30 to 18:00. EV and BESS are charged from 10:30 to 15:00. This allows V2G operation from 20:00 to 22:00 when $P_{g,1}^{out}$ reaches its peak of 36.1 kW. Microgrids 2 and 4 perform analogously to microgrid 1, except for the lower power consumption during the night. In microgrid 3, on the other hand, EV charge is supplied by PV after the first route, and it is extended for a longer duration in order to limit the energy absorbed from the grid.

Pursuing the economic target, microgrids are pushed to inject power into the grid by performing V2G, predominantly in the evening hours when revenues for discharge are higher. With this aim, PV production is mostly dedicated to charging the EV more than the BESS.

This target still ensures a reduction in losses, especially due to contribution of DC microgrid power exports to the grid.

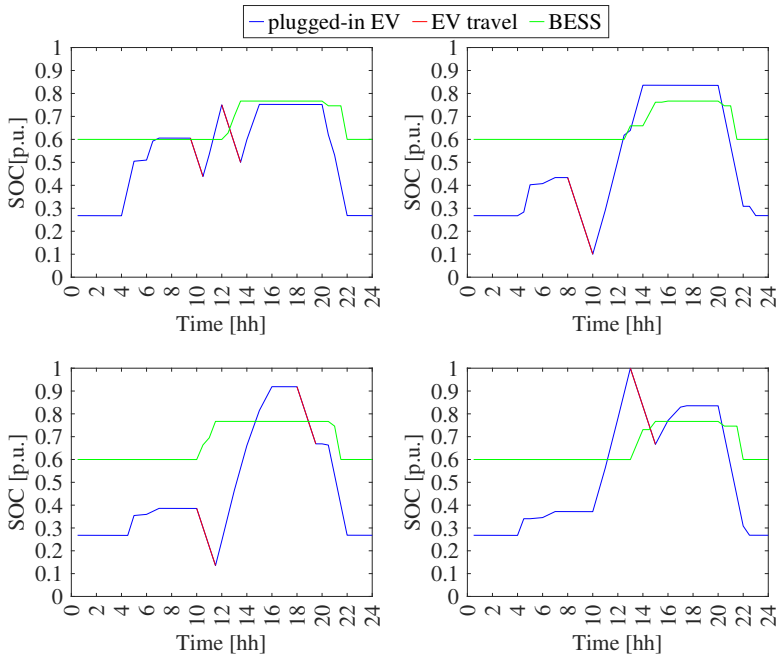

Figure 4.53: EV and BESS SOC levels in microgrid 1 (a), 2 (b), 3 (c), and 4 (d).

SOC levels of EV and BESS for each microgrid are shown in Fig. 4.53. In all microgrids, BESS have a limited operating range between 60.98% and 76.68%, whereas the capacity range of EVs is almost entirely exploited. In addition, BESS is not used to charge EV, as this process would imply higher costs due to wearing, and also because it is more convenient for EV to be charged first by PV and then by the grid; in particular, the EV in microgrid 1 reaches its maximum charge value of 75.25% at 15:00 as a result of being charged by PV after the end of its second travel. EV in microgrid 2 reaches the minimum permitted charge value of 10% at 10:00, while it reaches the maximum value of 83.59% at 14:00 after being charged by PV . In microgrid 3, the vehicle also reaches the minimum SOC value, while PV-supplied charge allows it to reach a maximum SOC of 91.9% at 16:00. Finally, in microgrid 4 EV fully charges as its journey starts later than the EVs in the other microgrids.

Costs related to bought and sold energy, along with BESS and EV wearing costs, EV charging costs, V2G revenues and net costs for all microgrids are all collected in Table 4.17. Generally, the presence of economic target for microgrid leads to higher remuneration for

selling energy to the grid exploiting V2G features. This results in a negative daily net cost for all microgrids. It can be seen that microgrid 1 incurs the highest cost for energy purchasing (3.19 €), as well as the highest revenue for energy selling (-10.28 €). The highest remuneration for V2G services are obtained by microgrids 2 and 4 (-11.57 €), as well as the total costs. BESS and EV wearing costs are almost the same for all microgrids, along with costs for EV charging.

Table 4.17: Daily cost components of DC microgrids.

	MG 1	**MG 2**	**MG 3**	**MG 4**
Purchased Energy [€]	3.19	1.40	0.90	0.76
Sold Energy [€]	-10.28	-9.44	-7.95	-8.94
BESS wearing [€]	0.30	0.30	0.30	0.30
EV wearing [€]	2.82	2.98	2.66	2.98
EV charge [€]	11.30	11.30	11.30	11.30
V2G revenue [€]	-9.87	-11.57	-8.17	-11.57
$Cost_{MG,b}$ [€]	-2.54	-5.02	-0.95	-5.16

4.8 LEC approach for DC microgrids integrated in MV grids: cost benefit analyses

With the aim of studying the behaviour that the aggregation of microgrids would have in pursuing a community target, assuming that a grid load is involved into the community and that the supply of it is marked by an incentive, it is possible to calculate the total daily community costs for different types of load. In these considerations, the amount of power flows on the distribution network is not considered, given that no constraints (e.g. on cable ampacity) is violated. In particular, assuming that the DC microgrids are interfacing with the grid as a single entity, the total power exchange of this entity with the external system is the sum of the power exchanged by each of the microgrids, $P_{MGS}(t)$ (positive if absorbed by the community, negative if delivered to the grid or null, if there is no exchange with the grid). As in (4.51), $P_{MGS}(t)$ is the algebraic sum of absorbed power $P^{in}_{MGS}(t)$ and delivered power $P^{out}_{MGS}(t)$, that are expressed as in (4.52a) and (4.52b). Furthermore, the quantity $P^{exch}_{MGS}(t)$ is defined as the amount of power exchanged at time t among microgrids,

equal to the minimum between $P^{in}_{MGS}(t)$ and $P^{out}_{MGS}(t)$ (4.53).

$$P_{MGS}(t) = P^{in}_{MGS}(t) - P^{out}_{MGS}(t) \;\; \forall t \in [1; N_T] \tag{4.51}$$

$$P^{in}_{MGS}(t) = \sum_{b}^{n_{MG}} P^{in}_{g,b}(t) \;\; \forall t \in [1; N_T] \tag{4.52a}$$

$$P^{out}_{MGS}(t) = \sum_{b}^{n_{MG}} P^{out}_{g,b}(t) \;\; \forall t \in [1; N_T] \tag{4.52b}$$

$$P^{exch}_{MGS}(t) = \min \left[P^{in}_{MGS}(t); P^{out}_{MGS}(t) \right] \;\; \forall t \in [1; N_T] \tag{4.53}$$

Furthermore, the relation among community load $P_{load,LEC}(t)$, power exchanged by microgrids $P_{MGS}(t)$, power absorbed (sold) by the energy community $P^{in}_{LEC}(t)$ ($P^{out}_{LEC}(t)$) and exchanged $P^{exch}_{LEC}(t)$ is expressed in (4.54).

$$P_{MGS}(t) + P_{load,LEC}(t) = P^{exch}_{LEC}(t) + P^{in}_{LEC}(t) - P^{out}_{LEC}(t) \;\; \forall t \in [1; N_T] \tag{4.54}$$

Depending on $P_{MGS}(t)$ sign, three cases are modelled. In the first one, if $P_{MGS}(t) > 0$ it means that power from the whole entity of microgrids is required from the grid; therefore, there is no power exchanged inside the community to feed the load and no power sold to the grid. If $P_{MGS}(t) < 0$ and also $|P_{MGS}(t)| > P_{load,LEC}(t)$, then the group of microgrids can provide power to the load within the community and sell the excess to the external grid, without any power purchase. In the third case $P_{MGS}(t) < 0$ and also $|P_{MGS}(t)| < P_{load,LEC}(t)$ occur, thus part of the load required power is provided by microgrids, while the residual part is covered by power purchase from the energy provider. The three cases are reported in (4.55)-(4.57).

$$if \;\; P_{MGS}(t) > 0 \Rightarrow \begin{cases} P^{exch}_{LEC}(t) = 0 \\ P^{out}_{LEC}(t) = 0 \\ P^{in}_{LEC}(t) = P_{MGS}(t) + P_{load,LEC}(t) \end{cases} \tag{4.55}$$

$$if \;\; P_{MGS}(t) < 0, |P_{MGS}(t)| > P_{load,LEC}(t) \Rightarrow \begin{cases} P^{exch}_{LEC}(t) = P_{load,i}(t) \\ P^{out}_{LEC}(t) = |P_{MGS}(t)| - P_{load,LEC}(t) \\ P^{in}_{LEC}(t) = 0 \end{cases} \tag{4.56}$$

$$if \;\; P_{MGS}(t) < 0, |P_{MGS}(t)| < P_{load,LEC}(t) \Rightarrow \begin{cases} P^{exch}_{LEC}(t) = |P_{MGS}(t)| \\ P^{out}_{LEC}(t) = 0 \\ P^{in}_{LEC}(t) = P_{load,LEC}(t) - |P_{MGS}(t)| \end{cases} \tag{4.57}$$

A schematic representation of power exchanges can be found in Figg. 4.54-4.56.

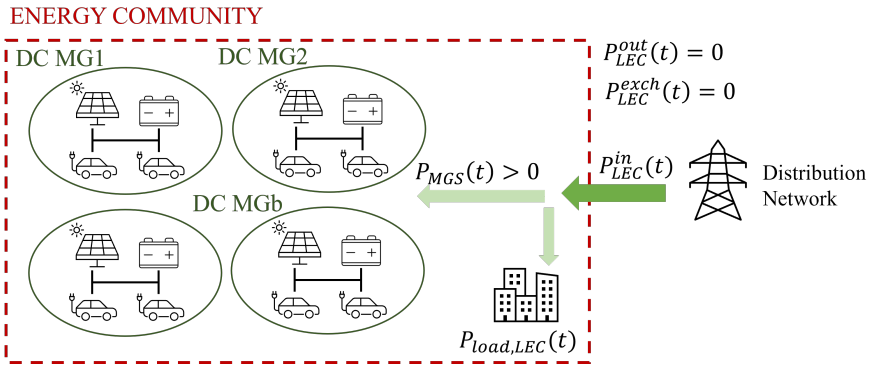

Figure 4.54: Power exchanges between energy community and distribution grid in case (4.55).

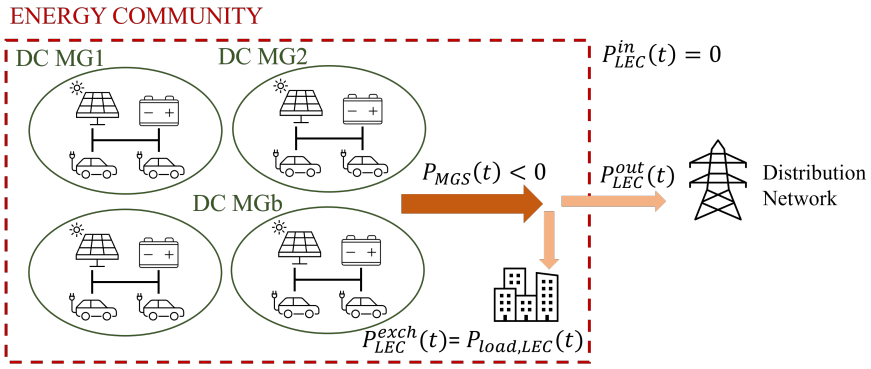

Figure 4.55: Power exchanges between energy community and distribution grid in case (4.56).

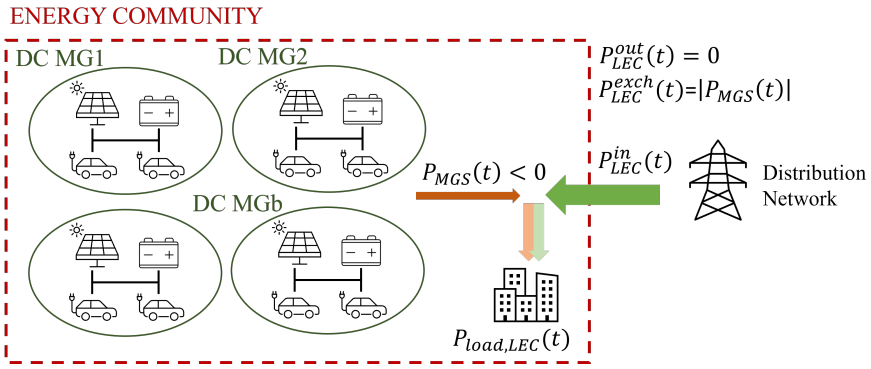

Figure 4.56: Power exchanges between energy community and distribution grid in case (4.57).

4.8.1 Evaluation of LEC costs

With the purpose of evaluating benefits deriving from the formation of the energy community, a comparison between daily costs in the absence and presence (thus considering incentive for the load supply) of the community is carried out.

In the absence of the community, both the power required by the microgrids and the power required by the load are purchased from the grid at the predetermined purchase price. Therefore, assuming that the power selling and buying prices $r_g^{out}(t)$ and $c_g^{in}(t)$ are the same for each b-th microgrid as reported in Fig. 4.50, without community formation, the total daily cost $C^{w/oLEC}$ is expressed by the following relation (4.58).

$$C^{w/oLEC} = \Delta T \cdot \sum_{t}^{N_T} \Big\{ c_g^{in}(t) \cdot P_{MGS}^{in}(t) - r_g^{in}(t) \cdot P_{MGS}^{out}(t) + \\ + c_g^{in}(t) \cdot P_{load,LEC}(t) \Big\} \tag{4.58}$$

Considering the aggregation of microgrids in the energy community, total cost accounts also for incentive (ξ expressed in €/MWh) for internal power exchanges inside the community, given by exchange among microgrids $P_{MGS}^{exch}(t)$, and community power supply $P_{LEC}^{exch}(t)$ to the load. The expression for evaluating cost C^{LEC} is reported in (4.59).

$$C^{LEC} = \Delta T \cdot \sum_{t}^{N_T} \Big\{ c_g^{in}(t) \cdot P_{LEC}^{in}(t) - r_g^{in}(t) \cdot P_{LEC}^{out}(t) + \\ -\xi \cdot \Big[P_{LEC}^{exch}(t) + P_{MGS}^{exch}(t) \Big] \Big\} \tag{4.59}$$

4.8.2 Analysis of results

The economic benefit deriving from LEC aggregation is evaluated for 3 load profiles, specifically the ones connected at nodes 26, 31 and 15, in order to establish which typology of load is more economically convenient for being integrated within the LEC. Load at node 26 refers to a commercial utility, and has a 22.48 kW peak at 12:00, and a daily energy request of 412.88 kWh. Load at node 31 refers to a commercial utility too, but with higher demand peak (57.11 kW at 10:30 and 11:30) and daily energy (1032.2 kWh). Load at node 15 refers to a residential utility with a peak of 59.67 kW at 12:30 and requires daily 949.9 kWh (the relevant profiles are reported in Fig. 4.57).

The incentive assumed is referred to the draft of the Ministry of the Environment and Energy Security made public after 199/2021 Legislative Decree. This incentive, as in [124], is valid on the energy shared within energy communities integrating renewable energy sources that start operating after December 16^{th} 2021, with installed power not exceeding 1 MW and that share energy with users connected to the same MV distribution network (deriving from a single HV /MV transformer station). Therefore, the incentive ξ is the sum of the fix tariff of 120 €/MWh (as in [70]) and the avoided grid costs for transport (corresponding to 8.48 €/MWh, according to [125]), for a total of 128.48 €/MWh.

In the case under study, the power exported by the whole entity of microgrids depicted as well in Fig. 4.57, is concentrated in the evening hours, while between 04:00 and 05:30 they constitute an additional load for the grid. In particular, at 20:30 and 22:00, it exceeds all loads demand, thus the excess is necessarily fed into the grid without incentive. Considering the integration of load at node 26, in the case of the creation of an energy community, the total cost is -0.017 €, so a remuneration is obtained, while in the case where it is not created, a cost of 21.79 € has to be sustained. Aggregating user 31, the costs amount to 71.96 € in

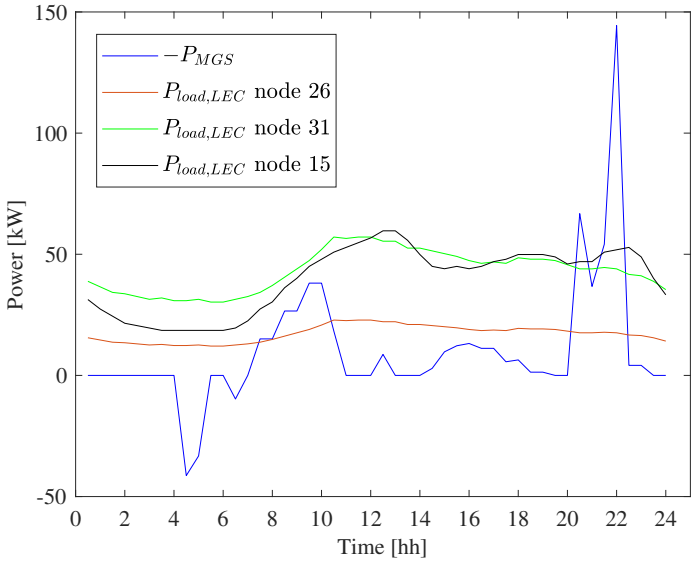

Figure 4.57: Power exchanges of all microgrids and load profiles considered.

the case of community and 105.26 € otherwise, while considering load 15 they amount to 62.82 € in the case of community and 97.44 € in the case of non-creation. Therefore, the community presents a higher saving (of 34.84%) by integrating residential load 15 rather than load 31 (31.18%). The results are collected in Table 4.18. Daily values of P_{MGS} and P_{LEC}^{exch} evaluated for each load are reported in Table 4.19: the total daily P_{MGS} is negative, meaning that the group of microgrids complexly export energy to the grid. As the power required by load increases (e.g. node 15 load) P_{LEC}^{exch} also increases, since energy is covered by microgrids inside the LEC.

Table 4.18: Cost comparison in the absence and in the presence of LEC of DC microgrids.

Load at node 26		**Load at node 31**		**Load at node 15**	
$C^{w/oLEC}$	C^{LEC}	$C^{w/oLEC}$	C^{LEC}	$C^{w/oLEC}$	C^{LEC}
21.79 €	-0.017 €	105.26 €	71.96 €	97.44 €	62.82 €

Table 4.19: Daily values of P_{MGS} and P_{LEC}^{exch} for each load considered.

Load at node 26		**Load at node 31**		**Load at node 15**	
P_{MGS}	P_{LEC}^{exch}	P_{MGS}	P_{LEC}^{exch}	P_{MGS}	P_{LEC}^{exch}
-487.5 kW	283.1 kW	-487.5 kW	446.3 kW	-487.5 kW	466.5 kW

Chapter 5

Conclusions and future work

In this thesis the integration of EVs into DC microgrid and distribution grids, with possible aggregated frameworks such as LECs by means of optimal procedures for energy management, has been investigated. The work has been framed into the activities of CONNECT and PROGRESSUS EU H2020 projects.

A performance analysis of the optimal procedures has been carried out firstly considering DC-based EVSI involving PV and BESS, taking into account technical and economic targets, and considering different EV usage patterns and PV availability levels. The influence of incentives and prices for V2G exploitation has been investigated, as well as the impact of fast-charging station integration into the microgrid. Furthermore, the possibility of internal reserve provision for coping with PV generation and EVs uncertainties has been studied. These procedures have been implemented into cloud-based platform for energy management of the DC microgrid Use Case of the PROGRESSUS project, along with preliminary tests on system assets. Simulations have shown that a more intense use of V2G operation has been observed when the objective does not involve wearing costs of EVs batteries. Moreover, the presence of a consistent PV availability has led to lower operation costs, while EV usage has affected possible exploitation in V2G mode. The comparison of occurring conditions deriving from the definition of proper technical and economic indicators able to provide synthetic information, could allow the EVSI EMS to adopt the best strategy. Considering different scenarios based on a set of structural, operating, and eco-

nomic conditions, the system without BESS show that V2G exploitation for power selling to the distribution grid is encouraged by more attractive selling prices more than by renewable energy availability. Moreover, the system involving BESS efficiently responds to price variations as well, giving a significant contribution to energy selling during the interval when the spike price occurs, and yielding lower daily economic effort. The integrated architecture for DC microgrid has proved to effectively achieve the controllability of EVs and the bidirectional power exchanges. The proposed stochastic energy management procedure has shown that up and down reserve levels are guaranteed during daily microgrid operation with a fair confidence level, proving that BESS and EV operations, when suitably managed, could be useful to compensate uncertainties, although implying higher operation costs. The influence of storage efficiency and wearing costs has implied a preference for EVs to support this function. A feasible integration of the EV fast-charging station into the DC microgrid has been demonstrated, although this implies an increase of cable and converter losses with respect to the case without the fast-charging, along with operational costs and energy exchanges with the utility grid. Considering a technical target implies that EVs are more actively involved, with consequently reduction of losses with the respect of the economic target. Furthermore, the implementation of optimal procedures into the energy management platform has shown a correct data exchange and visualization on platform dashboards.

The aggregation of DC microgrids into a LEC framework has shown that EV-based microgrids take advantage with respect to the other prosumers of the community from PV availability, BESS and EVs, and sell energy to the distribution grid and to the other prosumers, according to higher selling prices. Furthermore, the presence of revenues for EV discharging encourages V2G exploitation, with respect to the use of dedicated BESS.

The stochastic approach implemented in this framework of a two-stage scheduling procedure revealed that positive and negative reserve levels are guaranteed considering both provision only by BESS and by BESS and EVs. When the reserve is provided only by the BESS units, no significant modification of the scheduled power exchange within the

microgrid has been observed with respect to the case without reserve service. Whereas, when both BESS units and EV batteries provided reserve, a variation of schedules and daily cost reduction have been observed for EV-based microgrids, even in the absence of reserve revenues/costs. The proposed chance-constrained approach has resulted to provide more efficient solution with respect to stochastic scenario evaluation, showing that the reserve schedule has implied the attainment of better performances in terms of technical and economic objectives with reasonable computational effort.

The environmental and economic impact of EV parking lot operation in the presence and absence of a BESS has been discussed considering uncontrolled and smart charging techniques. Results have shown that BESS operation has been useful to reduce EV carbon intensity and charging costs. In particular, while considering environmental target, carbon emission reduction has been achieved, especially for high BESS capacity levels and in scenarios of EV fast charging rates, and operational costs are higher in fast charging scenarios than in low charge ones, independently from BESS size and the season. Some significant cost reductions have been observed considering economic target and high-capacity BESS, along with carbon emission reduction in the sole winter season. The exploitation of EV smart charging has allowed a less intense exploitation of BESS, ensuring its longer life, and the attainment of objective values similar to higher BESS sizes with uncontrolled charging.

The investigation on EV integration on distribution grids at different penetration levels has shown that the strategy based on V2G implies lower total energy and power losses, with respect to controlled and uncontrolled charging. Furthermore, the exploitation of V2G functionality has led to peak shaving, thus reducing losses and increasing the grid power quality, in terms of voltage deviations. Simulation results have shown that EV plug-in position within the grid (in particular at residential buses) could enhance V2G exploitation.

When integrating clusters of EV stations in MV and LV grids, grid loss and total load increases have occurred, although technical limitations on voltages and flow rates are satisfied, therefore correct and safe EV integration has proved feasible even with high penetration levels. Moreover, simulation results have pointed out how V2G functionality has been

affected by grid conditions. In fact, when stringent voltage limitations were imposed, EVs have been pushed to support the grid during demand peaks. Furthermore, since V2V behavior has been observed among different nodes in the grid, potentials for energy community realizations has been envisaged.

Finally, a multi-objective methodology for DC-based EVSI integrated into MV grids has been adopted for investigating possible aggregation in energy communities. Results have shown that technical and economic targets for the whole distribution grid and for each DC microgrid can be achieved, as reduced energy losses are detected with respect to the case without DC microgrid. Moreover, resources inside each microgrid are optimally programmed and V2G functionality has been exploited to inject power into the grid predominantly in the evening hours when revenues for discharge are higher. Simulations have allowed to assess the economic benefits from the aggregation of microgrids with grid loads in a LEC configuration. In particular, the aggregation of microgrids into LEC is more convenient when incentivising the feeding of a residential rather than a commercial user.

The studies carried out in this thesis, employing real device data of the use case demonstrator has led to individuate the operating strategies for the efficient deployment of EVs in DC microgrid as well as in LECs and distribution network ensuring proper technical, economic and environmental performances.

5.1 Future developments

The studies presented in this thesis have laid the groundwork for further developments. The potential directions for future research are listed as follows:

- tests on DC microgrid demonstrator in order to establish a proper communication between field assets and energy management system, in order to send correctly the optimized set-points to physical devices by the energy management platform, since the permanent connection procedure to the distribution grid is still ongoing,
- the increase of daily cost due to BESS employment for reserve provision could be

mitigated by considering the avoided cost of power purchase at grid connection point, making BESS usage convenient,

- the inclusion of revenues for reserve provision service exploited by EVs and BESS, along with the consideration of not only reserve levels within the DC microgrid, but also an aggregated reserve of the LEC,
- the analysis of optimal strategies for ancillary service provision in the energy market and regulation market by microgrids and systems of microgrids in order to reach economic targets,
- the development of control strategies analyzing interactions between community and microgrid operation both on day-ahead and real-time scale, with the aim of implementing them into the energy management system of the real installation,
- the evaluation of the impacts of higher EV penetration levels on the transmission network.

Bibliography

[1] United Nations Environment Programme (UNEP), "Emissions gap report 2023: Broken record – temperatures hit new highs, yet world fails to cut emissions (again)," 2023-11, Available online.

[2] European Commission, *COMMUNICATION FROM THE COMMISSION TO THE EUROPEAN PARLIAMENT, THE COUNCIL, THE EUROPEAN ECONOMIC AND SOCIAL COMMITTEE AND THE COMMITTEE OF THE REGIONS 'Fit for 55': delivering the EU's 2030 Climate Target on the way to climate neutrality.* 2021, Available online.

[3] European Parliament, *Regulation (EU) 2019/631 of the European Parliament and of the Council of 17 April 2019 setting CO2 emission performance standards for new passenger cars and for new light commercial vehicles, and repealing Regulations (EC) No 443/2009 and (EU) No 510/2011.* 2019, Available online.

[4] IEA, "Global ev outlook 2023.," 2023, License: CC BY 4.0, Available online.

[5] Energy & Strategy, "Smart mobility short report 2023," 2023, Available online.

[6] European Parliament, *REGULATION OF THE EUROPEAN PARLIAMENT AND OF THE COUNCIL on the deployment of alternative fuels infrastructure, and repealing Directive 2014/94/EU.* 2021, Available online.

[7] European Commission, *Regulation (EU) 2023/1804 of the European Parliament and of the Council of 13 September 2023 on the deployment of alternative fuels infrastructure, and repealing Directive 2014/94/EU (Text with EEA relevance).* 2023, Available online.

[8] European Alternative Fuels Observatory, "Road: reports by country.," Available online.

[9] Terna and Snam, "Documento di descrizione degli scenari 2022," 2022, Available online.

[10] A. Ahmadian, B. Mohammadi-IVatloo, and A. Elkamel, *Electric Vehicles in Energy Systems*. Springer, 2020.

[11] T. Pothinun and S. Premrudeepreechacharn, "Power quality impact of charging station on mv distribution networks: A case study in pea electrical power system," in *2018 53rd International Universities Power Engineering Conference (UPEC)*, pp. 1–6, 2018.

[12] R. Jarvis and P. Moses, "Smart grid congestion caused by plug-in electric vehicle charging," in *2019 IEEE Texas Power and Energy Conference (TPEC)*, pp. 1–5, 2019.

[13] H. Ramadan, A. Ali, and C. Farkas, "Assessment of plug-in electric vehicles charging impacts on residential low voltage distribution grid in hungary," in *2018 6th International Istanbul Smart Grids and Cities Congress and Fair (ICSG)*, pp. 105–109, 2018.

[14] A. Zaidi, K. Sunderland, and M. Conlon, "Impact assessment of high-power domestic ev charging proliferation of a distribution network," *IET Generation, Transmission & Distribution*, vol. 14, no. 24, pp. 5918–5926, 2020.

[15] S. Rahman, I. A. Khan, A. A. Khan, A. Mallik, and M. F. Nadeem, "Comprehensive review & impact analysis of integrating projected electric vehicle charging load to the existing low voltage distribution system," *Renewable and Sustainable Energy Reviews*, vol. 153, p. 111756, 2022.

[16] J. Stiasny, T. Zufferey, G. Pareschi, D. Toffanin, G. Hug, and K. Boulouchos, "Sensitivity analysis of electric vehicle impact on low-voltage distribution grids," *Electric Power Systems Research*, vol. 191, p. 106696, 2021.

[17] C.-M. Chan, H.-R. Liou, and C.-N. Lu, "Operation of distribution feeders with electric vehicle charging loads," in *2012 IEEE 15th International Conference on Harmonics and Quality of Power*, pp. 695–700, 2012.

[18] Y. Yu, D. Reihs, S. Wagh, A. Shekhar, D. Stahleder, G. R. C. Mouli, F. Lehfuss, and P. Bauer, "Data-driven study of low voltage distribution grid behaviour with increasing electric vehicle penetration," *IEEE Access*, vol. 10, pp. 6053–6070, 2022.

[19] M. Nour, H. Ramadan, A. Ali, and C. Farkas, "Impacts of plug-in electric vehicles charging on low voltage distribution network," in *2018 International Conference on Innovative Trends in Computer Engineering (ITCE)*, pp. 357–362, 2018.

[20] Z. Xie, W. Qi, C. Huang, and H. Li, "Effect analysis of ev optimal charging on dg integration in distribution network," in *2019 IEEE 8th International Conference on Advanced Power System Automation and Protection (APAP)*, pp. 525–528, 2019.

[21] H. Wang, K. Zeng, J. Liu, B. Du, and Y. Tang, "Power flow analysis of the economic dispatch considering the flexible ev charging," in *2020 IEEE 4th Conference on Energy Internet and Energy System Integration (EI2)*, pp. 2885–2888, 2020.

[22] D. McCarthy and P. Wolfs, "The hv system impacts of large scale electric vehicle deployments in a metropolitan area," in *2010 20th Australasian Universities Power Engineering Conference*, pp. 1–6, 2010.

[23] A. M. Sanchez, G. E. Coria, A. A. Romero, and S. R. Rivera, "An improved methodology for the hierarchical coordination of pev charging," *IEEE Access*, vol. 7, pp. 141754–141765, 2019.

[24] H. Turker and S. Bacha, "Optimal minimization of plug-in electric vehicle charging cost with vehicle-to-home and vehicle-to-grid concepts," *IEEE Transactions on Vehicular Technology*, vol. 67, no. 11, pp. 10281–10292, 2018.

[25] K. Clement-Nyns, E. Haesen, and J. Driesen, "The impact of vehicle-to-grid on the distribution grid," *Electric Power Systems Research*, vol. 81, no. 1, pp. 185–192, 2011.

[26] S. Iqbal, A. Xin, M. U. Jan, H. ur Rehman, A. Masood, S. A. Abbas Rizvi, and S. Salman, "Aggregated electric vehicle-to-grid for primary frequency control in a microgrid- a review," in *2018 IEEE 2nd International Electrical and Energy Conference (CIEEC)*, pp. 563–568, 2018.

[27] M. S. H. Nizami, M. J. Hossain, and K. Mahmud, "A coordinated electric vehicle management system for grid-support services in residential networks," *IEEE Systems Journal*, vol. 15, no. 2, pp. 2066–2077, 2021.

[28] A. Pal, A. Bhattacharya, and A. K. Chakraborty, "Allocation of ev fast charging station with v2g facility in distribution network," in *2019 8th International Conference on Power Systems (ICPS)*, pp. 1–6, 2019.

[29] H. B. Sonder, L. Cipcigan, and C. E. Ugalde-Loo, "Voltage analysis on mv/lv distribution networks with the integration of dc fast chargers," in *2020 6th IEEE International Energy Conference (ENERGYCon)*, pp. 260–265, 2020.

[30] M. Mohiti, H. Monsef, and H. Lesani, "A decentralized robust model for coordinated operation of smart distribution network and electric vehicle aggregators," *International Journal of Electrical Power & Energy Systems*, vol. 104, pp. 853–867, 2019.

[31] J. García-Villalobos, I. Zamora, J. San Martín, F. Asensio, and V. Aperribay, "Plug-in electric vehicles in electric distribution networks: A review of smart charging approaches," *Renewable and Sustainable Energy Reviews*, vol. 38, pp. 717–731, 2014.

[32] D. Mehlig, H. ApSimon, and I. Staffell, "Emissions from charging electric vehicles in the uk," *Transportation Research Part D: Transport and Environment*, vol. 110, p. 103430, 2022.

[33] J. Huber, K. Lohmann, M. Schmidt, and C. Weinhardt, "Carbon efficient smart charging using forecasts of marginal emission factors," *Journal of Cleaner Production*, vol. 284, p. 124766, 2021.

[34] C. G. Hoehne and M. V. Chester, "Optimizing plug-in electric vehicle and vehicle-to-grid charge scheduling to minimize carbon emissions," *Energy*, vol. 115, pp. 646–657, 2016.

[35] J. Li, G. Wang, X. Wang, and Y. Du, "Smart charging strategy for electric vehicles based on marginal carbon emission factors and time-of-use price," *Sustainable Cities and Society*, vol. 96, p. 104708, 2023.

[36] N. Brinkel, W. Schram, T. AlSkaif, I. Lampropoulos, and W. van Sark, "Should we reinforce the grid? cost and emission optimization of electric vehicle charging under different transformer limits," *Applied Energy*, vol. 276, p. 115285, 2020.

[37] Y. Krim, M. Sechilariu, F. Locment, and A. Alchami, "Global cost and carbon impact assessment methodology for electric vehicles' pv-powered charging station," *Applied Sciences*, vol. 12, no. 9, 2022.

[38] Y. Wen, Y. Chen, P. Wang, A. Rassol, and S. Xu, "Photovoltaic–electric vehicles participating in bidding model of power grid that considers carbon emissions," *Energy Reports*, vol. 8, pp. 3847–3855, 2022.

[39] L. Bartolucci, S. Cordiner, V. Mulone, M. Santarelli, F. Ortenzi, and M. Pasquali, "Pv assisted electric vehicle charging station considering the integration of stationary first- or second-life battery storage," *Journal of Cleaner Production*, vol. 383, p. 135426, 2023.

[40] L. S. A. Grande, I. Yahyaoui, and S. A. Gómez, "Energetic, economic and environmental viability of off-grid pv-bess for charging electric vehicles: Case study of spain," *Sustainable Cities and Society*, vol. 37, pp. 519–529, 2018.

[41] M. Sufyan, N. Rahim, M. Muhammad, C. Tan, S. Raihan, and A. Bakar, "Charge coordination and battery lifecycle analysis of electric vehicles with v2g implementation," *Electric Power Systems Research*, vol. 184, p. 106307, 2020.

[42] S. Kaur, T. Kaur, R. Khanna, and P. Singh, "A state of the art of dc microgrids for electric vehicle charging," in *2017 4th International Conference on Signal Processing, Computing and Control (ISPCC)*, pp. 381–386, 2017.

[43] K. Sayed, A. G. Abo-Khalil, and A. S. Alghamdi, "Optimum resilient operation and control dc microgrid based electric vehicles charging station powered by renewable energy sources," *Energies*, vol. 12, no. 22, 2019.

[44] H. Bevrani, B. François, and T. Ise, *Microgrid dynamics and control*. John Wiley & Sons, 2017.

[45] W. Wu, Y. Chen, A. Luo, L. Zhou, X. Zhou, L. Yang, Y. Dong, and J. M. Guerrero, "A virtual inertia control strategy for dc microgrids analogized with virtual synchronous machines," *IEEE Transactions on Industrial Electronics*, vol. 64, no. 7, pp. 6005–6016, 2017.

[46] Y. Wu, D. Chrenko, A. Ravey, and A. Miraoui, "Coordinated control of a fast v2g charging station with pv generation and energy storage systems," in *2017 IEEE Vehicle Power and Propulsion Conference (VPPC)*, pp. 1–6, 2017.

[47] S. Kaur, T. Kaur, R. Khanna, and P. Singh, "A state of the art of dc microgrids for electric vehicle charging," in *2017 4th International Conference on Signal Processing, Computing and Control (ISPCC)*, pp. 381–386, 2017.

[48] K. Sayed, A. Abo-Khalil, and A. S. Alghamdi, "Optimum resilient operation and control dc microgrid based electric vehicles charging station powered by renewable energy sources," *Energies*, vol. 12, p. 4240, 11 2019.

[49] L. Novoa and J. Brouwer, "Dynamics of an integrated solar photovoltaic and battery storage nanogrid for electric vehicle charging," *Journal of Power Sources*, vol. 399, pp. 166–178, 2018.

[50] J. L. Torres-Moreno, A. Gimenez-Fernandez, M. Perez-Garcia, and F. Rodriguez, "Energy management strategy for micro-grids with pv-battery systems and electric vehicles," *Energies*, vol. 11, no. 3, 2018.

[51] A. Garg, S. Shaosen, L. Gao, X. Peng, and P. Baredar, "Aging model development based on multidisciplinary parameters for lithium-ion batteries," *International Journal of Energy Research*, vol. 44, no. 4, pp. 2801–2818, 2020.

[52] X. Lu, N. Liu, Q. Chen, and J. Zhang, "Multi-objective optimal scheduling of a dc micro-grid consisted of pv system and ev charging station," in *2014 IEEE Innovative Smart Grid Technologies - Asia (ISGT ASIA)*, pp. 487–491, 2014.

[53] P. Wang, W. Wang, N. Meng, and D. Xu, "Multi-objective energy management system for dc microgrids based on the maximum membership degree principle," *Journal of Modern Power Systems and Clean Energy*, vol. 6, no. 4, pp. 668–678, 2018.

[54] L. Wang, Q. Li, R. Ding, M. Sun, and G. Wang, "Integrated scheduling of energy supply and demand in microgrids under uncertainty: A robust multi-objective optimization approach," *Energy*, vol. 130, pp. 1–14, 2017.

[55] B. Ye, X. Shi, X. Wang, and H. Wu, "Optimisation configuration of hybrid ac/dc microgrid containing electric vehicles based on the nsga-ii algorithm," *The Journal of Engineering*, vol. 2019, no. 10, pp. 7229–7236, 2019.

[56] W. Su, S. S. Yu, H. Li, H. H.-C. Iu, and T. Fernando, "An mpc-based dual-solver optimization method for dc microgrids with simultaneous consideration of operation cost and power loss," *IEEE Transactions on Power Systems*, vol. 36, no. 2, pp. 936–947, 2021.

[57] R. Ghotge, Y. Snow, S. Farahani, Z. Lukszo, and A. van Wijk, "Optimized scheduling of ev charging in solar parking lots for local peak reduction under ev demand uncertainty," *Energies*, vol. 13, no. 5, 2020.

[58] S. Li, H. Wu, X. Bai, and S. Yang, "Optimal dispatch for pv-assisted charging station of electric vehicles," in *2019 IEEE PES GTD Grand International Conference and Exposition Asia (GTD Asia)*, pp. 854–859, 2019.

[59] Q. Yan, B. Zhang, and M. Kezunovic, "Optimized operational cost reduction for an ev charging station integrated with battery energy storage and pv generation," *IEEE Transactions on Smart Grid*, vol. 10, no. 2, pp. 2096–2106, 2019.

[60] H. Zhao, H. Lu, B. Li, X. Wang, S. Zhang, and Y. Wang, "Stochastic optimization of microgrid participating day-ahead market operation strategy with consideration of energy storage system and demand response," *Energies*, vol. 13, no. 5, 2020.

[61] S. S. Reddy, V. Sandeep, and C.-M. Jung, "Review of stochastic optimization methods for smart grid," *Frontiers in Energy*, vol. 11, pp. 197–209, 2017.

[62] European Commission, "Energy union package communication," 2015.

[63] European Commission and Directorate-General for Energy, *Clean energy for all Europeans*. Publications Office, 2019.

[64] *Directive (EU) 2018/2001 of the European Parliament and of the Council of 11 December 2018 on the promotion of the use of energy from renewable sources.* 2018, Available online.

[65] *Directive (EU) 2019/944 of the European Parliament and of the Council of 5 June 2019 on common rules for the internal market for electricity and amending Directive 2012/27/EU.* 2019, Available online.

[66] *Directive 2009/72/EC of the European Parliament and of the Council of 13 July 2009 concerning common rules for the internal market in electricity and repealing Directive 2003/54/EC.* 2009, Available online.

[67] Repubblica Italiana, *Legge 28 febbraio 2020, n. 8. Gazzetta ufficiale della Repubblica Italiana n.51 del 29 Febbraio 2020*. 2020.

[68] ARERA, *Deliberazione 4 agosto 2020 - 318/2020/R/EEL.* 2020.

[69] Ministero dello sviluppo economico (MiSE), *Individuazione della tariffa incentivante per la remunerazione degli impianti a fonti rinnovabili inseriti nelle configurazioni sperimentali di autoconsumo collettivo e comunità energetiche rinnovabili*. 2020.

[70] M. dell'Ambiente e della Sicurezza Energetica (MASE), *Decreto MASE n.414 del 07/12/2023.* 2024, Available online.

[71] Q. Li, Y. Liao, K. Wu, L. Zhang, J. Lin, M. Chen, J. M. Guerrero, and D. Abbott, "Parallel and distributed optimization method with constraint decomposition for energy management of microgrids," *IEEE Transactions on Smart Grid*, vol. 12, no. 6, pp. 4627–4640, 2021.

[72] B. Zhou, J. Zou, C. Y. Chung, H. Wang, N. Liu, N. Voropai, and D. Xu, "Multi-microgrid energy management systems: Architecture, communication, and scheduling

strategies," *Journal of Modern Power Systems and Clean Energy*, vol. 9, no. 3, pp. 463–476, 2021.

[73] J. L. Martínez-Ramos, A. Marano-Marcolini, F. P. García-López, F. Almagro-Yravedra, A. Onen, Y. Yoldas, M. Khiat, L. Ghomri, and N. Fragale, "Provision of ancillary services by a smart microgrid: An opf approach," in *2018 International Conference on Smart Energy Systems and Technologies (SEST)*, pp. 1–6, 2018.

[74] M. Alowaifeer, M. Alkhraijah, A. P. S. Meliopoulos, and S. Grijalva, "Grid services optimization from multiple microgrids," *IEEE Transactions on Smart Grid*, vol. 13, no. 1, pp. 8–19, 2022.

[75] M. Mao, Y. Wang, L. Chang, and Y. Du, "Operation optimization for multi-microgrids based on centralized-decentralized hybrid hierarchical energy management," in *2017 IEEE Energy Conversion Congress and Exposition (ECCE)*, pp. 4813–4820, 2017.

[76] W. Zhang and Y. Xu, "Distributed optimal control for multiple microgrids in a distribution network," *IEEE Transactions on Smart Grid*, vol. 10, no. 4, pp. 3765–3779, 2019.

[77] A. Sinha, P. Malo, and K. Deb, "A review on bilevel optimization: From classical to evolutionary approaches and applications," *IEEE Transactions on Evolutionary Computation*, vol. 22, no. 2, pp. 276–295, 2018.

[78] E. Fernandez, M. Hossain, K. Mahmud, M. S. H. Nizami, and M. Kashif, "A bi-level optimization-based community energy management system for optimal energy sharing and trading among peers," *Journal of Cleaner Production*, vol. 279, p. 123254, 2021.

[79] S. Bahramara, M. Parsa Moghaddam, and M. Haghifam, "A bi-level optimization model for operation of distribution networks with micro-grids," *International Journal of Electrical Power & Energy Systems*, vol. 82, pp. 169–178, 2016.

[80] C. Guo, X. Wang, Y. Zheng, and F. Zhang, "Optimal energy management of multi-microgrids connected to distribution system based on deep reinforcement learning," *International Journal of Electrical Power & Energy Systems*, vol. 131, p. 107048, 2021.

[81] D. Wang, F. Locment, and M. Sechilariu, "Modelling, simulation, and management strategy of an electric vehicle charging station based on a dc microgrid," *Applied Sciences*, vol. 10, no. 6, 2020.

[82] J. Zhang, Y. Zhang, T. Li, L. Jiang, K. Li, H. Yin, and C. Ma, "A hierarchical distributed energy management for multiple pv-based ev charging stations," in *IECON 2018 - 44th Annual Conference of the IEEE Industrial Electronics Society*, pp. 1603–1608, 2018.

[83] M. Shin, D.-H. Choi, and J. Kim, "Cooperative management for pv/ess-enabled electric vehicle charging stations: A multiagent deep reinforcement learning approach," *IEEE Transactions on Industrial Informatics*, vol. 16, no. 5, pp. 3493–3503, 2020.

[84] H. Kikusato, K. Mori, S. Yoshizawa, Y. Fujimoto, H. Asano, Y. Hayashi, A. Kawashima, S. Inagaki, and T. Suzuki, "Electric vehicle charge–discharge management for utilization of photovoltaic by coordination between home and grid energy management systems," *IEEE Transactions on Smart Grid*, vol. 10, no. 3, pp. 3186–3197, 2019.

[85] A. Borghetti, F. Napolitano, S. Rahmani-Dabbagh, and F. Tossani, "Scenario tree generation for the optimization model of a parking lot for electric vehicles," in *2017 AEIT International Annual Conference*, pp. 1–6, 2017.

[86] M. Dicorato, G. Forte, M. Trovato, C. B. Muñoz, and G. Coppola, "An integrated dc microgrid solution for electric vehicle fleet management," *IEEE Transactions on Industry Applications*, vol. 55, no. 6, pp. 7347–7355, 2019.

[87] S. Bruno, C. Iurlaro, M. L. Scala, and M. Menga, "Integration of operating reserve constrains in the predictive optimal dispatch of energy and storage resources in small islands," in *2022 IEEE International Conference on Environment and Electrical Engineering and 2022 IEEE Industrial and Commercial Power Systems Europe (EEEIC / I&CPS Europe)*, pp. 1–6, 2022.

[88] G. Mohy-ud din, K. M. Muttaqi, and D. Sutanto, "A cooperative energy transaction model for vpp integrated renewable energy hubs in deregulated electricity markets," *IEEE Transactions on Industry Applications*, vol. 58, no. 6, pp. 7776–7791, 2022.

[89] X. Deng, Q. Zhang, Y. Li, T. Sun, and H. Yue, "Hierarchical distributed frequency regulation strategy of electric vehicle cluster considering demand charging load optimization," in *2020 IEEE 3rd Student Conference on Electrical Machines and Systems (SCEMS)*, pp. 959–969, 2020.

[90] Y. Li, B. Wang, Z. Yang, J. Li, and G. Li, "Optimal scheduling of integrated demand response-enabled community-integrated energy systems in uncertain environments," *IEEE Transactions on Industry Applications*, vol. 58, no. 2, pp. 2640–2651, 2022.

[91] J. Liu, H. Chen, W. Zhang, B. Yurkovich, and G. Rizzoni, "Energy management problems under uncertainties for grid-connected microgrids: A chance constrained programming approach," *IEEE Transactions on Smart Grid*, vol. 8, no. 6, pp. 2585–2596, 2017.

[92] C. Orozco, A. Borghetti, B. De Schutter, F. Napolitano, G. Pulazza, and F. Tossani, "Intra-day scheduling of a local energy community coordinated with day-ahead multistage decisions," *Sustainable Energy, Grids and Networks*, vol. 29, p. 100573, 2022.

[93] S. Bahramara, P. Sheikhahmadi, G. Chicco, A. Mazza, F. Wang, and J. P. S. Catalão, "Modeling the microgrid operator participation in day-ahead energy and reserve markets considering stochastic decisions in the real-time market," *IEEE Transactions on Industry Applications*, vol. 58, no. 5, pp. 5747–5762, 2022.

[94] Y. Cui, Z. Hu, and H. Luo, "Optimal day-ahead charging and frequency reserve scheduling of electric vehicles considering the regulation signal uncertainty," *IEEE Transactions on Industry Applications*, vol. 56, no. 5, pp. 5824–5835, 2020.

[95] N. Rezaei, A. Khazali, M. Mazidi, and A. Ahmadi, "Economic energy and reserve management of renewable-based microgrids in the presence of electric vehicle aggregators: A robust optimization approach," *Energy*, vol. 201, p. 117629, 2020.

[96] S. Bahramara, P. Sheikhahmadi, A. Mazza, and G. Chicco, "Day-ahead self-scheduling from risk-averse microgrid operators to provide reserves and flexible ramping ancillary services," *International Journal of Electrical Power & Energy Systems*, vol. 142, p. 108381, 2022.

[97] X. Yan, C. Gao, M. Song, T. Chen, J. Ding, M. Guo, X. Wang, and D. Abbes, "An igdt-based day-ahead co-optimization of energy and reserve in a vpp considering multiple uncertainties," *IEEE Transactions on Industry Applications*, vol. 58, no. 3, pp. 4037–4049, 2022.

[98] Z. Liu, L. Wang, and L. Ma, "A transactive energy framework for coordinated energy management of networked microgrids with distributionally robust optimization," *IEEE Transactions on Power Systems*, vol. 35, no. 1, pp. 395–404, 2020.

[99] W. Huang, W. Zheng, and D. J. Hill, "Distributionally robust optimal power flow in multi-microgrids with decomposition and guaranteed convergence," *IEEE Transactions on Smart Grid*, vol. 12, no. 1, pp. 43–55, 2021.

[100] PROGRESSUS Project https://progressus-ecsel.eu/.

[101] M. Dicorato, R. Sbrizzai, M. Trovato, and G. Forte, "Optimal operation and reserve provision planning for an ev-oriented dc microgrid," in *2019 IEEE International Conference on Environment and Electrical Engineering and 2019 IEEE Industrial and Commercial Power Systems Europe (EEEIC / I&CPS Europe)*, pp. 1–6, 2019.

[102] C. Heumann and M. S. Shalabh, *Introduction to statistics and data analysis*. Springer, 2016.

[103] B. Aluisio, S. Bruno, L. De Bellis, M. Dicorato, G. Forte, and M. Trovato, "Dc-microgrid operation planning for an electric vehicle supply infrastructure," *Applied Sciences*, vol. 9, no. 13, 2019.

[104] ARERA, "Electricity prices for customers.," 2018, Available online.

[105] M. Dicorato, G. Tricarico, F. Marasciuolo, G. Forte, and M. Trovato, "Performance analysis of ev stations optimal operation in dc microgrid configurations," in *2020 IEEE International Conference on Environment and Electrical Engineering and 2020 IEEE Industrial and Commercial Power Systems Europe (EEEIC / I&CPS Europe)*, pp. 1–6, 2020.

[106] K. Ginigeme and Z. Wang, "Distributed optimal vehicle-to-grid approaches with consideration of battery degradation cost under real-time pricing," *IEEE Access*, vol. 8, pp. 5225–5235, 2020.

[107] M. Ansari, M. Zadsar, H. Zareipour, and M. Kazemi, "Resilient operation planning of integrated electrical and natural gas systems in the presence of natural gas storages," *International Journal of Electrical Power & Energy Systems*, vol. 130, p. 106936, 2021.

[108] Solcast, "Irradiance and weather data," Available online.

[109] ARERA, "Condizioni economiche per i clienti del mercato tutelato," Available online.

[110] GME (Gestore Mercati Energetici), "Dati storici mgp," Available online.

[111] DEOP (Distributed Energy Optimization), "Product sheet and specific terms (specification document)," *Siemens Spa*, 2017.

[112] S. Lilla, C. Orozco, A. Borghetti, F. Napolitano, and F. Tossani, "Day-ahead scheduling of a local energy community: An alternating direction method of multipliers approach," *IEEE Transactions on Power Systems*, vol. 35, no. 2, pp. 1132–1142, 2020.

[113] A. Bemporad and M. Morari, "Control of systems integrating logic, dynamics, and constraints," *Automatica*, vol. 35, no. 3, pp. 407–427, 1999.

[114] G. Ferrari-Trecate, P. Letizia, and M. Spedicato, "Optimization with piecewise affine cost functions," 2001.

[115] Nationagrid ESO, "National carbon intensity forecast," Available online.

[116] Elexon, "System price analysis report.," Available online.

[117] V. Vita, "Development of a decision-making algorithm for the optimum size and placement of distributed generation units in distribution networks," *Energies*, vol. 10, no. 9, 2017.

[118] UKERC, "Energy data centre: Data catalogue.," Available online.

[119] Power Research Electronics (PRE), "Datasheet "power research eletronics 10 kw v2g ev charger module"," 2019.

[120] ADAC, "Elektroautos im test: So hoch ist die reichweite wirklich.," Available online.

[121] T. He, J. Zhu, J. Zhang, and L. Zheng, "An optimal charging/discharging strategy for smart electrical car parks," *Chinese Journal of Electrical Engineering*, vol. 4, no. 2, pp. 28–35, 2018.

[122] T. Alquthami, A. Alsubaie, M. Alkhraijah, K. Alqahtani, S. Alshahrani, and M. Anwar, "Investigating the impact of electric vehicles demand on the distribution network," *Energies*, vol. 15, no. 3, 2022.

[123] C. Mateo, G. Prettico, T. Gómez, R. Cossent, F. Gangale, P. Frías, and G. Fulli, "European representative electricity distribution networks," *International Journal of Electrical Power & Energy Systems*, vol. 99, pp. 273–280, 2018.

[124] RSE, "Dossier 19/2023: CER e Autoconsumo collettivo: alcune simulazioni numeriche alla luce della nuova regolazione," 2023.

[125] ARERA, *Delibera 27 Dicembre 2022 727/2022/R/eel. Definizione, ai sensi del decreto legislativo 199/21 e del decreto legislativo 210/21, della regolazione dell'autoconsumo diffuso. Approvazione del Testo Integrato Autoconsumo Diffuso (TIAD).* 2022.